LIQUID CRYSTALLINE SIDE CHAIN POLYSILOXANES WITH 4-AMINO-4'-STILBENECARBOXYLIC ESTER MESOGENS

By

MARIETTA O. BAUTISTA

Bachelor of Science

University of the Philippines at Los Banos

Los Banos, Laguna, Philippines

1982

Submitted to the Faculty of the
Graduate College of the
Oklahoma State University
in partial fulfillment of
the requirements for
the Degree of
DOCTOR OF PHILOSOPHY
May, 1992

LIQUID CRYSTALLINE SIDE CHAIN POLYSILOXANES
WITH 4-AMINO-4'-STILBENECARBOXYLIC
ESTER MESOGENS

Thesis Approved

Warren T. Ford
Thesis adviser

J. Paul Hawkins

Elizabeth M. Holt

Richard L. Purdy

Thomas C. Collins
Dean of the Graduate College

PREFACE

The aim of this research is to prepare side chain polymers that will exhibit liquid crystalline properties. Liquid crystal (LC) is the intermediate phase between the crystalline solid and isotropic liquid. The molecules in the LC phase are free to move about in the same fashion as in liquids, but as they do so, they tend to remain oriented in a certain direction. Liquid crystals are commonly known for their application as displays for watches, clocks, calculators and other digital displays.

In this work, the side chain polysiloxanes were prepared by the hydrosilylation of a preformed polymer with a terminal alkene which becomes the side chain. The flexibility of the polysiloxane backbone allows the preparation of polymers having low glass transition temperature, T_g. With flexible alkylene spacer, which partially decouples the motions of the side chains and the polymer backbone, production of a room-temperature LC phase can be realized. High isotropization temperature and broad LC phase transition temperature range are also observed.

The characterization of side chain liquid crystalline polysiloxanes with 4-amino-4'-stilbenecarboxylic ester mesogens was undertaken using differential scanning calorimetry, polarizing microscope, and high temperature X-ray diffraction. The utilization of these materials for nonlinear optical applications were also examined. The monolayer behavior of the side chain polysiloxanes were investigated by Langmuir-Blodgett (LB) methods. The deposition of monolayers of the polysiloxanes onto a substrate (e.g. quartz glass) was also performed.

ACKNOWLEDGMENTS

I would like to express sincere appreciation to my adviser, Dr. Warren T. Ford, for his guidance, patience, encouraging words and valuable advice throughout my graduate program. I wish to thank him for giving me the opportunity to broaden my scientific and personal experience by sending me to work in University of Florida. Appreciation is also extended to Dr. Elizabeth M. Holt, Dr. J. Paul Devlin, Dr. Mark G. Rockley and Dr. Richard C. Powell for serving on my advisory committee.

I wish to extend my appreciation to Dr. Randolph S. Duran for allowing me to work in his laboratory at the University of Florida. His valuable knowledge of liquid crystals and Langmuir-Blodgett films has enhanced my understanding of these two subjects. Special thanks to Dr. Matthias Naumann for his intelligent contribution to the analyses of the X-ray diffraction patterns and microscopic textures of my polysiloxanes. I am grateful to all of Dr. Duran's students, specially Angie Thibodeaux, for their warm welcome and for adopting me in their research group for a few months.

Sincere appreciation is given to Dr. Roger J. Reeves for doing the second harmonic generation experiments in Dr. Powell's laboratory and for his unfailing assistance in matters concerning nonlinear optical studies.

I wish to thank all my fellow graduate students and the postdocs in our group, specially Dr. Haribabu, for their help and friendship over the years. Many thanks also go to all the graduate students in our department who shared my frustrations and successes.

I extend a sincere thank you to all my friends who have made my life in Stillwater, Oklahoma, meaningful. Special mention to Edgar Miranda for his friendship and moral support.

A note of thanks is also extended to staff members in the Department of Chemistry of Oklahoma State University for technical assistance.

My sincerest gratitude is extended to my parents for their love, understanding and encouragement throughout my education. I would like to dedicate my work in memory of my father. I am also grateful to my brother and sisters for their love and moral support.

Special thanks to the LORD for watching over me.

Lastly, I would like to acknowledge the Department of Chemistry of Oklahoma State University for their financial support throughout my graduate study.

TABLE OF CONTENTS

Chapter Page

LIST OF TABLES

LIST OF FIGURES

LIST OF SPECTRA

ABSTRACT

Solid, liquid, and gas are the three states of matter. A solid consists of molecules or ions that are fixed in a specific position. Strong attractive forces hold the molecules in place. Hence, three-dimensional order is maintained in a crystalline solid. On the other hand, the forces holding the molecules together in the liquid state are much weaker. Thus, the molecules are free to move randomly and the order is much less than in a solid. Solids are hard and difficult to deform while liquids flow and are easily deformed. In a gas, the molecules move randomly as in liquids, but the attractive forces are not strong enough to hold the molecules close together. A gas can be deformed even more easily than a liquid. A phase is a sample of matter with uniform properties. A state of matter can have one or more phases. Increasing the temperature of a substance increases the molecular motions and the phase is changed at a precise temperature. A completely disordered phase is called isotropic. Thus, most liquids and gases are isotropic. Liquid crystal (LC) is an intermediate phase between the crystalline solid and the isotropic liquid. When a solid melts to an LC phase, the material flows as a liquid, but the molecules retain order in one or two dimensions. Although, an LC phase is anisotropic, it is more similar to a liquid than to a crystalline solid because it only possesses a small amount of order.

The purpose of this work was to prepare and understand the properties liquid crystal polymers (LCPs) which have the shape of a comb. A polymer is a substance consisting of giant molecules formed as chains or networks from smaller molecules (monomers) of the same kind. In the comb-shaped LCPs, relatively long rod-shaped side branches bound to the main chain comprise the teeth and the backbone of a comb, respectively. The comb polymers were made by a reaction that binds the teeth to a preformed polymer backbone of poly(methylhydrosiloxane), a polymer similar to that of

silicone oil and silicone rubber which is among the most flexible polymers known. The flexibility of the backbone allows the preparation of polymers having low glass transition temperature, T_g (the temperature at which a rubbery liquid changes to a glass or vice versa). A spacer chain was placed between the main chain and the side chain to allow main chain motion without disturbing the orientation of the side chains which gives the LC properties of the polymers.

The LC properties of the comb-shaped polymers were examined using a differential scanning calorimeter (DSC), a polarizing microscope, and a high temperature X-ray diffractometer. DSC detects the temperatures at which change of phase occurs and measures the energy change of a phase transition. A LC phase is best observed by a microscope. Due to the orientational order of LCs, polarized light is transmitted. The arrangement of the molecules in different phases is obtained from the X-ray diffractometer. One or two LC phases were observed for each polymer depending on the size of the side chains.

LCs are commonly known for their application as displays (LCD) for watches, calculators and other digital displays. In this work, the polymers were investigated for possible nonlinear optical applications. The polymers prepared in the laboratory showed promising nonlinear optical response which can be compared to materials currently used as laboratory standards.

CHAPTER I

INTRODUCTION

Liquid Crystals

Liquid crystal (LC) refers to a phase which is intermediate between the crystalline solid and the isotropic liquid.[1] A substance in this state is strongly anisotropic in some of its properties although it exhibits a certain degree of fluidity, which in some cases may be comparable to that of an ordinary liquid.[2] A substance having long-range order of the molecular positions in one or two dimensions but not the three dimensional order of a solid state crystal is called a liquid crystal.

The melting of a crystalline substance is a familiar phase transition. The highly structured solid melts to the isotropic liquid phase at a well-defined temperature and with a characteristic heat of fusion. However, a number of organic compounds do not melt directly from crystalline solid to isotropic liquid. Instead, the substance passes through an intermediate phase, a mesophase. In this case, two phase transitions are involved: at a lower temperature, a transition from crystalline solid to mesophase, and at a higher temperature, a transition from mesophase to isotropic liquid. The term LC phase has been used interchangeably with mesophase. The molecular units that lead to mesophases are called mesogens. Transitions into these phases may be brought about by purely thermal processes (thermotropic mesomorphism) or by the influence of solvent (lyotropic mesomorphism). Thermotropic LCs are pure substances, and temperature changes cause the appearance and disappearance of the mesophases. Lyotropic LCs are mixtures of two

different substances, and the mesophase is dependent on the concentration of one component in another.

The first observations of mesomorphic behavior were made towards the end of the nineteenth century by F. Reinitzer[3] and O. Lehmann[4]. The person generally given credit for discovering LCs is Reinitzer. In 1888, he noted that a carefully purified sample of cholesteryl benzoate melted at 146.6 °C to give a cloudy liquid, and when further heated, turned into a clear liquid at 180.6 °C. The following year, Lehmann confirmed Reinitzer's observations using a polarizing microscope equipped with a hot stage. Lehmann remained the dominant figure in LC research in the early twentieth century. After years of experiments, it has become clear what type of compound is likely to be liquid crystalline at some temperature.[5] First of all, the molecule must be elongated in shape, that is, it must be significantly longer that it is wide. Second, the molecule must have some rigidity in its central region. Finally, it seems to be advantageous if the ends of the molecules are somewhat flexible. In 1977, it was established that relatively flat, disc-shaped molecules with flexible side chains may also form stable mesophases.[6]

The great majority of liquid crystalline substances are based on the following general structure:[7]

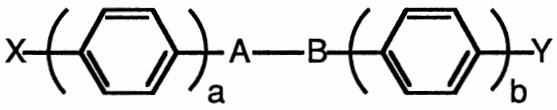

These structures possess a) two terminal groups, X and Y, usually on the long axis of the molecule, b) two or more (a and b) aromatic, usually benzene rings, (or more rarely, heteroaromatic and/or cycloaliphatic rings), and c) one or more bridging groups, A-B, that bind the rings together. A range of terminal substituents such as alkyl, alkoxy and cyano has been used and studied intensively. The nature of the central linkage is of great importance and it usually contains multiple bonds (e.g.-CH=N-, -N=N-, and -CO_2-) that

maintain the rigidity and linearity of the molecules. Several biphenyl systems with no central unit other than the inter-ring C-C bond were also found to exhibit LC properties.

Depending on the detailed molecular geometry, a system may pass through one or more mesophases before it transforms into the isotropic liquid. In 1922, G. Freidel[8] proposed the classification of the different LC phases into three types: nematic, cholesteric and smectic, based mainly on optical studies. The nematic LC (from the Greek word nematos, meaning thread) has a high degree of long range translational order. The molecules are on the average oriented with their long axes approximately parallel with one another. The cholesteric mesophase is also a nematic type of LC except that it is composed of optically active molecules. A more proper name for this phase is chiral nematic LC (chiral simply means twisted). Mesophases in which the molecules are approximately packed together in layers are known collectively as smectic phases (from smectos, meaning soap). In these phases, not only is the small amount of orientational order of LCs present but there is also a small amount of positional order. In the early 1960s, systematic studies of the classification of smectic LCs were undertaken by H. Sackmann and D. Demus.[9,10] They developed the "miscibility rule", which states that LCs are of the same type if they are miscible in all proportions (i.e., all liquid crystalline modifications which exhibit an uninterrupted series of mixed crystals in binary systems without contradiction can be marked with the same symbol). Microscopic textures, the order in which different phases appear in compounds with more than one smectic phase, and X-ray diffraction patterns were also used in their classification work. They introduced the now-common identification of different smectic phase types by capital letters: A, B, C, etc. Smectic A (S_A) phase is the least ordered of all smectic phases. The molecules in this phase have their long axes on the average perpendicular to the layer plane. Smectic B (S_B) phase differs from S_A in that the molecular centers in each layer are hexagonally close packed. Smectic C (S_C) phase is a tilted form of S_A, that is, the molecules are tilted with

respect to the layer planes. The most common LC phases with rod-shaped mesogens (N, S_A and S_C) are shown in Figure 1.[11]

Thermal analysis is important in characterizing LC phases. A knowledge of both the temperature and the heat of transition is necessary for the evaluation of the type and degree of order present in a system. Differential scanning calorimetry (DSC) has greatly facilitated the determination of temperatures, heats of transition, and heat capacity of various phases. DSC involves the comparison of the sample with an inert reference (indium is usually used) during a dynamic heating or cooling program. By comparing the transitions between the various types of phases, certain regularities are observed. The melting enthalpies always possess the highest values. The transition enthalpies connected with the LC phases do not exceed about 7.08 kJ/mol, in most cases, they are considerably smaller. Phase transitions connected with strong structural changes are connected with high transition enthalpies while phase transitions with small structural changes are represented with small ΔH. Identification of liquid crystalline phases begins with an investigation of the textures of the phases by means of microscopic observations in polarized light on a heated stage. Changes in texture within a temperature range indicate the occurrence of phase transitions. However, the generation of typical textures is not always possible. Sometimes transitions between LC phases are accompanied by only slight changes. The textures that appear are often those of the phase which resulted from cooling (paramorphism). The features of the various textures are caused by the existence of different kinds of defects. To obtain an impression of the structure of the unit aggregates of a phase, the thermal data and microscopic textures must be combined with the X-ray findings. X-ray diffraction provides information concerning the arrangement and mode of packing of molecules and the types of order present in a mesophase. The X-ray diffraction pattern of nonoriented samples (powder pattern) can be divided into inner rings at small angles, and outer rings at large angles. The inner rings are indicative of longer layer spacings while the outer rings correspond to shorter preferred

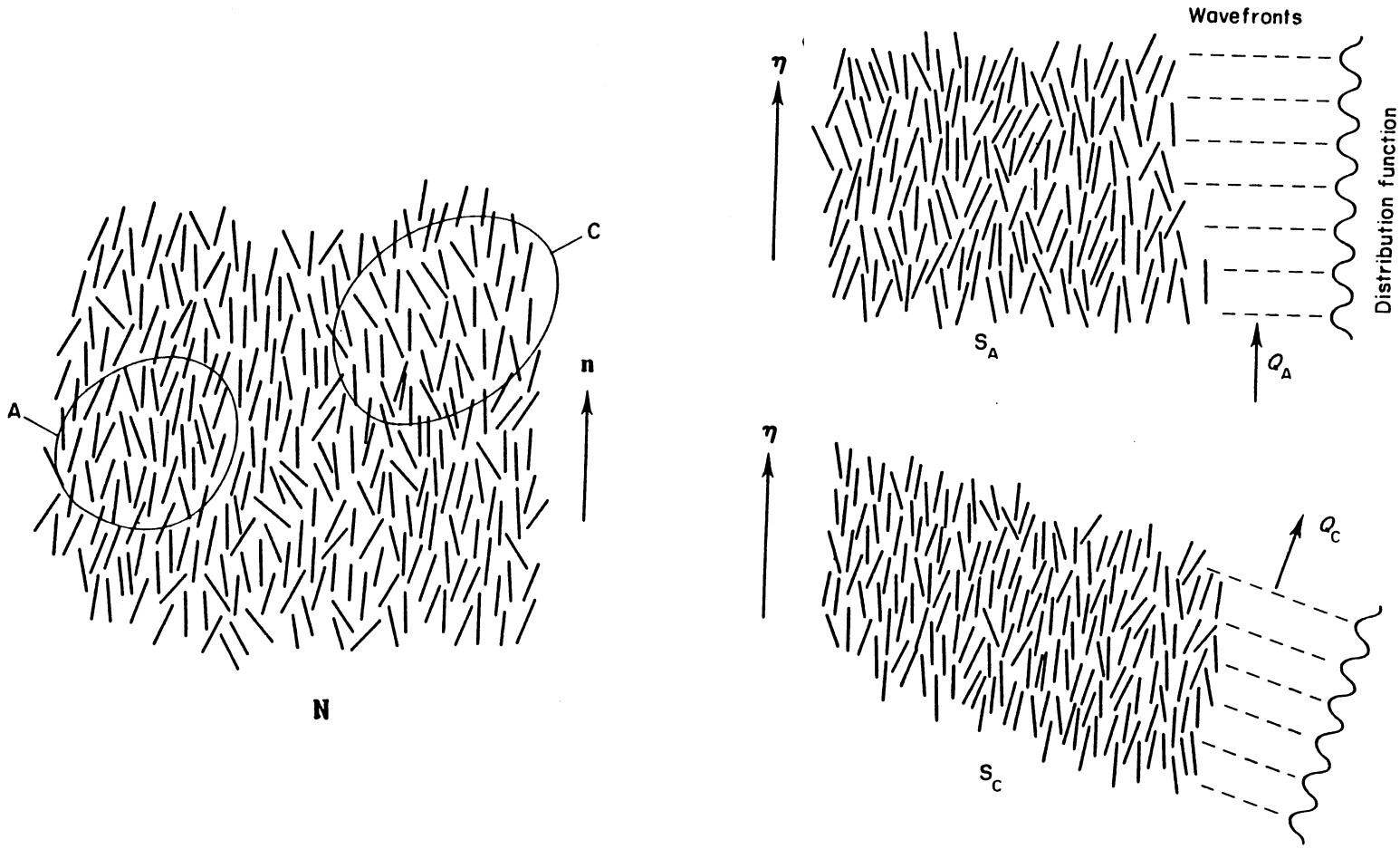

Figure 1. Schematic representation of nematic (N), smectic A (S_A) and smectic C (S_C) structures. Regions A and C in the nematic drawing represent local fluctuations of S_A- and S_C- type structural correlations. (Taken from Leadbetter, ref. 11).

spacings occurring in the lateral packing arrangement of the molecules. The spacings are calculated using Bragg's equation.

$$n\lambda = 2d \sin\theta$$

where n is an integer number and in normal usage is considered to be one, λ is the wavelength of the radiation in use, d is the distance between spacings, and θ is the angle of incidence or diffraction. The appearance of a broad halo or a sharp ring furnishes a qualitative indication of the degree of order. This method gives the principal reticular spacings but no information about the spatial orientation of these planes. Reliable characterization of molecular arrays by X-ray diffraction is possible only in oriented samples. The X-ray patterns of nematics and smectics differ mainly in their characteristics at small angles. Nematic patterns present a diffuse ring corresponding to distances equal to the molecular length, which indicates that there is no order in the direction of the molecular long axes. In contrast, X-ray patterns obtained from smectics present one or several sharp rings (usually two orders are observed) which are indicative of a periodic lamellar structure, corresponding to the smectic layers.

The spontaneous, anisotropic orientation of low molecular weight mesogenic molecules in the LC state inspired some interest in introducing these LC properties into macromolecules. This brought out a new aspect in polymer science, that is, the realization of LC polymers. The combination of the polymer-specific characteristics of mechanical strength and processability with the anisotropic, physical characteristics of the LC state promises interesting and novel materials. A general introduction to LC polymers will be presented and the types of thermotropic LC polymers will be pointed out. The discussion will concentrate on LC polymers containing rod-like mesogenic groups in the side chains of macromolecules.

The definition of the LC state of low molar mass LCs and LC polymers does not differ. The positional and orientational long range order for low molar mass LCs is related to the single molecules, whereas the order for polymers can be related either to the entire macromolecule or to the monomer unit of the macromolecule, depending on the chemical constitution of the LC polymers. LC polymers have wider mesophase temperature ranges and often more ordered LC phases than low molar mass LCs. In contrast to low molar mass LCs, which usually crystallize on cooling, noncrystallizable polymers harden to anisotropic glasses upon cooling from a LC phase. The LC structure characteristic of the mesophase is then preserved in a glassy state. As in low molar mass LCs, the LC properties can be examined by differential scanning calorimetry, polarizing microscopy, X-ray diffraction and other techniques. However, the high viscosity and the broad phase transition temperature ranges of the LC polymers make the investigation difficult due to slow change in their supramolecular structures.

L. Onsager (1949)[12] and P. Flory (1956)[13] adapted conventional lattice methods to describe a theory of non-melting, rigid, rod-shaped polymers. They predicted that a solution of hard, asymmetric polymers should separate into two phases, an ordered mesophase and an isotropic phase, above a threshold concentration. In the case of rod-like polymers, the ratio of the length of the longitudinal molecular axis to the length of the transverse axis of the macromolecules was found to govern the concentration at which phase separation occurs. This was experimentally confirmed in 1956 for a polypeptide which formed a stable, rod-shaped helical conformation in solution.[14] In the 1960s, researchers at Du Pont discovered that certain aromatic polyamides such as poly(p-phenylene terephthalamide) exhibited anisotropic properties in concentrated solution. As a result, the well-known ultra-high-modulus Kevlar aramid fiber which forms an LC phase only in solution was developed.[15]

The first reported observations of thermotropic LC behavior in polymers were made in the mid-1970s by A. Roviello and A. Sirigu[16] and by W. Jackson and H.

Kuhfuss[17]. The former study dealt with the preparation and characterization of poly-alkanoates from p,p'-dihydroxy-α,α'-dimethyl benzalazine and diacyl chlorides while the materials described in the latter study were aromatic-aliphatic copolyesters prepared by the reaction of *p*-acetoxybenzoic acid and poly(ethylene terephthalate). Since then there has been considerable research on polymers of this type which are called main chain liquid crystal polymers (MCLCPs).

The preparation of MCLCPs can be realized by linking together suitable mesogenic monomers.[18] The units are linked together through suitable functional groups, A and B, located at the ends of the mesogenic monomer. The monomers usually undergo a condensation reaction to form the polymer.

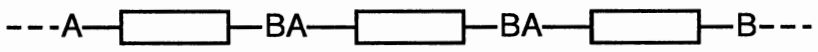

The linkages between B and A and the mesogen cores (▭) may be direct, giving a rigid type of backbone or of a flexible nature, e.g., an alkylene chain, giving a polymer backbone with alternating rigid (mesogenic) and flexible segments.

The basic structures in MCLCPs are benzene rings interlinked at para positions:

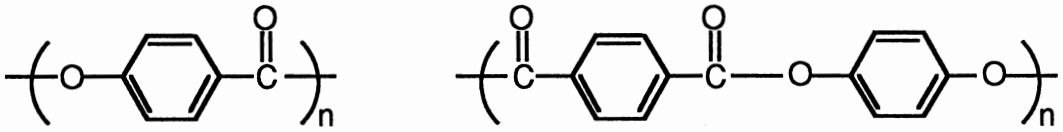

These rod-like polymers are insoluble and do not fuse without the occurrence of decomposition. Hence, it is necessary to lower the melting point to a melt processable range without destroying LC formation. There are three possible ways of modifying the rigid, rod-shaped basic structure.[19,20] First, the linearity of the macromolecule can be reduced by a less symmetric comonomer unit or a voluminous aromatic side group. Second, the rigid mesogenic groups are attached via a flexible spacer, e.g., alkyl or alkoxy

chain. With increasing length of the flexible chain between the mesogenic groups, not only is the melting point of the polymer lowered, but the mesogenic groups have an increasing tendency to order in a layer-like manner. Finally, linear macromolecules are substituted laterally with mesogenic groups via a flexible chain. These groups behave as chemically-bound solvent molecules and thereby reduce the polymer-polymer interactions and thus the melting point.

A great many aromatic polyesters and copolyester which show thermotropic LC behavior have been synthesized because they can be prepared by the traditional methods of condensation polymerization.[21] Although, other MCLCPs such as polyazomethines[22], polyesteramides[23], polyamides[24], and polyethers[25,28] have also been prepared. Recently, MCLC polyhydrocarbons have been synthesized for the first time.[27]

Prior to 1978, numerous investigations concerning the synthesis of polymers with low molar mass LC compounds attached directly to their backbones were reported, although these materials failed to exhibit LC behavior. Direct linkage, except in a few cases, gives only glasses with an anisotropy of structure that is lost at the glass transition. Coupled with steric interactions between the side groups, the tendency toward a statistical distribution of chain conformations hinders the ordered arrangement of the mesogenic groups and LC formation is suppressed.

In 1977, Shibaev and Plate[28] proposed that for the formation of an LC structure, a certain mobility of the side groups is required, which, in spite of the presence of the main chain, permits attainment of a definite order in the arrangement of the mesogenic side chains. In order to overcome steric hindrance to packing of the side chains, it is necessary to remove the mesogenic side groups some distance away from the main chain. To prove their proposal, thermotropic polymers containing cholesterol were synthesized and characterized.

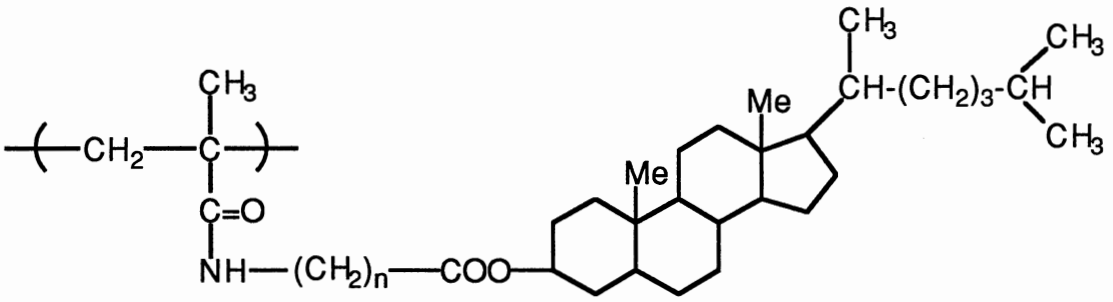

Table I.[a] Transition Temperatures of Cholesterol Containing Polymers[b]

n	T_g, °C	T_f, °C	$T_{a\text{-}i}$, °C
2	185 decomp.	-	-
5	130	200	220
6	130	190	215
8	130	180	200
10	125	150	185
11	120	135	180

[a]Ref. 28. [b]T_g = glass temperature, T_f = flow temperature, $T_{a\text{-}i}$ = temperature of transition from anisotropic to isotropic melt.

At temperatures below $T_{a\text{-}i}$, the polymers (where $n \geq 5$) were in the flow state, in the form of a mobile, viscous, anisotropic liquid. The flow caused movement of the birefringent regions, similar to the behavior of low molar mass LCs. Thus, the authors were the first to bring about and observe formation of an LC phase in cholesterol containing polymers in the high elastic and viscous flow states. They noted that the temperature interval covering the appearance of segmental mobility combined with optical anisotropy is dependent on the length of the methylene "bridge" joining the cholesterol group to the main chain.

Finkelmann and his coworkers[29] in 1978 introduced their model considerations for the realization of SCLCPs. They postulated that in the liquid state, the motions of the polymer main chain have to be decoupled from those of the anisotropically oriented

mesogenic side chains. The decoupling is then possible if flexible spacer groups are inserted between the main chain and the rigid mesogenic side chains.

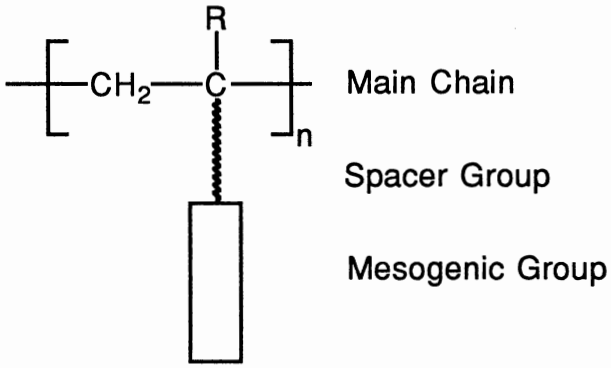

On the basis of this model, they expected that in spite of the statistical conformation of the main chain, an anisotropic orientation of the mesogenic side chain is possible. Furthermore, the main chain imposes little or no restriction on the orientation of the mesogenic side chains. To prove their model considerations, they synthesized SC polymers using suitable monomers of benzoic acid phenyl esters.

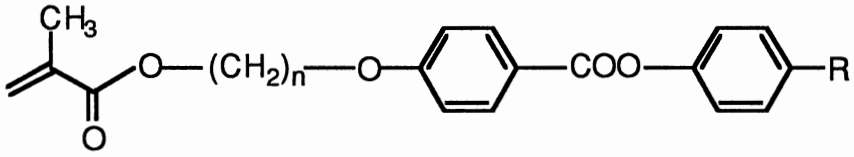

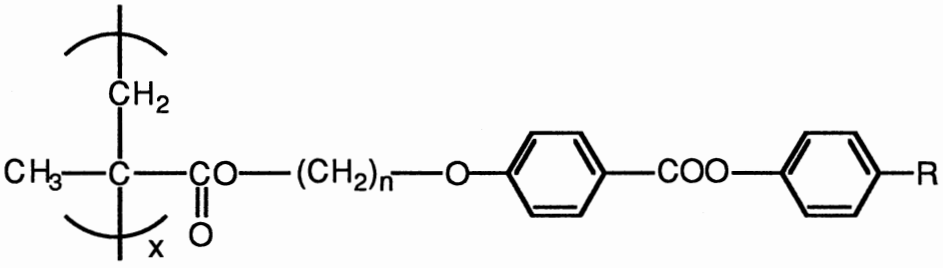

Table II shows that the SC polymers exhibit enantiotropic nematic or smectic phases depending on the substituent, thereby confirming their model considerations. The

decoupling of the side groups by using a flexible spacer allows the main chain motion to occur without disturbance of the anisotropic arrangement of the side chains. The polymer then may exhibit LC properties.

Table II.[a] Structures and Properties of Spacer Carrying Liquid Crystalline Monomers and Polymers

n	R	Phase transition[b] (°C) Monomer	Polymer
2	OCH_3	C 69 I	g 101[c] N 121 I
2	OC_3H_7	C 67 I	g 120[d] S 129 I
2	CN	C 84 I	amorphous
2	OC_6H_{13}	C 59 I	g 100[d] S 140 I
2	C_6H_4-OCH_3	C 108 N 211 I	[e] N 177 I
3	C_6H_5	C 105 I	[e] S 170 N 187 I
3	C_6H_4-OC_2H_5	C 123 N 202 I	g 120[c] S 300 I
6	OCH_3	C 47 I	g 95[c] N 105 I
6	OC_6H_{13}	C 47 N 53 I	g 60[c] S 115 I
6	C_6H_5	C 64 S 68 N 92 I	g 130[d] S 164 N 184 I

[a]Ref. 29. [b]C = crystal, N = nematic, S = smectic, I = isotropic liquid, g = glass transition. [c]Glass transition was determined by DSC measurement. [d]Glass transition was determined as softening points with the polarizing microscope. [e] not determined.

Further investigation by the same group of researchers used polymers with biphenyl moieties as mesogenic group.[30]

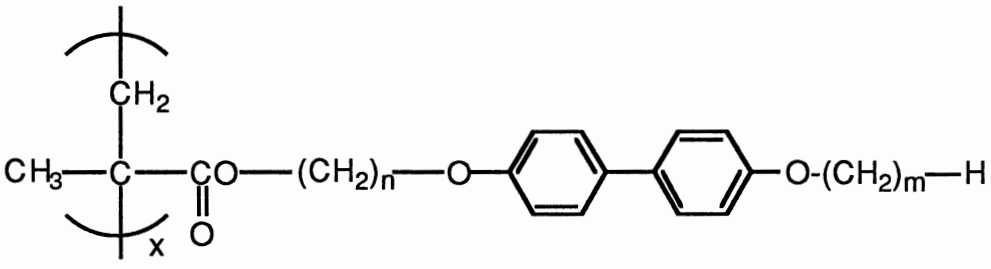

With the exception of the p'-unsubstituted biphenyl derivative, all polymers exhibit the postulated thermotropic LC phases. If the biphenyl group is substituted with a short spacer (n = 2) and the short substituent (m = 1), a nematic polymer phase is observed, whereas the polymers with n = 6 and m > 1 showed smectic phases. The results are consistent with the behavior of low molar mass LC biphenyl derivatives. Therefore, they were able to verify the validity of the model considerations that LC polymer phases can be routinely realized analogous to conventional LCs.

Following the introduction of the spacer model of SCLCPs, numerous SCLCPs have been synthesized using a variety of different polymer backbones[31,32] and a large number of known mesogenic molecules[7] as side chain components. Typical spacer groups consist between 3 and 12 methylene units. However, oligooxyethylene[33] or oligosiloxane[34] units may be used to enhance the degree of decoupling through a more flexible spacer.

SCLCPs can be prepared by three different types of polymerization as shown in Figure 2.[35] The most common method is to introduce into a mesogenic molecule a reactive group capable of undergoing addition polymerization.[36] In most cases, the polymerizable group is a methacrylate or an acrylate, which forms a flexible backbone. This type of SCLCPs have been the most widely synthesized by free radical polymerization in solution with common initiators such as azobisisobutyronitrile (AIBN). Anionic[37,38], group transfer[39] and cationic[40,41] polymerizations have been used to obtain different tacticities, molecular weights and polydispersities and to vary the nature of the polymer backbone.

The second possibility is to introduce into the low molecular weight mesogen a reactive group capable of undergoing a polycondenzation reaction. In this way, polymers containing heteroatoms in the backbone can be synthesized. Polycondensation reactions have been successfully applied to the preparation of SCLC polyesters[42] with flexible, semiflexible and rigid backbones.

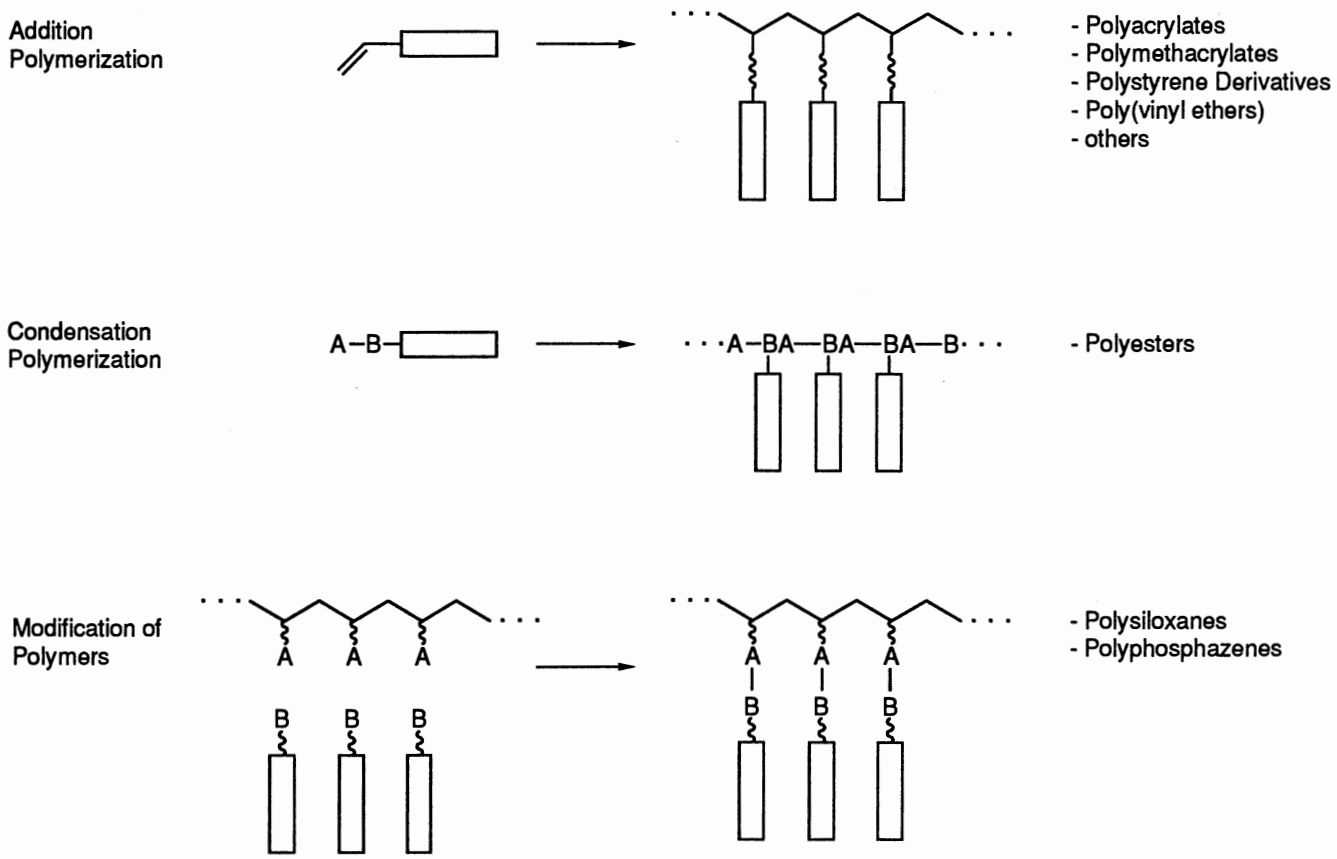

Figure 2. Different methods of preparation of side chain liquid crystalline polymers.

The third synthesis route starts with reactive polymers. They can be modified to mesogenic side-chain polymers by using suitable reactive mesogenic monomers.[43] SCLC polysiloxanes are usually prepared by an addition process, commencing with a preformed polymer backbone which contains reactive functional groups (Si-H) to which the mesogenic groups are appended. In this case, a quantitative addition reaction can be easily detected by the disappearance of the Si-H vibrational absorption. This type of reaction is carried out in the presence of an appropriate platinum catalyst, e.g. $H_2PtCl_6 \cdot 6H_2O$ in isopropyl alcohol[44-46] (Speier's catalyst), or divinyltetramethyldisiloxane platinum[47], or dicyclopentadienylplatinum (II) chloride[48].

The replacement of the hydrocarbon polymer main chain by a polysiloxane main chain, which is characterized by high flexibility of the chain segments, is expected to produce polymers with glass transitions at low temperatures. Finkelmann and Rehage[49] prepared SCLC polysiloxanes with benzoic acid 4-substituted phenyl esters in the side chains.

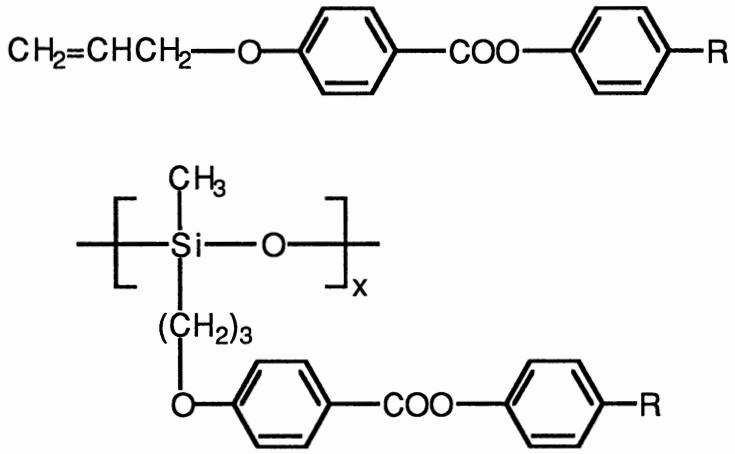

In Table III, the phase transitions for the purified polysiloxanes are summarized. This is the first case that LC homopolymers are obtained , which exhibit LC phase at room temperature. A nematic polymer exists if the benzoic acid phenyl ester group is substituted with a methoxy group, whereas smectic phases exist if a nitrile or hexyloxy group is the

substituent. According to these results, the type of the LC phase of the polysiloxanes is determined by the substituents of the mesogenic moiety. This is in accordance with results obtained for SCLC polymethacrylates.

Table III.[a] Phase Transitions of Monomers and Their Corresponding Polysiloxanes

R	Phase transition temperatures[b] (°C) Monomers	Polysiloxanes
OCH_3	C 89 I	g 15 N 61 I
OC_6H_{13}	C 61 N 77 I	g 15 S 112 I
CN	C 103 I	g 20 S 61 I

[a]Ref. 49. [b]C = crystalline, N = nematic, I = isotropic liquid, g = glass transition, S = smectic.

The glass transition temperatures were not lowered to a great extent, as expected from the glass transition temperature of pure poly(dimethylsiloxane) (T_g = -127 °C). For an effective lowering of T_g, the interactions of the mesogenic side groups have to be weakened. One possible way is to dilute the mesogenic groups along the main chain with non-mesogenic segments. This was realized by the preparation of side chain copolysiloxanes.[50]

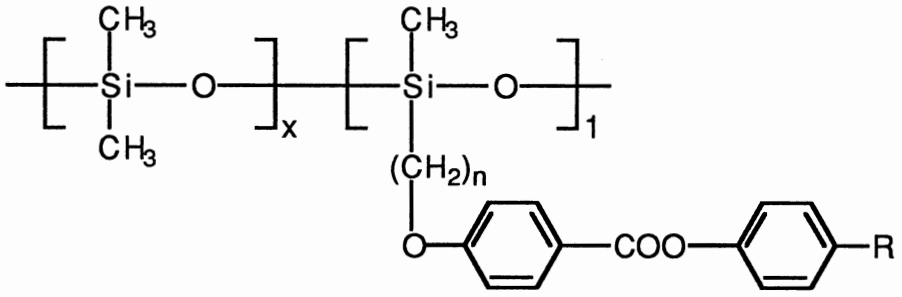

where x = 3, 5, 10 ; n = 3, 5, 11

R = OCH_3, CN

Insertion of a short dimethylsiloxane segment (x = 3) into the main chain between the mesogenic group resulted in a decrease of T_g (range from -22 to -45 °C). However, only polymers with longer spacer chains (n = 5 or 11) exhibited LC phases (smectic). With further reduction of the contents of mesogenic groups in the polymer (x = 5 or 10), T_g is lowered continuously towards the value of pure poly(dimethylsiloxane). Reported glass transition temperatures of the copolysiloxanes ranges from -46 to -53 °C for x = 5 and -112 to -119 °C for x = 10. From the results, the authors found that short spacer (n = 5) do not contribute very much to the stability of the LC phase, and the phase disappears at a dilution of x = 10. With long alkyl spacer (e.g., n = 11), the range of liquid crystallinity is not influenced by the dilution of the mesogenic groups in the main chain.

In a recent study, Percec and Tomazos[51] reported the synthesis and characterization of polymethacrylates and polyacrylates containing mesogenic groups based on 4-hydroxy-4'-methoxy-α-methylstilbene and the corresponding polysiloxanes. The authors observed that all of their polymethacrylates exhibit enantiotropic liquid crystalline mesophases. The isotropization transition temperature decreases with the decrease of the flexible spacer length from n =11 to n = 6 and then increases again. The isotropization enthalpy increases with the increase in the spacer length. The polymethacrylate containing only two methylenic units in the spacer displays only a nematic mesophase. Polymers containing intermediate spacer length display both smectic and nematic mesophases, while the polymethacrylate with n = 11 displays only a smectic mesophase. The polymethacrylate with n =11 is the only one to exhibit side-chain crystallization. This side-chain crystallization is strongly kinetically controlled and can be best observed during the first heating scan. An increase in the degree of polymerization gives rise to a decrease in the rate of crystallization. Crystallization is depressed so much that it does not appear at temperatures above T_g when the polymer is scanned on both heating and cooling at 20 °C/min. Attainment of equilibrium, which would lead to a

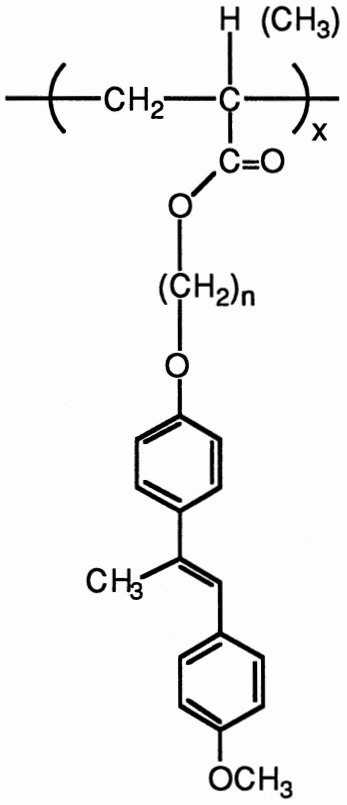

n = 2, 3, 6, 8, 11

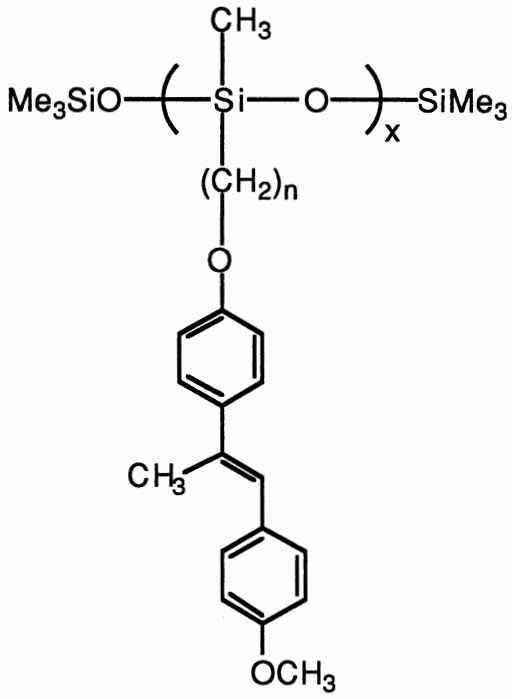

n = 3, 6, 8, 11

crystalline polymer, would require careful annealing and involve an extended period of time. The polyacrylates behave similarly to the polymethacrylates with the exception that all undergo side-chain crystallization. For long spacers, this crystallization is observable on any DSC scan. However, for shorter spacers, it can be observed mostly on the first heating scan or upon annealing. All of the polysiloxanes undergo side-chain crystallization, and their isotropization transition temperatures are higher than those of the corresponding polymethacrylates or polyacrylates. When making the latter comparison, one has to be aware of the fact that the flexible spacer of polysiloxanes contain only the methylenic units while the flexible spacer in polymethacrylates and polyacrylates contains the methylenic units plus an oxygen and a carbonyl group. Therefore, the flexible spacer of the polysiloxanes is in fact shorter than the one of the polymethacrylates or

polyacrylates. The type of mesophase displayed by polysiloxanes is determined, as in the case of other backbones, only by the length of the spacer. However, the ease of side-chain crystallization can transform the highest temperature mesomorphic phase from enantiotropic (mesophase observed, as reversible, both on heating and on cooling) into monotropic (mesophase which can be observed only on cooling). This is the case of the polysiloxanes containing eight and six methylenic units within their spacer.

The general conclusion derived from this study is that the spacer length dictates the nature of the mesophase exhibited by a certain polymer. However, the nature of the polymer backbone dictates the thermal stability of the mesophase and the ease of side-chain crystallization. Flexible backbones tend to give rise to higher thermal stability of the mesophase and simultaneously increase ease of side-chain crystallization. This last effect may lead to the transformation of enantiotropic mesophases into monotropic mesophases.

The systematic investigations of SCLCPs show that a long spacer group allows the side chain to be relatively independent of the backbone, and hence show that the same regularities with respect to LC properties for SCLCPs and their low molar mass analogues. This is particular true for the order parameters and the behavior in the electric field. A short spacer length results in less organizational freedom and hence the phase transitions of the mesogenic side chain are influenced more by the backbone.

The orientational long-range order of the molecules in the nematic phase is described by the order parameter S

$$S = \frac{1}{2}\langle 3\cos^2\theta - 1\rangle$$

The angle θ denotes the mean deviation of molecular axis with respect to the symmetry axis of the orientational distribution function of the molecular axes. This description can also be applied to SCLCPs, if the polymer main chain is neglected and only the mesogenic

side groups are considered. This order parameter directly reflects the anisotropy of the polymers. The order parameter of LCPs can be determined from the data on IR- and UV-dichroism of added dye, isomorphic (same mesophase) to liquid crystal, from X-ray analysis, from NMR or ESR measurements.[31,32] The values of S for some LCPs are given in Table IV.[32]

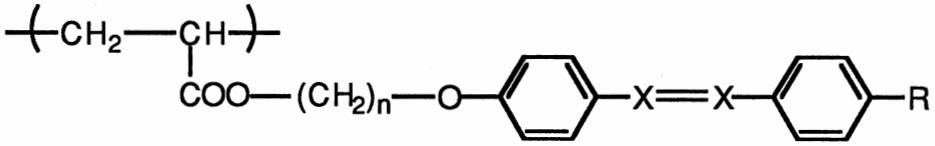

Table IV.[a] Values of Order Parameter S for Some LCPs Determined by Different Methods.

X=X	R	n	mesophase[b]	S	method of determination
-	CN	5	N	0.45	NMR
CH=N	CN	6	N	0.50	guest-host dichroism
COO	OCH3	2	N	0.65	ESR
COO	OCH3	6	S	0.92	ESR
COO	OCH3	6	S	0.85	NMR
CH=N	CN	11	S	0.91	X-ray analysis

[a]Ref. 32. [b]N = nematic, S = smectic.

Polymers exhibit lower values of S at a fixed reduced temperature (T_m/T_c, where T_m is the measuring temperature and T_c is the clearing temperature) compared with that of the corresponding monomers, while the slope of the temperature dependence curve is very similar. S remains constant at temperatures below T_g. This is one of the most important properties of SCLCPs. The LC order freezes in at Tg and remains unchanged in the glassy state of the system. Therefore, anisotropic glasses having anisotropic physical properties are obtained.

LC molecules can possess permanent or induced dipole moments both along and across the long axis of the molecule. The molecule will orient so the larger of the two dipoles lies along the electric field. If the dipole moment is along the long axis of the molecule, then an electric field causes the molecular long axis of the liquid crystal to lie parallel to the field. However, if the dipole moment lies across the long axis, then the presence of electric field causes the molecular long axis to orient perpendicular to the field. The strength of the electric field necessary to orient the director (direction of preferred orientation of molecular long axis) of a liquid crystal is relatively low since the director of a liquid crystal is usually free to orient in any direction. The freedom of liquid crystal molecules to change orientation while maintaining some orientational order among the molecules produces this delicate response to electric fields. Polymers with a flexible spacer of sufficient length (> 4 -CH_2-) have similar responses to electric field.[31] The field strength for the reorientation is directly related to the anisotropy of the dielectric constants of the mesogenic monomer unit of the polymer.

The combination of electric field-induced orientation in the LC state and the durable storage of the alignment in the glassy state of polymers offers new prospects for applications. The preparation and characterization SCLCPs with polarized mesogenic moieties which can be processed in the form of optically clear films and exhibit nonlinear optical properties have generated tremendous interest.

Langmuir-Blodgett Films

The Langmuir-Blodgett (LB) technique[52-54] is a useful tool for systematic preparation of well-defined thin films of side chain polymers. An insoluble monolayer is usually characterized by its pressure (Π) - area (A) curve (or isotherm). The isotherm shows the relationship between the observed surface pressure (related to the average interaction between neighboring molecules) and the area occupied on the liquid surface by the molecules of the film. Most LB films are made by spreading surface active molecules

(surfactants) at an air/water interface (Figure 3), and measurements can be performed by a film balance while varying the film area by compression between barriers.

The apparatus (shown in Figure 3) generally used consists of a surface pressure measuring device mounted on a trough equipped with suitable barriers. Most often, a rectangular trough is used, with the pressure detector near one end. The two fundamentally different film balances are the Wilhelmy type (shown in Figure 3) and the Langmuir type. In the Wilhelmy method, an absolute measurement is made by determining the force due to surface tension on a plate or other object suspended so that it is partially immersed in the liquid, and this is compared with a similar absolute measurement on a clean surface. The Langmuir method, on the other hand, utilizes a

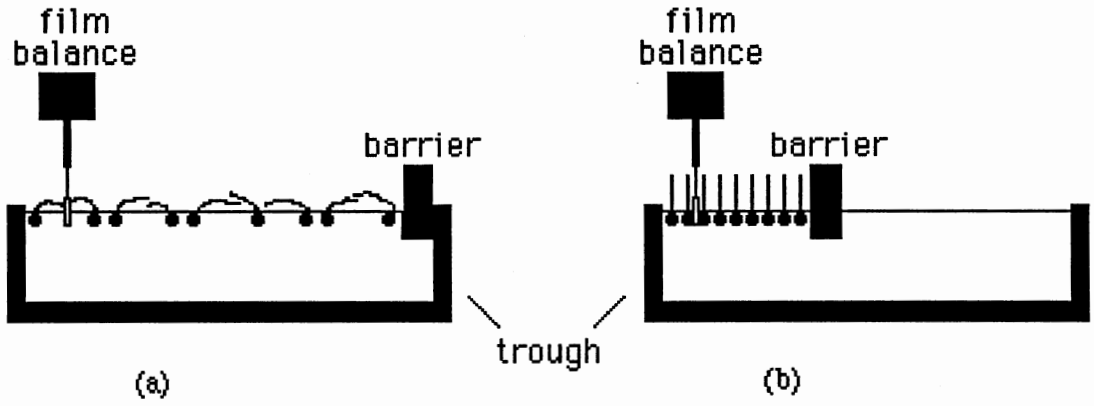

Figure 3. Monolayer of a surfactant on a water surface: (a) the monolayer before compression and (b) the monolayer after compression.

direct differential measurement. A clean portion of the liquid surface is separated from the monolayer-covered area by a partition and the force acting on this is measured. The partition usually consists of a movable float connected to a conventional balance with which the magnitude of the force is determined.

The molecules in monolayers could exist in three different states, more or less analogous to three dimensional liquids, solids or gases. Various monolayer states

represent different degrees of molecular freedom or order, resulting from the intermolecular forces in the film and the subphase. In the case of low molar mass substances, the three film states are generally referred to as condensed (solid) films, expanded films (liquid) and gaseous films.

A generalized Π-A isotherm for a film of simple molecules may be represented as in Figure 4.[54] The gaseous state of monolayers is conceptually the simplest and has followed a two-dimensional analysis corresponding to that of the ordinary three-dimensional matter. The molecules in such films are floating about in the surface layer far apart so that they exert relatively little force on one another. Such monolayers are characterized experimentally by a surface pressure which approaches zero asymptotically, as the area available to the film is increased, and by a constant surface potential, showing no variation from place to place in the film. The surface viscosity of gaseous monolayers is also very low. In principle, any monolayer-forming substance will exist as a gaseous film if the molecules are sufficiently widely separated. It is suggested that the average conformation of a flexible chain molecule in the gaseous monolayer is more nearly parallel to the water surface than vertically extended.

At the opposite extreme from the gaseous monolayers are the condensed films in which the molecules are arranged in nearly their closest possible packing. This type of film, which can be thought of as much like a two-dimensional crystal, is common, easily studied and is usually thought of as the typical monolayer. In this film, the molecules stand nearly upright with their terminal polar groups in the water and their long chains closely packed. The Π-A plots are nearly straight and very steep, indicating low compressibility in the condensed monolayers. This reflects the presence of strong chain-chain interactions which hold the molecules in their closest-packed arrangement, with little dependence on surface pressure. Condensed films are highly incompressible and often exhibit high surface viscosity.

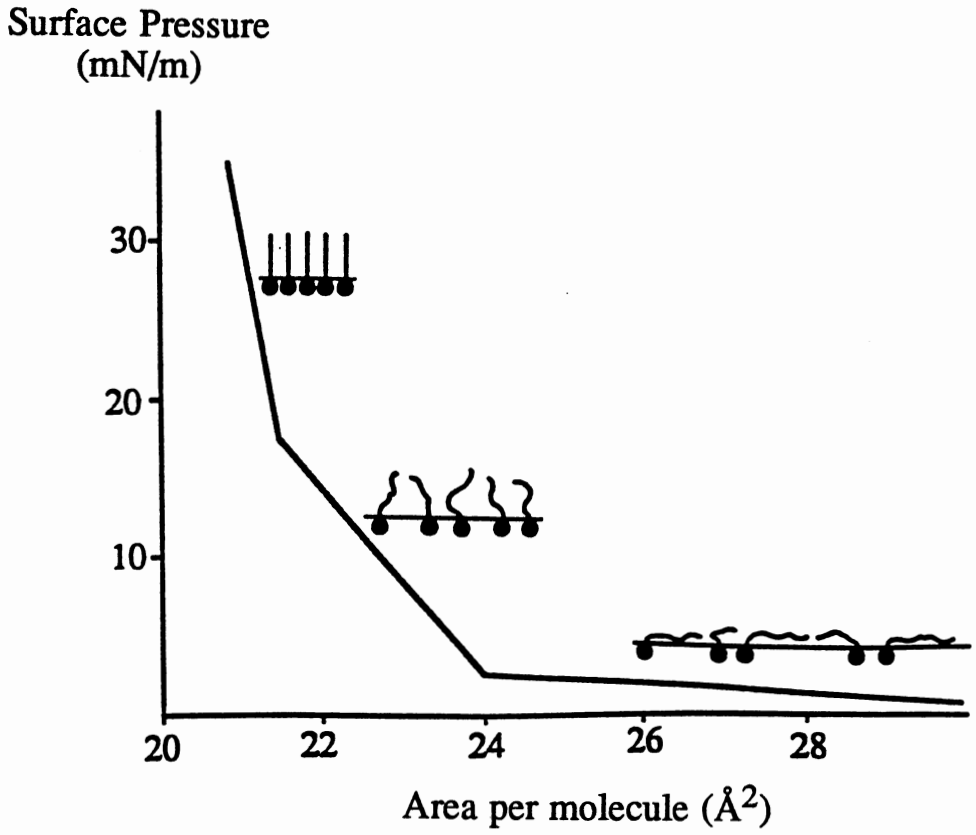

Figure 4. A general Π-A isotherm of a monolayer of a simple molecule. (Taken from Ulman, ref. 54).

Intermediate in molecular area between gaseous and condensed films of simple molecules are the expanded monolayers. The Π-A diagrams of these films show considerable curvature, although they approach the $\Pi = 0$ axis at a fairly steep angle, rather than asymptotically as in the case of gaseous monolayers. The films have low surface pressure with little tendency for the film-forming molecules to become widely separated on the surface. The molecular area is typically two or three times as large as the molecular cross section. The surface potential does not show fluctuation, indicating that the films are homogeneous and the surface viscosity is low. Apparently, in expanded films, the conformation is in some way intermediate between the condensed films and the gaseous films. The hydrophobic portions of the molecules in an expanded film are in random, rather than regular, orientation, only the polar functional groups being constrained to be in contact with the subphase.

In general, the Π-A diagrams for well-spread polymer films on aqueous subphases are rather featureless by comparison with the variety of curves which have been obtained for monolayers of smaller molecules. The curves are smooth, without marked discontinuities, and show no evidence of phase transformation in the stable monolayer region. The surface pressure is low at large specific areas, but increases more or less rapidly when the film is compressed to the point where the macromolecules themselves occupy most of the available surface. The polymer films can be divided into condensed and expanded classes. Monolayers of the expanded type are fluid and exhibit a gradual rise in surface pressure on compression and a well-defined and complete collapse. Condensed polymer films are best identified by their high viscosity or rigidity, together with a much steeper Π-A isotherm. Qualitative interpretation of the Π-A characteristics of polymer monolayers have generally been proposed in terms of compressibility or rearrangement of the polymer chains on compression in the film.

The classical materials of monolayer studies are surfactants, which have a molecular structure composed of a large nonpolar or hydrophobic portion, the hydrocarbon chain, and at one end a polar or hydrophilic functional group, such as -COOH or -OH. The polar groups tend to confer water solubility, while the hydrophobic part prevents it. The balance between them determines whether a molecule will form an insoluble monolayer. Interactions between and within the monolayer-forming molecules, both in the film and in bulk phases are important. Better packings of the molecules enhance intermolecular dispersion forces between the chains in adjacent molecules, thus stabilizing the molecules in the film. However, if intermolecular attractions are too strong, it will be difficult to produce a monolayer even when a suitable polar group is present. Another factor which must be considered is volatility; the substance must not evaporate too rapidly for measurements to be made.

In the case of high polymeric substances, somewhat different criteria apply. Formation of stable monolayers of macromolecules depends on sufficient attraction for the subphase surface to overcome bulk cohesion. A high degree of insolubility is not required. It is only necessary that the individual monomer units have a finite free energy of adsorption from the bulk solution to the surface for a monolayer to be stable. It is also possible to spread monolayers of insoluble polymers. In this case, the criteria of spreadability are similar to those for simple, nonpolymeric materials.

Many monolayers can be compressed to pressures considerably higher than their equilibrium spreading pressures. Eventually, however, it is found impossible to increase the surface pressure further, and the area of the film decreases if the pressure is maintained constant, or the pressure falls if the film is held at constant area. This condition is referred to as the collapse point of the monolayer under the given experimental conditions. When collapse occurs, molecules are pushed up from the surface, maintaining the integrity of the two-dimensional array, in a ridge two molecules thick. The ridge finally breaks off and

lies on the remaining monolayer film as a collapsed film. The collapse pressure is the pressure at which molecules are first pushed out of the monolayer.

In the case of large polymeric molecules, over-compression of a stable monolayer may lead to rearrangements of the polymer chains. It seems reasonable to expect that on compression some molecules or parts of molecules could be displaced from the surface. The LB method is a mechanical means of forming an oriented monomolecular thin film which can be subsequently deposited on solid plate (or substrate). A schematic diagram illustrating a common form of LB deposition is shown in Figure 5.[55] In this example, the substrate is hydrophilic and the first monolayer is transferred as the substrate is raised through the subphase. The substrate may be placed in the subphase before the monolayer is spread, or may be lowered into the subphase through the compressed monolayer. Since the spread molecules are usually amphiphilic in nature, there is often a strong tendency for the Y-type deposition to form multilayers having head-to-head and tail-to-tail stacking and a center of symmetry. In the example shown in Figure 5, a multilayer structure containing only an odd number of layers can be produced. However, if the solid substrate is hydrophobic, a monolayer will be deposited as it is first lowered into the subphase, thus a Y-type film containing an even number of monolayers can be fabricated.

Noncentrosymmetric films are difficult to obtain by classical LB techniques (X-type or Z-type deposition, where transfer occurs only on the downstroke or upstroke, respectively) and frequently much synthetic effort is necessary to find ways to induce this behavior. Schematic diagrams and the expected molecular arrangement for the two types of layers are shown in Figure 6.[55]

Nonlinear Optical Materials

If electric, magnetic or electromagnetic (optical) fields act on materials, the building blocks of the materials (atoms, ions, electrons) will experience forces and be displaced through translation or rotation by those forces. When an electromagnetic field interacts

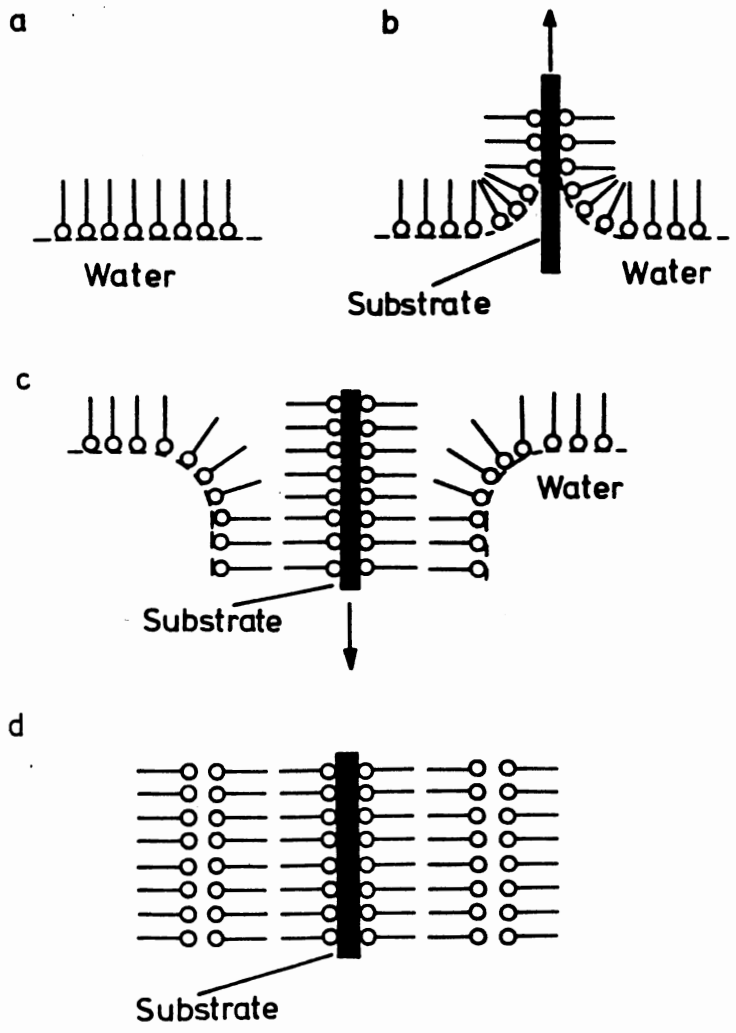

Figure 5. Deposition of multilayers onto a hydrophilic substrate by the LB technique with Y-type structure: (a) compressed monolayer, (b) first upstroke, (c) subsequent downstroke, (d) head-to-head and tail-to-tail configuration (Y-type). (Taken from Petty and Barlow, ref. 55).

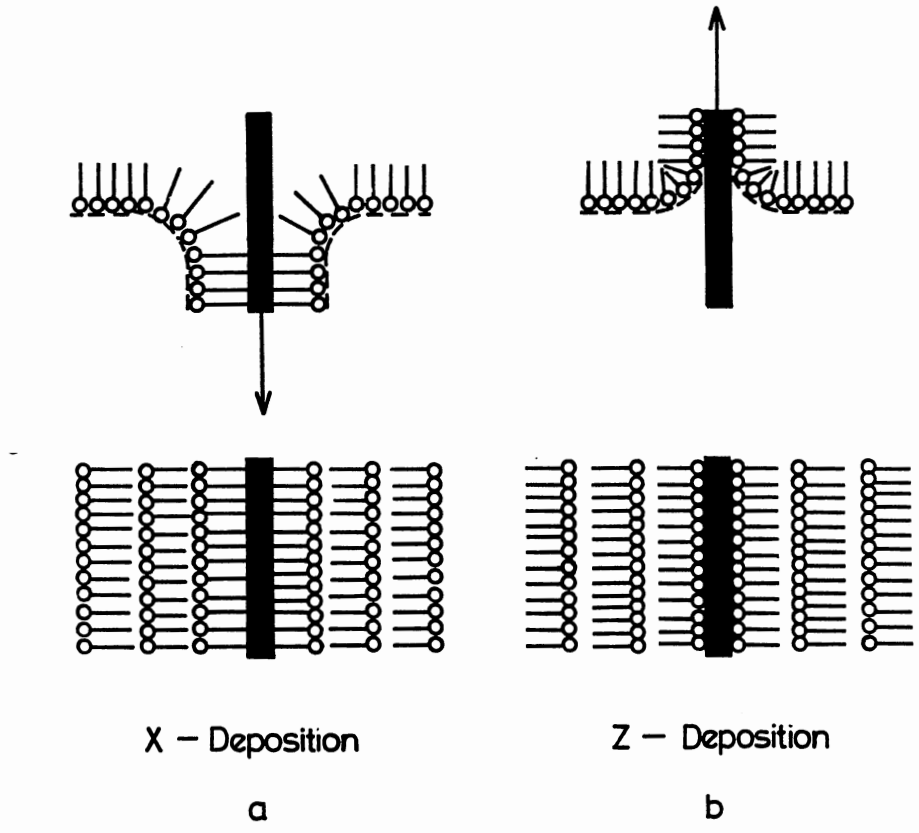

Figure 6. X-type (a) and Z-type (b) deposition with their respective structures. (Taken from Petty and Barlow, ref. 55).

with a molecule or a medium consisting of many molecules, the oscillating field polarizes the materials. The positive and negative charges in the constituent molecules move in opposite directions, so that an oscillating electric dipole is induced in the materials. The induced dipole per unit volume is called polarization, P. For small applied field strengths, the polarization is linearly proportional to the strength of the electromagnetic field and the optical response is linear.

Nonlinear optical (NLO) materials exhibit nonlinear polarizations when subjected to the above mentioned fields. The induced polarization depends on higher orders of the field strength. Generally, only applied field strengths as strong as those of lasers lead to observation of such nonlinearities. Nonlinear electric polarizations in materials can give rise to a number of optically nonlinear phenomena such as frequency doubling, frequency tripling and four-wave mixing.

The fundamental concepts[56] of nonlinear optics and their relationships to chemical structures will be briefly summarized. In the dipolar approximation, the polarization p_i induced in an atom or molecule by an external field E can be written as

$$p_i = \alpha_{ij} \cdot E_j + \beta_{ijk} \cdot\cdot E_j E_k + \gamma_{ijkl} \cdots E_j E_k E_l + \ldots$$

where the subscripts i, j, k, and l refer to the molecular coordinate system, E_j, E_k, and E_l denote components of the applied field, and the tensor quantities α, β, and γ, are often referred to as the polarizability, hyperpolarizability, and second hyperpolarizability, respectively. The analogous expression for macroscopic or bulk media is

$$P_I = \chi^{(1)}_{IJ} \cdot E_J + \chi^{(2)}_{IJK} \cdot\cdot E_J E_K + \chi^{(3)}_{IJKL} \cdots E_J E_K E_L + \ldots$$

where the coefficients $\chi^{(1)}$, $\chi^{(2)}$, and $\chi^{(3)}$, are similar in meaning to their microscopic counterparts. The even tensors β and $\chi^{(2)}$ are zero in centrosymmetric media. This

restriction plays an important role in the development of second order NLO materials. The odd order tensors have no symmetry restriction. NLO effects are called resonant when the material absorbs the incident laser light and nonresonant when the light is not absorbed.

The history of NLO effects in organic materials goes back about two decades. Urea was one of the early organic systems to demonstrate the potential of achieving large optical nonlinearities in organic crystals. To obtain a $\chi^{(2)}$ response, an organic crystal must be noncentrosymmetric, or a noncrystalline organic material must be polarized into a noncentrosymmetric order by an electric field. Various theoretical approaches to calculate microscopic second order nonlinearities, β, have been used. One such calculation is a perturbation approach using a two-level model. Within the concept of perturbation expansion, a two-level model predicts large β for molecular structures having large transition dipole moments and large differences between the permanent dipole moments of the ground and excited states. Therefore, materials composed of molecules having conjugated π-electron donor and acceptor substituents at the ends of a delocalized π-electron system have significant second order $\chi^{(2)}$ properties.[57] The low lying charge-transfer states in the donor-acceptor substituted structures such as 4-dimethylamino-4'-nitrostilbene (DANS)

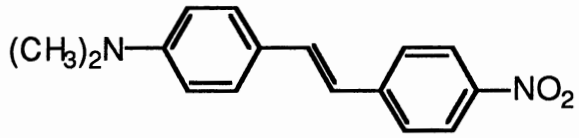

provide such a large change in the dipole moment upon excitation, and hence DANS is expected to exhibit large β. Second order polarizabilities are known for a large number of organic structures and can be estimated for new structures from ground state dipole moments, solvatochromic UV-visible spectral data, and the lowest energy electronic transition frequency relative to the incident laser frequency. A common technique for

measuring the value of β is electric field induced second harmonic generation (EFISH). In this method, a dc electric field is applied across a solution of the compound to be tested, a laser beam is passed through the solution, and the intensity of the generated second harmonic light is measured. Note that EFISH does not measure the individual tensor components β_{ijk}, but measures β_x which is the sum of certain β_{ijk} components.

$$\beta_x = \beta_{xxx} + 1/3\ (\beta_{xyy} + 2\beta_{yxy} + \beta_{xzz} + 2\beta_{zxz})$$

The most commonly studied second order NLO property of solid materials is second harmonic generation (SHG) or frequency doubling, a practical technique in laser technology. The SHG nonlinear coefficient d is often reported and is related to $\chi^{(2)}$ by

$$\chi^{(2)}_{IJK} = 2d_{IJK}$$

The nonlinear coefficient d_{33} (d_{333} or d_{zzz}) does not contribute to phase-matched SHG and is the largest nonlinear coefficient in poled polymers. Using a 1064 nm pulsed Nd-YAG laser, the absolute second harmonic conversion efficiency is determined by measuring the ratio of the 532 ($I^{2\omega}$) and the 1064 (I^{ω}) nm signal intensities and applying corrections for the relative responses of the monochromator and photomultiplier tube to the two wavelengths.

In recent years, it has been found that organic molecules or polymers show larger second order NLO responses than the conventional inorganic materials. Poled polymers are one of the most promising approaches to the development of new materials for second order NLO applications. This approach could lead to early utilization of polymers in devices. Processing of polymers is relatively easy and inexpensive compared with conventional substrates derived from materials such as $LiNbO_3$, and the choice of NLO-active materials is large and not limited to compound crystallizing noncentrosymmetrically.

Disadvantages of this approach include the need for the relatively complex and difficult electric field poling process, the broad orientational distribution function, the dilution of the nonlinear chromophore in the matrix, and concerns about long-term stability of the metastable poled state. Much of the efforts are focused on the preparation of materials with significantly high concentration of NLO-active species, readily attainable orientational order, and best thermal stability.

Several researchers reported[58-61] the observation of SHG in glassy polymers such as polystyrene (PS) and poly(methyl methacrylate) (PMMA) doped with optically characterized second harmonic generating dyes such as 4-dimethylamino-4'-nitrostilbene (DANS), 2-methyl-4-nitroaniline (MNA) and 4-[ethyl(2-hydroxyethyl)-amino]-4'-nitroazobenzene (disperse red - DR). The second harmonic coefficient, d_{33}, of spin coated films (~4 μm) of the azo dye in PMMA, measured at a fundamental wavelength of 1580 nm, was $6.0 \pm 1.3 \times 10^{-9}$ esu.[58] This value is approximately five times that of potassium dihydrogen phosphate (KDP). Films of PS and PMMA with DANS showed d_{33} value of about 2×10^{-9} esu (fundamental wavelength of 1064 nm).[59,60] This can be compared to the d_{33} values of 0.55×10^{-9} esu for KDP or 7.1×10^{-9} esu for lithium niobate, current inorganic industry standards.

The optical quality of the spin-coated films onto indium tin oxide (ITO) coated glass are extremely important. The films must be defect and pinhole free, so that the sample does not break down under the high applied electric field and the amount of the scattering due to surface ripples or other defects must be minimal for proper measurement. The films were coated with a thin layer of gold to improve contact with the poling apparatus electrodes. The electric field is applied perpendicular to the film. The ITO substrate served as the bottom electrode, and a second piece of ITO glass served as the top electrode. The NLO-chromophores in the polymer matrix were aligned using a strong dc electric field (from 0.3 to 0.5 MV/cm) at temperatures near or above (about 5 °C) T_g, and the aligned materials have been hardened into the glassy state with the field still on.

Corona poling has also been used to align doped glassy polymers. Hampsch and coworkers[62,63] used corona discharge generated by a sharp tungsten needle biased with up to 5000 V and placed 0.6 cm above and normal to the polymer film spin-coated onto soda-lime glass. The corona current was between 1-3 μA. Typical film thicknesses ranged from 1.8 to 2.5 μm. Gas (air, He or N_2) continually flowed across the film throughout the entire measurement. The intense electric field generated at the needle tip during the corona process accelerates nearby free electrons to velocities high enough to impact-ionize gas molecules in their path, creating ions with the same polarity as the needle. Ion current carriers form a space charge between the electrodes, since the ambient gases are good insulators. The reactive ions accelerate toward the grounded film and accumulate near the surface, generating a very high electric field across the film. This field orients the dopants thereby inducing second order nonlinear activity. For in situ measurement of the SHG intensity, poling was performed at ambient temperature in a controlled atmosphere of air or nitrogen using a Plexiglas box with quartz windows. Significant SHG signal can be observed even when poling doped PMMA films at room temperature. This was not observed when using contact poling. Corona poling is a powerful method for creating a large potential across the film that efficiently orients the NLO dopants noncentrosymetrically in the polymer matrix. The major advantage of this method is the fact that only the bare, low conductivity polymer surface is charged. Impurities, defects, and pinholes, therefore, cause only relatively small local currents and do not result in short circuiting the whole sample. As a consequence, very high breakdown field strengths are readily achieved.

Films of such dyes in glassy polymers give strong SHG signals but lack temporal stability in the glassy state at room temperature. The loss in SHG intensity with time is due to the rotation of the dye molecules in areas of locally high free volume and/or mobility and relaxation of the polymer chains after poling, thus giving the dopant

molecules greater freedom to rotate. Moreover, the low solubility of the dye in the polymer limits the number density of the active NLO component.

The use of polyimide as host in a guest-host thin film was demonstrated to exhibit electro-optic response stable at temperature up to 150 °C.[64] The polyimide which is imidized at 250 °C with a dc poling field between coplanar electrodes aligns the nonlinear optical guest. The imidization process involves the generation of water, and so the electric current across the electrodes was monitored to check for dielectric breakdown.

Better temporal stability is obtained in dyes dissolved in a LCP instead of a non mesogenic amorphous polymer such as PMMA.[65] This is because the stable state of a LCP is anisotropic, and the long molecular axis of the dye aligns with director of the liquid crystal.

Another alternative is to connect the active NLO chromophore to the polymer backbone. These materials have greater effectiveness because they have a higher molar concentration of the NLO species (for larger nonlinear susceptibility), decreased mobility (for greater temporal stability) and greater overall film homogeneity (for less scattering loss).[66-68] NLO polymers provide a number of advantages over low molar mass organic molecules, including lower dielectric constant, greater processing flexibility, and improved mechanical properties. Thin films from an amorphous polyacrylate that incorporated p-nitroaniline as side groups with one methylene spacer chain exhibited a very high second order nonlinear coefficient, $d_{33} = 31$ pm/V.[69] The films were poled by a corona discharge and the SHG intensities were simultaneously (*in situ*) measured. The d_{33} coefficient decreased approximately 40% after 5 days (from the time the poling field was turned off at temperature below T_g) and then stabilized. Methyl methacrylate copolymers with nonlinear optical 4-alkoxy-4'-alkylsulfone stilbene side chains[70], which are transparent down to 410 nm resulted in a reasonably high nonlinearity ($d_{33} \leq 9$ pm/V).[71] Thin-film samples were prepared by spin coating onto ITO covered glass substrate. A fairly stable, polar orientation has been obtained by means of electric field poling with a corona

discharge at temperatures which are about 20 K below the T_g's of these polymers. The side chain concentration was limited by the occurrence of semi-crystallinity, giving rise to large scattering losses.

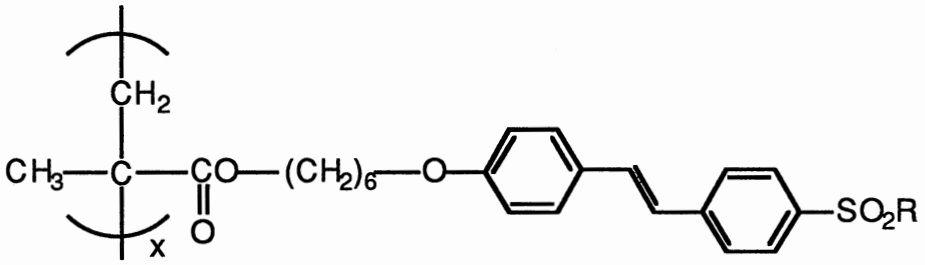

$R = CH_3$, C_6H_{13}

Incorporation of the dye into a highly cross-linked epoxy network can significantly enhance the temporal stability but does not prevent entirely decay of the SHG with time.[72,73] Eich and his coworkers[74] reported cross-linked polymers with NLO molecules covalently incorporated into a rigid network. The NLO moieties are cemented in their positions and cannot undergo local reorientational movements like doped or side group NLO polymers, where none or only one geometrical position of each NLO group is linked to the polymer backbone. In this method, a soluble prepolymer is first prepared that contains cross-linking sites attached to the NLO-active groups. Films of the prepolymer prepared by spin coating or from the melt, are heated (precured) to enable some chemical cross-linking and thus increase T_g to an optimum for poling. The precured polymer is then heated above its T_g and subjected to a high electric field to obtain the desired alignment of NLO moities. Subsequent chemical cross-linking (curing) under electric field continues to advance the Tg. Hence, the freezing-in of the noncentrosymmetric order is achieved.

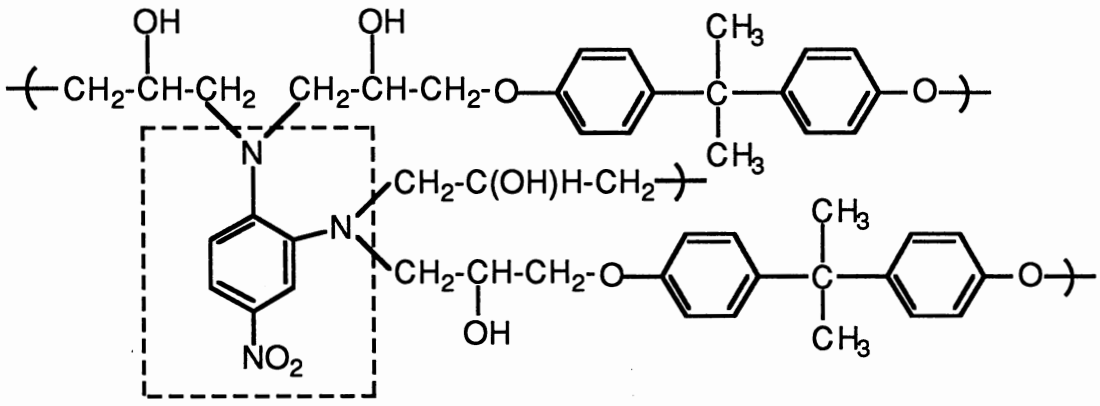

Films of high optical quality showed d_{33} = 13.5 and d_{31} = 3 pm/V for the corona poled, cured polymer, which remained completely stable after over 500 hours at ambient temperature. Furthermore, no tendency of decay in SHG signal even at 85 °C was observed.

Jungbauer and coworkers[75] reported forming a network polymer from two NLO-active monomers, bifunctional N,N-(diglycidyl)-4-nitroaniline and trifunctional N-(2-aminophenyl)-4-nitroaniline. In this case, every NLO moiety is connected to the network by a single covalent bond. After full cure under corona poling at 120 °C, the sample exhibited at ambient temperature d_{33} = 50 pm/V and d_{31} = 16 pm/V at 1064 nm fundamental wavelength. The nonlinear coefficients were stable even at 80 °C. The same group observed that films of an epoxy polymer containing 4-amino-4'-nitrotolane chromophores, which were poled by corona discharge, showed very large nonlinear coefficients of d_{33} = 89 pm/V, which is three times as large as that of lithium niobate (d_{33} = 30 pm/V), and d_{31} = 25 pm/V for incident light of 1060 nm wavelength.[76] The large d_{33} value can be accounted for by the long conjugated length and a large contribution from the resonance enhancement in the tolane moiety.

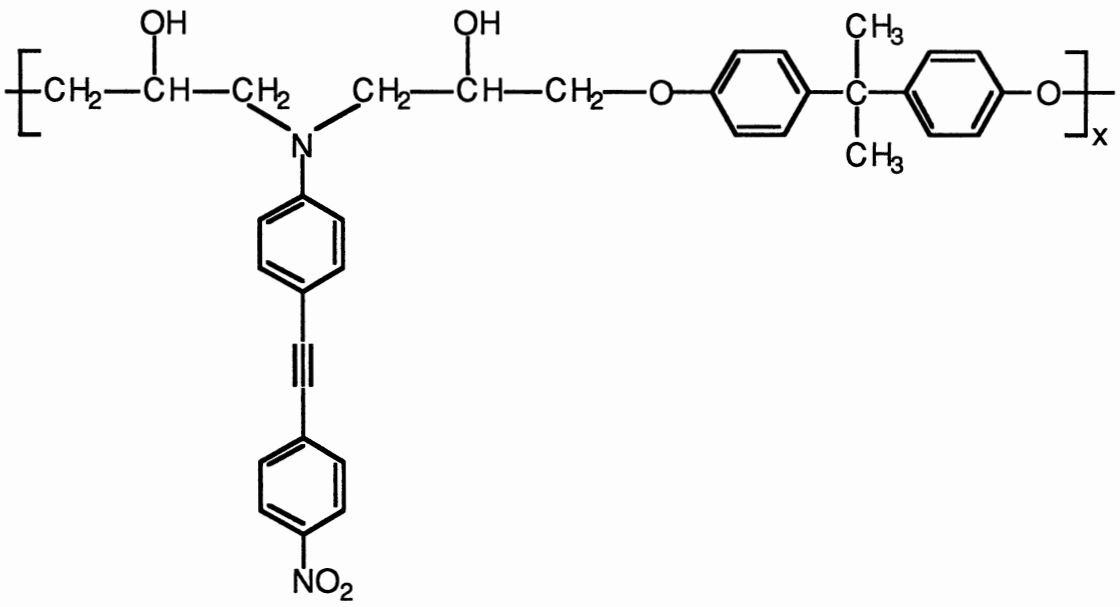

Another class of polymers was obtained by photo-crosslinking reactions between the photosensitive chromophores functionalized into NLO molecules and the same or related chromophores appended into a polymer, acting as the matrix.[77-79] New cross-linking materials with NLO moieties, where the nonlinear species has a large molecular hyperpolarizability (e.g., donor, acceptor derivatized azo, stilbene and azomethine dyes) were investigated.[77,78]

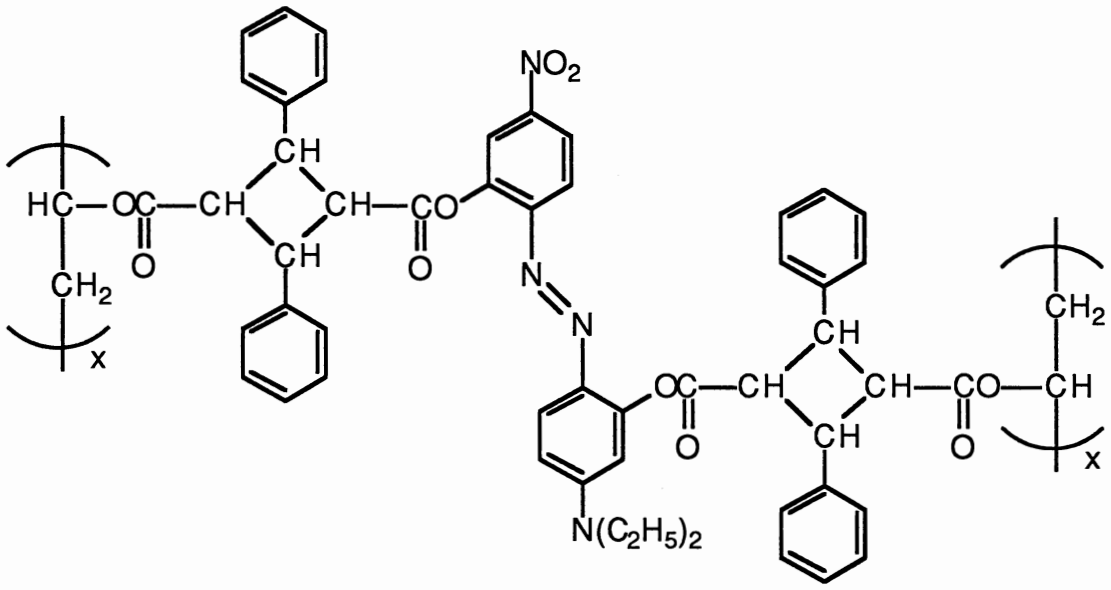

Noncentrosymmetric organization of NLO molecules in the polymer matrix was introduced by corona poling and the system was photo-crosslinked in the poled state, which yields material with excellent optical quality and stable, and large nonlinear coefficients. The second harmonic coefficient of the polymer film, d_{33}, was in the range of 15 to 30 pm/V. Orientation of the chromophore showed stability for over long period of time at temperatures ranging from 60 °C to 85 °C.

Temporal stability is also expected to improve when the NLO structure is the mesogen of a LCP. A LCP retains anisotropic structure indefinitely, whereas an amorphous polymer relaxes after electrical poling. The advantage of using LCPs is that these polymers can be ordered in the liquid crystalline phase at elevated temperature and this oriented mesophase may be cooled rapidly to below its glass transition temperature (T_g) to freeze in the mesophase order. For an ideal smectic LC, there is an ordering factor of about 0.9 (Table IV), giving an enhanced polar order and the possibility of increasing the macroscopic second order susceptibility by a factor of 5 over amorphous polymers poled at the same field strength. This is due to spontaneous alignment of the dipoles above T_g, giving natural axial order and hence greater ease of alignment.

SCLCPs are more promising than MCLCPs because they have thermotropic mesophases at lower temperatures (typically 25 - 200 °C) and their responses to applied electric and magnetic fields are faster. Low temperature mesophases allow rapid alignment of samples at temperatures where they are chemically stable, and films can be prepared without the need for solvent. SCLC copolymers containing dyes can be macroscopically oriented and the orientation can be locked in below T_g. Moreover, the order parameters of these SCLC copolymers are higher than monomeric dyes dissolved in LCP.[80,81]

A typical NLO side chain liquid crystalline polymer is illustrated below.

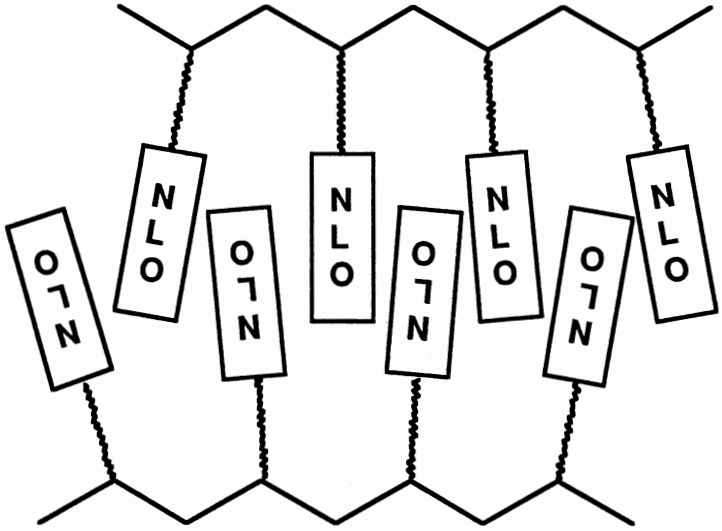

The structure consists of a mesogenic side chain which is also a NLO chromophore. The NLO side chains are usually conjugated stilbenes, or analogous diazo or azomethine systems with donor and acceptor groups at opposite ends of the conjugated system. The addition of a hydrocarbon chain produced a long rod-like anisotropic molecule with the desired LC properties. For SHG experiments, it is important that the LCPs possess polar side chains of positive dielectric anisotropy. Most of the SCLCPs that are known to form efficient SHG films have the donor substituent in the spacer chain and the acceptor at the end of the side chain.[82,83]

Leslie and his coworkers[84] investigated the first series of NLO side chain liquid crystalline polymers. The mesogen/NLO unit is 4-hydroxy-4'-nitrobiphenyl.

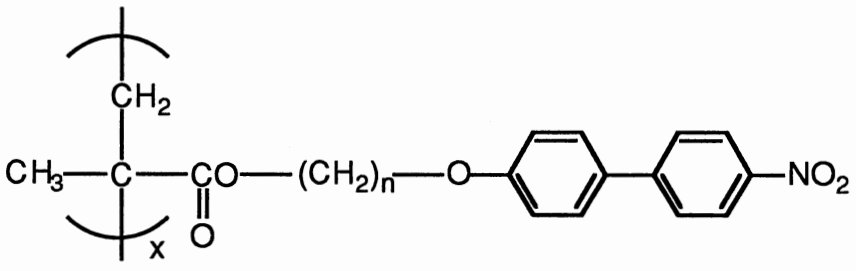

Table V.[a] NLO Side Chain Polymer Properties.

n	Phase[b]	T_g (°C)	T_i (°C)
2	I	-	-
3	N	85	100
5	N	45	72
6	N	40	64
8	N	35	75
11	S_A	20	95
12	S_A	10	80

[a]Ref. 84. [b]I = isotropic, N = nematic, S_A = smectic A, T_g = glass transition temperature, T_i = isotropization temperature.

Free-standing films were prepared by pressing the polymer melt between two conductive glass surfaces. Poling was done by applying an electrical field across the samples at elevated temperature. The authors reported that the polymer films showed SHG signals.

McCulloch and Bailey[85] studied a series of polymers based on the polystyrene backbone with different mesogenic/NLO side chains.

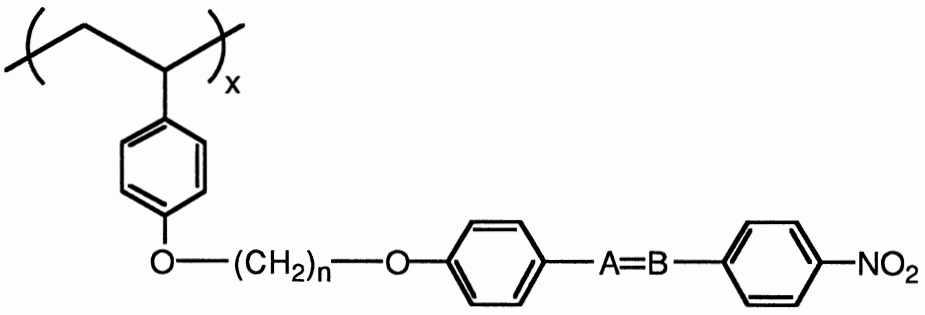

where n = 6, 8 or 10
A = CH or N
B = CH or N

The polystyrene was chosen due to its high optical transparency over a wide frequency range, its high dielectric strength and its relatively high T_g. Polystyrene has a much higher refractive index than polyacrylates and polysiloxanes. The polystyrene system also has good film-forming ability and is chemically stable. Relatively high T_gs were observed especially for the shorter spacer lengths (n = 6). As the spacer length increased, the relatively large enthalpy change at the isotropization temperature (T_i) indicated a smectic LC phase. An estimate of the magnitude of β was made using the solvatochromic shift technique. The values obtained were found to be dependent on the solvent system employed. Using the solvent shift from THF to cyclohexane, the following values for the 3 main polymer systems relative to p-nitroaniline were obtained.

Table VI.[a] β Values from Solvatochromic Method.

Compound	β (expt)
p-nitroaniline	10
stilbene (CH=CH)	28
diazo (N=N)	25
azomethine (CH=N)	16

[a]Ref. 85.

Preliminary electrical poling work was carried out. Partial alignment was achieved as confirmed by optical microscopy and SHG at 1064 nm, but considerable difficulty was encountered with dielectric breakdown, probably due to impurities in the backbone polymers.

A recent study by Pfeiffer and Haase[86] used LC polymethacrylates with a nitrostilbene mesogen in the side chain.

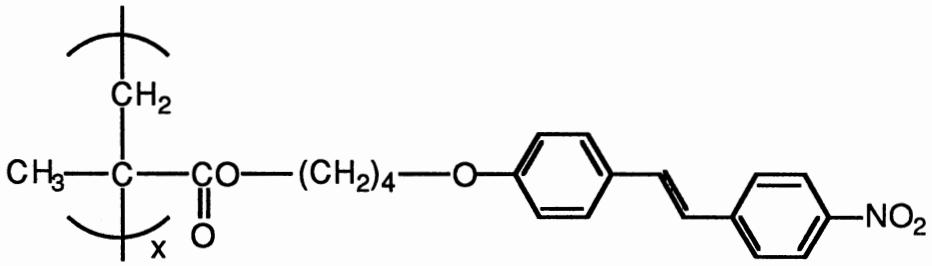

In order to achieve a LC material with high T_g and only a nematic phase, the spacer length should be small. The authors showed that the SCLC polymethacrylates can be easily aligned using strong magnetic fields. A superconducting magnet with a field strength of 7 T was used and a completely transparent film of 75 μm thickness was obtained. In the glassy state (above room temperature), no relaxation could be found in the frequency range under investigation. This means that once an orientation of the mesogens is achieved, this can be frozen in the glassy state.

An earlier experiment by our group reported SHG responses on films of a SCLC polyacrylates with stilbene mesogen in which the donor substituent (amino group) is at the end of the side chain and the acceptor (ester group) in the spacer chain.[87] Absolute SHG conversion efficiencies approached 10^{-7}, which are typical values for organic films.

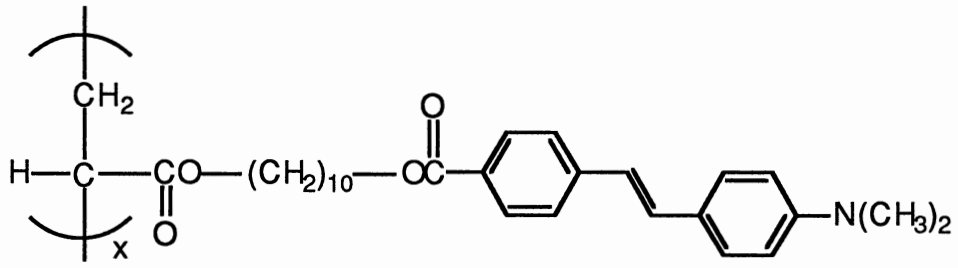

Acentric Langmuir-Blodgett (LB)[55,56] films represent a promising approach to high-efficiency SHG materials. This approach offers the advantage of being able to assemble a film layer by layer. Considerable effort has gone into the synthesis of

amphiphiles, characterization of mono- and multilayered films and measurement of their second NLO properties.

Aktsipetrov and his coworkers[88] in 1983 were the first to report on SHG from LB multilayers, using 4-octadecylamino-4'-nitroazobenzene as the amphiphile.

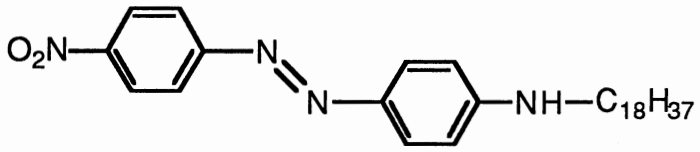

In this experiment, they measured SHG in reflection from the surface, thus learning about molecular orientation in two dimensions. The monolayer on the surface has a $\chi^{(2)}$ value of 2.8 x 10^{-8} esu . They also reported the preparation of Y- and Z-type LB films from this compound. For the centrosymmetric Y-type five-layer film, deposited onto SiO_2 hydrophilic surface, the measured $I^{2\omega}$ was an order of magnitude lower than that of the monolayer. However, for the Z-type five-layer film, deposited onto a hydrophobic surface, they found that $I^{2\omega}$ increased with the number of layers.

The amphiphilic properties of the molecule were improved by adding a carboxylate group.[89,90] Another important change was to shorten the alkyl chain from 18 to 12 carbons, thus increasing the surface energy of the monolayer.

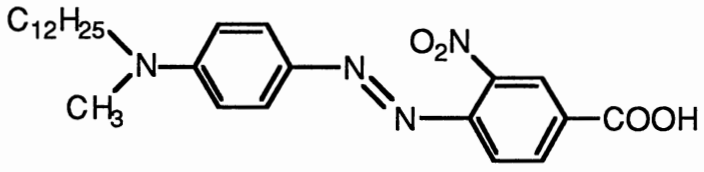

As a result, the energy difference between the head-group and tail-group surfaces decreased and the stability of Z -type film increased. Z-type films with and without Cd^{2+} in the subphase were obtained. Cd^{2+} often gives more stable monolayers of carboxylic acids on water. The SHG measurements for the Cd^{2+}-stabilized film at an incident angle

of 45° yielded a large signal (532 nm). A $\chi^{(2)}$ value of 6.7 x 10^{-6} esu was obtained for the film, the largest reported so far in the literature. This major enhancement is due both to the proximity of the second harmonic frequency (2ω = 532 nm) to the absorption maximum (λ_{max} = 504 nm without Cd^{2+} and 464 nm with Cd^{2+}) and to the large number of π-electrons in the molecule.

Multiple dippings of 4-[N-(4-carboxypentyl)-N-methylamino]-4'-nitrostilbene resulted in suspected Z-type deposition with the molecules oriented in a head-to-tail, head-to-tail fashion, where the carboxylic acid group is the head.[91]

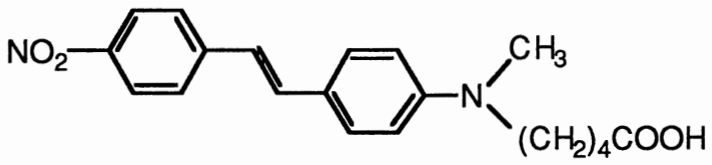

Deposition occurred on the withdrawal only and the quantity of monolayer transferred was equivalent to 60% substrate coverage for each dip. Dipping (20 times) gave a clearly visible red coating which for the hydrophilic microscope slide exhibited strong SHG with a 1064 nm Nd/YAG laser. The coated substrate still showed areas of similar strong SHG after 12 weeks when testing ceased.

Noncentrosymmetric multilayer structure of merocyanine amphiphiles were first reported by Daniel and Smith.[92] They introduced long-chain amines ($C_{18}H_{37}NH_2$) as the counter layer in their ABAB system. The monolayers were exposed to ammonia or methylamine to deprotonate the dyes. Girling and his coworkers[93] reported the first SHG measurements on merocyanine LB film. They alternated layers of the C_{22} derivative with layers of ω-tricosenoic acid as the intermediate layer and obtained β_z of 2.42 x 10^{-27} esu for the dye, which is resonance-enhanced at 2ω (533 nm).

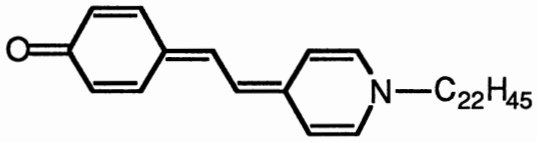

The chromophore that has received the most attention for fabrication of LB mono- and multilayers is that of the hemicyanine.[94,95] The first report on LB films from hemicyanine was given by Girling and his coworkers.[96] Both monolayers and ABAB multilayers with ω-tricosenoic were prepared and the tilt angle of the chromophore in the monolayer was estimated to be 37°, and a β_z value of 2.29 x 19^{-28} esu.

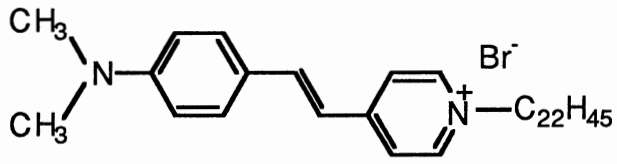

Ashwell prepared LB Y-type film structures of the C_{18} derivative hemicyanine interleaved with 4,4'-dioctadecyl-3,5,3',5'-tetramethyldipyrrylmethene hydrobromide.[97] This two-legged amphiphilic molecule was synthesized specifically as a compatible spacer, the principle being that the hemicyanine tail might penetrate and fasten the interleaving LB layers. Quadratic SHG enhancement has been obtained for 300 layer films.

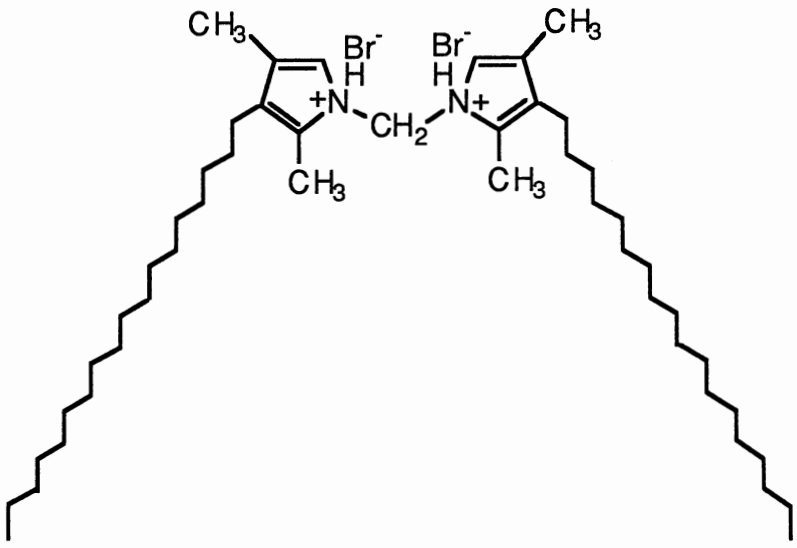

LB films of 2-docosylamino-5-nitropyridine have been introduced as noncentrosymmetric multilayers, exhibiting strong SHG.[98]

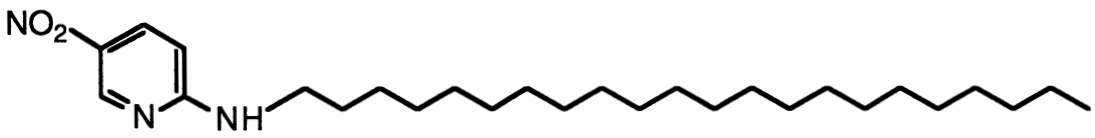

Films were found to display significant anisotropy with respect to the dipping direction. Preferential orientation of the chromophore was established by SHG measurements and by polarized UV-vis spectroscopy of monolayer and multilayer (40 layers) samples. At 20 mN/m, monolayers showed their maximum absorption at 387 nm. The polarized spectra demonstrated that the monolayer was isotropic. The optical densities for parallel and perpendicular absorption are identical within experimental error. In contrast, the polarized spectra of the 40 layered-film showed a ratio of optical densities parallel and perpendicular to the dipping direction to be 1.6. A tilt angle of the alkyl chains of 37° obtained from X-ray measurements is in good agreement with the calculated value of 36.5°, obtained from the area per molecule (32 $Å^2$) found for monolayers on the water surface. Well-ordered Y-type LB multilayers of the same compound were reported to exhibit second order NLO effects, although they have a Y-type, herringbone-like structure.[99]

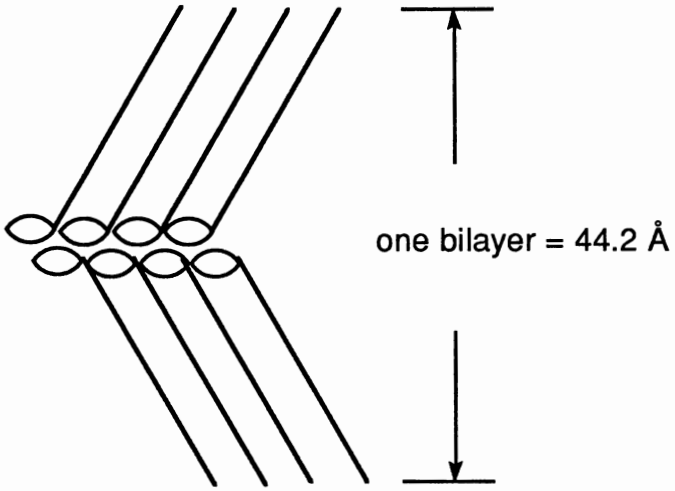

It is believed that this structure is the reason for the nonlinear optical properties of the LB films, which yielded d_{33} = 7.8 pm/V for λ =1064 nm and d_{33} = 2.0 for λ = 1318 nm. For these experiments, samples of different thickness (880, 1770 and 2210 Å) derived from X-ray measurements were used. The order within the layers is most likely caused by interlayer hydrogen bridging between the amino and the nitro groups of adjacent molecules.

The formation of LB films from low molar mass amphiphiles and their SHG responses have been studied.[55,56,100,101] However the use of polymeric amphiphiles either in the Y- or Z-type deposition is becoming attractive because of the thermal stability and possibly, amorphous nature of the films.

Carr and Goodwin[102] reported the first SHG signal from an LB film of a side chain copolysiloxane.

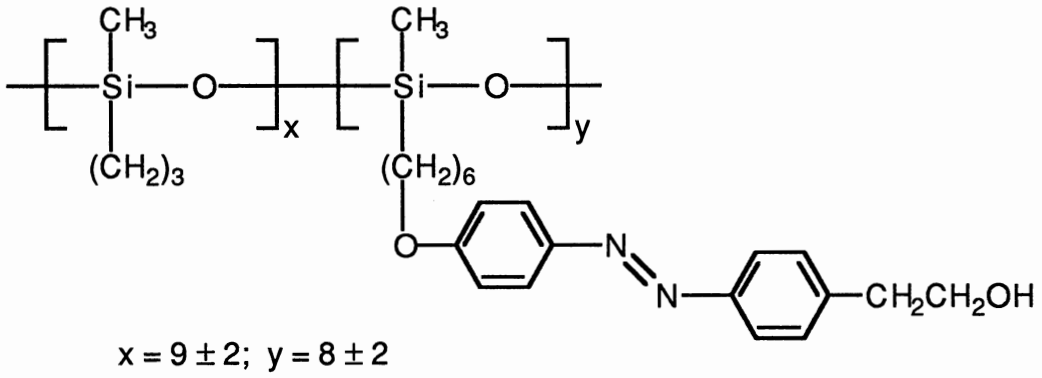

x = 9 ± 2; y = 8 ± 2

The interesting features in this system are the lack of a long alkyl chain and the fact that the hydrophilic head group (OH) is on the pendant chromophore, thus allowing for the polymer to serve as a hydrophobic blanket in the monolayer. A condensed phase is formed at Π = 20 mN/m and the average area occupied per chromophoric side group is approximately 38 $Å^2$ at Π = 30 mN/m. Furthermore, when the monolayers were maintained at this surface pressure, no significant change in the surface area was detected over a period of 64 hours, indicating no tendency for film rearrangement, collapse or

dissolution. Thus, the side chain polysiloxane forms exceptionally stable monolayers. A β_z value of 8.4 x 10^{-29} esu for the repeat unit was obtained.

Anderson and his coworkers[103] prepared two hydrophilic side chain copolyethers with hemicyanine as pendant groups extending toward the hydrophobic region.

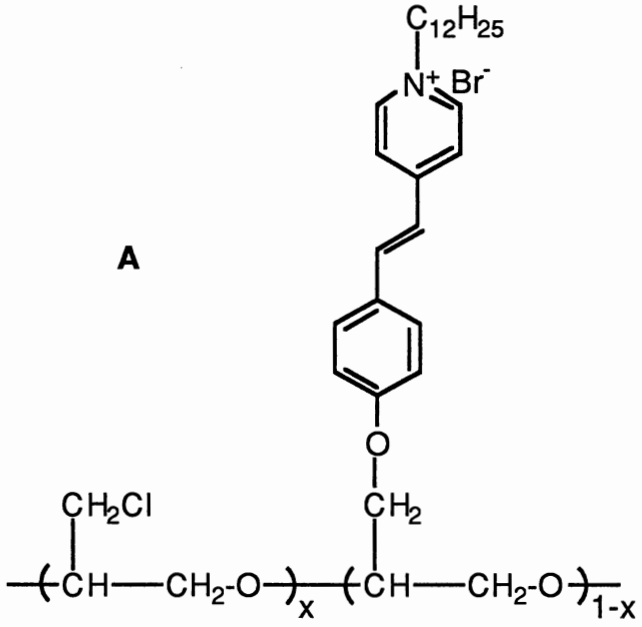

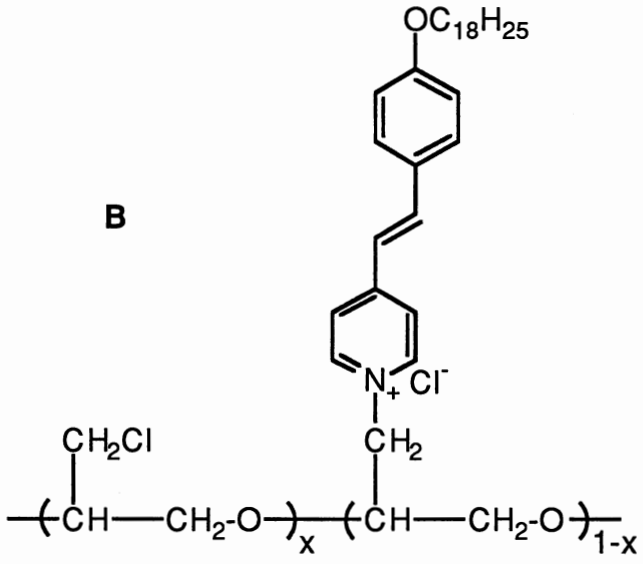

In polymer A, the alkyl chain is connected to the pyridine acceptor, while in polymer B, it is connected to the oxygen donor. The compression isotherms for the two polymers showed that at a surface pressure of 35 mN/m, the surface area per chromophore unit is 27 $Å^2$ for polymer A and 40 $Å^2$ for polymer B. These values are reasonable since A has 43 repeat units with 47% chromophore load, and B has 11 repeat units with 33% load. The area per molecule for the hemicyanine chromophore is approximately 30 $Å^2$ at 35 mN/m. The results suggested that the hydrophilic polyether repeat units that do not have a chromophore side chain may be looping down into the subphase and not occupying any space at the air-water interphase. This is the first true noncentrosymmetric, stable Y-type multilayer of a polymeric amphiphile, where the chromophores are with their dipole pointing in the same direction, i.e., they have additive effect. They prepared films up to eight monolayers (four AB bilayers). Second harmonic radiation (532 nm) was detected for the optically active bilayers which are interleaved with an optically inert material such as arachidic acid. The SHG response increased quadratically with respect to the number of AB bilayers. The ability to probe the orientation and concentration dependence of the harmonic intensity makes SHG a useful structural probe.

Monolayer film formation has been observed for a liquid crystalline copolymer containing a second order NLO side chain.[104] The isotherm is generally smooth and rather featureless and does not display any phase transitions in the stable monolayer region. The film was pictured as having an orientation on the subphase that would be governed by the polar groups of the side chains of the copolymer. The authors assumed that the polar groups were lying flat on the subphase surface while the hydrocarbon backbone protruded away from the surface as shown below. The isotherm showed the film beginning to condensed at about 67 $Å^2$ per monomer unit which is in excellent agreement with the value (67 $Å^2$) obtained from the calculations using standard bond lengths and thicknesses, thus confirming the orientational model. The films

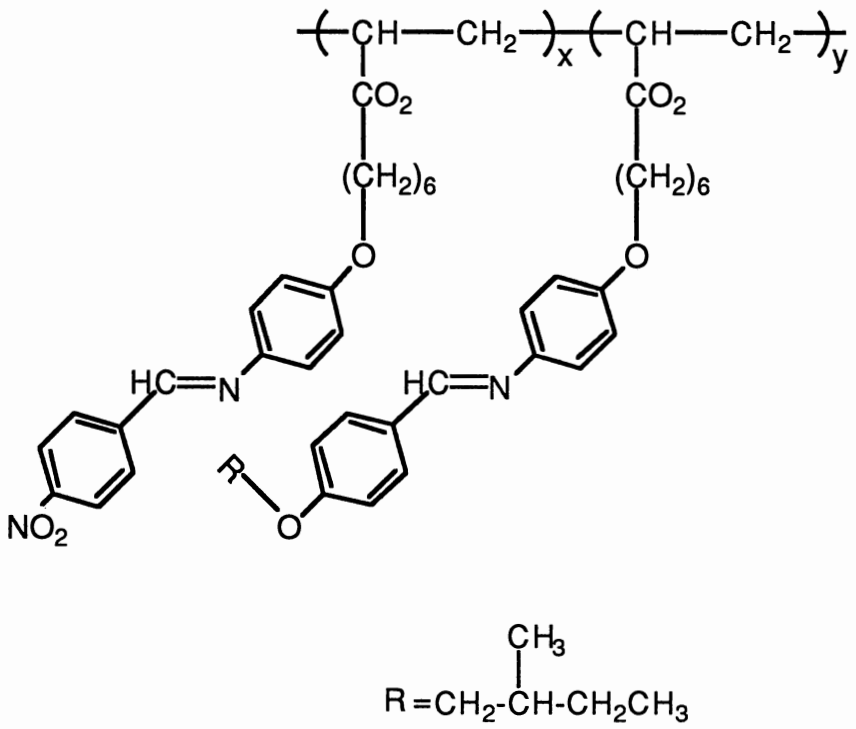

were successfully transferred via the horizontal dipping technique. Results from UV-visible and attenuated total reflection-IR (ATR-IR) spectra have shown that the films transferred onto substrates exhibit the inherent orientational properties of LB films. Due to the high viscosity of polymers, using horizontal lifting to transfer monolayers may be the approach to allow mass production of high quality NLO devices.

The degree of alignment of LB films of two SCLC copolymers[100,101] were studied by Tredgold, Hodge and coworkers.[107] These copolymers formed good LB layers by Y-deposition with deposition ratios near unity for both up and down strokes. Films approximately 670 monolayers thick (0.9 to 1.4 μm) were made with both copolymers. Comparison of apparently equivalent peaks, from X-ray diffraction patterns, for cast and LB materials always leads to the layer spacing of the LC film being rather

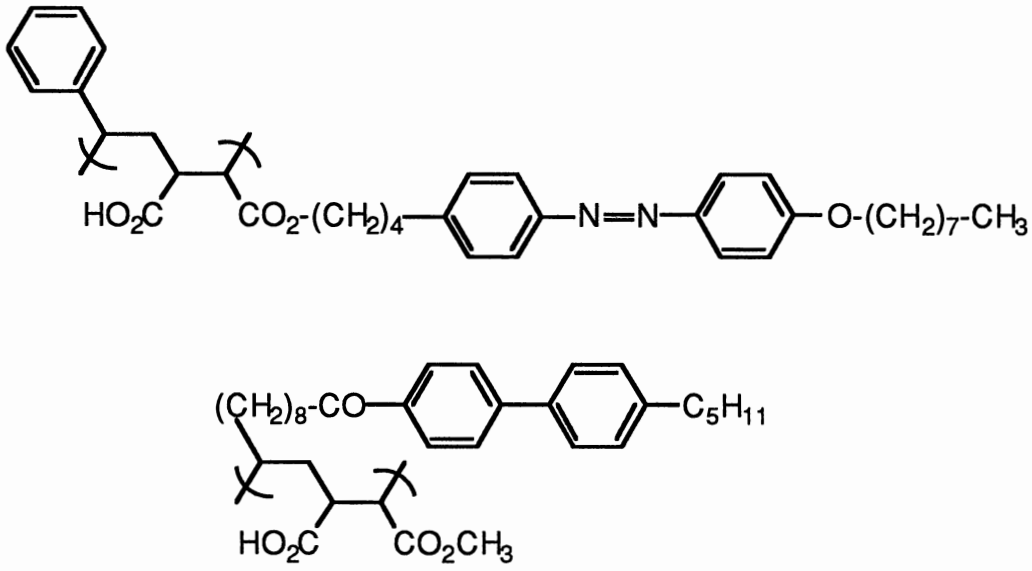

larger than the layer spacing of the equivalent cast film, due to the incorporation of water in the LB films. The layer spacing is reduced by heating, which drives off the water. LB films having similar thickness as the cast films were totally unresponsive to a magnetic field.

The LB technique is an important method of providing oriented assemblies of organic molecules and side chain polymers, giving rise to the fabrication of large second order NLO films. This technique can be used to prepare ultrathin noncentrosymmetric films of SCLCPs having NLO chromophores for the study of SHG. Unfortunately, these films, particularly the alternating layer type, involve a painfully tedious method of preparation. They tend to be fragile and the nonlinear component is quite diluted by the ineffective aliphatic chains. Thermal and photochemical stability of the NLO-active moiety is also a major concern. Much progress remains to be made in molecular and polymer design and synthesis as well as in deposition processes before this approach constitutes a practical alternative for second order nonlinear materials. Therefore, their use is recommended primarily as models to probe nonlinearities of various molecular species incorporated into a film.

REFERENCES

1. Saeva, F. D., Ed. *Liquid Crystals, The Fourth State of Matter*; Marcel Dekker, Inc.: New York, 1979.
2. Chandrasekhar, S. *Liquid Crystals*; Cambridge University Press: London, 1977.
3. Reinitzer, F. *Monatsh. Chem.* **1888**, 9,421.
4. Lehmann, O. *Z. Phys. Chem.* **1889**, 4, 462.
5. Collings, P. J. *Liquid Crystals, Nature's Delicate Phase of Matter*; Princeton University Press: New Jersey, 1990.
6. Chandrasekhar, S.; Sadashiva, B. K.; Suresh, K. A. *Pramana* **1977**, 9, 471-480.
7. Kelker, H.; Hatz, R. *Handbook of Liquid Crystals*; Verlag Chemie: Weinheim, 1980.
8. Freidel, G. *Ann. Phys.* **1922**, 18, 273-474.
9. Sackmann, H.; Demus, D. *Mol. Cryst.* **1966**, 2, 81-102.
10. Sackmann, H.; Demus, D. *Mol. Cryst. Liq. Cryst.* **1973**, 21, 239-273.
11. Leadbetter, A. J. In *Thermotropic Liquid Crystals*; Gray, G. W., Ed.; John Wiley & Sons: Chichester, U. K., 1987; pp 1-27.
12. Onsager. L. *Ann. New York Acad.* Sci. **1949**, 51, 627-659.
13. Flory, P. J. *Proc. R. Soc. London Ser.* A **1956**, 234, 60-73.
14. Robinson, C. *Trans. Faraday Soc.* **1956**, 52, 571-592.
15. Kwolek, S. L.; Morgan, P. W.; Sorenson, W. R. E. I. du Pont de Nemours & Co. U.S. 3 063 966, 1962; *Chem. Abstr.* **1969**, 58, 6964.
16. Roviello, A.; Sirigu, A. *J. Polym. Sci., Polym. Lett. Ed.* **1975**, 13, 455-463.

17. Jackson, W. J.; Kuhfuss, H. F. *J. Polym. Sci., Polym. Chem. Ed.* **1976**, 14, 2043-2058.

18. Finkelmann, H. In *Thermotropic Liquid Crystals*; Gray, G. W., Ed.; John Wiley & Sons: Chichester, U. K., 1987; pp 145-170.

19. Finkelmann, H. *Angew. Chem. Int. Ed. Engl.* **1987**, 26, 816-824.

20. Noel, C.; Navard, P. *Prog. Polym. Sci.* **1991**, 16, 55-110.

21. Chapoy, L. L., Ed. *Recent Advances in Liquid Crystalline Polymers*; Elsevier Applied Science Publishers: New York, 1985.

22. Griffin, A. C.; Britt, T. R.; Hung, R. S. L.; Steele, M. L. *Mol. Cryst. Liq. Cryst.* **1984**, 105, 305-314.

23. Khan, A. H.; McIntyre, J. E.; Milburn, A. H. *Polymer* **1983**, 24, 1610-1614.

24. Griffin, A. C.; Britt, T. R.; Campbell, G. A. *Mol. Cryst. Liq. Cryst. Lett.* **1982**, 82, 145-150.

25. Percec, V.; Shaffer, T. D.; Nava, H. *J. Polym. Sci., Polym. Lett. Ed.* **1984**, 22, 637-647.

26. Jonsson, H.; Werner, P. E.; Gedde, U. W.; Hult, A. *Macromolecules* **1989**, 22, 1683-1689.

27. Memeger, W. *Macromolecules* **1989**, 22, 1577-1588.

28. Shibaev, V. P.; Plate, N. A. *Vysokomol. Soedin.* **1977**, A19, 923-972 (Translated in *Polymer Sci. U.S.S.R.* **1977**, 19, 1065-1122).

29. Finkelmann, H.; Ringsdorf, H.; Wendorff, J. H. *Makromol. Chem.* **1978**, 179, 273-276.

30. Finkelmann, H.; Happ, M.; Portugal, M.; Ringsdorf, H. *Makromol. Chem.* **1978**, 179, 2541-2544.

31. Finkelmann, H.; Rehage, G. *Adv. Polym. Sci.* **1984**, 60/61, 99-172.

32. Shibaev, V. P.; Plate, N. A. *Adv. Polym. Sci.* **1984**, 60/61, 173-252.

33. Kostromin, S. G.; Shibaev, V. P.; Plate, N. A. *Liq. Cryst.* **1987**, 2 195-200.

34. Engel, M.; Hisgen, B.; Keller, R.; Krender, W.; Reck, B.; Ringsdorf, H.; Schmidt, H. W.; Tschirner, P. *Pure Appl. Chem.* **1985**, 57, 1009-1014.

35. Finkelmann, H. In *Polymer Liquid Crystals*; Ciferri, A.; Krigbaum, W. R.; Meyer, R. B., Eds.; Academic Press: New York, 1982; pp 35-62.

36. Percec, V.; Pugh, C. In *Side Chain Liquid Crystal Polymers*; McArdle, C. B., Ed.; Blackie and Sons: Glasgow, U. K., 1989; pp 30-105.

37. Frosini, V.; Levita, G.; Lupinacci, D.; Magagnini, P. L. *Mol. Cryst. Liq. Cryst.* **1981**, 66, 21-36.

38. Hahn, B.; Wendorff, J. H.; Portugall, M.; Ringsdorf, H. *Coll. Polym. Sci.* **1981**, 259, 875-884.

39. Kreuder, W.; Webster, O. W.; Ringsdorf , H. *Makromol. Chem., Rapid Commun.* **1986**, 7, 5-13.

40. Rodriguez-Parada, J. M.; Percec, V. *J. Polym. Sci., Polym. Chem.* Ed. **1986**, 24, 1363-1378.

41. Rodriguez-Parada, J. M.; Percec, V. *J. Polym. Sci., Polym. Chem.* Ed. **1987**, 25, 2269-2279.

42. Reck, B.; Ringsdorf, H. *Makromol. Chem., Rapid Commun.* **1985**, 6, 291-299.

43. Gray, G. W. In Side Chain Liquid Crystal Polymers; McArdle, C. B., Ed.; Blackie and Sons: Glasgow, U. K., 1989; pp 106-129.

44. Gemmell, P. A.; Gray, G. W.; Lacey, D. *Mol. Cryst. Liq. Cryst.* **1985**, 122, 205-218.

45. Gray, G. W.; Lacey, D.; Nestor, G.; White, M. S. *Makromol. Chem., Rapid Commun.* **1986**, 7, 71-76.

46. Nestor, G.; White, M. S.; Gray, G. W.; Lacey, D.; Toyne, K. J. *Makromol. Chem.* **1987**, 188, 2759-2767.

47. de Marignan, G.; Teyssie, D.; Boileau, S.; Malthete, J.; Noel, C. *Polymer*, **1988**, 29, 1318-1322.

48. Apfel, M. A.; Finkelmann, H.; Janini, G. M.; Laub, R. J.; Luhmann, B.-H.; Price, A.; Roberts, W. L.; Shaw, T. J.; Smith, C. A. *Anal. Chem.* **1985**, 57, 651-658.

49. Finkelmann, H.; Rehage, G. *Makromol. Chem., Rapid Commun.* **1980**, 1, 31-34.

50. Ringsdorf, H.; Schneller, A. *Makromol. Chem., Rapid Commun.* **1982**, 3, 557-562.

51. Percec, V.; Tomazos, D. *Macromolecules* **1989**, 22, 2062-2069.

52. Gaines, G. L., Jr. "*Insoluble Monolayers at Liquid-Gas Interfaces*", Interscience: New York, 1966.

53. Roberts, G., Ed. *Langmuir-Blodgett Films*, Plenum Press: New York, 1990.

54. Ulman, A. *An Introduction to Ultrathin Organic Films from Langmuir-Blodgett to Self-Assembly*, Academic Press: New York, 1991.

55. Petty, M. C.; Barlow, W. A. In *Langmuir-Blodgett Films*; Roberts, G., Ed.; Plenum Press: New York, 1990; pp 93-132.

56. Prasad, P. N.; Williams, D. J. *Introduction to Nonlinear Optical Effects in Molecules and Polymers*; John Wiley & sons, Inc.: New York, 1991.

57. Prasad, P. N.; Ulrich, D. R., Eds. *Nonlinear Optical and Electroactive Polymers*; Plenum Press: New York, 1988.

58. Small, R. D.; Singer, K. D.; Sohn, J. E.; Kuzyk, M. G.; Lalama, S. J. *Proc. SPIE* **1986**, 682, 160-169.

59. Singer, K. D.; Sohn, J. E.; Lalama, S. J. *Appl. Phys. Lett.* **1986**, 49, 248-250.

60. Hampsch, H. L.; Yang, J.; Wong, G. K.; Torkelson, J. M. *Macromolecules*, **1988**, 21, 526-528.

61. Hampsch, H. L.; Yang, J.; Wong, G. K.; Torkelson, J. M. *Polym. Commun.* **1989**, 30, 40-43.

62. Hampsch, H. L.; Torkelson, J. M.; Bethke, S. J.; Grubb, S. G. *J. Appl. Phys.* **1990**, 67, 1037-1041.

63. Hampsch, H. L.; Yang, J.; Wong, G. K.; Torkelson, J. M.; *Mat. Res. Soc. Symp. Proc.* **1990**, 173, 625-630.

64. Wu, J. W.; Valley, J. F.; Ermer, S.; Binkley, E. S.; Kenney, J. T.; Lipscomb, G. F.; Lytel, R. *Appl. Phys. Lett.* **1991**, 58, 225-227.

65. Meridith, G. R.; VanDusen, J. G.; Williams, D. J. *Macromolecules* **1982**, 15, 1385-1389.

66. Ye, C.; Marks, T. J.; Yang, J.; Wong, G. K. *Macromolecules* **1987**, 20, 2322-2324.

67. Ye, C.; Minami, N.; Marks, T. J.; Yang, J.; Wong, G. K. *Macromolecules* **1988**, 21, 2899-2901.

68. Dai, D.-R.; Marks, T. J.; Yang, J.; Lundquist, P. M.; Wong, G. K. *Macromolecules* **1990**, 23, 1891-1894.

69. Eich, M.; Sen, A.; Looser, H.; Bjorklund, G. C.; Swalen, J. D.; Twieg, R.; Yoon, D. Y. *J. Appl. Phys.* **1989**, 66, 2559-2567.

70. Nijhuis, S.; Rikken, G. L. J. A.; Havinga, E. E.; ten Hoeve, W.; Wynberg, H.; Meijer, E. W. *J. Chem. Soc., Chem. Commun.* **1990** 1093-1094.

71. Rikken, G. L. J. A.; Seppen, C. J. E.; Nijhuis, S.; Meijer, E. W. *Appl. Phys. Lett.* **1991**, 58, 435-437.

72. Hubbard, M. A.; Marks, T. J.; Yang, J.; Wong, G. K. *Chem. Mater.* **1989**, 1, 167-169.

73. Park, J.; Marks, T. J.; Yang, J.; Wong, G. K. *Chem. Mater.* **1990**, 2, 229-231.

74. Eich, M.; Reck, B.; Yoon, D. Y.; Wilson, C. G.; Bjorklund, G. C. *J. Appl. Phys.* **1989**, 66, 3241-3247.

75. Jungbauer, D.; Reck, B.; Twieg, R.; Yoon, D. Y.; Willson, C. G.; Swalen, J. D. *Appl. Phys. Lett.* **1990**, 56, 2610-2612.

76. Jungbauer, D.; Teraoka, I.; Yoon, D. Y.; Reck, B.; Swalen, J. D.; Twieg, R.; Willson, C. G. *J. Appl. Phys.* **1991**, 69, 8011-8017.

77. Mandal, B. K.; Kumar, J.; Huang, J.-C.; Tripathy, S. *Makromol. Chem., Rapid Commun.* **1991**, 12, 63-68.

78. Mandal, B. K.; Chen, Y. M.; Lee, J. Y.; Kumar, J.; Tripathy, S. *Appl. Phys. Lett.* **1991**, 58, 2459-2460.

79. Mandal, B. K.; Jeng, R. J.; Kumar, J.; Tripathy, S. K. *Makromol. Chem. Rapid Commun.* **1991**, 12, 607-612.

80. Ringsdorf, H.; Schmidt, H.-W. *Makromol. Chem.* **1984**, 185, 1327-1344.

81. Ringsdorf, H.; Schmidt, H.-W.; Baur, G.; Kiefer, R.; Windscheid, F. *Liq. Cryst.* **1986**, 4, 319-325.

82. Wendorff, J. H.; Eich, M. *Mol. Cryst. Liq. Cryst.* **1989**, 169, 133-166.

83. Noel, C.; Friedrich, C.; Leonard, V.; Le Barny, P.; Ravaux, G.; Dubois, J. C. *Makromol. Chem., Macromol. Symp.* **1989**, 24, 283-301.

84. Leslie, T. M.; DeMartino, R. N.; Choe, E. W.; Khanarian, G.; Haas, D.; Nelson, G.; Stamatoff, J. B.; Stuetz, D. E.; Teng, C.-C.; Yoon, H.-N. *Mol. Cryst. Liq. Cryst.* **1987**, 153, 451-477.

85. McCulloch, I. A.; Bailey, R. T. *Proc. SPIE* **1989**, 1147, 134-140.

86. Pfeiffer, M.; Haase, W.; *Proc. SPIE* **1990**, 1337, 234-245.

87. Ford, W. T.; Bautista, M.; Zhao, M.; Reeves, R. J.; Powell, R. C. *Mol. Cryst. Liq. Cryst.* **1991**, 198, 351-356.

88. Aktsipetrov, O. A.; Akhmediev, N. N.; Mishina, E. D.; Novak, V. R. as reported by Ulman, A. In *An Introduction to Ultrathin Organic Films from Langmuir-Blodgett to Self-Assembly*, Academic Press: New York, 1991; p 348.

89. Ledoux, I.; Josse, D.; Vidakovic, P.; Zyss, J.; Hann, R. A.; Gordon, P. F.; Bothwell, B. D.; Gupta, S. K.; Allen, S.; Robin, P.; Chastaing, E.; Dubois, J. C. *Europhys. Lett.* **1987**, 3, 803-809.

90. Loulergue, J. C.; Dumont, M.; Levy, Y.; Robin, P.; Pocholle, J. P.; Papuchon, M. *Thin Solid Films* **1988**, 160, 399-405.

91. Barton, J. W.; Buhaenko, M.; Moyle, B.; Ratcliffe, M. *J. Chem. Soc., Chem. Commun.* **1988**, 488-489.

92. Daniel, M. F.; Smith, G. W. *Mol. Cryst. Liq. Cryst. Lett.* **1984**, 102, 193-198.

93. Girling, I. R.; Cade, N. A.; Kolinsky, P. V.; Montgomery, C. M. *Electron. Lett.* **1985**, 21, 169-170.

94. Cross, G. H.; Peterson, I. R.; Girling, I. R.; Cade, N. A.; Goodwin, M. J.; Carr, N.; Sethi, R. S.; Marsden, R.; Gray, G. W.; Lacey, D.; McRoberts, A. M.; Scrowston, R. M.; Toyne, K. J. *Thin Solid Films* **1988**, 156, 39-52.

95. Stroeve, P.; Saperstein, D. D.; Rabolt, J. F. *J. Chem. Phys.* **1990**, 92, 6958-6967.

96. Girling, I. R.; Kolinsky, P. V.; Cade, N. A.; Earls, J. D.; Peterson, I. R. *Opt. Commun.* **1985**, 55, 289.

97. Ashwell, G. J. *Mat. Res. Soc. Symp. Proc.* **1991**, in press.

98. Decher, G.; Klinkhammer, F.; Peterson, I. R.; Steitz, R. *Thin Solid Films* **1989**, 178, 445-451.

99. Bosshard, Ch.; Kupfer, M.; Gunter, P.; Pasquier, C.; Zahir, S.; Seifert, M. *Appl. Phys. Lett.* **1990**, 56, 1204-1206.

100. Popovitz-Biro, R.; Hill, K.; Landau, E. M.; Lahav, M.; Leiserowitz, L.; Sagiv, J.; Hsiung, H.; Meredith, G. R.; Vanherzeele, H. *J. Am. Chem. Soc.* **1988**, 110, 2672-2674.

101. Popovitz-Biro, R.; Hill, K.; Shavit, E.; Hung, D. J.; Lahav, M.; Leiserowitz, L.; Sagiv, J.; Hsiung, H.; Meredith, G. R.; Vanherzeele, H. *J. Am. Chem. Soc.* **1990**, 112, 2498-2506.

102. Carr, N.; Goodwin, M. J. *Makromol. Chem., Rapid Commun.* **1987**, 8, 487-493.

103. Anderson, B. L.; Hall, R. C.; Higgins, B. G., Lindsay, G.; Stroeve, P. Kowel, S. T. *Synth. Metals* **1989**, 28, D683-D688.

104. Carpenter, M. M.; Prasad, P. N.; Griffin, A. C. *Thin Solid Films* **1988**, 161, 315-324.

105. Vickers, A. J.; Tredgold, R. H.; Hodge, P.; Khosdel, E.; Girling, I. *Thin Solid Films* **1985**, 134, 43-48.

106. Jones, R.; Tredgold, R. H.; Hoorfar, A.; Allen, R. A.; Hodge, P. *Thin Solid Films* **1985**, 134, 57-66.

107. Ali-Adib, Z.; Tredgold, R. H.; Hodge, P.; Davis, F. *Langmuir* **1991**, 7, 363-366.

CHAPTER II

SYNTHESES AND CHARACTERIZATION OF LIQUID CRYSTALLINE SIDE CHAIN POLYSILOXANES WITH 4-AMINO-4'-STILBENECARBOXYLIC ESTER MESOGENS

Introduction

Organic compounds, polymers and liquid crystalline polymers (LCPs) have generated considerable interest as potential materials for nonlinear optical (NLO) applications.[1] Side-chain liquid crystalline polymers (SCLCPs)[2] are interesting materials because they combine the properties of polymers and those of liquid crystals of low molecular weight.

SCLCPs with polarizable aromatic mesogens are good candidates for thin-film second order NLO materials. Most of the polymers that have been prepared and known to form second harmonic generation (SHG) films have the donor substituent in the spacer chain and the acceptor at the end of the side chain.[3-12] A series of side-chain polyacrylates with polarized 4-(dimethylamino)-4'-stilbenecarboxylic ester mesogens,[13] with the donor substituent at the end of the side chain and the acceptor in the spacer chain, was reported to form optically clear thin films and one of them exhibited a strong SHG response.[14] Problems were encountered in the development of the liquid crystalline phases of these side chain polyacrylates. Long annealing times were needed to observe phase transitions in the DSC and microscopic textures. It is therefore of some interest to exchange the

hydrocarbon polymer main chain by a polysiloxane main chain, which is characterized by high flexibility of the chain segments. It is hoped that the change in the polymer backbone will give easily developed liquid crystalline phases.

My research focuses on the preparation of liquid crystalline polysiloxanes with polarized 4-amino-4'-stilbenecarboxylic ester mesogens in the side chains. The transition temperatures and phase assignments of both the monomers and the polysiloxanes have been determined by thermal analysis, optical microscopy, and X-ray diffraction. Monolayer behavior of the polysiloxanes has been investigated by LB methods. LB Films were prepared from the monolayers of the polysiloxanes for future SHG studies.

The SCLC polysiloxanes prepared are given below.

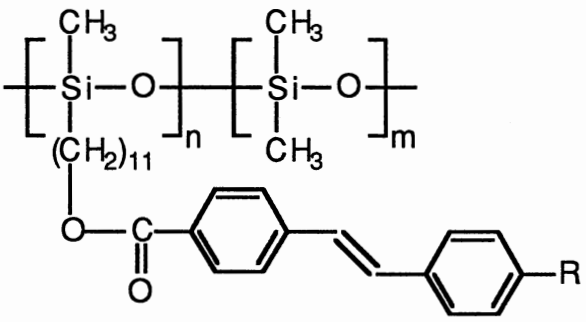

R = —N(CH$_3$)$_2$ **HPS-1**, n = 60, m = 0
CPS-1, n = 9, m = 8

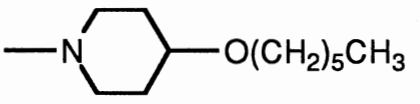

HPS-2, n = 60, m = 0
CPS-2, n = 9, m = 8

Experimental Section

Materials. 4-Hydroxypiperidine, acetic anhydride, 80% NaH dispersed in mineral oil, 1,4,7,10,13-pentaoxacyclopentadecane (15-crown-5), bromohexane, 4-fluorobenzaldehyde, methyl 4-(hydroxymethyl)benzoate, thionyl chloride, triethyl

phosphite, 4-(N,N-dimethylamino)benzaldehyde, 10-undecen-1-ol, nickel acetylacetonate hydrate, and hexachloroplatinic acid were obtained from Aldrich and were used without further purification. Purities of the reagents were checked by ^{1}H NMR and ^{13}C NMR. Syntheses were run in air unless otherwise stated. Kodak chromagram sheets (silica gel with fluorescent indicator) were used for all thin layer chromatography (TLC) experiments.

The poly(hydromethyl)siloxane (PHMS) with a reported DP of 45 to 90, was obtained from Wacker while the poly(hydromethylsiloxane-co-dimethylsiloxane) (PHMS-PDMS) (50 - 55 wt% hydromethyl) with a reported molecular weight of 900 - 1000, was obtained from Petrarch. Table VII reports the average molecular weights, M_w/M_n, and DP of the two polysiloxanes, PHMS and PHMS-PDMS, used in the experiment as obtained by GPC and ^{29}Si NMR analyses.

Table VII. Characterization of Commercial Polysiloxanes

Polymer (Source)	GPC[a]			^{29}Si NMR[b]	
	M_n	M_w	M_w/M_n	M_n	DP
PHMS (Wacker)	3800	10 400	2.7	3762	60 ± 3
PHMS-PDMS (Petrarch)	1050	1800	1.8	1294	17 ± 1 (9 : 8)

[a] Analyses in toluene solution at 25 °C and flow rate of 1 mL/min. A refractive index detector (Waters Differential Refractometer R401) was used and calibration was based on cubic fit values using polystyrenes of $M_n = (0.800 - 100) \times 10^3$ as standards. [b] End group analysis (see appendix, spectrum 15).

Measurements. ^{1}H NMR and ^{13}C NMR spectra were recorded on a Varian XL-300 instrument at 300 MHz and 75 MHz, respectively. ^{29}Si NMR spectra were recorded

on a Varian XL-400 instrument at 79 MHz, and the experimental conditions are reported in Table VIII. IR spectra were obtained on a Perkin-Elmer 681 instrument. A Varian DMS 200 spectrophotometer was used for UV-visible measurements. Synthesized materials were sent to Galbraith Laboratories, Inc. for elemental analyses.

Table VIII. ^{29}Si NMR Experimental Conditions

Solvent	$CDCl_3$
Reference	TMS (0.05%)
Polymer concentration[a]	10 - 20% (w/v)
Paramagnetic relaxation agent, $Cr(acac)_3$[a]	1% (w/v)
Acquisition temperature	ambient
Acquisition time	1.989 s
Pulse width	20.0 μs
Pulse delay	1.500 s
Transients	1600 - 26 500
Decoupler mode[a]	NNY[b]

[a] As reported by Gray and coworkers.[15] [b] Decoupler is on only during spectral acquisition.

Molecular weights obtained by gel permeation chromatography (GPC) were conducted with a Waters 590 pump equipped with a Rheodyne injector with a 20-μL sample loop, a Beckman 153 analytical 254-nm UV detector, and an Interactive Microware data station. GPC analyses were performed at 25 °C using three PL gel columns of 10^2, 10^3, 10^4 Å obtained from Polymer Laboratories, Ltd. THF was the solvent at a flow rate of 1 mL/min and polystyrenes of $M_n = (0.8 - 600) \times 10^3$ were the standards for calibrations using the cubic fit values. Solutions (~10 mg polymer/mL THF) were filtered through a 0.5 μm PTFE membrane (Alltech Associates, Inc.) before injection into the chromatograph.

Differential scanning calorimetry (DSC) measurements were performed with a Perkin Elmer DSC-2 instrument equipped with a TADS 3600 data station. Two separate scans were done for each of the side chain polysiloxanes. The baseline on each scan was optimized. The first scan was done from -123 °C to 77 °C with the use of liquid nitrogen as coolant. Helium was used as purge gas for the sample holder enclosure while the dry box was purged with nitrogen. The second scan was performed from 37 °C to about 250 °C, using nitrogen as purge gas for both the sample holder enclosure and dry box. For the second scan, the temperatures and heats of transitions were calibrated with indium as the standard. Scans were typically done at a rate of 20 K/min. Glass transition temperatures (T_g) were read at the midpoint of the change in the heat capacity.

The phase transition behaviors and mesomorphic textures were observed with a Nikon OPTIPHOT-POL microscope with crossed polarizers and equipped with a Mettler FP82 hot stage controlled by a Mettler FP80 thermoregulator. Observations were made at rates between 10 and 1 K/min and transition temperatures quoted are from extrapolation to zero rate. In many cases the polymeric samples were quite viscous in the mesophase, and annealing at elevated temperatures for several hours was necessary to obtain good textures.

X-ray diffraction powder measurements were performed with Cu-Kα radiation, using a Philips APD 3720 high temperature X-ray diffractometer equipped with a tantalum heating plate controlled by a thermoregulator. The sample chamber was purged with helium gas during each measurement. Prior to the X-ray measurements, the sample was heated above the clearing point to erase any previous thermal history and then cooled to the desired temperatures for measurement.

LB measurements were performed with KSV 5000 instruments equipped with one barrier for unsymmetrical compression and both floating barrier and Wilhelmy plate surface pressure sensors. Monolayers were spread on the water subphase from chloroform solutions (approx. 0.5 mg/mL) and were compressed at barrier speeds of 25

to 5 mm/min. All measurements were done at about 27 to 30 °C. The monolayers were characterized at the air-water interface by measurement of the film surface pressure, Π, vs mean molecular area, Mma, isotherms. The hysteresis behavior by compression and subsequent expansion of the monolayer was also investigated. The temporal stability of the monolayers was checked by isobaric creep measurements as well as pressure drop measurements at constant surface area.

Quartz microscope slides (25 mm x 25 mm x 2 mm) were used for dipping experiments. They were thoroughly cleaned with chromic acid solution and rinsed five to six times with deionized water to provide hydrophilic surfaces. For hydrophobic substrates, the cleaned slides were first soaked in a chloroform-methanol (1:2) solution for one hour and chloroform for another hour. The slides were then treated with a silanization solution (containing 70 mL of decahydronaphthalene, 30 mL chloroform and approximately 5 mL of octadecyltrichlorosilane) for 24 h at room temperature. The hydrophobized slides were stirred in chloroform, chloroform-methanol (1:2) solution and methanol, each for 15 min. The success of the hydrophobization was tested by dipping the treated slide into water. When it was quickly pulled out, the hydrophobic slide looked dry. The cleaning and the hydrophobization of the slides were all done in covered wide-mouth bottles and slides were stored in cleaned, dried bottles.

Monolayers were spread on the water subphase and were symmetrically compressed using two barriers at a speed of 5 mm/min. Monolayer transfer was carried out at constant surface pressure of 20 mN/m and at this time, the barrier speed was reduced to a maximum of 1.0 mm/min. The monolayers were allowed to stabilize for about 30 min before dipping the substrate at a slow speed of 1.0 mm/min. The substrate was withdrawn at the same speed as the dipping speed.

N-Acetyl-4-hydroxypiperidine (2). To a solution of 4-hydroxypiperidine (247 mmol, 25.0 g) and acetic anhydride (247 mmol, 23.5 mL), an equivalent amount of anhydrous K_2CO_3 was added. The reaction mixture was stirred at room temperature for 6

h under dry air. The progress of the reaction was monitored by TLC using ethyl acetate : acetone (1:1) as eluant. After 12 h, no 4-hydroxypiperidine was detected. The product was extracted with CH_2Cl_2 and the solid K_2CO_3 was filtered off. The solvent was removed by rotavap and the pure product was collected by distillation at approximately 130 °C and 0.25 mmHg. The yield was 28.47 g (81%). ^1H NMR ($CDCl_3$) δ 1.52 and 1.87 (2 m, 4 H, CH_2), 2.09 (s, 3 H, $CH_3C=O$), 3.21, 3.72 and 4.04 (3 m, 4 H, NCH_2), 3.90 (m, 1 H, OCH), 4.31 (s, 1 H, OH). ^{13}C NMR ($CDCl_3$) δ 21.2 ($CH_3C=O$), 33.5 (CH_2), 34.2 (CH_2), 38.8 (NCH_2), 43.6 (NCH_2), 66.2 (OCH), 168.9 (C=O). IR (neat, cm^{-1}) 3060 - 3700 (O-H), 2940, 2890, 1630 (C=O), 1490, 1460, 1440, 1370, 1270, 1240, 1090, 1050. Anal. Calcd for $C_7H_{13}NO_2$: C, 58.72; H, 9.15; N, 9.78. Found: C, 58.67; H, 9.37; N, 9.68.

N-Acetyl-4-hexyloxypiperidine (3). A sample of 88 mmol (2.64 g) 80% NaH dispersed in mineral oil was washed three times with pentane under N_2. To a stirred slurry of NaH in 20 mL of dry DMF, 80 mmol (11.45 g) of compound **2** (dried at room temperature under vacuum prior to the reaction) and 5 mmol (1 mL) of 15-crown-5 were added under N_2 and the mixture was stirred at room temperature for 15 min. An equimolar amount of 1-bromohexane (80 mmol; 11.25 mL) was added and the mixture was allowed to stand at room temperature for 48 h. The mixture was poured into 150 mL ice-water and the product was extracted three times with ether. The combined ether extracts were washed three times with H_2O and the final extract was dried over anhydrous Na_2SO_4. The ether was removed by rotavap and the pure product was collected by reduced pressure distillation at 120 °C and 0.25 mmHg. The yield was 7.46 g (41%). ^1H NMR ($CDCl_3$) δ 0.90 (t, 3 H, CH_3), 1.31 (m, 6 H, $(CH_2)_3CH_3$), 1.57 (m, 4 H, OCH_2CH_2 and $OCHCH_2$), 1.83 (m, 2 H, $OCHCH_2$), 2.09 (s, 3 H, $CH_3C=O$), 3.27, 3.65 and 3.90 (3 m, 4 H, NCH_2), 3.47 (overlapping t and m, 3 H, OCH and OCH_2). ^{13}C NMR ($CDCl_3$) δ 14.1 (CH_3), 21.5 ($CH_3C=O$), 22.6 (CH_3CH_2), 25.9 ($(CH_2)_2CH_2$), 30.0 (OCH_2CH_2), 30.6 ($OCHCH_2$), 31.7 ($CH_3CH_2CH_2$ and $OCHCH_2$), 38.8 (NCH_2),

43.7 (NCH_2), 68.2 (OCH_2), 73.8 (OCH), 168.8 (C=O). IR (neat, cm^{-1}) 2940, 2860, 1650 (C=O), 1440, 1360, 1280, 1240, 1110, 1050. Anal. Calcd for $C_{13}H_{25}NO_2$: C, 68.68; H, 11.08; N, 6.16. Found: C, 69.36; H, 10.69; N, 6.04.

4-Hexyloxypiperidine (4). A mixture of compound **3** (30 mmol; 6.82 g) and 3.5 M H_2SO_4 (300 mmol, 86 mL) was refluxed overnight. The mixture was poured into 150 mL ice-water. NaOH pellets were added to make the solution basic. The product was extracted three times with ether and the combined ether extracts were washed three times with H_2O. The final extract was dried over anhydrous Na_2SO_4 and concentrated by rotavap. The pure product was collected by reduced pressure distillation at 80 °C and 0.25 mmHg. The yield was 4.68 g (84%). ^1H NMR ($CDCl_3$) δ 0.90 (t, 3 H, CH_3), 1.34 (m, 6 H, (CH_2)$_3CH_3$), 1.41 and 1.91 (2m, 4 H, OCHCH_2), 1.54 (s, 1H, NH), 1.56 (quintet, 2 H, J = 7 Hz, OCH_2CH_2), 2.60 and 3.08 (2 m, 4 H, NCH_2), 3.32 (m, 1 H, OCH), 3.44 (t, 2 H, J = 7 Hz, OCH_2). ^{13}C NMR ($CDCl_3$) δ 14.1 (CH_3), 22.7 (CH_3CH_2), 25.9 ((CH_2)$_2CH_2$), 30.1 (OCH_2CH_2), 31.7 ($CH_3CH_2CH_2$), 33.2 ($OCHCH_2$), 44.7 (NCH_2), 67.8 (OCH_2), 75.6 (OCH). IR (neat, cm^{-1}) 3280 (N-H), 2940, 2860, 2740, 1470, 1450, 1360, 1320, 1160, 1110, 1040, 1000, 770. Anal. Calcd for $C_{11}H_{23}NO$: C, 71.30; H, 12.51; N, 7.56. Found: C, 70.89; H, 12.23; N, 7.59.

4-(4'-Hexyloxy-1-piperidino)benzaldehyde (5). Equimolar quantities of compound **4** (27.8 mmol, 5.15 g) and 4-fluorobenzaldehyde (27.8 mmol, 3.45 g) with 3.84 g of anhydrous K_2CO_3 in 5 mL of DMSO were stirred and heated under N_2 at 90 °C for 48 h. The progress of the reaction was monitored by TLC using $CHCl_3$: hexane (1:1) as eluant. After 48 h, the absence of the starting aldehyde was noted. The reaction mixture was then poured into 250 mL of H_2O and the precipitate was filtered. After several recrystallizations from ethanol-water, the yield was 5.88 g (73%) and the melting point was 42-44 °C. ^1H NMR ($CDCl_3$) δ 0.89 (t, 3 H, CH_3), 1.33 (m, 6 H, (CH_2)$_3CH_3$), 1.57 (quintet, 2 H, J = 7 Hz, OCH_2CH_2), 1.70 and 1.94 (2 m, 4 H, OCHCH_2), 3.21 and 3.70 (2 m, 4 H, NCH_2), 3.47 (t, 2 H, J = 7 Hz, OCH_2), 3.61 (m, 1

H, OCH), 6.91 (d, 2 H, J = 9 Hz, Ar H3 and H5), 7.73 (d, 2 H, J = 9 Hz, Ar H2 and H6), 9.76 (s, 1 H, HC=O). ^{13}C NMR ($CDCl_3$) δ 14.1 (CH_3), 22.6 (CH_3CH_2), 25.9 ($(CH_2)_2CH_2$), 30.1 (OCH_2CH_2), 30.6 ($OCHCH_2$), 31.7 ($CH_3CH_2CH_2$), 44.9 (NCH_2), 68.2 (OCH_2), 73.9 (OCH), 113.4 (Ar C3 and C5), 126.5 (Ar C1), 132.0 (Ar C2 and C6), 154.8 (Ar C4), 190.3 (C=O). IR (KBr, cm^{-1}) 2960, 2940, 2860, 1680 (C=O), 1620 (C=C), 1380, 1250, 1230, 1180, 1120, 1100, 1080, 810. UV-vis ($CHCl_3$) λ_{max} = 338 nm ($\varepsilon = 2.79 \times 10^4\ M^{-1}\ cm^{-1}$). Anal. Calcd for $C_{18}H_{27}NO_2$: C, 74.70; H, 9.40; N, 4.84. Found: C, 74.98; H, 9.62; N, 4.86.

Methyl 4-(chloromethyl)benzoate (7). Methyl 4-(hydroxymethyl)benzoate (100 mmol, 16.96 g) was dissolved in 110 mmol (8.10 mL) of thionyl chloride. The reaction mixture was allowed to stand in the hood under dry air for 16 h and was refluxed for 30 min in an oil bath. The solution was poured into 100 mL of ice-water and the product was extracted three times with 60 mL portions of ether. The combined ether extracts were washed twice with 60 mL portions of saturated aqueous sodium bicarbonate and once with 60 mL of H_2O. The final extract was dried over anhydrous Na_2SO_4. The ether was distilled off by rotavap and the product was obtained by distillation at 109 °C and 10 mmHg. The melting point of the product was 39-40 °C (lit.[16] mp 39 - 40 °C) and the yield was 15.88 (55%). ^1H NMR ($CDCl_3$) δ 3.90 (s, 3 H, OCH_3), 4.60 (s, 2 H, $ClCH_2$), 7.45 (d, 2 H, Ar H3 and H5), 8.02 (d, 2 H, Ar H2 and H4). ^{13}C NMR ($CDCl_3$) δ 43.5 ($ClCH_2$), 52.0 (OCH_3), 124.5 (Ar C3 and C5), 130.0 (Ar C1, C2 and C6), 142.0 (Ar C4), 166.5 (C=O).

Diethyl p-(methoxycarbonyl)benzylphosphonate (8). A mixture of 40 mmol (7.38 g) of compound **7** and 50 mmol (8.66 mL) of triethyl phosphite was refluxed for 1 h using an oil bath. At the end of the reflux period, the phosphate ester was allowed to cool to room temperature. The excess triethyl phosphite was distilled off under reduced pressure and then the product was obtained at 185 °C and 5 mmHg. The yield was 10.47 g (93%). Spectral analyses agreed with previous literature.[13]

4-(N,N-dimethylamino)-4'-carbomethoxy-*trans*-stilbene (9). A sample of 30 mmol (0.90 g) 80% NaH dispersed in mineral oil was washed three times with dry pentane under N_2. A solution of 30 mg of 15-crown-5 in 60 mL of dry THF was added. This reaction was done in the dark under N_2. To this stirred slurry, a solution of 4-(N,N-dimethylamino)benzaldehyde (40 mmol, 5.98 g) and compound **8** (40 mmol, 11.40 g) in 30 mL of THF was added dropwise at 0 °C. During the course of the reaction, a yellow precipitate formed. The mixture was stirred for 2 h at room temperature and poured into 400 mL of ice-water. The precipitate was filtered and washed with ether. After recrystallization from DMF, 9.16 g (81%) of greenish yellow powder was obtained. The melting transition temperature, obtained from the DSC, was 226 °C (lit.[13] T_m 229 °C). Spectral analyses agreed with previous literature.[13] UV-vis ($CHCl_3$) λ_{max} = 383 nm (ε = 2.94 x 10^4 M^{-1} cm^{-1}). Anal. Calcd for $C_{18}H_{19}NO_2$: C, 76.84; H, 6.81; N, 4.98. Found: C, 76.76; H, 6.85; N, 4.96.

4-(4-Hexyloxy-1-piperidino)-4'-carbomethoxy-*trans*-stilbene (10). The same procedure was followed as described above for **9** using a solution of **5** (20 mmol, 5.79 g) and compound **8** (20 mmol, 5.72 g) in 30 mL THF. After recrystallization from DMF, 7.07 g (84%) of greenish yellow powder was obtained. Three phase transitions were observed from the DSC scan (C 178 °C M_1 227 °C M_2 252 °C I). No microscopic texture was obtained due to the decomposition of the material at the isotropization temperature, which was not observed in the thermal analysis because this was done under nitrogen. ^{1}H NMR ($CDCl_3$) δ 0.89 (t, 3 H, CH_3), 1.31 (m, 6 H, $(CH_2)_3CH_3$), 1.57 (quintet, 2 H, J = 7 Hz, OCH_2CH_2), 1.71 and 1.97 (2 m, 4 H, $OCHCH_2$), 2.99 and 3.59 (2 m, 4 H, NCH_2), 3.47 (overlapping t and m, 3 H, J = 7 Hz, OCH and OCH_2), 3.91 (s, 3 H, CO_2CH_3), 6.91 (d, 2 H, J = 8.4 Hz, Ar H3 and H5), 6.95 (d, 1 H, J = 16.5 Hz, =$CHArCO_2R$), 7.12 (d, 1 H, J = 16.5 Hz, =$CHArNR_2$), 7.42 (d, 2 H, J = 8.4 Hz, Ar H2 and H6), 7.51 (d, 2 H, J = 8.2 Hz, Ar H2' and H6'), 7.99 (d, 2 H, J = 8.2 Hz, Ar H3' and H5'). ^{13}C NMR ($CDCl_3$) δ 14.1 (CH_3), 22.6

(CH_3CH_2), 25.9 ($(CH_2)_2CH_2$), 30.1 (OCH_2CH_2), 30.9 ($OCHCH_2$), 31.7 ($CH_3CH_2CH_2$), 46.6 (NCH_2), 52.0 (CO_2CH_3), 68.1 (OCH_2), 74.4 (OCH), 115.8 (Ar C3 and C5), 124.2 (=$CHArCO_2R$), 125.8 (Ar C2' and C6'), 127.3 (Ar C1), 127.9 (Ar C2 and C6), 128.1 (Ar C4'), 129.9 (Ar C3' and C5'), 131.1 (=$CHArNR_2$), 142.6 (Ar C1'), 151.1 (Ar C4), 167.0 (C=O). IR (KBr, cm^{-1}) 2960, 2940, 2860, 1720 (C=O), 1600 (C=C), 1520, 1440, 1410, 1370, 1290, 1190, 1180, 1110, 960, 840, 810, 770. UV-vis ($CHCl_3$) λ_{max} = 370 nm ($\varepsilon = 3.38 \times 10^4\ M^{-1}\ cm^{-1}$). Anal. Calcd for $C_{27}H_{35}NO_3$: C, 76.92; H, 8.37; N, 3.32. Found: C, 76.80; H, 8.42; N, 3.31.

10-Undecen-1-yl-4-(N,N-dimethylamino)-*trans*-stilbene-4'-carboxylate (MNR-1). A mixture of 5.0 mmol (1.41 g) of compound **9** and 25 mmol (5 mL) of ω-undecylenyl alcohol in 20 mL of xylene was treated with 1.0 mmol (0.27 g) of nickel acetylacetonate hydrate. The mixture was refluxed in the dark until no more of compound **9** could be detected by TLC using 15 % ethyl acetate in hexane as eluant. The mixture was allowed to pass through a filter paper to filter off the black solid that was formed. The black solid was washed several times with ethyl acetate using a total volume of 300 mL. The filtrate was washed three times with H_2O. The organic layer was dried over anhydrous Na_2SO_4 and then the solvent was removed by rotavap. The crude product was recrystallized from ethyl alcohol with a yield of 1.39 g (66%). ^1H NMR ($CDCl_3$) δ 1.37 (m, 12 H, $(CH_2)_6$), 1.76 (quintet, 2 H, J = 7 Hz, $CO_2CH_2CH_2$), 2.04 (q, 2 H, J = 7 Hz, =$CHCH_2$), 2.99 (s, 6 H, NCH_3), 4.30 (t, 2 H, J = 7 Hz, CO_2CH_2), 4.97 (m, 2H, =CH_2), 5.80 (m, 1 H, =CH), 6.71 (d, 2 H, J = 8.8 Hz, Ar H3 and H5), 6.92 (d, 1 H, J = 16.2 Hz, =$CHArCO_2R$), 7.15 (d, 1 H, J = 16.3 Hz, =$CHArNR_2$), 7.43 (d, 2 H, J = 8.8 Hz, Ar H2 and H6), 7.51 (d, 2 H, J = 8.4 Hz, Ar H2' and H6'), 7.98 (d, 2 H, J = 8.3 Hz, Ar H3' and H5'). ^{13}C NMR ($CDCl_3$) δ 25.9, 28.6, 28.8, 29.0, 29.1, 29.2 and 29.3 ($(CH)_7$), 33.6 (=$CHCH_2$), 40.2 (NCH_3), 64.8 (CO_2CH_2), 112.1 (Ar C3 and C5), 114.0 (=CH_2), 122.9 (=$CHArCO_2R$), 124.9 (Ar C1), 125.5 (Ar C2' and C6'), 127.8 (Ar C2 and C6), 128.1 (Ar C4'), 129.8 (Ar C3' and C5'), 131.2 (=$CHArNR_2$), 139.1

(=CH), 142.6 (Ar C1'), 150.3 (Ar C4), 166.5 (C=O). IR (KBr, cm^{-1}) 2920, 2860, 1710 (C=O), 1600 (C=C), 1530, 1360, 1280, 1200, 1180, 1110, 820. UV-vis ($CHCl_3$) λ_{max} = 381 nm ($\varepsilon = 3.05 \times 10^4\ M^{-1}\ cm^{-1}$). Anal. Calcd for $C_{28}H_{37}NO_2$: C, 80.15; H, 8.89; N, 3.34. Found: C, 80.52; H, 8.97; N, 3.31.

10-Undecen-1-yl-4-(4-hexyloxy-1-piperidino)-*trans*-stilbene-4'-carboxylate (MNR-2). The same procedure was followed as described above for **MNR-1** using a mixture of 5.0 mmol (2.10 g) of compound **10** and 25 mmol (5 mL) of ω-undecylenyl alcohol in 20 mL of xylene treated with 1.0 mmol (0.27 g) of nickel acetylacetonate hydrate. Recrystallization from ethyl alcohol gave a yield of 1.94 g (69%). ^1H NMR ($CDCl_3$) δ 0.89 (t, 3 H, CH_3), 1.37 (m, 18 H, $(CH_2)_6$ and $(CH_2)_3CH_3$), 1.57 (quintet, 2 H, J = 7 Hz, OCH_2CH_2), 1.73 (m, 4 H, $CO_2CH_2CH_2$ and $OCHCH_2$), 2.02 (m, 4 H, $=CHCH_2$ and $OCHCH_2$), 2.99 and 3.59 (2 m, 4 H, NCH_2), 3.47 (overlapping t and m, 3 H, J = 7 Hz, OCH and OCH_2), 4.30 (t, 2 H, J = 7 Hz, CO_2CH_2), 4.97 (m, 2H, $=CH_2$), 5.80 (m, 1 H, =CH), 6.91 (d, 2 H, J = 8.7 Hz, Ar H3 and H5), 6.96 (d, 1 H, J = 15.6 Hz, $=CHArCO_2R$), 7.14 (d, 1 H, J = 16.1 Hz, $=CHArNR_2$), 7.42 (d, 2 H, J = 8.7 Hz, Ar H2 and H6), 7.51 (d, 2 H, J = 8.4 Hz, Ar H2' and H6'), 7.99 (d, 2 H, J = 8.3 Hz, Ar H3' and H5'). ^{13}C NMR ($CDCl_3$) δ 14.1 (CH_3), 22.6 (CH_3CH_2), 25.9 ($(CH_2)_2CH_2$), 26.0, 28.7, 28.9, 29.1, 29.2, 29.4, 29.5 ($(CH_2)_7$), 30.1 (OCH_2CH_2), 30.9 ($OCHCH_2$), 31.7 ($CH_3CH_2CH_2$), 33.8 ($=CHCH_2$), 46.6 (NCH_2), 65.0 (CO_2CH_2), 68.1 (OCH_2), 74.4 (OCH), 114.1 ($=CH_2$), 115.8 (Ar C3 and C5), 124.2 ($=CHArCO_2R$), 125.8 (Ar C2' and C6'), 127.3 (Ar C1), 127.8 (Ar C2 and C6), 128.5 (Ar C4'), 129.9 (Ar C3' and C5'), 131.0 ($=CHArNR_2$), 139.2 (=CH), 142.4 (Ar C1'), 151.1 (Ar C4), 166.6 (C=O). IR (KBr, cm^{-1}) 2930, 2860, 1710 (C=O), 1600 (C=C), 1520, 1470, 1370, 1280, 1180, 1110, 820, 770. UV-vis ($CHCl_3$) λ_{max} = 369 nm ($\varepsilon = 2.97 \times 10^4\ M^{-1}\ cm^{-1}$). Anal. Calcd for $C_{37}H_{53}NO_3$: C, 79.38; H, 9.54; N, 2.50. Found: C, 78.86; H, 9.76; N, 2.42.

Polyhydrosilylation reaction procedure. The starting polysiloxane and a 10 mol% excess of the appropriate monomers, **MNR**, with respect to the Si-H bonds were dissolved in 30 ml of dry toluene (freshly distilled and dried over molecular sieves). A solution of equimolar amounts of chloroplatinic acid catalyst (H_2PtCl_6) and triethylamine in 2-propanol was added to give a Pt : alkene ratio of 0.0001. The reaction was carried out in the dark at 100 ^oC for about 48 h under Ar, until negligible Si-H absorption (2160 cm^{-1}) was detectable by IR spectroscopy. When no change in the Si-H absorption was observed, an equimolar amount of 1-octene to the original Si-H was added to the reaction mixture. The reaction was then allowed to proceed for several hours. The polymer was precipitated from a solution of chloroform by the slow addition of methanol with continuous stirring. Approximately 2 g of polymer was dissolved in about 30 mL of chloroform and a total of about 300 mL of methanol was consumed. The polymer was vacuum filtered through a fritted disc (fine porosity) Buchner funnel. The precipitation step was done six to seven times. In each precipitation, the purity of the polymers was checked by gel permeation chromatography, GPC. The side-chain polysiloxanes obtained were characterized and the data are listed below.

HPS-1. The procedure was followed as described above using a mixture of 0.41 g (6.5 mmol (Si-H)) of poly(hydromethylsiloxane) and 3.00 g (7.15 mmol) of **MNR-1** in 30 mL of dry toluene. Toluene was used in the precipitation process since the polymer is soluble in hot toluene while insoluble in cold toluene. Approximately 2.5 g of **HPS-1** was dissolved in about 25 mL of hot toluene. The hot solution was filtered quickly through a fluted filter paper. The solution was cooled to room temperature and then placed in an ice-bath. The polymer was vacuum filtered through a fritted disc (fine porosity) Buchner funnel. After the final precipitation, 2.15 g (69%) of greenish yellow powder was obtained. ^1H NMR ($CDCl_3$) δ 0.04 (Si-CH_3), 0.12 (terminal Si-CH_3), 0.49 (Si-CH_2), 0.84 (CH_3), 1.32 ((CH_2)$_6$ and (CH_2)$_8$), 1.69 ($CO_2CH_2CH_2$), 2.88 (NCH_3), 4.45 (CO_2CH_2), 6.64 (Ar H3 and H5), 6.86 (=$CHArCO_2R$), 7.06 (=$CHArNR_2$), 7.35 (Ar H2

and H6), 7.42 (Ar H2' and H6'), 7.92 (Ar H3' and H5'). ^{13}C NMR ($CDCl_3$) δ 17.7 (Si-CH_2), 23.1, 26.1, 28.8, 29.5, 29.6, 29.7, 29.8, 32.0 and 33.6 (($CH_2)_6$ and $(CH_2)_9$), 40.3 (NCH_3), 65.0 (CO_2CH_2), 112.1 (Ar C3 and C5), 123.0 (=$CHArCO_2R$), 125.0 (Ar C1), 125.6 (Ar C2' and C6'), 128.0 (Ar C2 and C6), 128.2 (Ar C4'), 129.9 (Ar C3' and C5'), 131.2 (=$CHArNR_2$), 142.6 (Ar C1'), 150.3 (Ar C4), 166.5 (C=O). ^{29}Si NMR ($CDCl_3$) δ -21.3 to -22.9 (CH_3-Si-CH_2). IR (KBr, cm^{-1}) 2920, 2850, 2150 (small peak, Si-H), 1710 (C=O), 1600 (C=C), 1520, 1410, 1360, 1280, 1260, 1180, 1100 - 1010 (Si-O), 840, 810, 770. UV-vis ($CHCl_3$) λ_{max} = 382 nm. Anal. Calcd for **HPS-1**: C, 72.45; H, 8.63; N, 2.90; Si, 6.02. Found: C, 71.32; H, 9.69; N, 2.12; Si, 7.87.

CPS-1. The procedure was followed as described above using a mixture of 0.93 g (6.5 mmol (Si-H)) of poly(hydromethyl-dimethylsiloxane) and 3.00 g (7.15 mmol) of **MNR-1** in 30 mL of dry toluene. After the final precipitation, 2.29 g (63%) of greenish yellow powder was obtained. ^1H NMR ($CDCl_3$) δ 0.04 (Si-CH_3), 0.12 (terminal Si-CH_3), 0.48 (Si-CH_2), 0.85 (CH_3), 1.25 (($CH_2)_6$ and $(CH_2)_8$), 1.72 ($CO_2CH_2CH_2$), 2.96 (NCH_3), 4.26 (CO_2CH_2), 6.67 (Ar H3 and H5), 6.88 (=$CHArCO_2R$), 7.11 (=$CHArNR_2$), 7.39 (Ar H2 and H6), 7.46 (Ar H2' and H6'), 7.95 (Ar H3' and H5'). ^{13}C NMR ($CDCl_3$) δ 1.1 (Si-CH_3), 1.2 (terminal Si-CH_3), 17.6 (Si-CH_2), 23.1, 26.1, 28.8, 29.4, 29.5, 29.7, 32.0 and 33.5 (($CH_2)_6$ and $(CH_2)_9$), 40.3 (NCH_3), 65.0 (CO_2CH_2), 112.3 (Ar C3 and C5), 123.0 (=$CHArCO_2R$), 125.0 (Ar C1), 125.6 (Ar C2' and C6'), 128.0 (Ar C2 and C6), 128.2 (Ar C4'), 129.9 (Ar C3' and C5'), 131.3 (=$CHArNR_2$), 142.7 (Ar C1'), 150.4 (Ar C4), 166.6 (C=O). ^{29}Si NMR ($CDCl_3$) δ -21.8 to -23.0 (CH_3-Si-CH_2 and CH_3-Si-CH_3), 6.8, 6.9, 7.1 and 7.2 (terminal Si). IR (KBr, cm^{-1}) 2960, 2920, 2850, 2150 (small peak, Si-H), 1710 (C=O), 1600 (C=C), 1520, 1410, 1360, 1280, 1260, 1180, 1100-1010 (Si-O), 840, 810, 770. UV-vis ($CHCl_3$) λ_{max} = 382 nm. Anal. Calcd for **CPS-1**: C, 67.00; H, 8.64; N, 2.48; Si, 10.52. Found: C, 66.05; H, 8.45; N, 2.30; Si, 10.39.

HPS-2. The procedure was followed as described above using a mixture of 0.25 g (4.0 mmol (Si-H)) of poly(hydromethylsiloxane) and 2.50 g (4.47 mmol) of **MNR-2** in 30 mL of dry toluene. After the final precipitation, 1.38 g (55%) of greenish yellow powder was obtained. ^{1}H NMR ($CDCl_3$) δ 0.05 (Si-CH_3), 0.51 (Si-CH_2), 0.86 (CH_3), 1.29 ((CH_2)$_3$, (CH_2)$_6$ and (CH_2)$_8$), 1.54 (OCH_2CH_2), 1.69 ($CO_2CH_2CH_2$ and $OCHCH_2$), 1.94 ($OCHCH_2$), 2.94 and 3.54 (NCH_2), 3.44 (OCH and OCH_2), 4.25 (CO_2CH_2), 6.87 (Ar H3, H5 and =$CHArCO_2R$), 7.08 (=$CHArNR_2$), 7.38 (Ar H2 and H6), 7.46 (Ar H2' and H6'), 7.96 (Ar H3' and H5'). ^{13}C NMR ($CDCl_3$) δ 14.1 (CH_3), 17.7 (Si-CH_2), 22.6 (CH_3CH_2), 23.1, 25.9, 26.1, 28.8, 29.5, 29.7, 29.8, 30.1, 30.2 and 33.6 ((CH_2)$_2$, (CH_2)$_6$ and (CH_2)$_9$), 30.9 ($OCHCH_2$), 31.7 ($CH_3CH_2CH_2$), 46.6 (NCH_2), 65.0 (CO_2CH_2), 68.0 (OCH_2), 74.5 (OCH), 115.8 (Ar C3 and C5), 124.2 (=$CHArCO_2R$), 125.8 (Ar C2' and C6'), 127.3 (Ar C1), 127.8 (Ar C2 and C6), 128.4 (Ar C4), 129.9 (Ar C3' and C5'), 130.9 (=$CHArNR_2$), 142.4 (Ar C1'), 151.1 (Ar C4), 166.5 (C=O). ^{29}Si NMR ($CDCl_3$) δ -21.4 to -23.2 (CH_3-Si-CH_2), 6.7 (terminal Si). IR (KBr, cm^{-1}) 2920, 2850, 2150 (small peak, Si-H), 1710 (C=O), 1600 (C=C), 1520, 1470, 1410, 1370, 1280, 1260, 1190, 1180, 1110-1010 (Si-O), 840, 810, 770. UV-vis ($CHCl_3$) λ_{max} = 371 nm. Anal. Calcd for **HPS-2**: C, 73.48; H, 9.28; N, 2.25; Si, 4.66. Found: C, 70.02; H, 9.04; N, 1.66; Si, 7.59.

CPS-2. The procedure was followed as described above using a mixture of 0.58 g (4.0 mmol (Si-H)) of poly(hydromethyl-dimethylsiloxane) and 2.50 g (4.47 mmol) of **MNR-2** in 30 mL of dry toluene. After the final precipitation, 1.70 g (60%) of greenish yellow powder was obtained. ^{1}H NMR ($CDCl_3$) δ 0.04 (Si-CH_3), 0.49 (Si-CH_2), 0.89 (CH_3), 1.30 ((CH_2)$_3$, (CH_2)$_6$ and (CH_2)$_8$), 1.56 (OCH_2CH_2), 1.72 ($CO_2CH_2CH_2$ and $OCHCH_2$), 1.95 ($OCHCH_2$), 2.96 and 3.55 (NCH_2), 3.44 (OCH and OCH_2), 4.27 (CO_2CH_2), 6.89 (Ar H3 and H5), 6.94 (=$CHArCO_2R$), 7.11 (=$CHArNR_2$), 7.40 (Ar H2 and H6), 7.48 (Ar H2' and H6'), 7.97 (Ar H3' and H5'). ^{13}C NMR ($CDCl_3$) δ 1.2 (Si-CH_3), 1.9 (terminal Si-CH_3), 14.1 (CH_3), 17.6 (Si-CH_2), 22.6 (CH_3CH_2), 23.1, 25.9,

26.1, 28.8, 29.4, 29.7, 30.1, 30.2 and 33.5 ($(CH_2)_2$, $(CH_2)_6$ and $(CH_2)_9$), 30.9 ($OCHCH_2$), 31.7 ($CH_3CH_2CH_2$), 46.6 (NCH_2), 65.0 (CO_2CH_2), 68.0 (OCH_2), 74.4 (OCH), 115.8 (Ar C3 and C5), 124.2 (=$CHArCO_2R$), 125.8 (Ar C2' and C6'), 127.3 (Ar C1), 127.8 (Ar C2 and C6), 128.5 (Ar C4'), 129.9 (Ar C3' and C5'), 131.0 (=$CHArNR_2$), 142.4 (Ar C1'), 151.1 (Ar C4), 166.5 (C=O). ^{29}Si NMR ($CDCl_3$) δ -21.8 to -22.9 (CH_3-Si-CH_2 and CH_3-Si-CH_3), 6.8, 6.9, 7.1 and 7.2 (terminal Si). IR (KBr, cm^{-1}) 2960, 2910, 2850, 2140 (small peak, Si-H), 1710 (C=O), 1600 (C=C), 1520, 1470, 1410, 1370, 1280, 1260, 1190, 1180, 1110-1010 (Si-H), 840, 810, 770. UV-vis ($CHCl_3$) λ_{max} = 369 nm. Anal. Calcd for **CPS-2**: C, 69.01; H, 9.21; N, 1.99; Si, 8.42. Found: C, 67.65; H, 9.09; N, 1.64; Si, 9.12.

Results

Synthesis. 4-(4'-n-Hexyloxy-1-piperidino)benzaldehyde, **5**, which is needed for the preparation of the stilbene precursor was synthesized as shown in Scheme 1. The success of each of the reactions was clearly monitored by ^1H NMR (Table IX). The first step was employed to protect the amino group of 4-hydroxypiperidine, **1**, prior to the alkylation of the hydroxyl group. Anhydrous potassium carbonate was needed to neutralize both the acetic acid formed in the reaction and any protonated amine. This would ensure that the amino group is free to react with the acetic anhydride, thus allowing the reaction go to completion. The reaction mixture was not washed with H_2O because the product is more soluble in H_2O than in any organic solvents. The acylated product **2** was white crystal and highly hygroscopic. The ^1H NMR spectrum showed the splitting of one of the multiplets corresponding to H1 and H5 into two multiplet signals and shifted downfield at 3.72 ppm and 4.04 ppm.

Scheme I

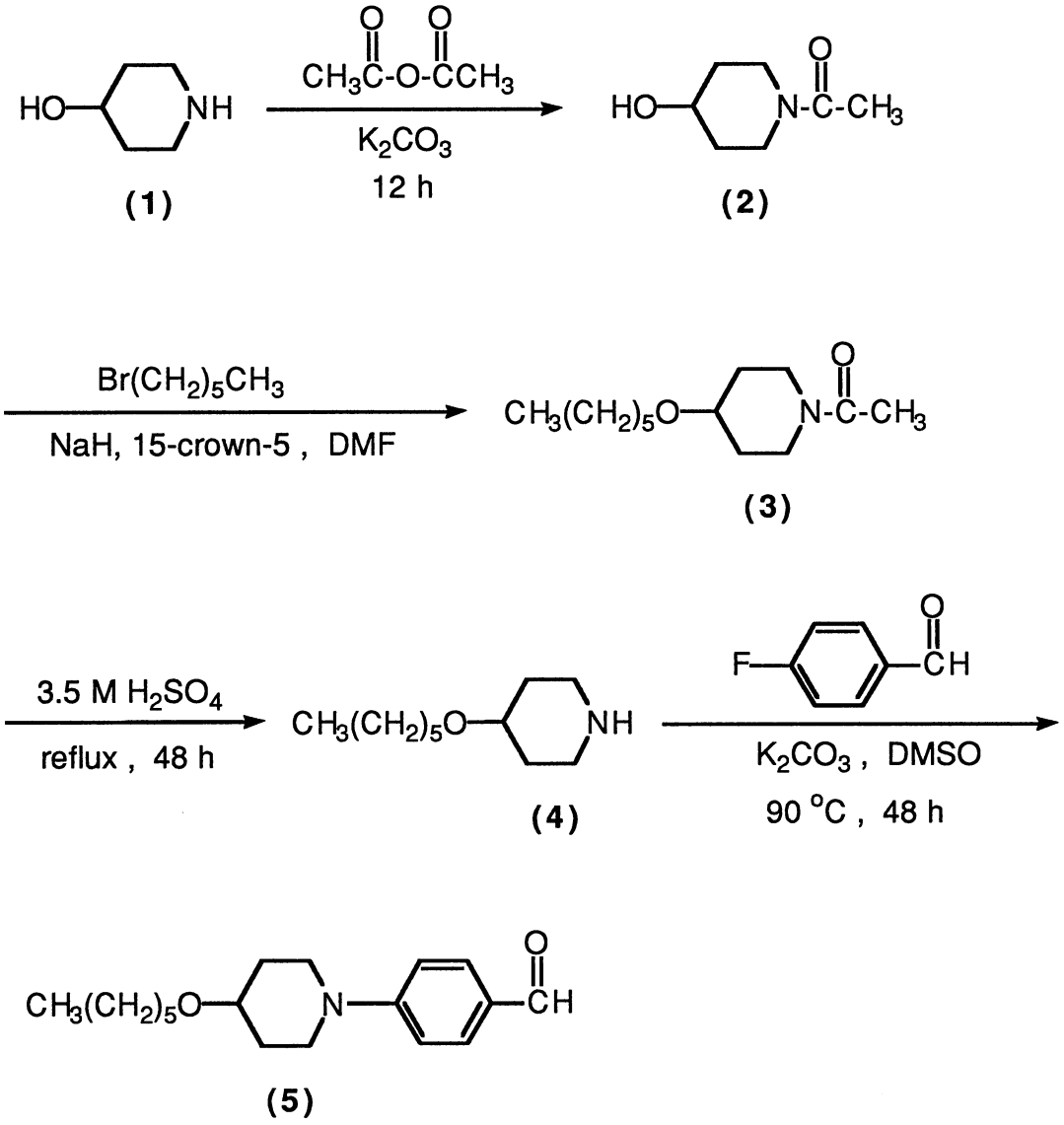
HO
NH
(1)
CH3C-O-CCH3
K2CO3
12 h
HO
N-C-CH3
(2)
Br(CH2)5CH3
NaH, 15-crown-5 , DMF
CH3(CH2)5O
N-C-CH3
(3)
3.5 M H2SO4
reflux , 48 h
CH3(CH2)5O
NH
(4)
F
CH
K2CO3 , DMSO
90 °C , 48 h
CH3(CH2)5O
N
CH
(5)

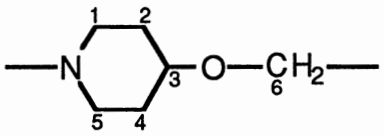

Table IX. ^{1}H NMR Chemical Shifts of Compounds **1 - 5**

compound	chemical shift, ppm						
	H1 and H5			H2 and H4		H3	H6
1	2.60	3.08		1.40	1.89	3.68	-
2	3.21	3.72	4.04	1.52	1.87	3.90	-
3	3.27	3.65	3.90	1.57	1.83	3.47	3.47
4	2.60	3.08		1.41	1.91	3.32	3.44
5	3.21	3.70		1.70	1.94	3.61	3.47

For the conversion of **2** to **3**, NaH dispersed in mineral oil was used instead of NaH powder since in an earlier experiment where NaH powder was used, a very small amount of the product was obtained. Added 15-crown-5 increased the reactivity of the alkoxide ion. The Na^+ was effectively trapped by the crown ether, making the alkoxide exposed to the alkyl halide. Due to the hygroscopic nature of **2**, the second step has to be done immediately after its collection from distillation. Otherwise, one has to keep it under nitrogen and prior to the second reaction, one has to dry **2** at room temperature under vacuum. This reaction produced a viscous colorless liquid. The ^{1}H NMR spectrum of **3** showed the upfield shifting of H3 from 3.90 ppm to 3.47 ppm with the overlapping of the triplet corresponding to H6.

The deprotection of **3** was a simple acid-catalyzed hydrolysis reaction. During the work-up, it is important to make the solution basic to extract the amine product in the ether

layer. After reduced pressure distillation, a colorless liquid was obtained. The ^{1}H NMR spectrum of **4** showed the two multiplet signals of H1 and H5 at the same positions as in **1**. The multiplet at 3.32 ppm for H3 separated from the triplet at 3.44 ppm of H6.

The final step is the production of **5** which was carried out under standard experimental conditions.[17] Anhydrous K_2CO_3 in the mixture was needed to neutralize the HF formed during the reaction. When the solution was poured into H_2O, it is necessary to stir the mixture thoroughly to remove the DMSO clinging to the precipitate. After several recrystallizations, a white feather-like solid was obtained. The ^{1}H NMR spectrum showed the downfield shifting of the multiplets corresponding to H1 and H5 from 2.60 ppm to 3.11 ppm and 3.08 ppm to 3.70 ppm. Moreover, one of the multiplets of H2 and H4 shifted downfield from 1.41 ppm to 1.70 ppm.

The preparation of the methyl stilbenes, **9** and **10**, and the monomers, **MNR-1** and **MNR-2** was performed as illustrated in Scheme 2. The phosphonate **8** was prepared from chlorinated methyl ester **7** with triethyl phosphite. All succeeding reactions should be carried out in the dark because of possible trans to cis isomerization of the stilbenes. As shown in the ^{1}H NMR spectra of the methyl stilbenes, **9** and **10**, only the trans isomers were present. The solubility of **10** in organic solvents has improved dramatically as compared to **9** because of the incorporation of the *n*-hexylpiperidino group at one end of the stilbene. During the preparation of NMR solutions, it was observed that **9** was slightly soluble in chloroform while **10** was very soluble in chloroform.

The transesterification of the methyl esters, **9** and **10**, was performed with the use of $Ni(acac)_2$[18] as the catalyst instead of concentrated H_2SO_4, which is commonly used. For this reaction to proceed faster, vigorous refluxing was needed to drive off the methyl alcohol which is formed in the reaction. It was also important not to use an excess of solvent. At the end of the reaction, TLC showed the absence of the starting methyl ester, thus making it easy to get pure products and high yields. The entire synthesis proceeded

Scheme II

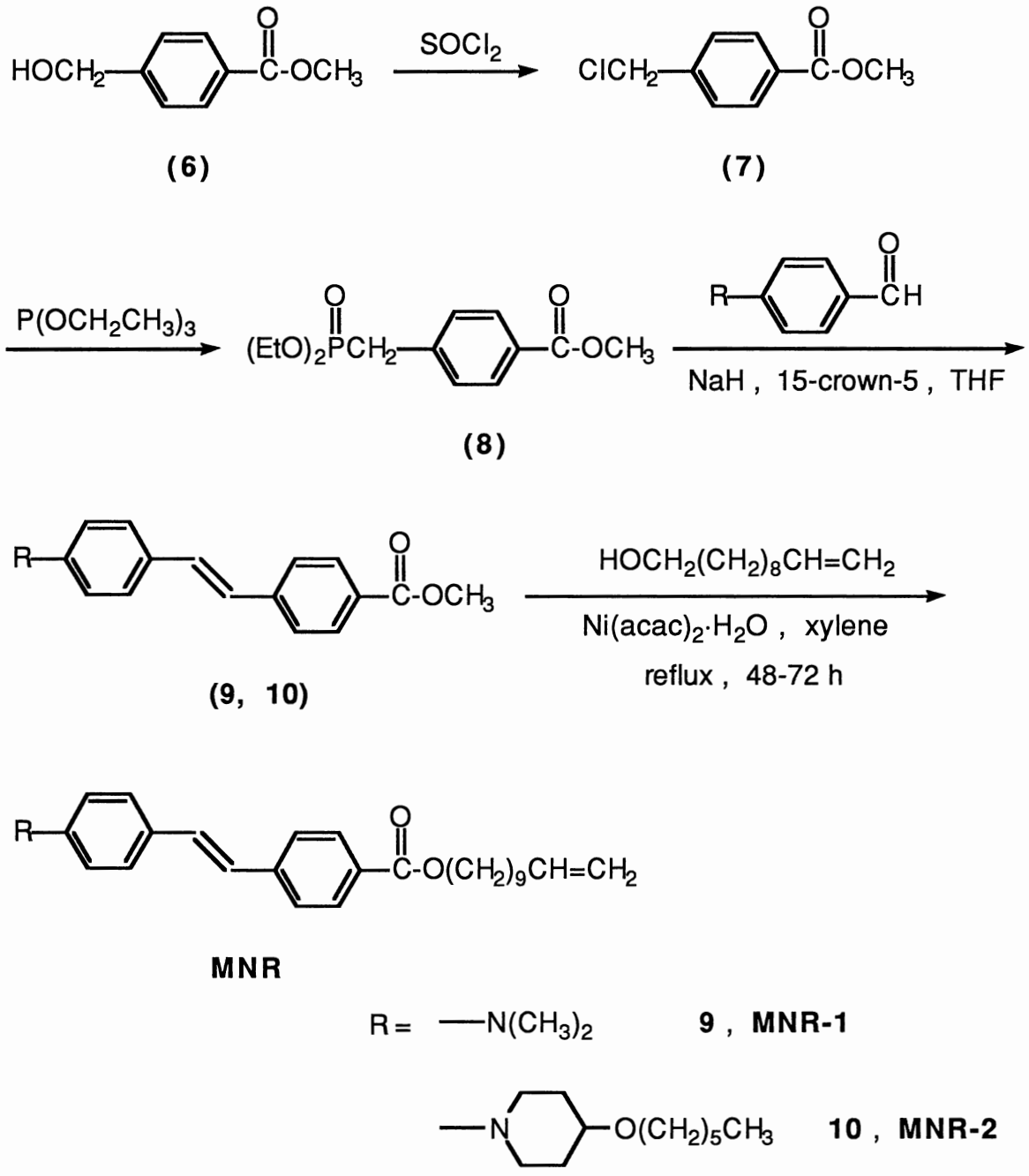
HOCH2
C-OCH3
SOCl2
ClCH2
C-OCH3
(6)
(7)
P(OCH2CH3)3
(EtO)2PCH2
C-OCH3
R
CH
NaH , 15-crown-5 , THF
(8)
R
C-OCH3
HOCH2(CH2)8CH=CH2
Ni(acac)2·H2O , xylene
reflux , 48-72 h
(9, 10)
R
C-O(CH2)9CH=CH2
MNR
R = —N(CH3)2
9 , MNR-1
—N
O(CH2)5CH3
10 , MNR-2

without detectable isomerization of the stilbene double bond as shown in the ^1H NMR spectra of the monomers, **MNR-1** and **MNR-2**.

Hydrosilylation of the monomers with either poly(hydromethyl)siloxane or the copolymer of 50% (hydromethyl)siloxane - 50% (dimethyl)siloxane in dry toluene was carried out in the presence of chloroplatinic acid in isopropyl alcohol (Scheme 3). An amount of triethylamine equivalent to the H_2PtCl_6 was added to this catalyst solution to neutralize the HCl, which otherwise would protonate the amino group of the monomers. Upon the addition of triethylamine, the solution became cloudy. Even after refluxing the mixtures for 48 hours, a small residual 2160 cm^{-1} band remained in the IR spectrum of the mixture, so 1-octene equimolar to the original amount of Si-H in the starting polysiloxane was added to try to consume remaining Si-H groups. This would enable most if not all the Si-H to react with the smaller alkene molecule. The ^{29}Si NMR spectra of the final side-chain polysiloxanes showed no peak at -37 ppm for the Si-H groups. However, ^1H NMR spectra indicated that 100 % conversion was not attained as shown by the presence of a small peak at 4.7 ppm for Si-H groups in the starting polysiloxanes. The % of unreacted Si-H groups in the polymers was estimated, by cut and weigh method. The octyl side-chain of **HPS-1** and **CPS-1** can also be estimated from the methyl signal of the octyl group in the ^1H NMR. However, this signal is superimposed with the methyl signal of the hexyl group for **HPS-2** and **CPS-2**, and so no estimate can be done on the octyl side-chain content. The percent conversion and the octyl side-chain content were also estimated from the results of elemental analyses of the polysiloxanes. Different combinations of Si-H, Si-octyl and Si-mesogen (Si-methyl was included for the copolymers) repeat units were considered, and the % C, H, N and Si were calculated. The combination that best fit the values (all elements were considered) obtained from the elemental analyses was selected. A summary of the calculated values is shown in Table X.

Table X. Analyses of Side-Chain Polysiloxanes on ^1H NMR and Elemental Analysis

polymer	% conversion of SiH		% octyl side-chain		% mesogen side chain	
	^1H NMR	EA	^1H NMR	EA	1H NMR	EA
HPS-1	91	96	12	29	79	67
CPS-1	93	100	10	11	83	89
HPS-2	94	85	-	27	-	58
CPS-2	93	100	-	11	-	89

GPC was used to check the purity of the polymers in each precipitation. At the final precipitation, **HPS-1** and **CPS-1** showed less than 1% monomer content while **HPS-2** and **CPS-2** showed 2 and 5% monomer content, respectively. GPC analyses of the molecular weights based on polystyrene standards and residual monomer contents are reported in Table XI.

Scheme III

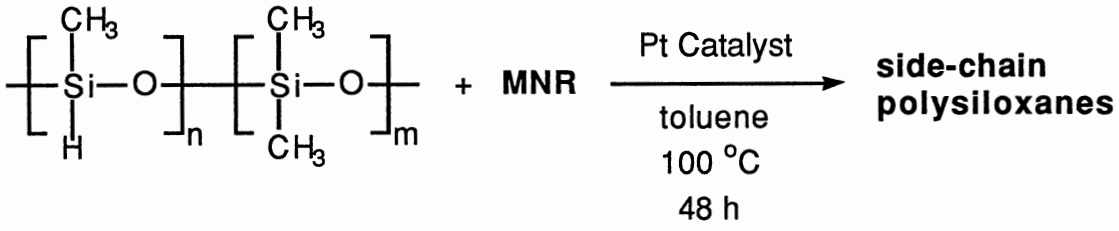

The purified polymers have molecular weight distributions, M_w/M_n, values ranging from 1.4 to 1.9. The M_w/M_n values for the SCLC homopolysiloxanes were lower than the starting polysiloxanes (Table I), which is due to the fractionation of oligomers. The same thing was observed for the SCLC copolysiloxanes. It has been reported that GPC analyses using polystyrene standards underestimate the molecular weights of SCLCPs

because the hydrodynamic volume of a comb-like polymer is smaller than that of polystyrene of the same weight.[19]

Table XI. GPC Analyses of Side-Chain Polysiloxanes

polymer	M_n	M_w	M_w/M_n	% monomer
HPS-1	6800	9800	1.4	<1
CPS-1	5400	8800	1.5	<1
HPS-2	19 400	37 600	1.9	2
CPS-2	7200	10 500	1.5	5

Liquid Crystal Phases. Phase transitions of the monomers and the polysiloxanes measured by DSC and microscopy are summarized in Table XII. The phase assignments are based on powder X-ray diffraction and polarizing microscopy.

Table XII. Phase Transition Temperatures of Monomers and Polysiloxanes

Sample	Phase transition temperature[a], °C (ΔH, kcal/mol of mesogen)								
MNR-1			C	146	I				
HPS-1			C	167-195 (4.84)	N	215[b]	I		
CPS-1	G	-35	C	146-178 (7.06)	S_A	183[b]	I		
MNR-2			C	109 (0.54)	S_B	172 (1.52)	S_A	183	I
HPS-2			C	110-118 (0.15)	S_B[c]	192-211 (1.0)	N	258[b]	I
CPS-2	G	-43	C	112-126 (0.27)	S_B	182-197 (1.04)	S_A	220[b]	I

[a] C = orthorhombic crystal or smectic E, I = isotropic liquid, N = nematic, G = glass, S_A = smectic A, S_B = smectic B. [b] Transition temperatures were determined by microscopy. All other data is from DSC. [c] Possibly an ordered nematic.

Two highly ordered mesophases of **MNR-2** were observed by thermal analysis while only a melting transition was observed for **MNR-1**. This shows that the hexyloxypiperidino chain increased the flexibility of the alkyl amino end of the dipolar stilbene, thus giving it a wider range of liquid crystalline properties. The powder X-ray diffraction pattern of the high temperature transition phase, Figure 7, of **MNR-2** showed a sharp peak at the small angle region, which is an indication of the presence of layers, and a diffuse peak at the wide angle region, which meant that the molecules are randomly arranged within the layers. This X-ray pattern is characteristic for smectic A or C. Figure 8 shows the X-ray pattern at 165 ^{o}C, which exhibits a sharp peak in the wide angle region in addition to the sharp peaks in the small angle region. This outer reflection corresponds to 110 and 200 reflections which indicates an ordered structure of the molecules within the smectic layers. The mesophase assigned at this temperature is smectic B. **MNR-2** exhibited the distinctive simple focal conic texture of a smectic A phase as shown in Figures 9A and 9B. The characteristic feature of the X-ray pattern of the powder-like sample of **MNR-1**, shown in Figure 10, pointed out a well-ordered structure in which the molecular long axes are orthogonal to layer planes. At first, this phase is thought to be a smectic E phase. However, the texture obtained in the microscope under crossed polarized light (Figure 11) suggests an orthorhombic crystalline structure.

There was no evidence of any glass transition for **HPS-1** by DSC in the range from -123 ^{o}C to 146 ^{o}C. This might be due to the small volume fraction of the siloxane backbone compared to the side-chain mesogen, making the glass transition too weak to detect. With strong dipole-dipole interactions between the mesogenic side chains, the polymers tend to behave as semicrystalline rather than glassy. Moreover, with the long flexible methylene spacer chain, the decoupling of the mesogenic moieties and the polymer backbone was maximized, thus promoting partial crystallization of the side chain. Due to the high viscosity of the polymer, broad peaks are observed in DSC scans. There is a tendency of the mesogenic side chains to behave differently from one domain to the other

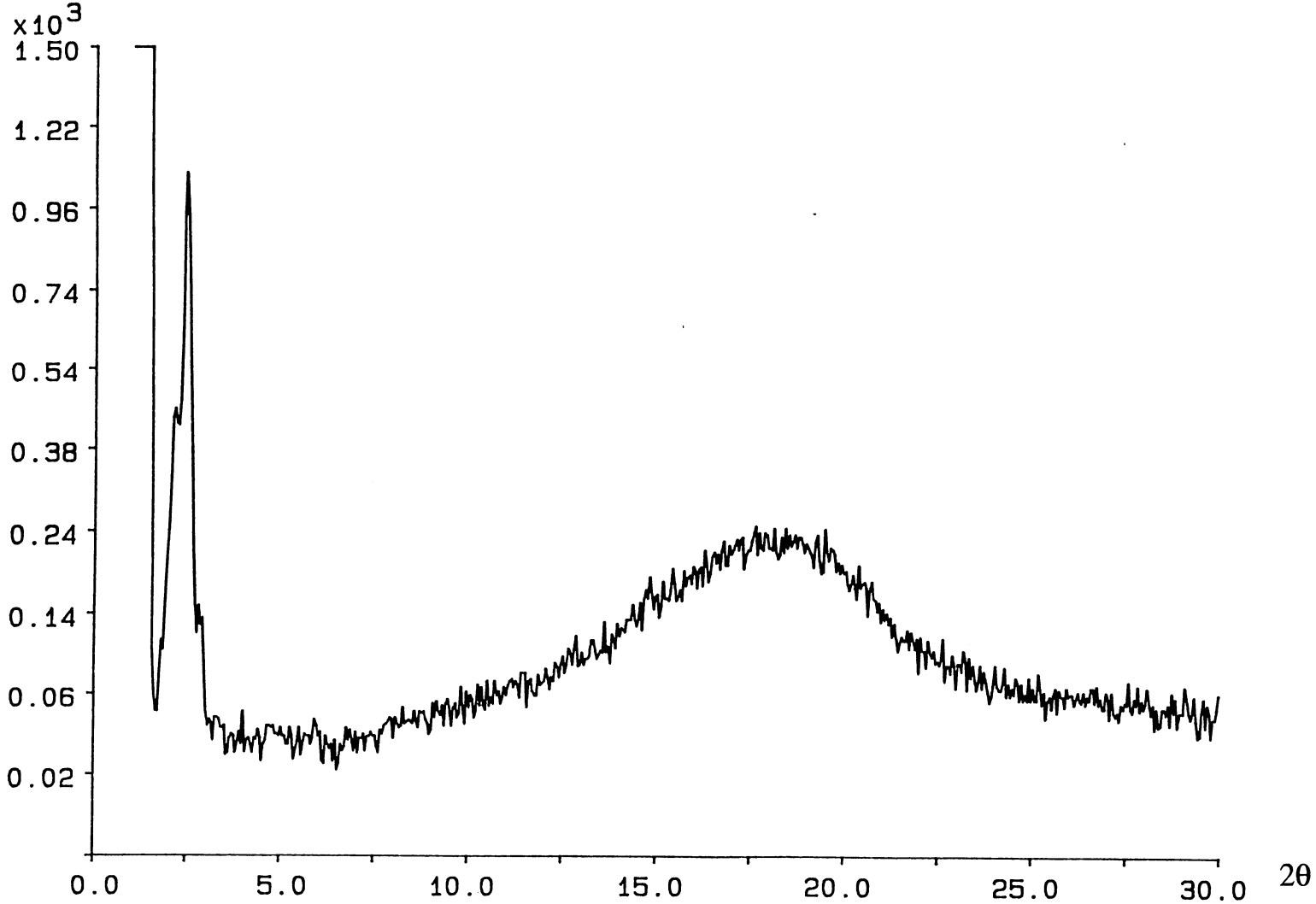

Figure 7. Powder X-ray diffraction pattern of **MNR-2** at 177 °C.

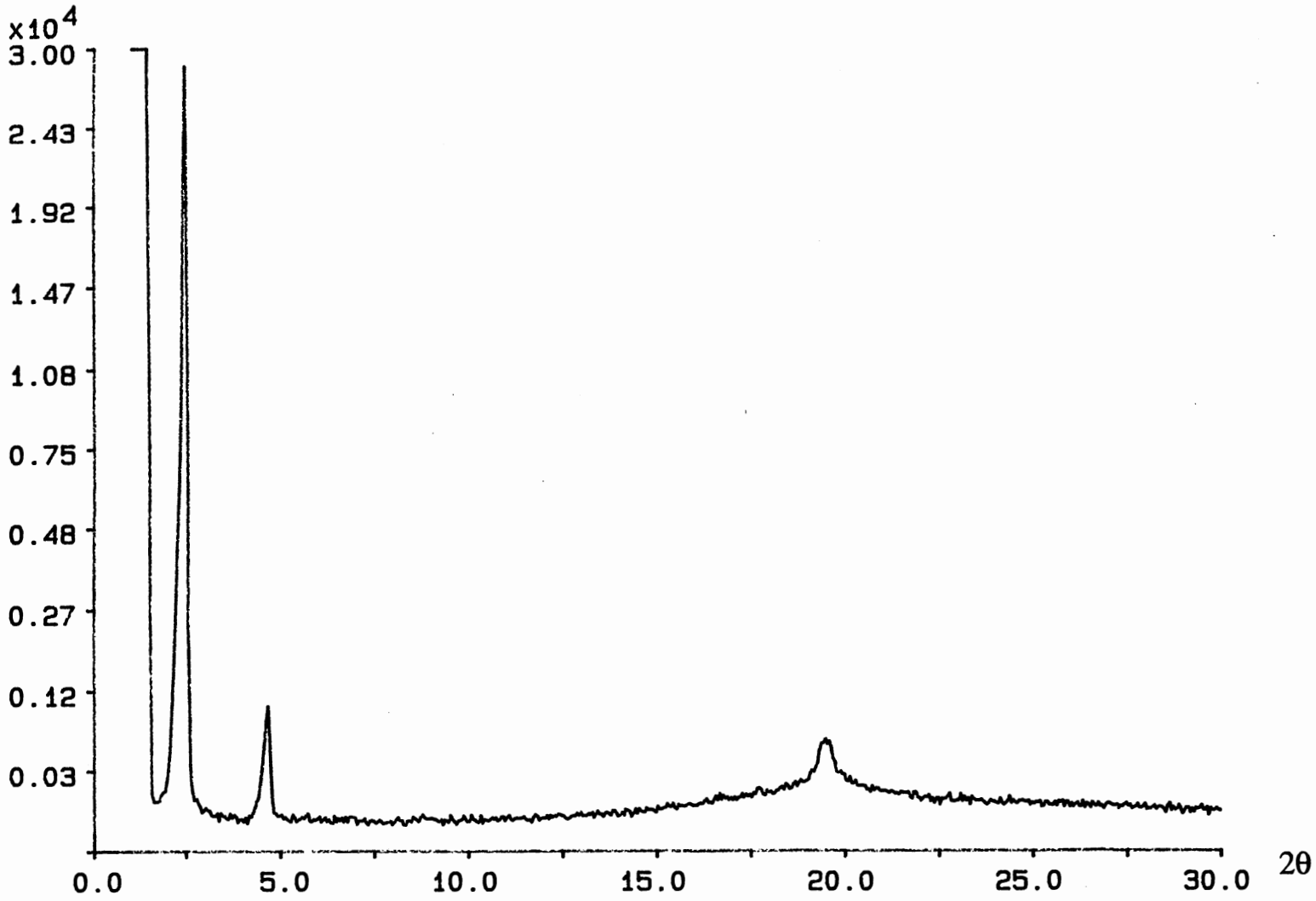

Figure 8. Powder X-ray diffraction pattern of **MNR-2** at 165 °C.

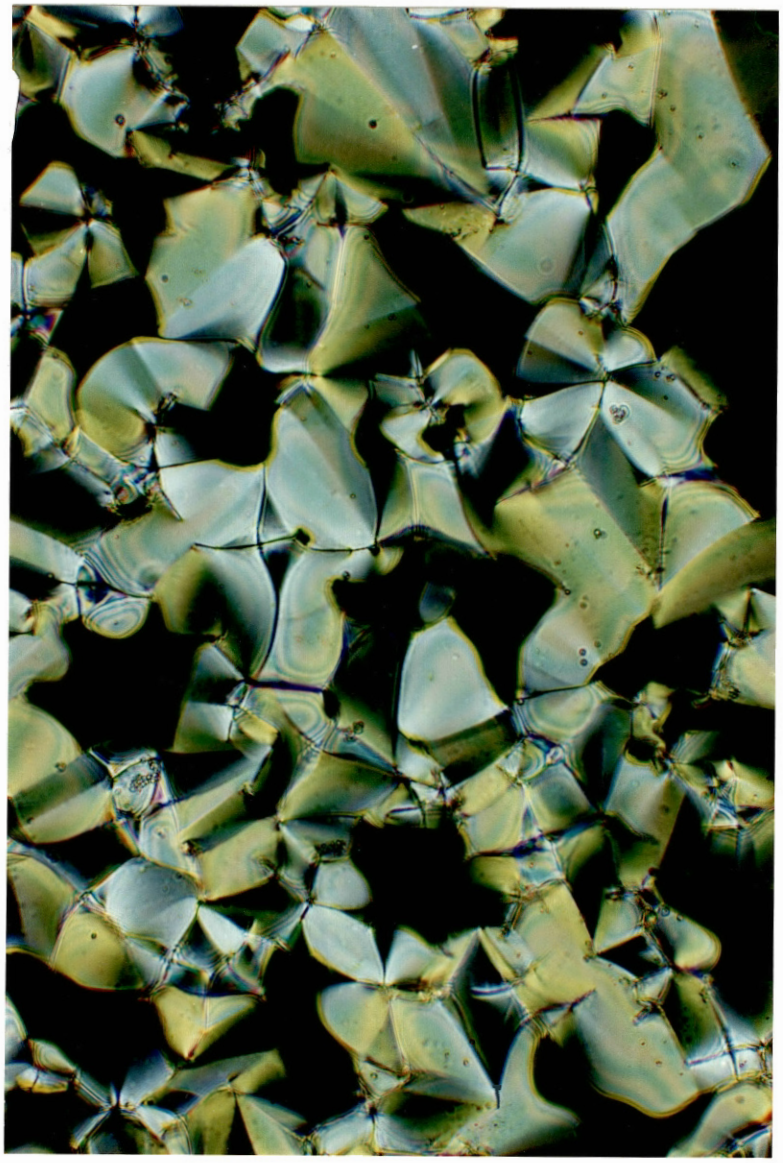

Figure 9A. Focal conic texture between crossed polarizers (300x) of **MNR-2** obtained at 165 ^{o}C upon cooling from the isotropic phase.

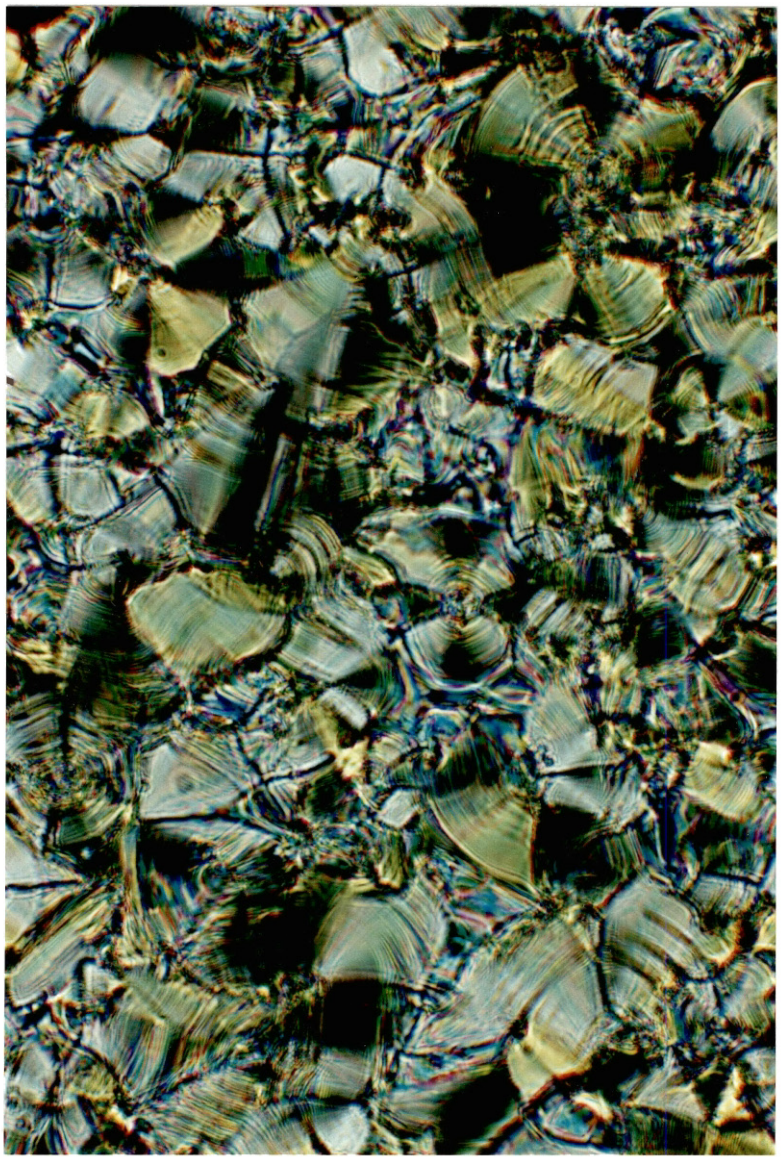

Figure 9B. Microscopic texture (300x) of **MNR-2** at 100 °C under crossed polarized light.

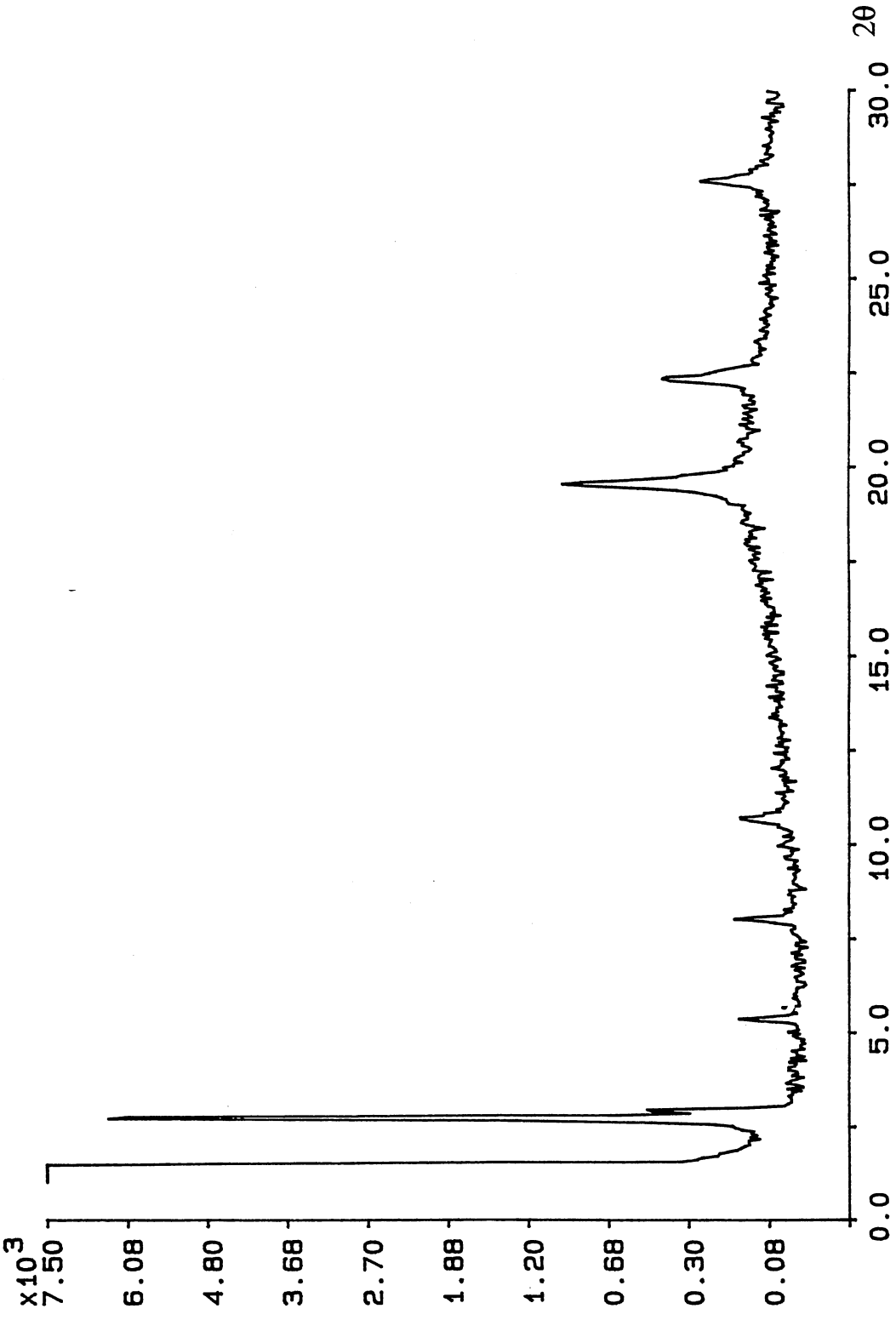

Figure 10. Powder X-ray diffraction of **MNR-1** at 135 °C.

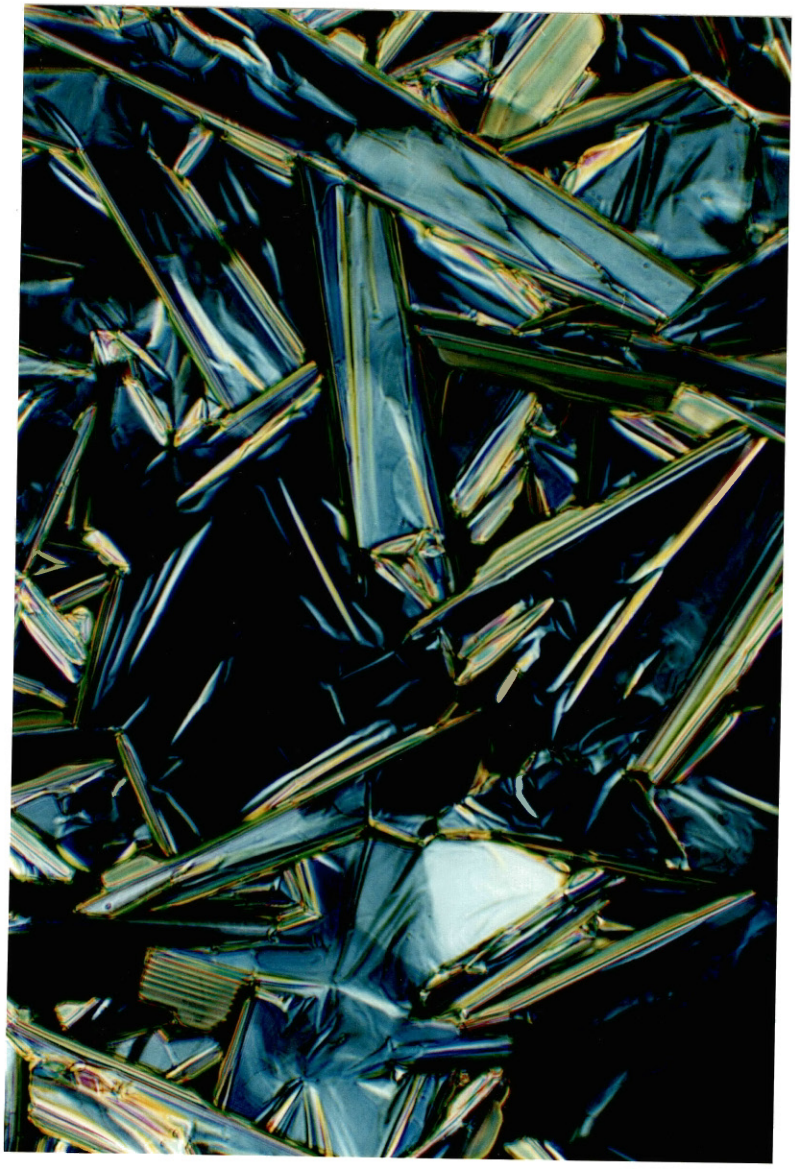

Figure 11. Microscopic texture between crossed polarizers (300x) of **MNR-1** at 139 °C.

and could experienced different heats of transition. Figures 12A and 12B show thermograms of **HPS-1** at different scan rates. Except for the first heating and cooling curves, there is no significant change in the phase transition temperatures and no resolution of the overlapping peaks. Therefore, only one mesophase was assigned for **HPS-1**, although the thermograms show three overlapping transitions at about 167 °C to 195 °C. I first thought that the lone transition was isotropization. However, when observed under the microscope with crossed polarized light, the isotropization temperature was much higher than that obtained in the DSC thermogram. The thermogram of a blend containing 90 wt% **HPS-1** and 10 wt% **MNR-1** was investigated to check the effect of having a substantial amount of monomer in the polymer sample. On the first heating scan, the melting transition of the monomer was evident (Figure 12C). However, in the second heating scan, this transition disappeared and only the overlapping peaks are observed. The phase transition temperature range recorded in the second heating is almost the same as the one obtained in "pure" **HPS-1**. The textural analysis of **HPS-1** was very difficult, due mainly to the high viscosity of the polymer even just below the isotropization temperature. Annealing at the desired temperature for hours or even days did not give a recognizable texture as shown in Figure 13. This is typical of high molecular weight smectic polymers. The powder X-ray diffraction pattern of the homopolysiloxane, **HPS-1**, showed the presence of a nematic phase. Figure 14 shows a diffuse peak in the wide angle region, which indicates the disordered arrangement of the molecules, although there is orientational order of the long molecular axes along the director. The absence of any sharp peaks in the small angle region meant the absence of translational periodicity along any direction. The DP of the homopolysiloxanes is 60, thus giving a very viscous polymer. The side-chain mesogens have difficulty in arranging themselves in layers, and so the less ordered mesophase was observed.

A very weak, wide glass transition with a midpoint at -35 °C, shown in Figure 15, was observed for **CPS-1** in the low temperature DSC scan. At the high temperature scan

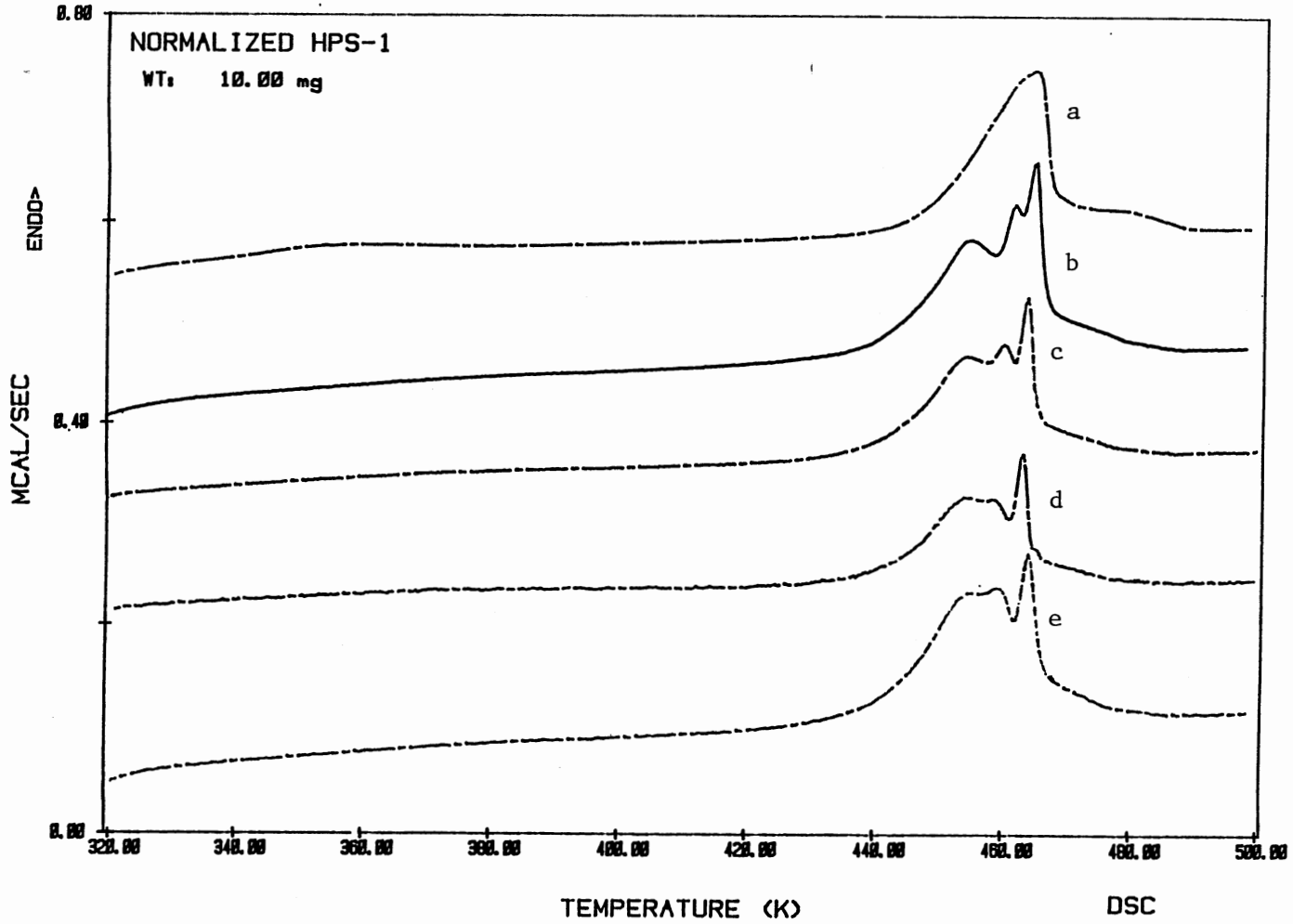

Figure 12A. Repeated DSC analyses of **HPS-1** at different heating rates: (a) first at 20 K/min; (b) second at 20 K/min; (c) 10 K/min; (d) 5 K/min; (e) 20 K/min.

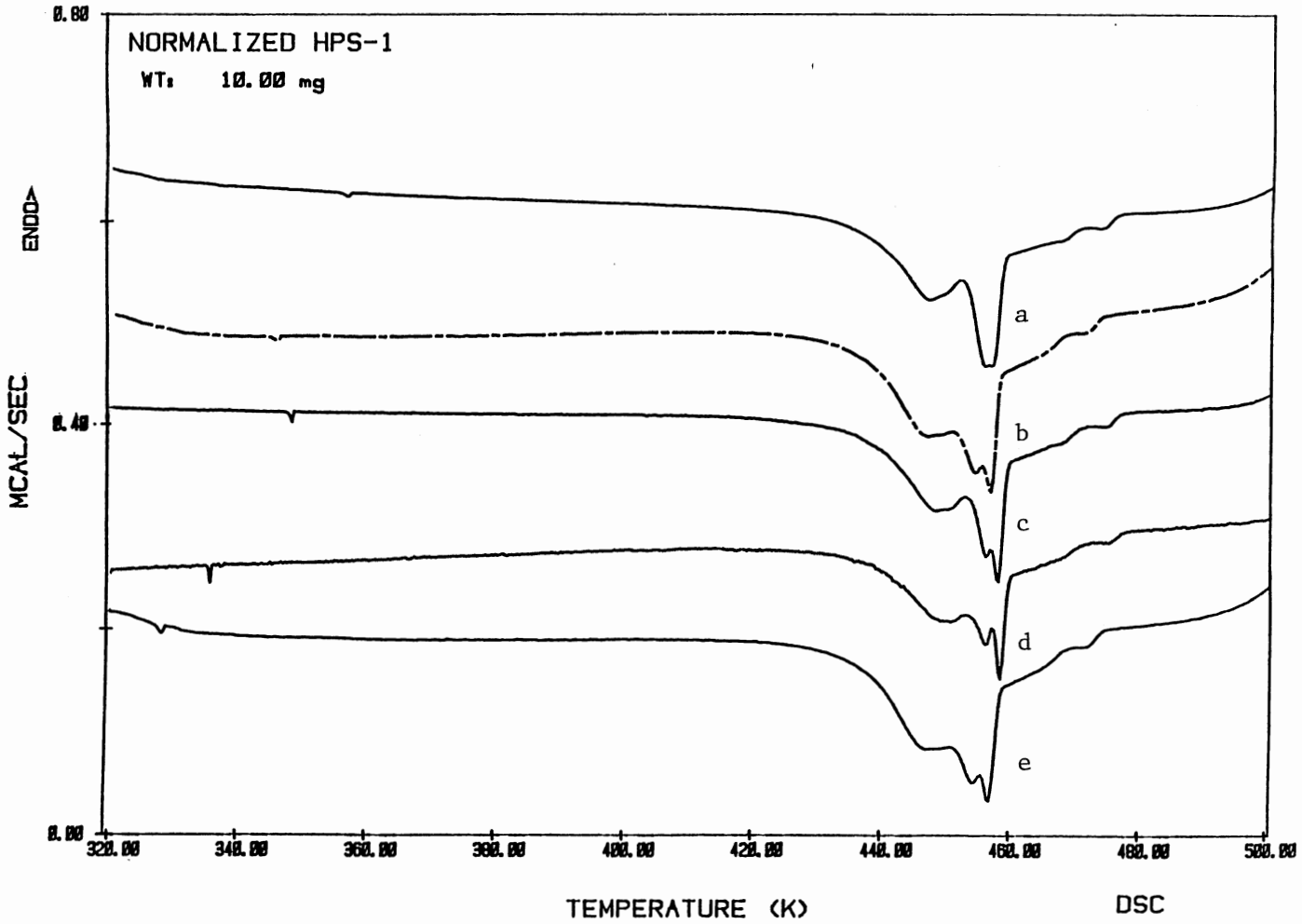

Figure 12B. Repeated DSC analyses of **HPS-1** at different cooling rates: (a) first at 20 K/min; (b) second at 20 K/min; (c) 10 K/min; (d) 5 K/min; (e) 20 K/min.

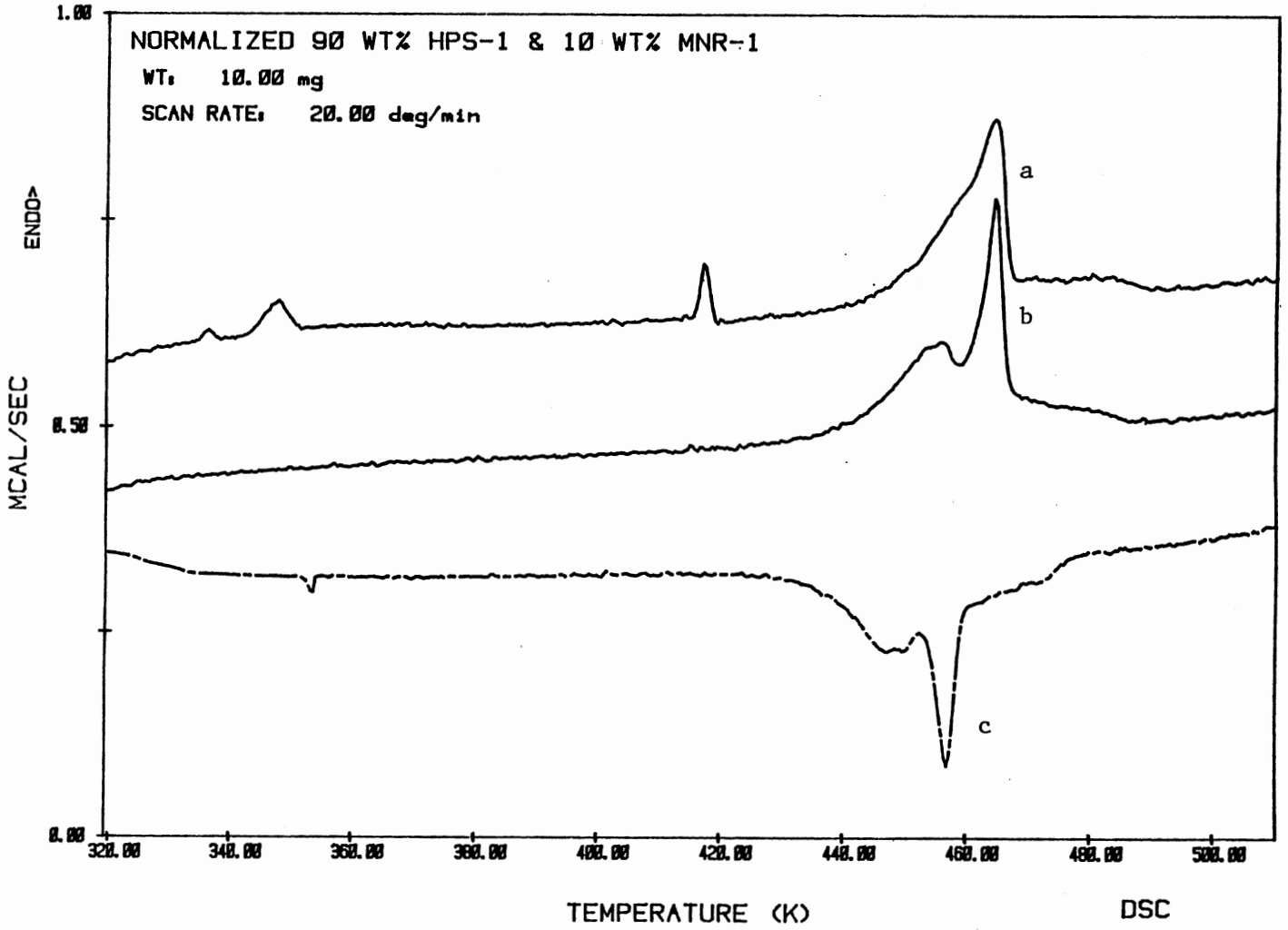

Figure 12C. DSC analyses of 90 wt% **HPS-1** and 10 wt% **MNR-1** blend at 20 K/min: (a) first heating; (b) first cooling; (c) second heating.

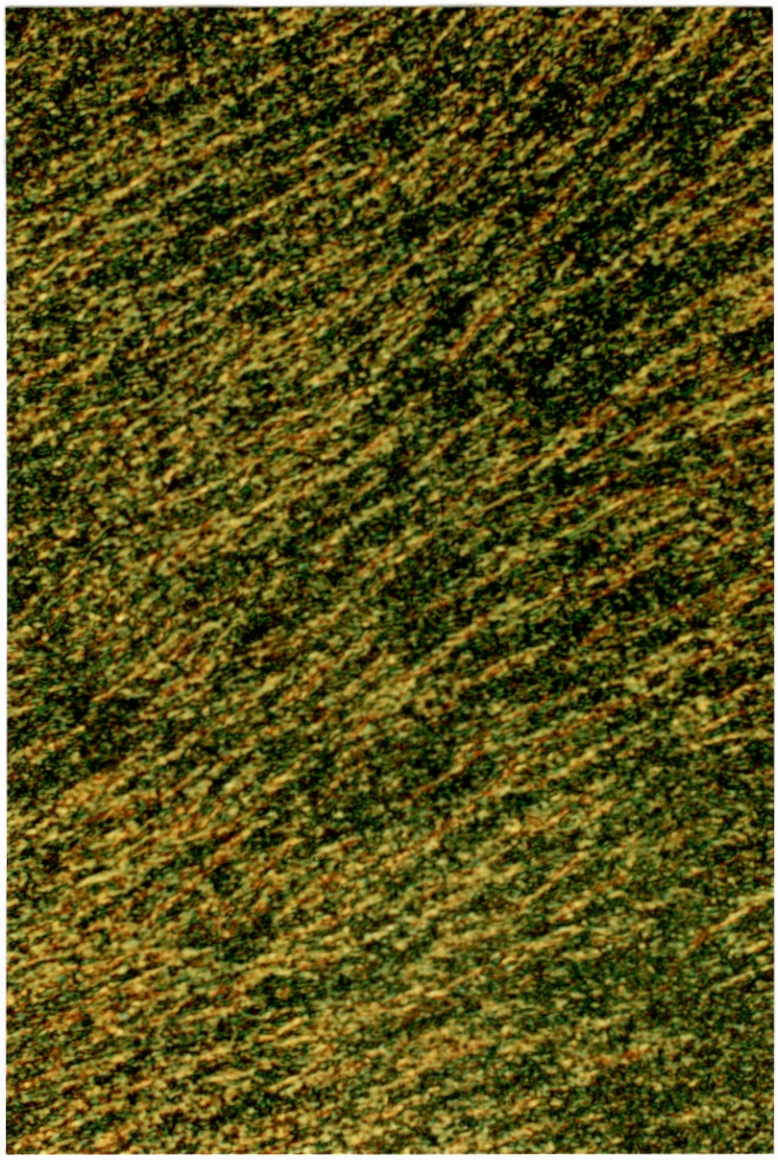

Figure 13. Microscopic texture between crossed polarizers (300x) of **HPS-1** after overnight annealing at 190 °C.

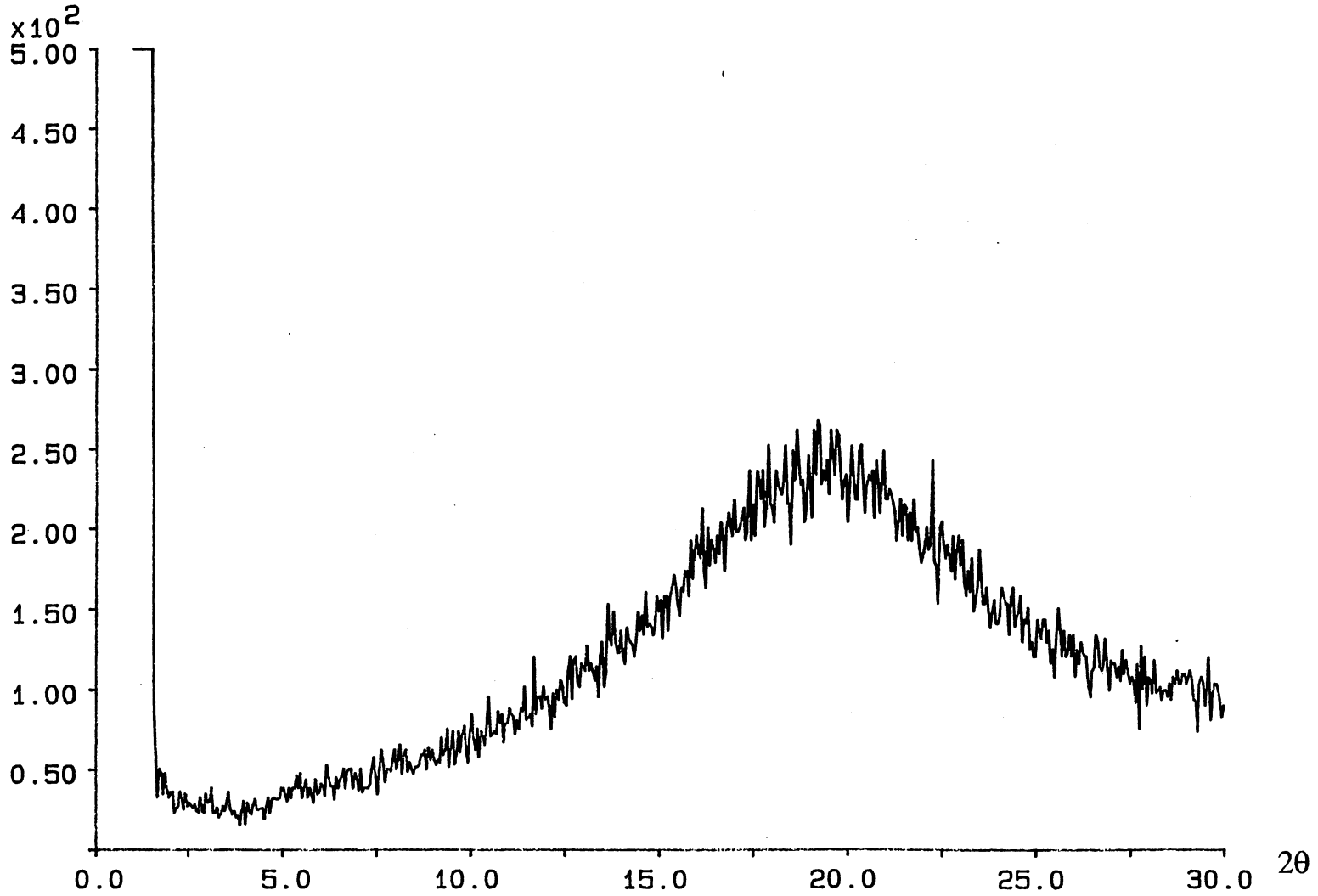

Figure 14. Powder X-ray diffraction pattern of **HPS-1** at 210 °C.

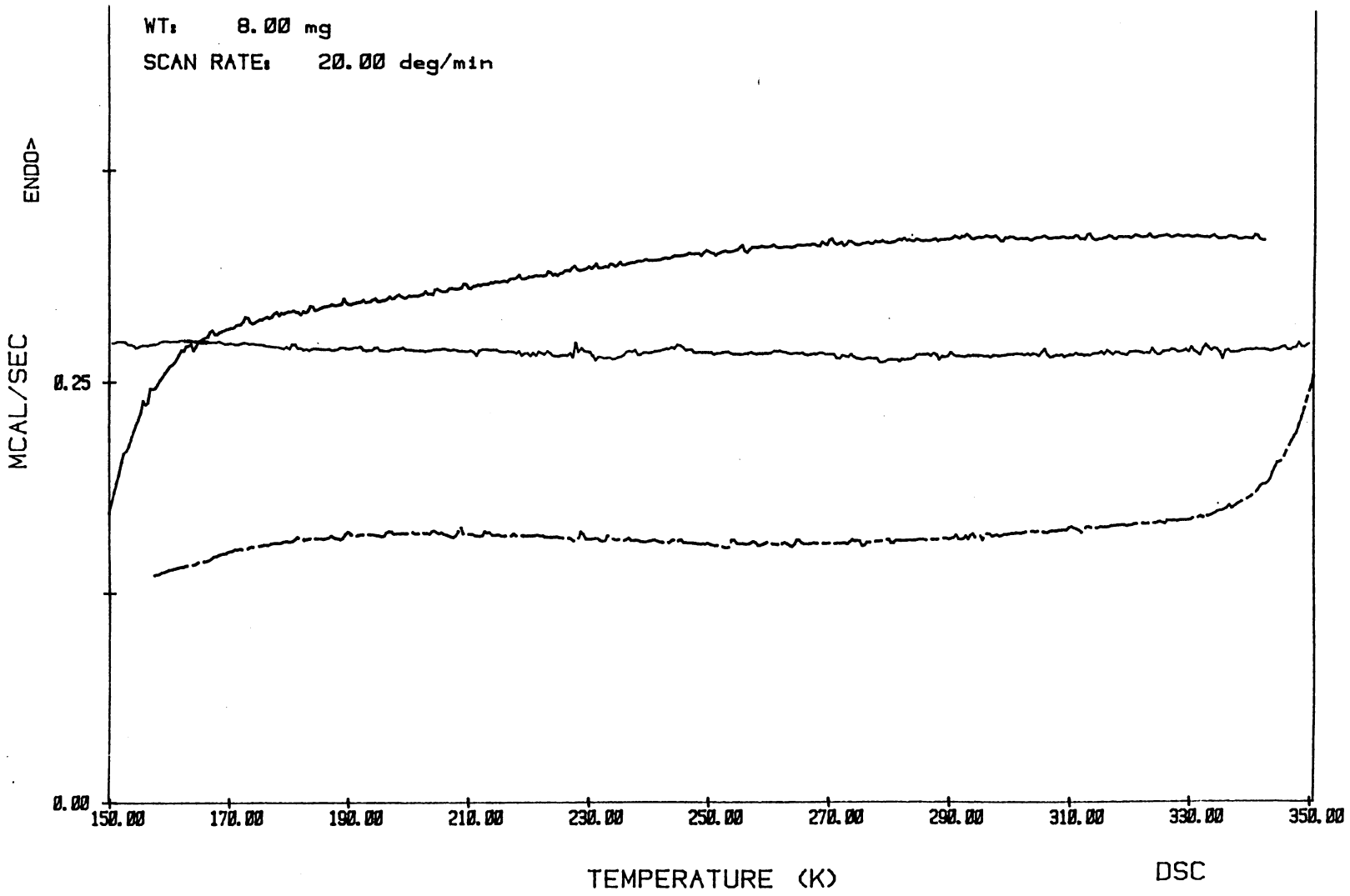

Figure 15. Subambient DSC thermograms of **CPS-1** at 20 K/min.

(Figure 16), only one mesophase was assigned, although it shows two overlapping peaks. As explained earlier, this is due to the high viscosity of the polymer and the way the mesogenic side chains order themselves. Similar thermograms were obtained at different scan rates. The X-ray pattern at 177 °C, shown in Figure 17, showed sharp peaks in the small angle region which is an indication of smectic layers, and a diffuse peak in the wide angle region, characteristic of the S_A phase. Figure 18 shows a fine grained texture under the microscope with plane polarized light.

The hexyloxypiperidinostilbene containing homopolysiloxane, **HPS-2**, like **HPS-1** showed no glass transition. At the high temperature DSC scan (Figure 19), two phase transitions and the usual overlapping of peaks were observed. Varying the scan rate did not show significant change in the thermograms. **HPS-2** had both a high temperature nematic and an ordered phase initially assigned as S_B from the powder X-ray diffraction pattern at 120 °C. However, this phase of **HPS-2** did not show any reflections in the small angle region, Figure 20, which means the absence of layers. This gives doubts on the presence of smectic B phase. It is possible that this mesophase is an ordered nematic with hexagonal structure rather than smectic B. Friedzon and his coworkers[20] reported a similar X-ray pattern and suggested that it was due to a new phase, N_B, in which the mesogenic groups were packed in a hexagonal array but without translational order in the direction of their long axes. Again, no sharp peaks were observed in the small angle region for the crystalline structure of **HPS-2** as shown in Figure 21. As in **HPS-1**, no microscopic texture was obtained for **HPS-2**.

Figure 22 shows a similar weak, wide glass transition with midpoint at -43 °C for **CPS-2**. As in **HPS-2**, two phase transitions, with overlapping peaks, were observed for **CPS-2** as shown in Figure 23. There was no significant change in the thermograms with varying scan rates. In addition to the observed high temperature S_A phase, which was assigned from the X-ray diffraction at 205 °C (Figure 24), a low temperature mesophase was observed for **CPS-2**, and assigned an S_B structure. The powder X-ray

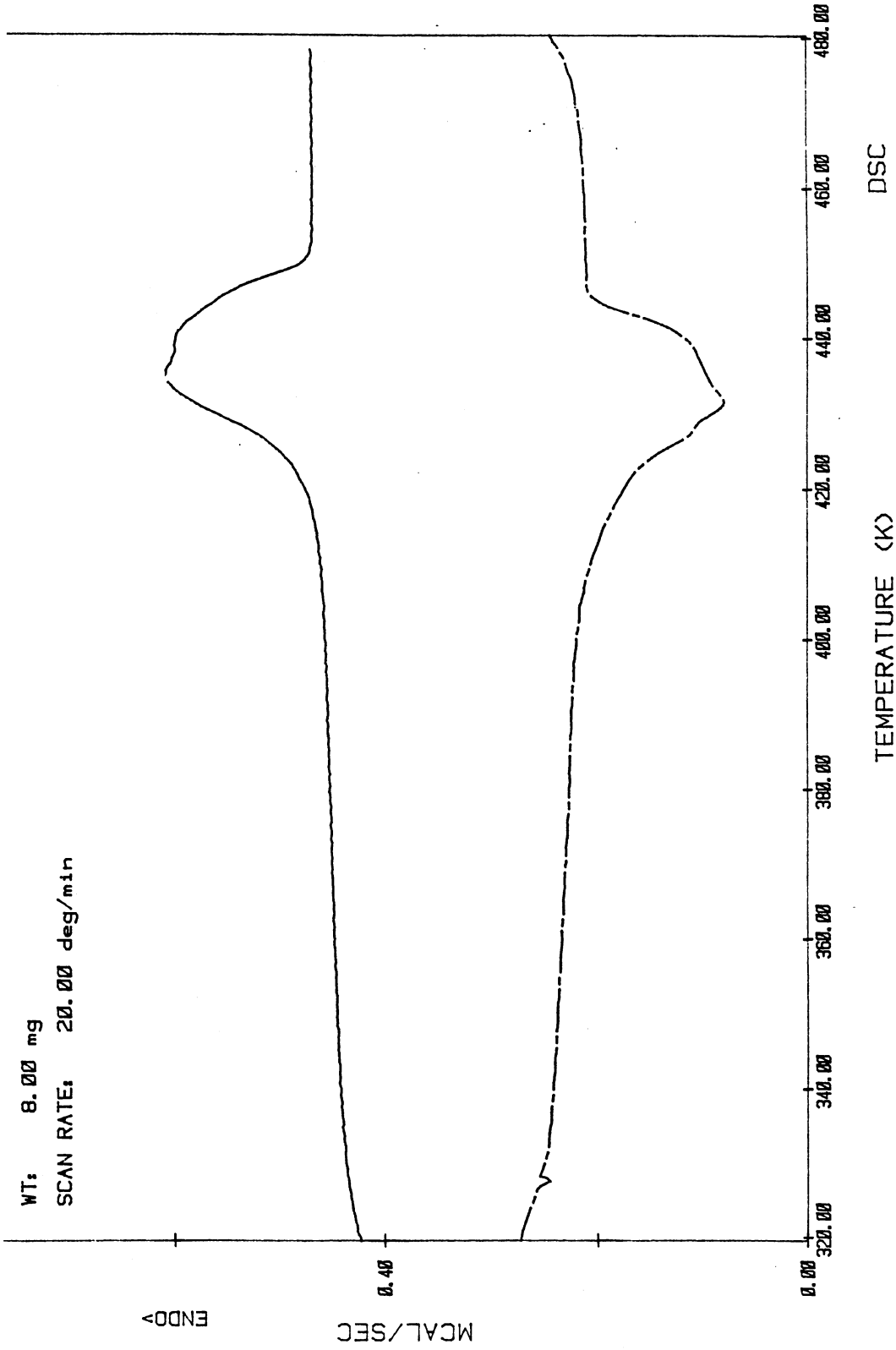

Figure 16. DSC thermograms of **CPS-1** at 20 K/min.

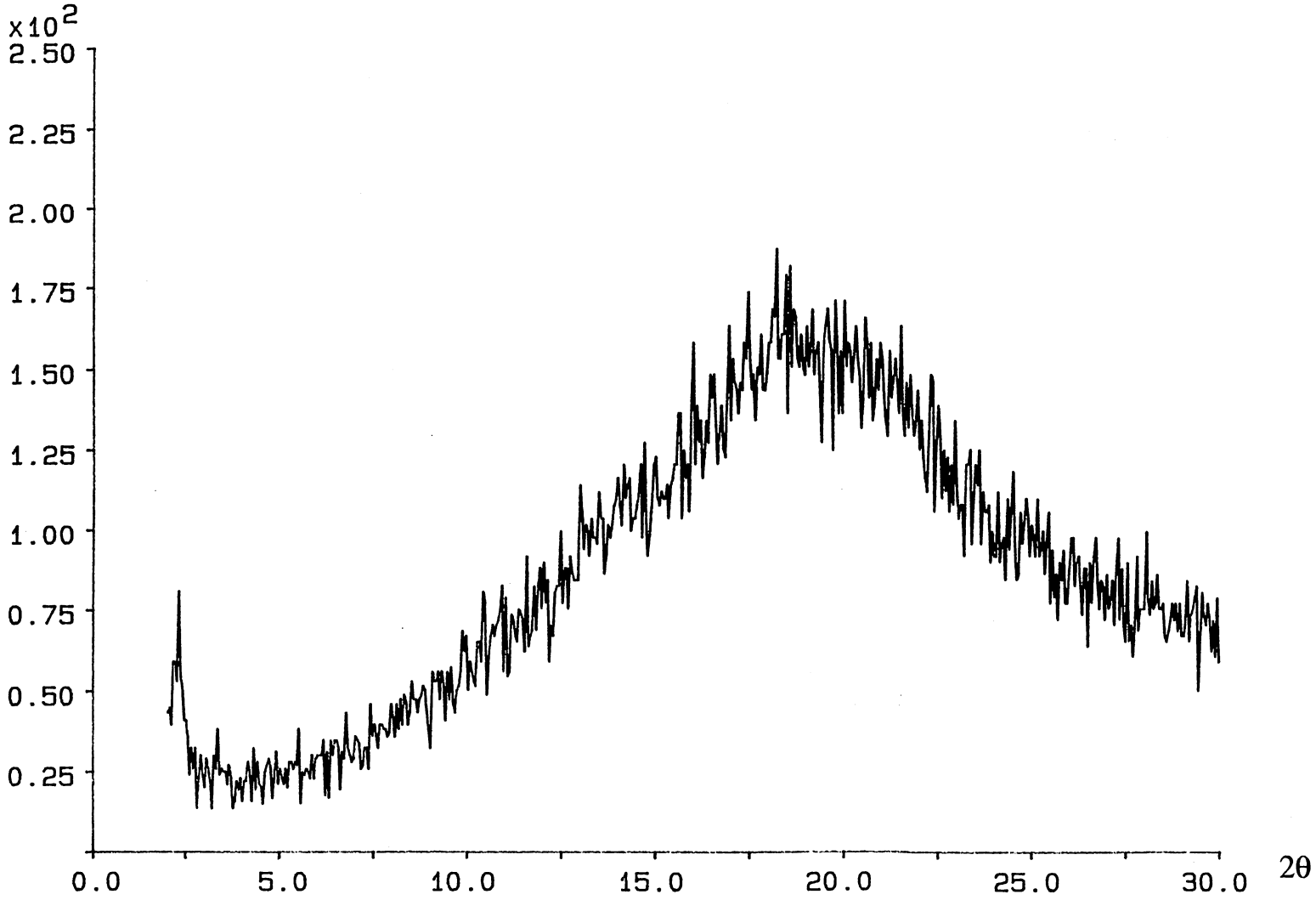

Figure 17. Powder X-ray diffraction pattern of **CPS-1** at 180 °C.

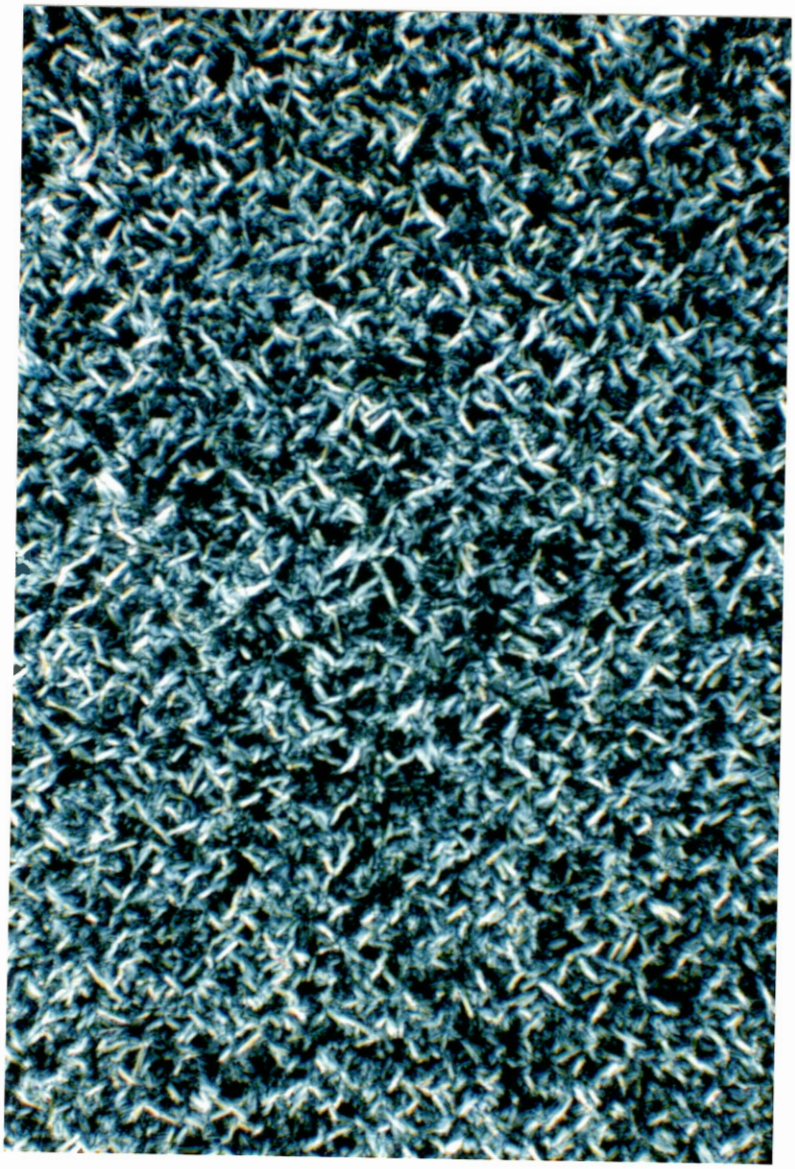

Figure 18. Microscopic texture between crossed polarizers (300x) of **CPS-1** after overnight annealing at 145 °C.

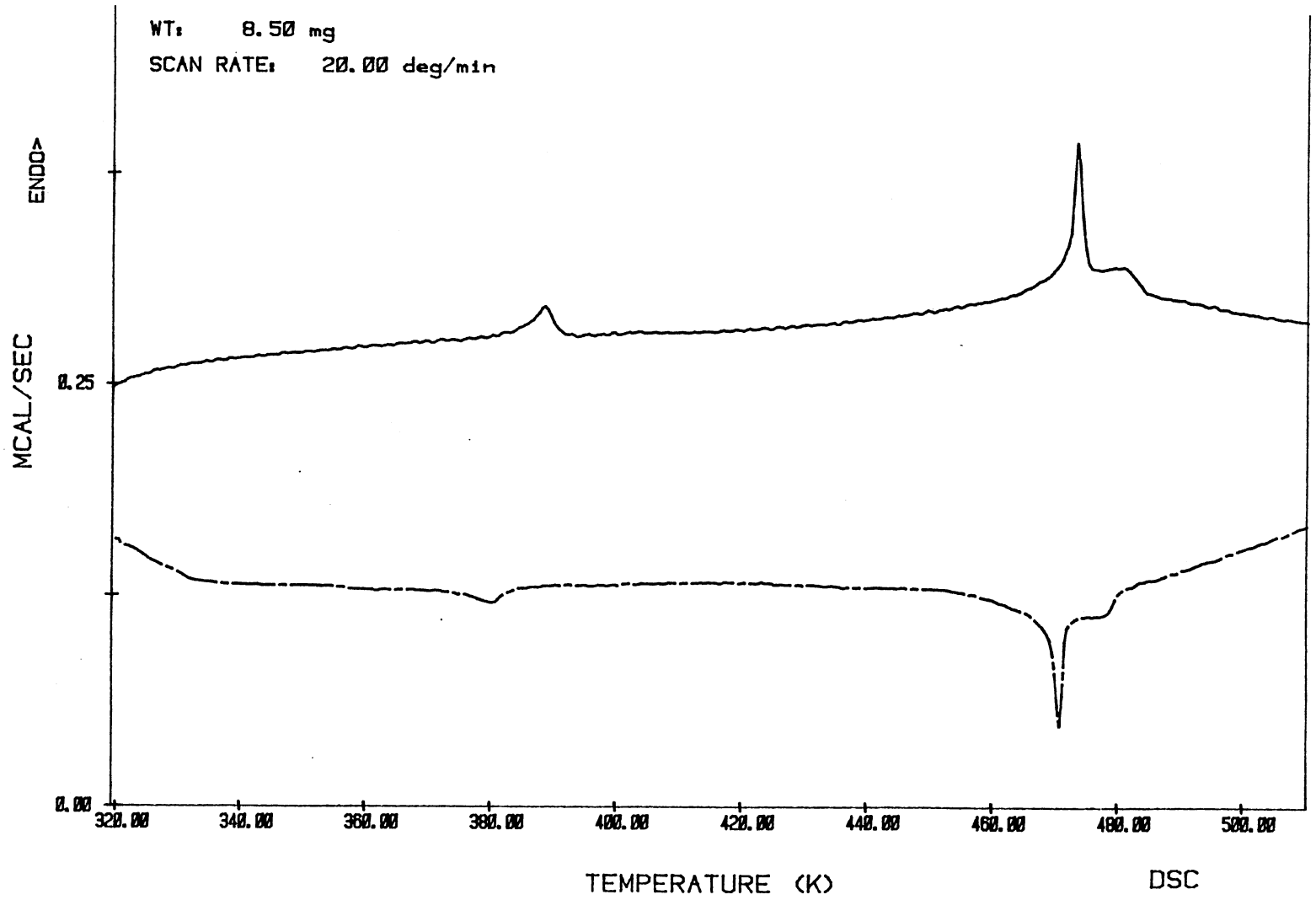

Figure 19. DSC thermograms of **HPS-2** at 20 K/min.

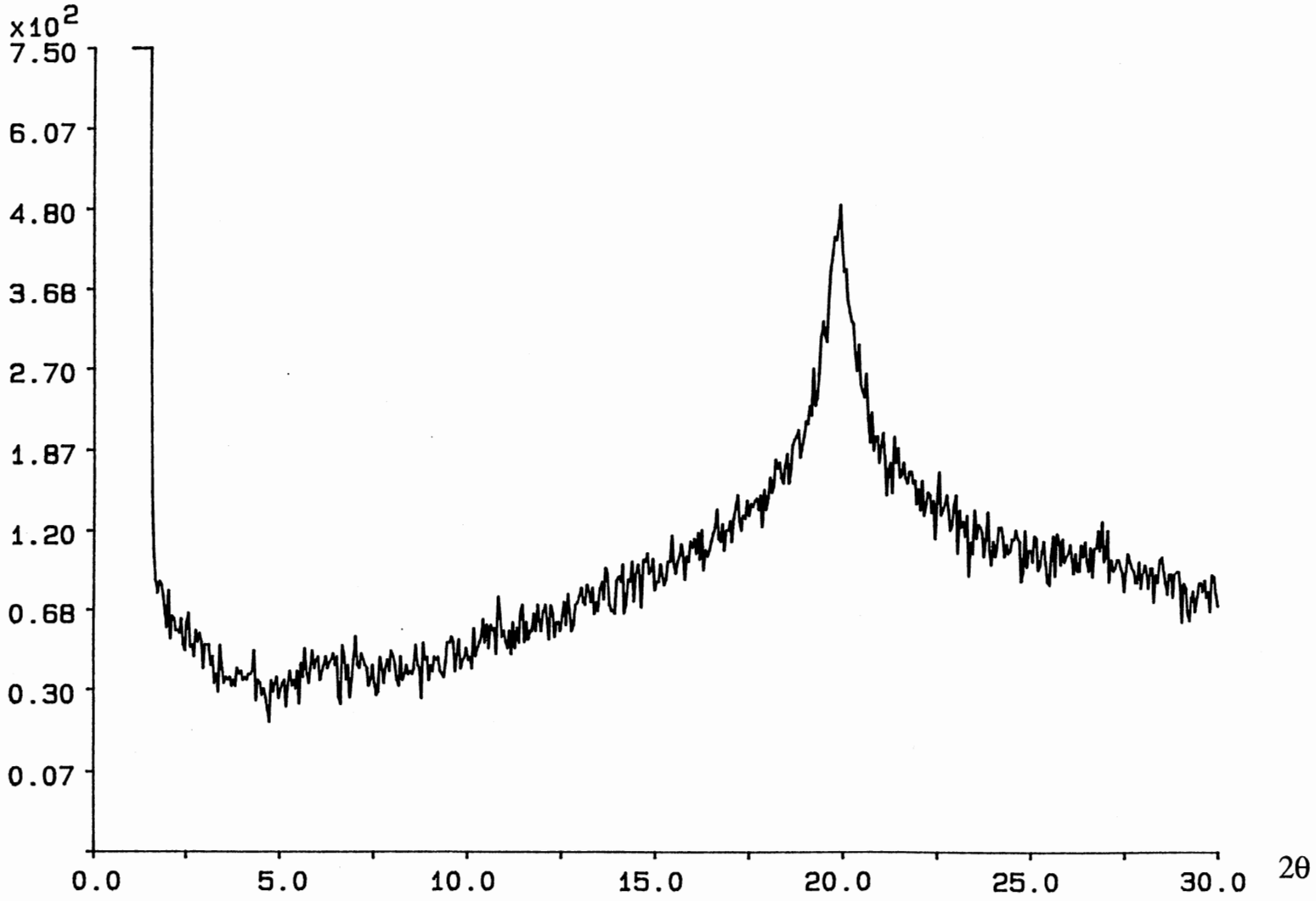

Figure 20. Powder X-ray diffraction pattern of **HPS-2** at 120 °C.

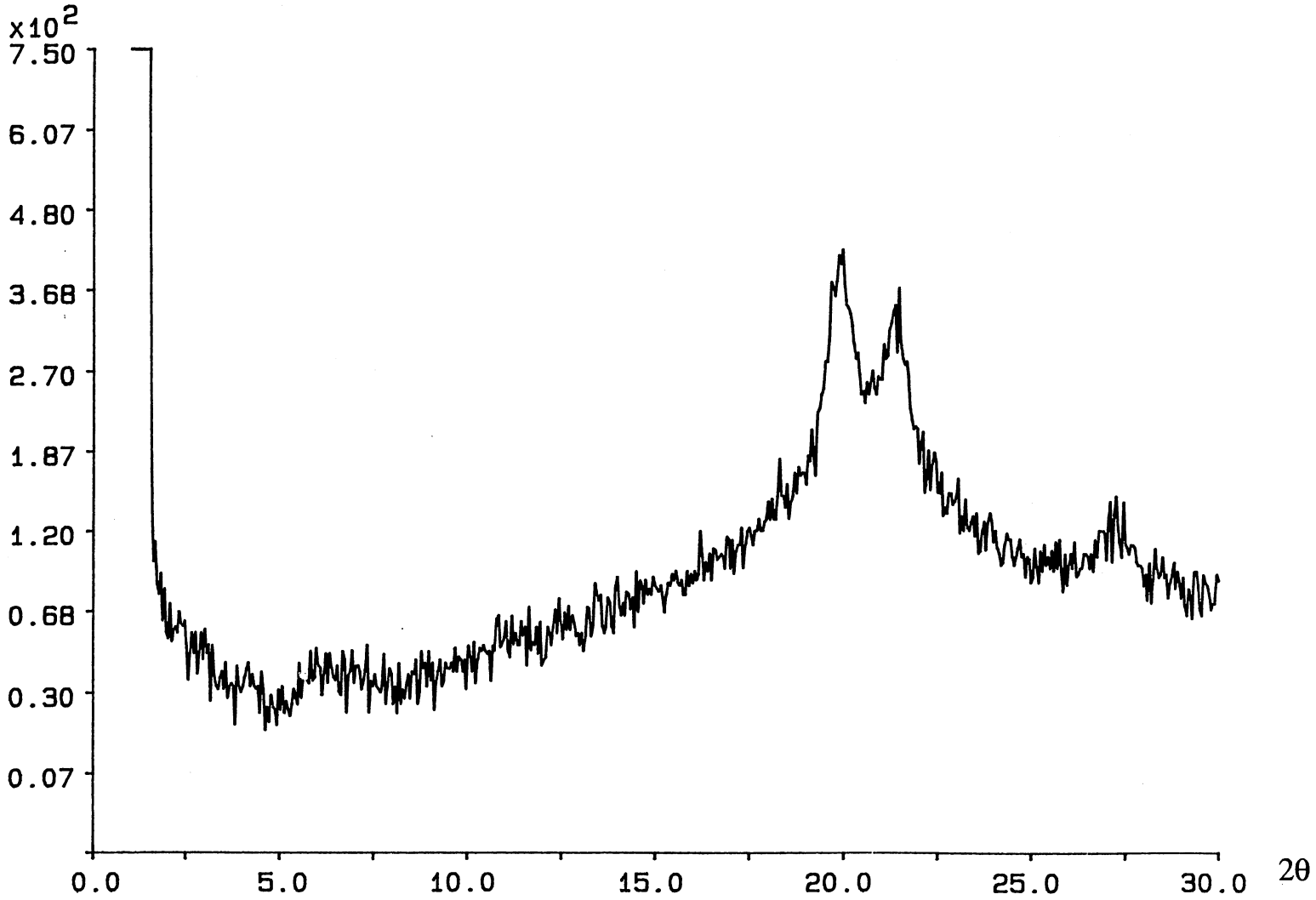

Figure 21. Powder X-ray diffraction pattern of **HPS-2** at 50 °C.

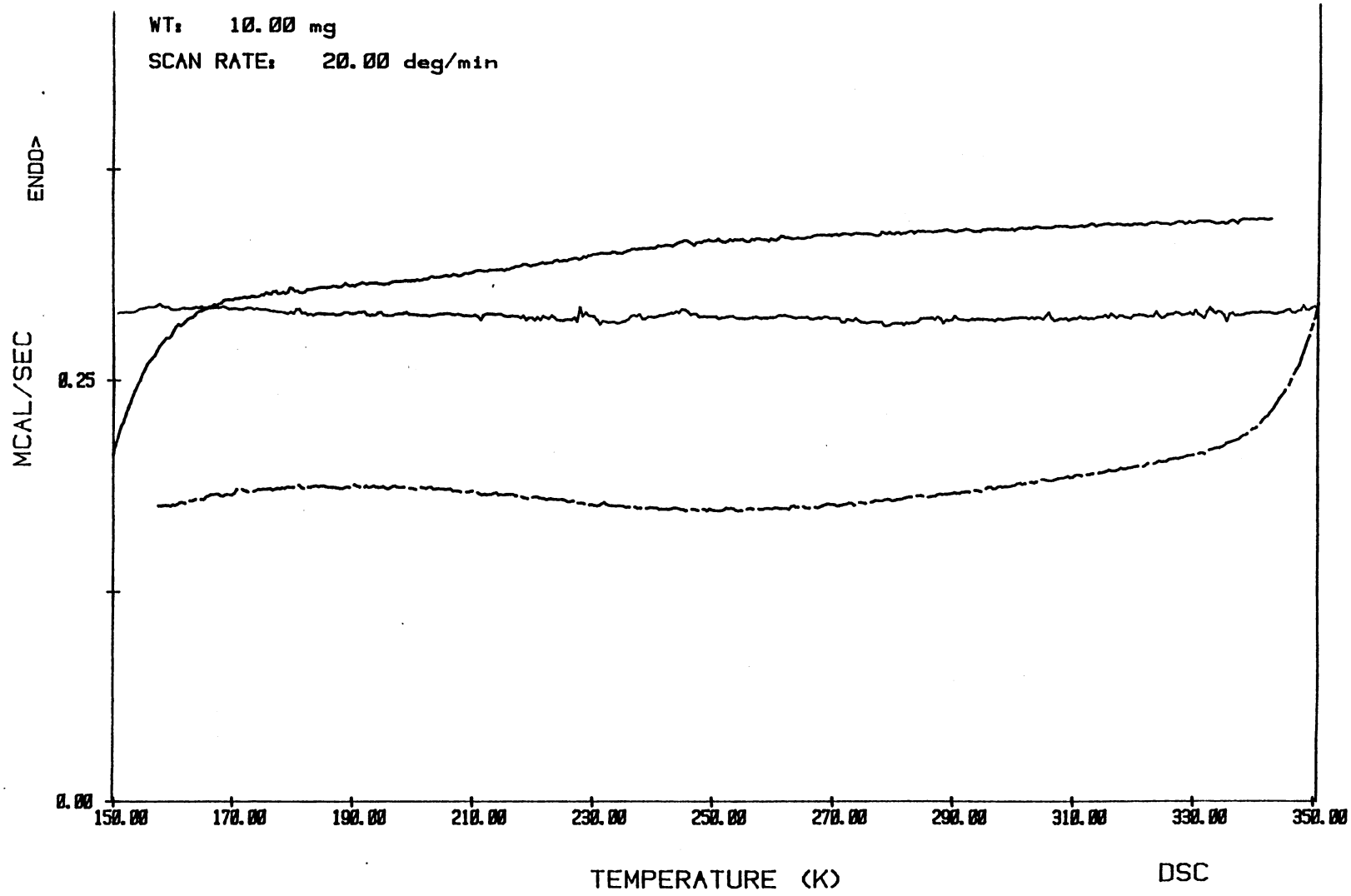

Figure 22. Subambient DSC thermograms of **CPS-2** at 20 K/min.

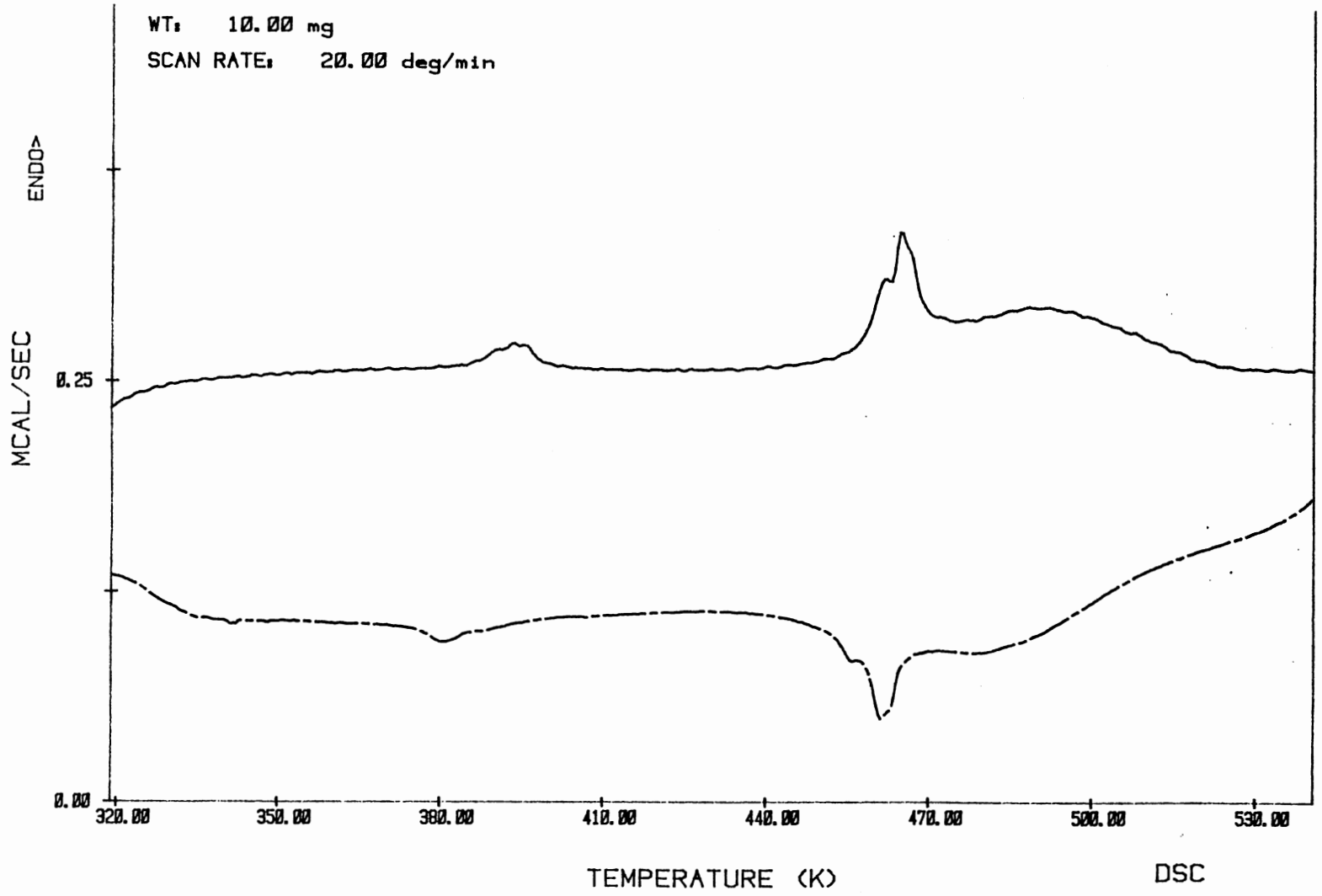

Figure 23. DSC thermograms of **CPS-2** at 20 K/min.

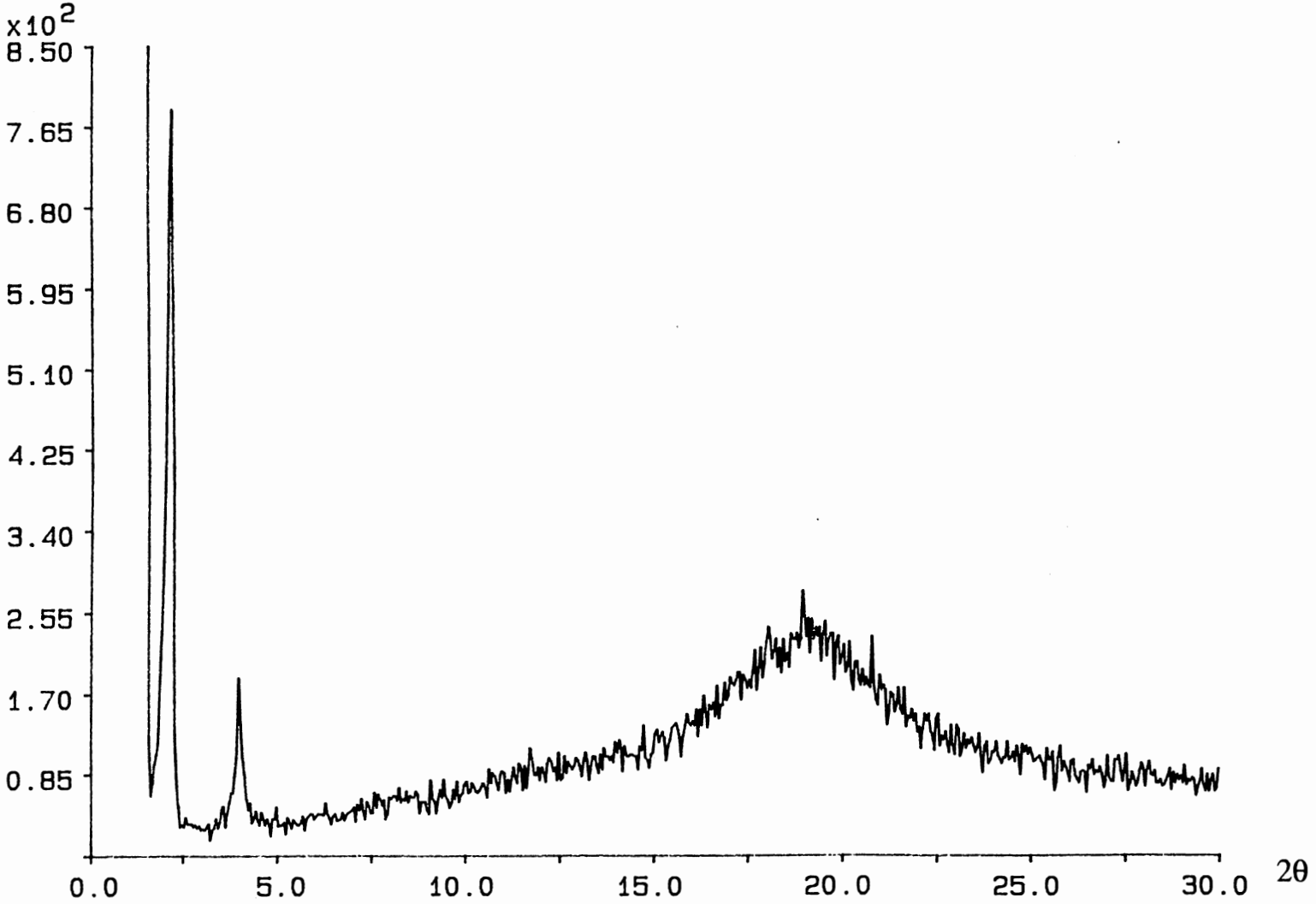

Figure 24. Powder X-ray diffraction pattern of **CPS-2** at 205 °C.

diffraction pattern at 171 °C (Figure 25) showed the typical sharp peaks in the small angle region denoting the presence of layers and a strong sharp peak in the wide angle region which corresponds to 110 and 200 reflections. Figures 26A and 26 B show the microscopic structure under crossed polarized light of **CPS-2** which is a typical fan-shaped for S_A phase.

The isotropization temperatures of all the side-chain polysiloxanes, which were not observed in the DSC, were obtained from the microscopic data. The heats of transition from the mesophase to the isotropic liquid phase are too small to observe in the DSC.

All of the polysiloxanes exhibited a low temperature crystalline phase identified by X-ray diffraction patterns and reported in Table XII. The long flexible methylene chain as spacer has efficiently decoupled the motions of the mesogenic group and the main chain, thus the polymers experienced side chain crystallization. Flexible backbones such as polysiloxanes tend to give rise to side chain crystallization. Figure 27 shows a sample X-ray pattern of this crystalline phase, taken at 150 °C for **HPS-1**. Three sharp peaks were observed in the wide angle region corresponding to 110, 200 and 210 reflections, which are characteristic wide angle reflections of an orthorhombic crystal. Sharp peaks were also observed in the small angle region which indicate that the molecules are arranged in layers. There is the possibility that this phase might be a S_E phase, which also gives the three reflections in the wide angle region. Though, to distinguish a smectic E phase from an orthorhombic crystal, X-ray diffraction studies would need to be performed on oriented samples.

Monolayers. The monolayers of the polysiloxanes were characterized by measurement of the film pressure (Π) vs mean molecular area (Mma, $Å^2$) isotherms. In this work, mean molecular area is defined as area per mesogenic repeat unit of the polysiloxane. The room temperature isotherms are shown in Figures 28 to 31 and were reproducible. The curves obtained for **HPS-1** and **CPS-1** were smooth, without any

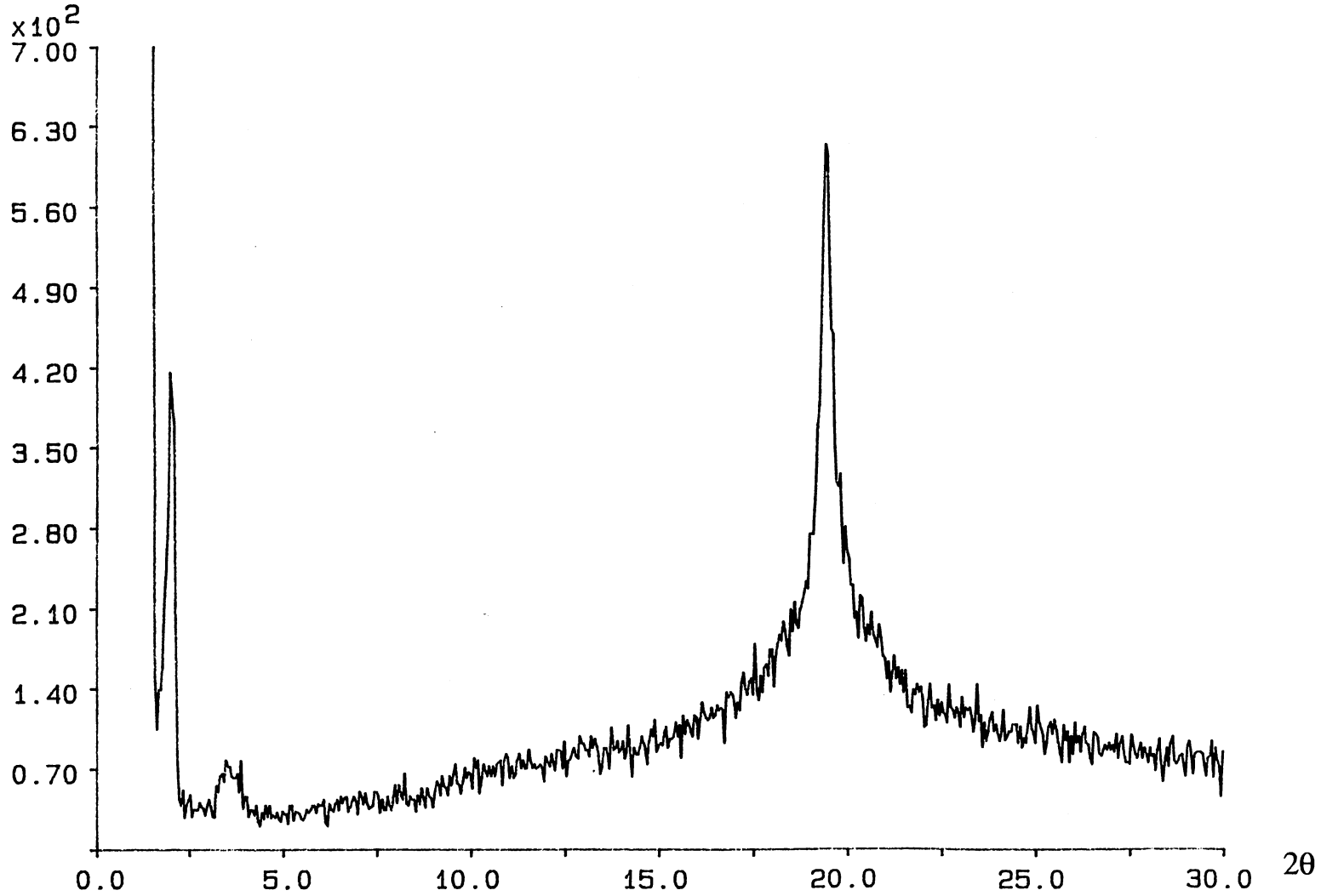

Figure 25. Powder X-ray diffraction pattern of **CPS-2** at 171 °C.

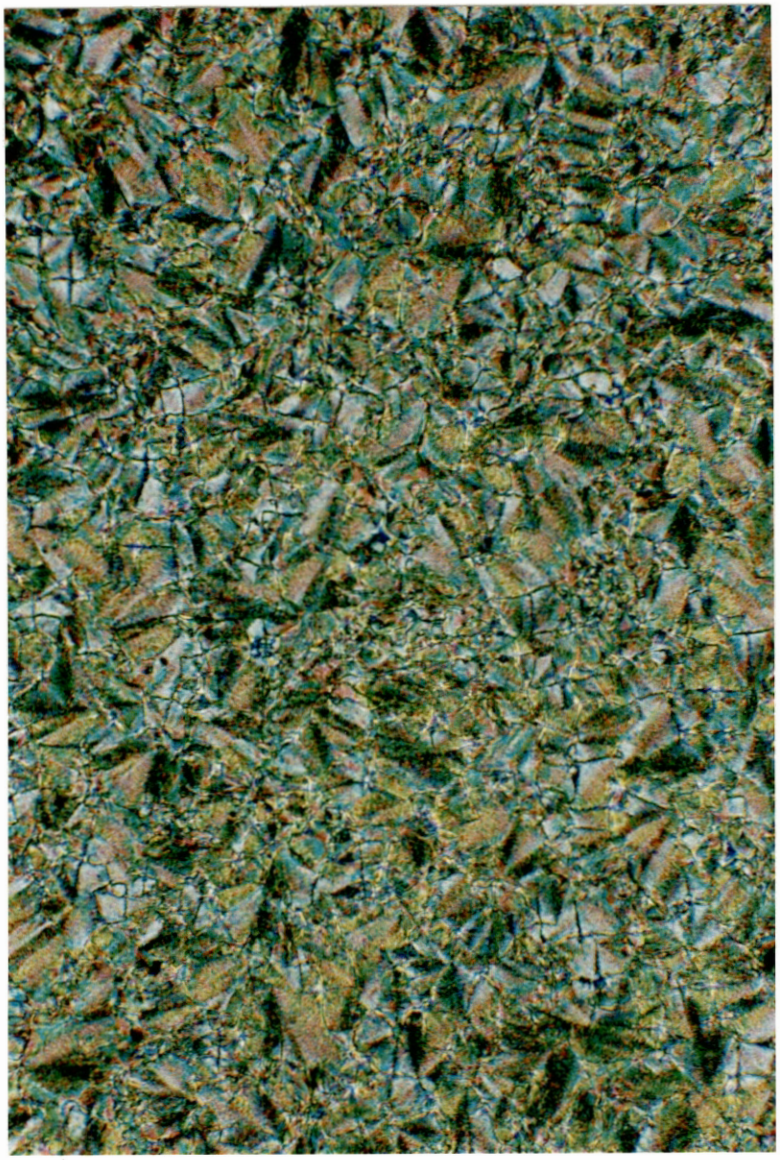

Figure 26A. Fan-like texture between crossed polarizers of **CPS-2** after overnight annealing at 175 °C.

Figure 26B. Microscopic texture (300x) of **CPS-2** after 30 min at 106 °C under crossed polarized light.

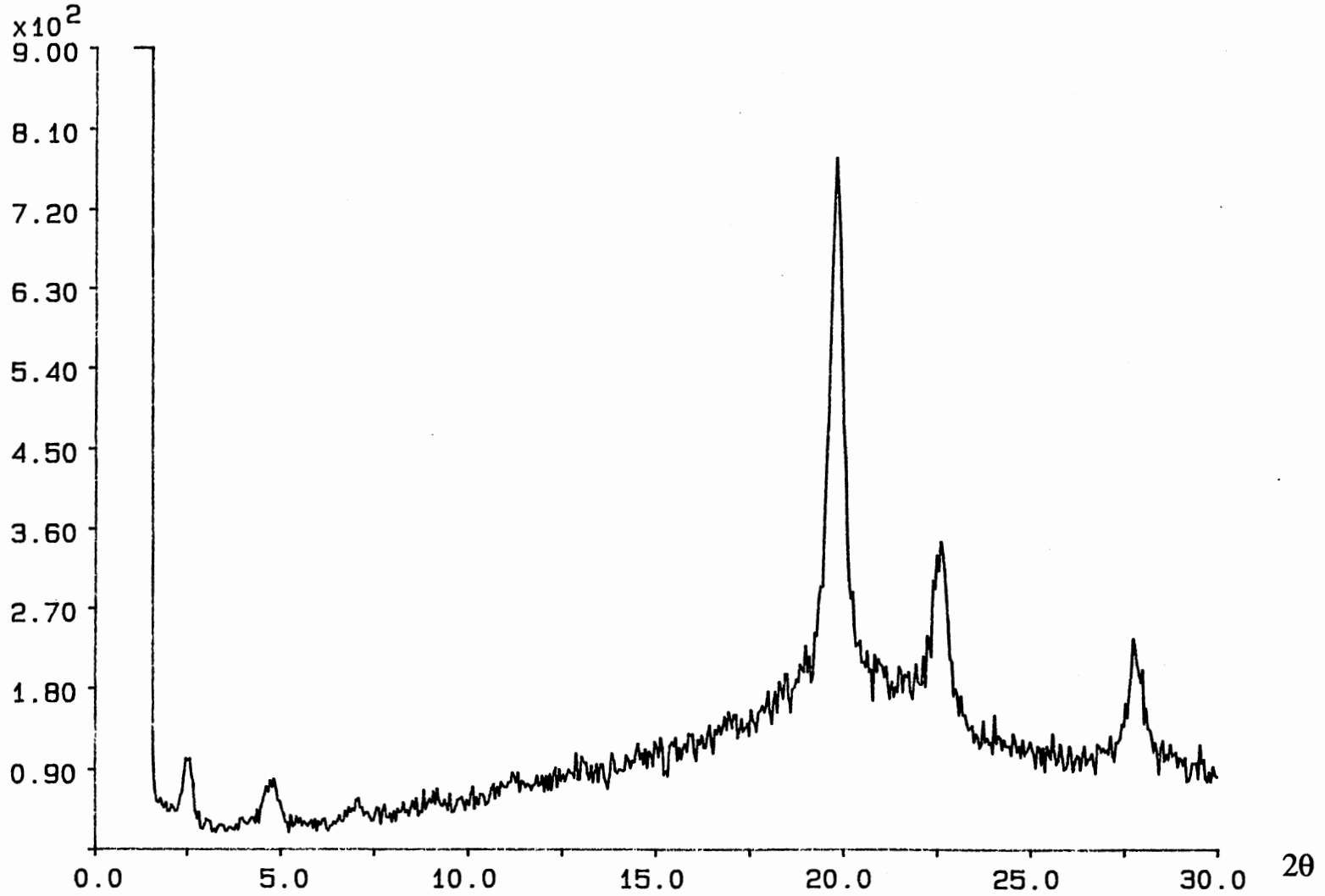

Figure 27. Powder X-ray diffraction pattern of **HPS-1** at 150 °C, illustrating an orthorhombic crystalline structure.

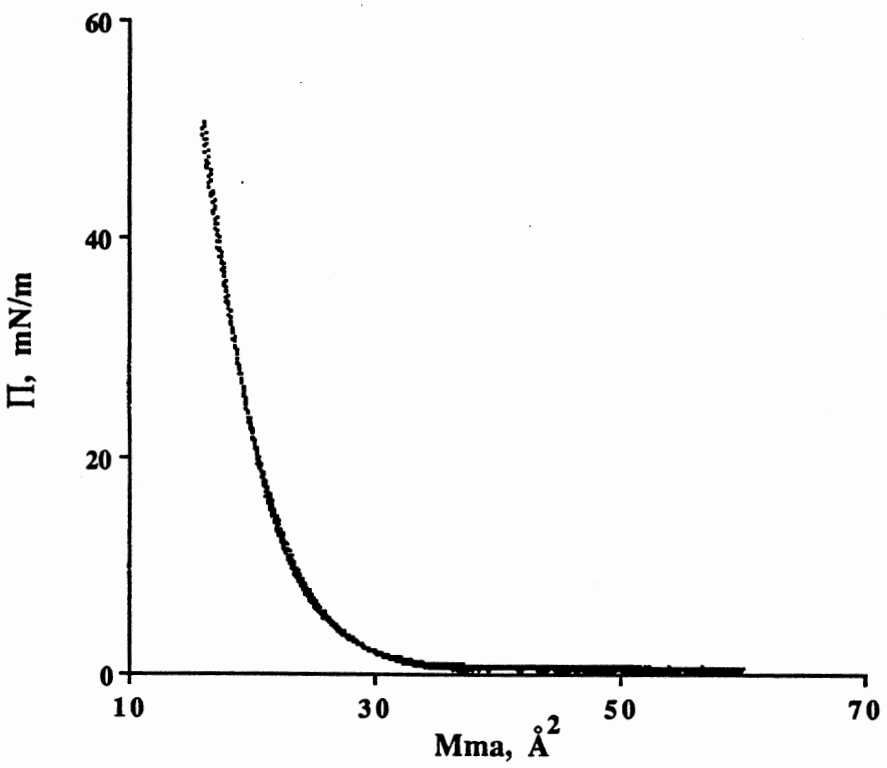

Figure 28. Surface pressure - area isotherm of **HPS-1** at room temperature.

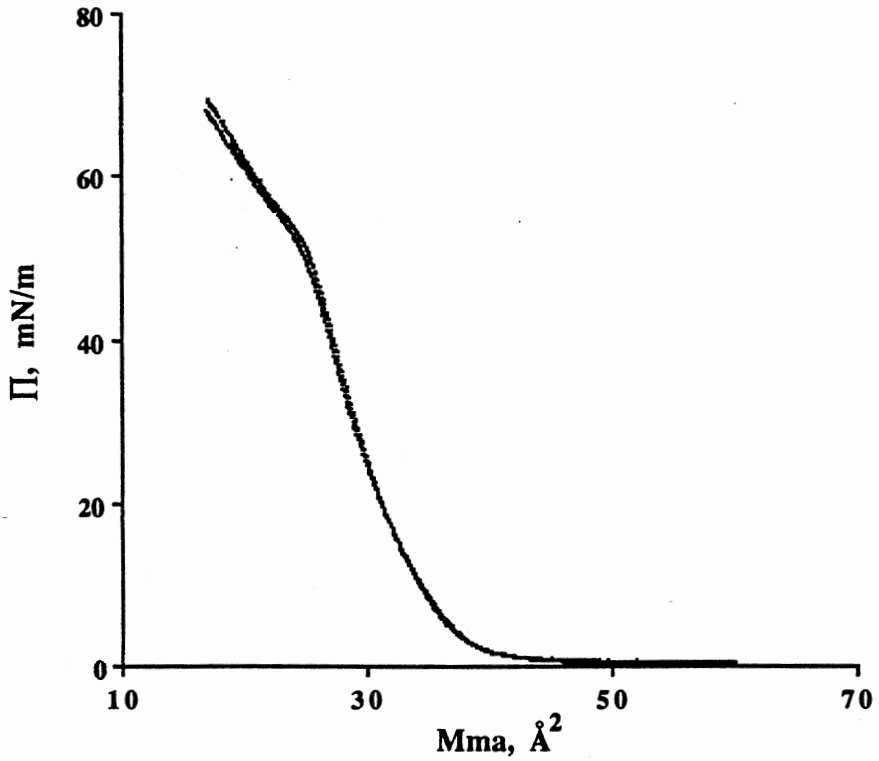

Figure 29. Surface pressure - area isotherm of **CPS-1** at room temperature.

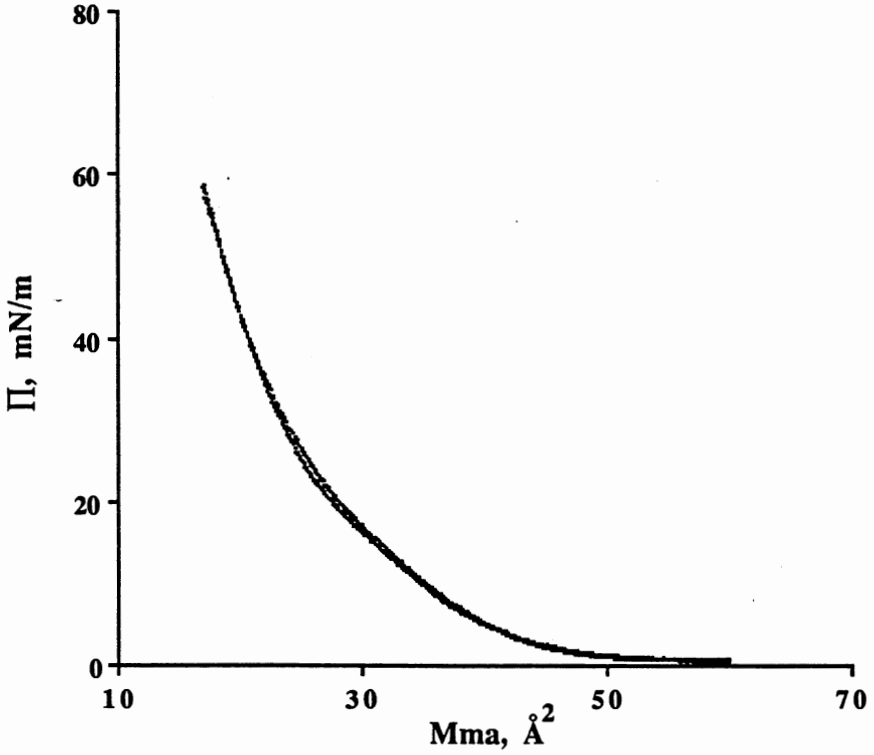

Figure 30. Surface pressure - area isotherm of **HPS-2** at room temperature.

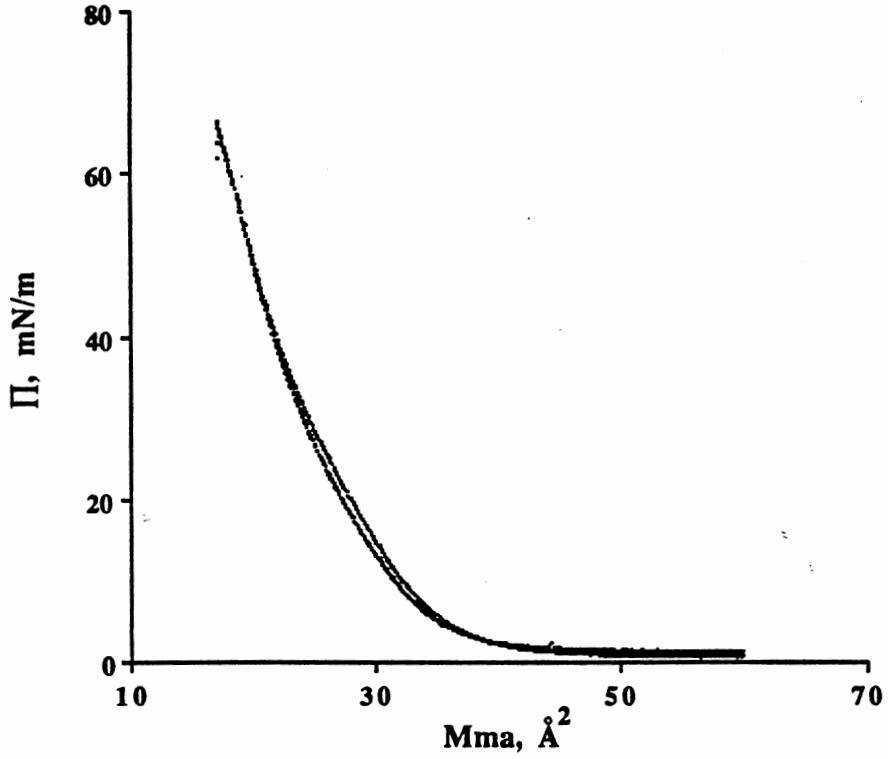

Figure 31. Surface pressure - area isotherm of **CPS-2** at room temperature.

observable discontinuities, and showed no evidence of phase transformations. The surface pressure was low at large surface areas, but increased more or less rapidly when the film was compressed to the point where the macromolecules occupied most of the available surface. Upon extrapolation of the steeply sloping linear region to zero surface pressure, the intercept gives the area per molecule of a closely packed monolayer. The minimum stable areas per repeat unit were ~23 $Å^2$ and ~34 $Å^2$ for **HPS-1** and **CPS-1**, respectively. The isotherms for **HPS-2** and **CPS-2** showed evidence of phase transitions just above 30 $Å^2$ to about 50 $Å^2$. **HPS-2** and **CPS-2** gave the same mean molecular area per repeat unit which is ~ 30 $Å^2$. Because the side-chain polysiloxane films exhibited high viscosities, it was necessary to use a Langmuir balance, rather than a Wilhelmy plate to measure surface pressure. The films can be compressed to about 40 mN/m with no apparent collapse. Only **CPS-1** showed a possible collapse of the monolayer at about 53 mN/m, which alternatively could be just a rearrangement of the polymer chains or side chains. The copolysiloxanes, **CPS-1** and **CPS-2**, showed less hysteresis upon compression and subsequent expansion of the monolayers on water than the homopolysiloxanes, **HPS-1** and **HPS-2** (Figures 32-35). Further compression-expansion runs showed a much improved hysteresis behavior than the first one for **CPS-1** and **CPS-2**. There was a bigger drop in the surface pressure for the homopolysiloxanes when the barriers were stopped for 1 minute before decompression. Figures 36-39 show the isobaric, 15 mN/m, surface areas as a function of time. The monolayers are stable at the given surface pressure, and similar behavior was observed for all polysiloxanes. There was a bigger decrease of the mean-molecular area during the first 30 minutes with **HPS-1** than with **CPS-1**. The same trend was observed in **HPS-2** as compared to that of **CPS-2**. Due to the greater movement of the long alkyl flexible side-chain mesogens, the drop of the mean molecular area for the first 30 minutes in **HPS-2** and **CPS-2** was much bigger than that in **HPS-1** and **CPS-1**. It took more time for the

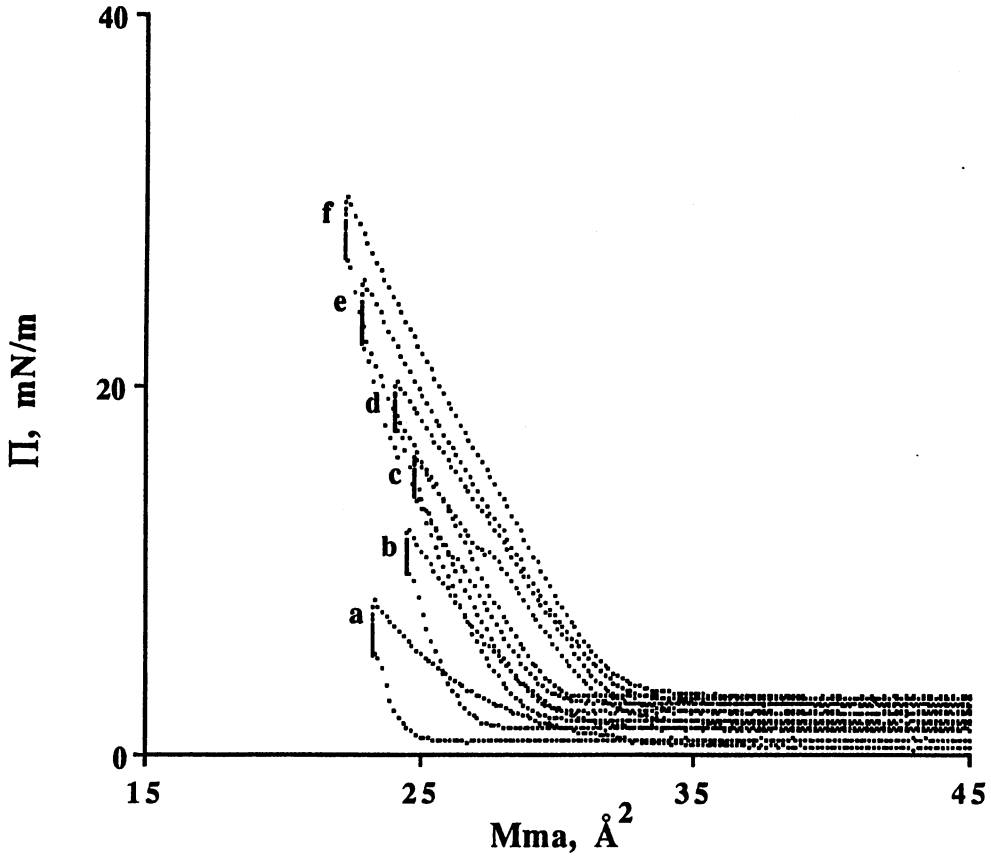

Figure 32. Hysteresis behavior of **HPS-1** monolayer at room temperature: barrier stopped at (a) 8 mN/m; (b) 12 mN/m; (c) 16 mN/m; (d) 20 mN/m; (e) 24 mN/m; (f) 30 mN/m.

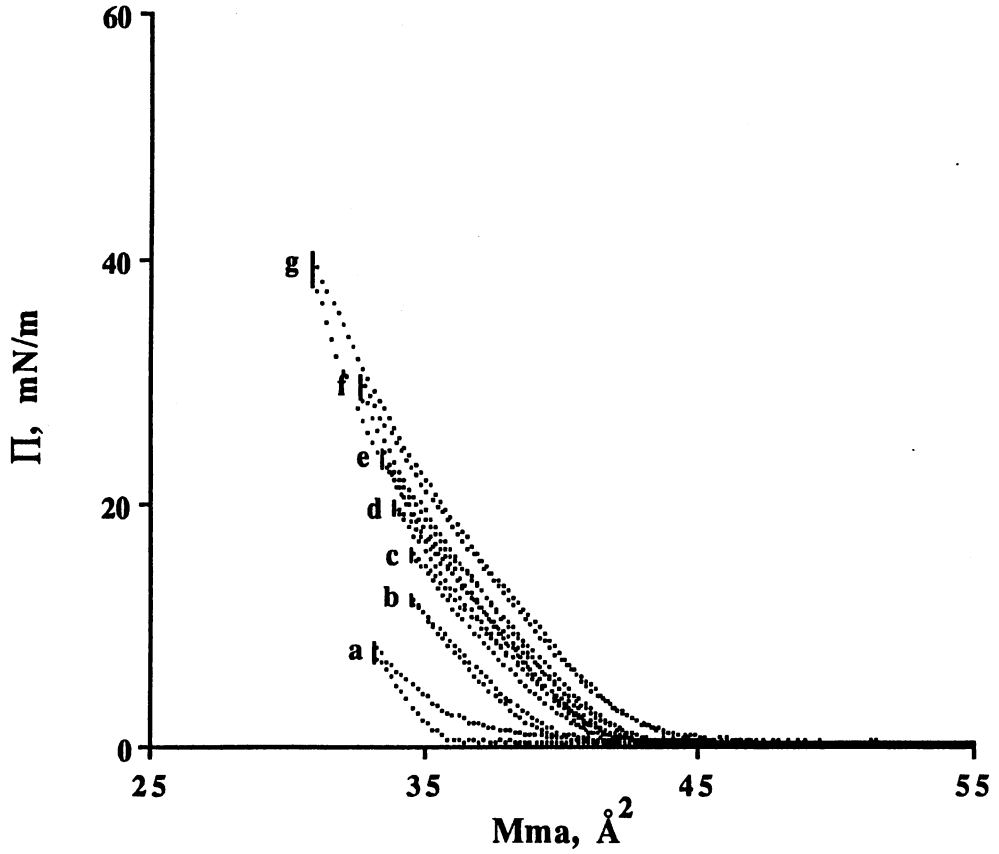

Figure 33. Hysteresis behavior of **CPS-1** monolayer at room temperature: barrier stopped at (a) 8 mN/m; (b) 12 mN/m; (c) 16 mN/m; (d) 20 mN/m; (e) 24 mN/m; (f) 30 mN/m; (g) 40 mN/m.

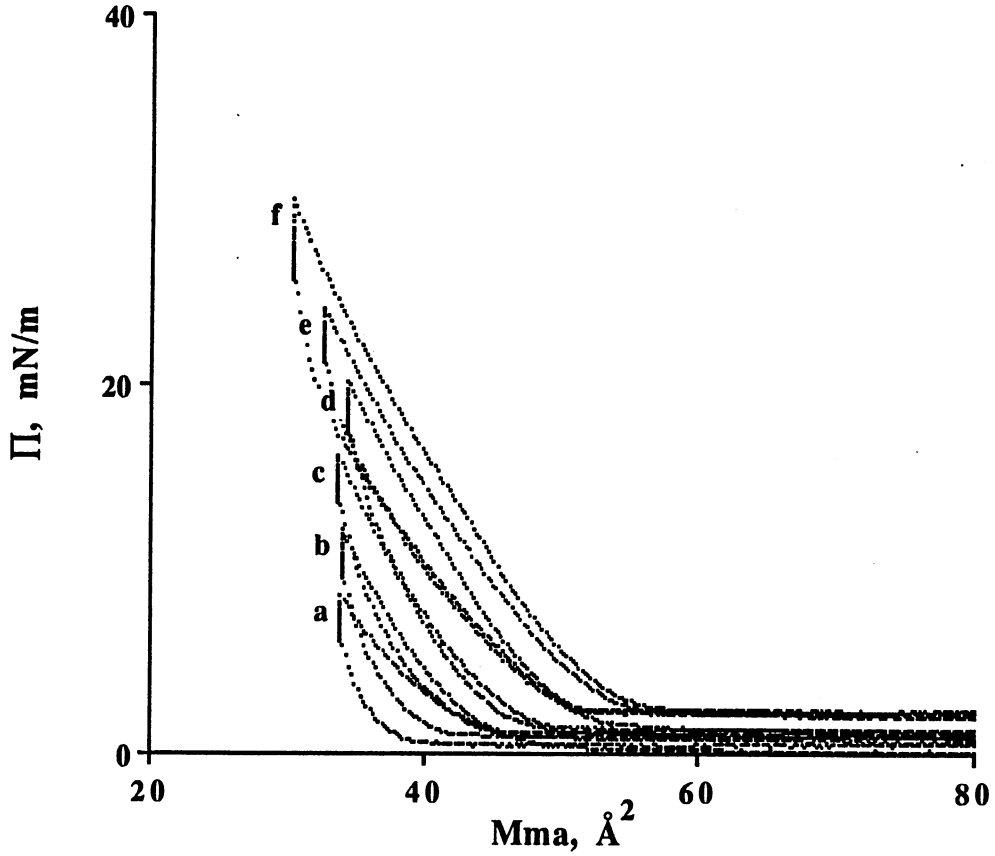

Figure 34. Hysteresis behavior of **HPS-2** monolayer at room temperature: barrier stopped at (a) 8 mN/m; (b) 12 mN/m; (c) 16 mN/m; (d) 20 mN/m; (e) 24 mN/m; (f) 30 mN/m.

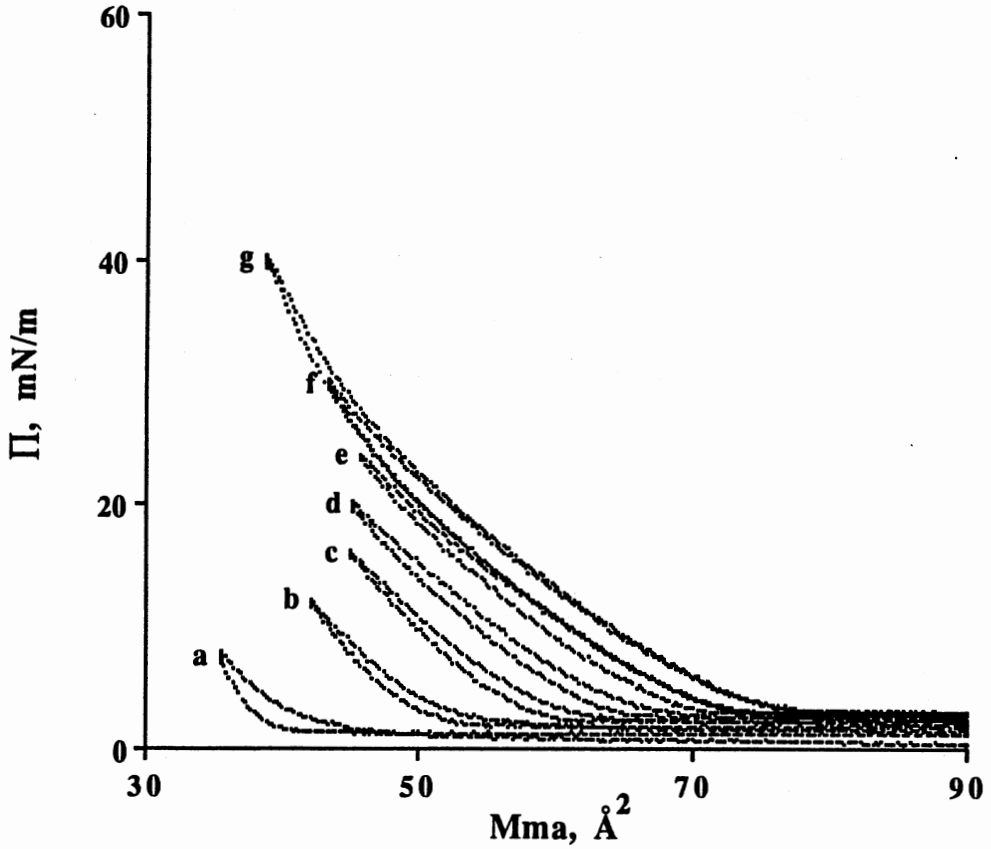

Figure 35. Hysteresis behavior of **CPS-2** monolayer at room temperature: barrier stopped at (a) 8 mN/m; (b) 12 mN/m; (c) 16 mN/m; (d) 20 mN/m; (e) 24 mN/m; (f) 30 mN/m; (g) 40 mN/m.

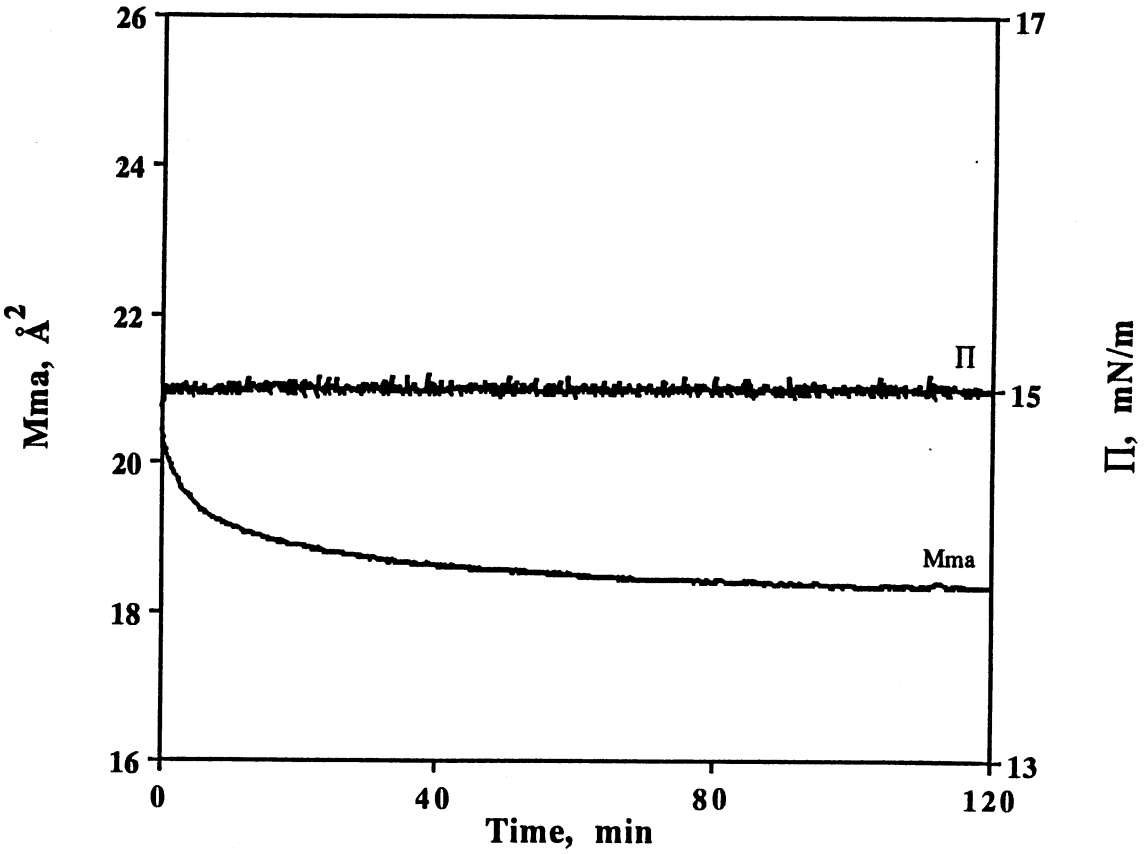

Figure 36. Isobaric creep measurement of **HPS-1** monolayer at room temperature.

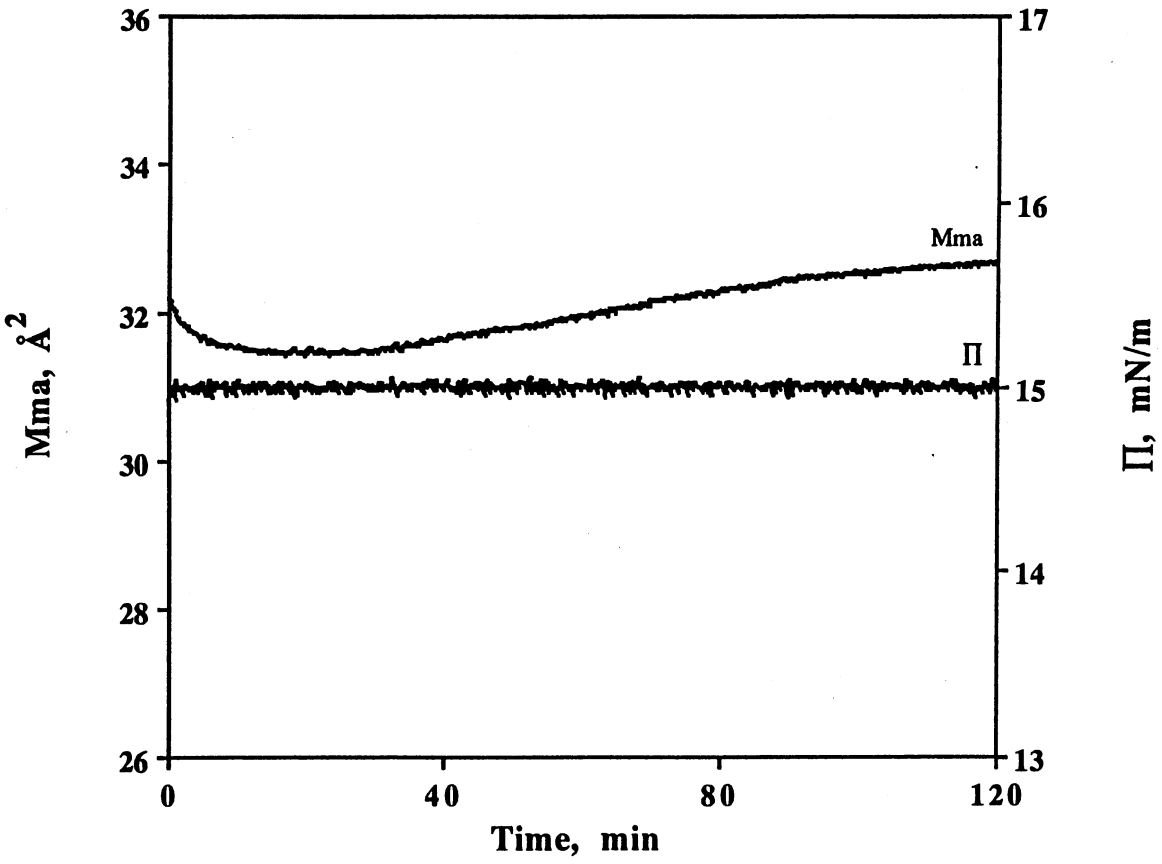

Figure 37. Isobaric creep measurement of **CPS-1** at room temperature.

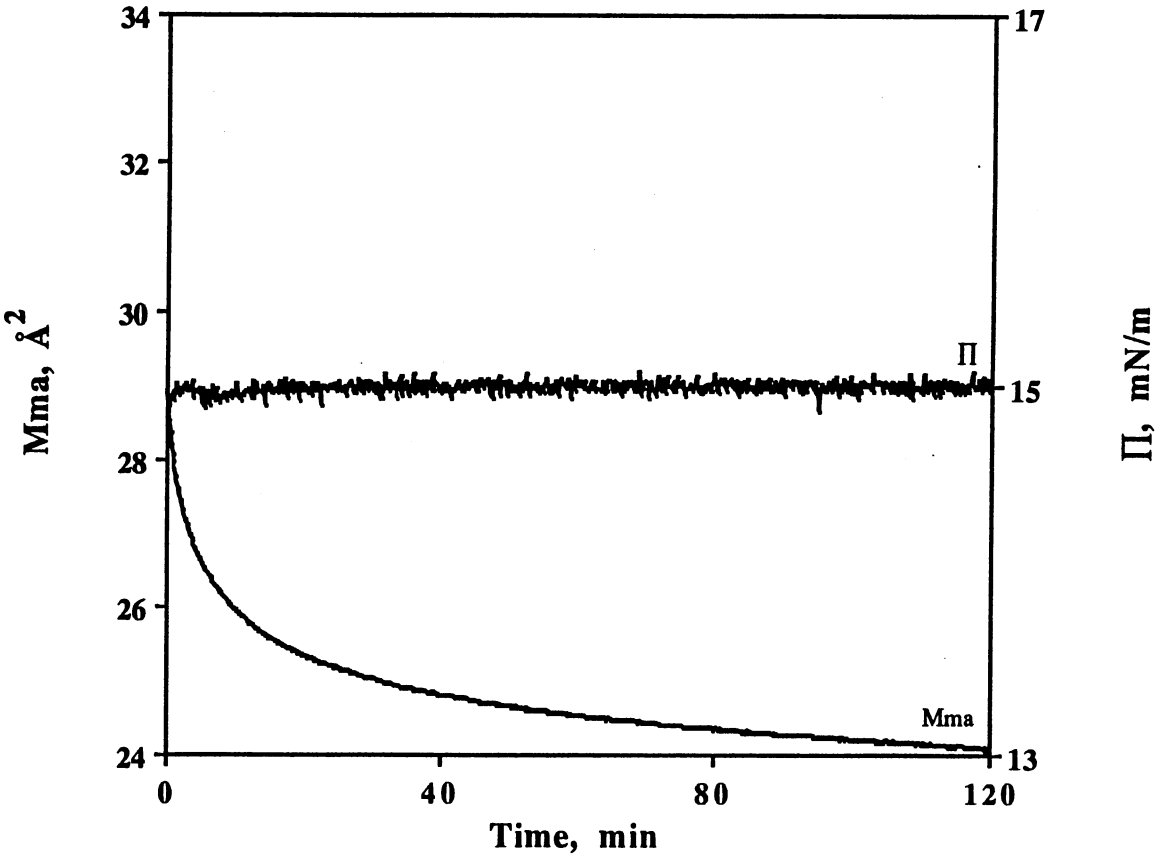

Figure 38. Isobaric creep measurement of **HPS-2** monolayer at room temperature.

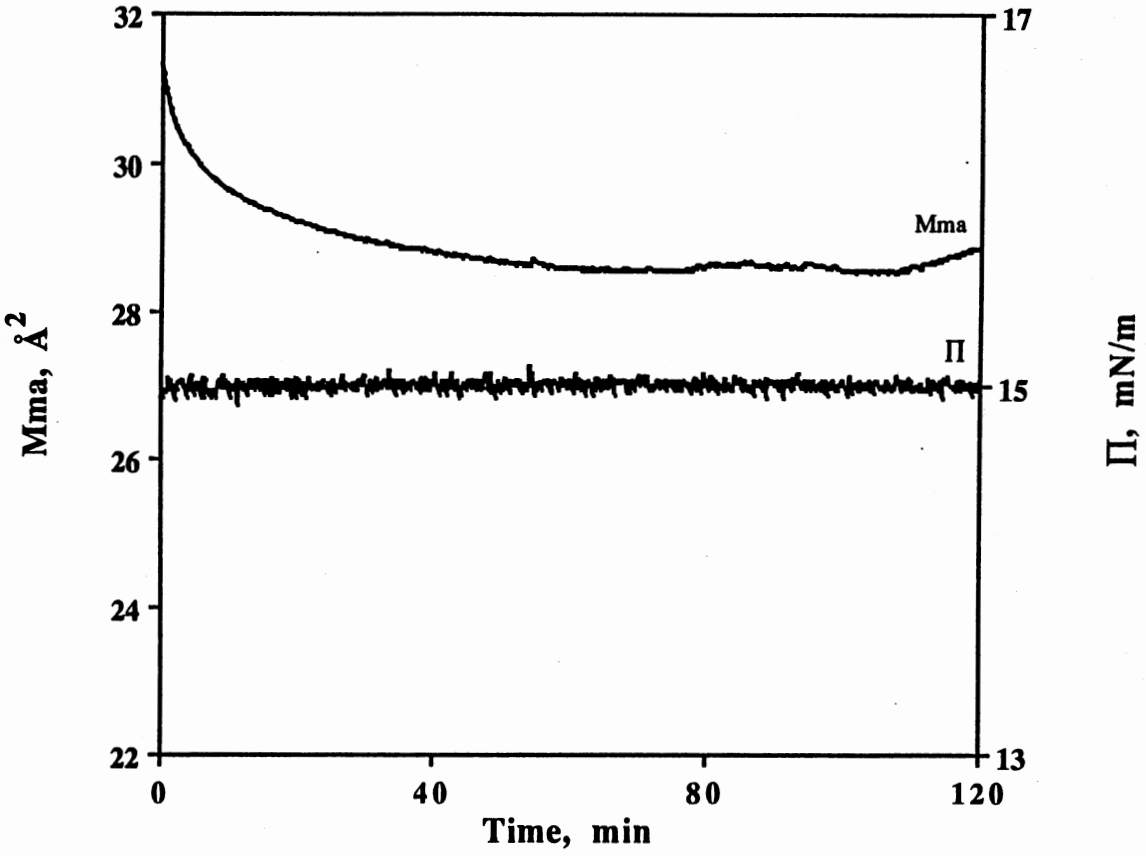

Figure 39. Isobaric creep measurement of **CPS-2** monolayer at room temperature.

mesogens to arrange themselves in the most stable conformation. Thus, it is necessary to wait for 30 minutes or more so as to allow the side-chain mesogens to orient themselves on the water subphase before any deposition is carried out.

Preliminary deposition experiments were performed on the polysiloxanes. Films were primarily deposited onto hydrophobic, octadecyltrichlorosilane-treated quartz slides. There was no deposition of the monolayers of the polysiloxanes onto a hydrophilic substrate. LB multilayers of **CPS-1** were obtained on hydrophobic substrate with a transfer ratio of 0.8 during the first dip, 0.3 during the first upstroke and a decreasing transfer ratio on succeeding dips, from 0.4 to 0.2. Thus, dipping was stopped after six layers were obtained. Monolayers of **CPS-2** also showed deposition, although the transfer ratios of the first dip and the first upstroke were only 0.5 and 0.2. Dipping was stopped after 4 layers. When the transferred monolayers were investigated by UV-vis, the **CPS-2** LB film showed spectrum, Figure 40, with an absorbance of 0.040 at λ_{max} = 336 nm and 0.035 at λ_{max} = 336 nm. Figure 41 presents the UV-vis spectrum of the **CPS-1** LB film. There is a considerable absorption in the range of 300 to 400 nm and an absorbance of approximately 0.070 at $\lambda_{max} \approx 250$ nm. **HPS-1** and **HPS-2** did not deposit onto the hydrophobic substrate.

Discussion

Synthesis. The protection of the amino group of **1** was necessary so as not to compete with the alkylation reaction of the hydroxyl group with bromohexane. The alkylation of **2** worked well when DMF was used as a solvent rather than THF. There was no product formed when THF was the solvent. It can be concluded that DMF is a better solvent for Na alkoxide, thus facilitating the contact of the alkoxide with the alkyl halide in solution. The yield of **3** was improved considerably because of the addition of catalytic amount of 15-crown-5. Crown ethers have the ability to solvate cations such as

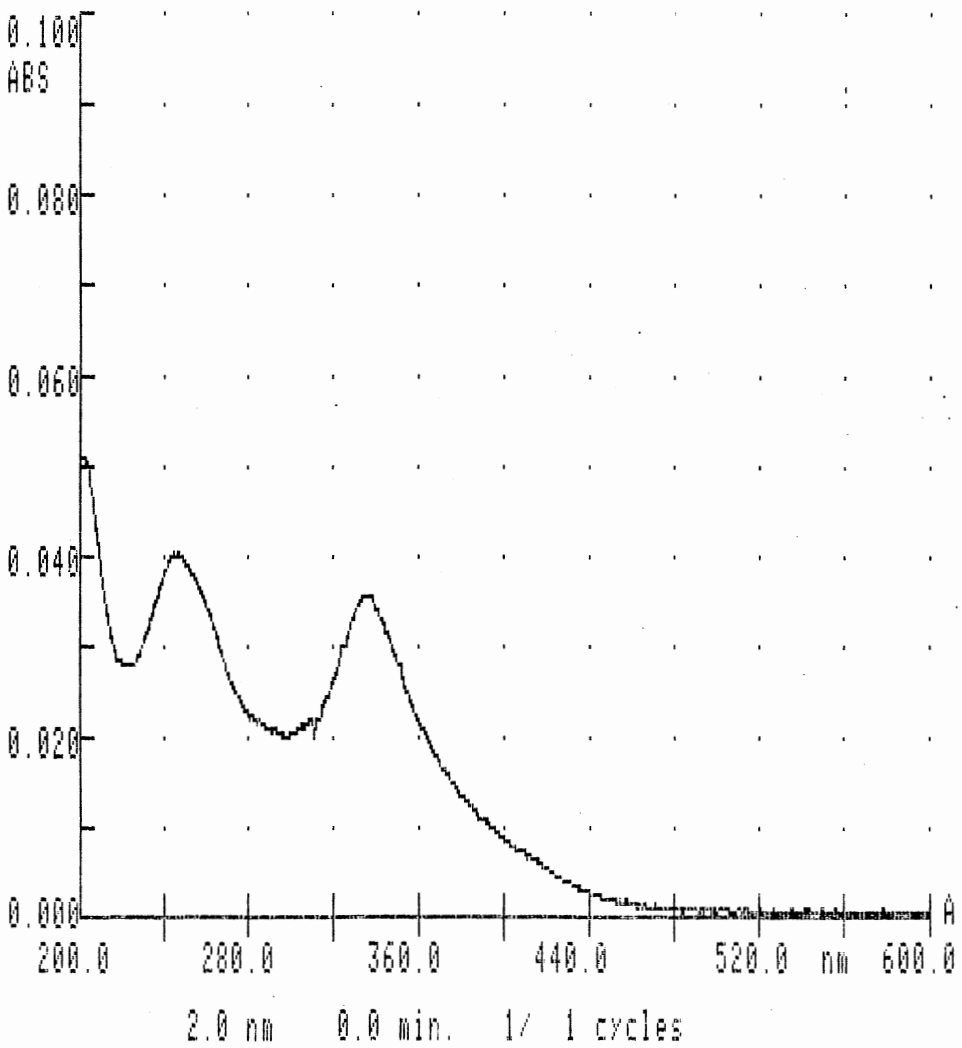

Figure 40. UV-vis spectrum of an LB film of **CPS-2**.

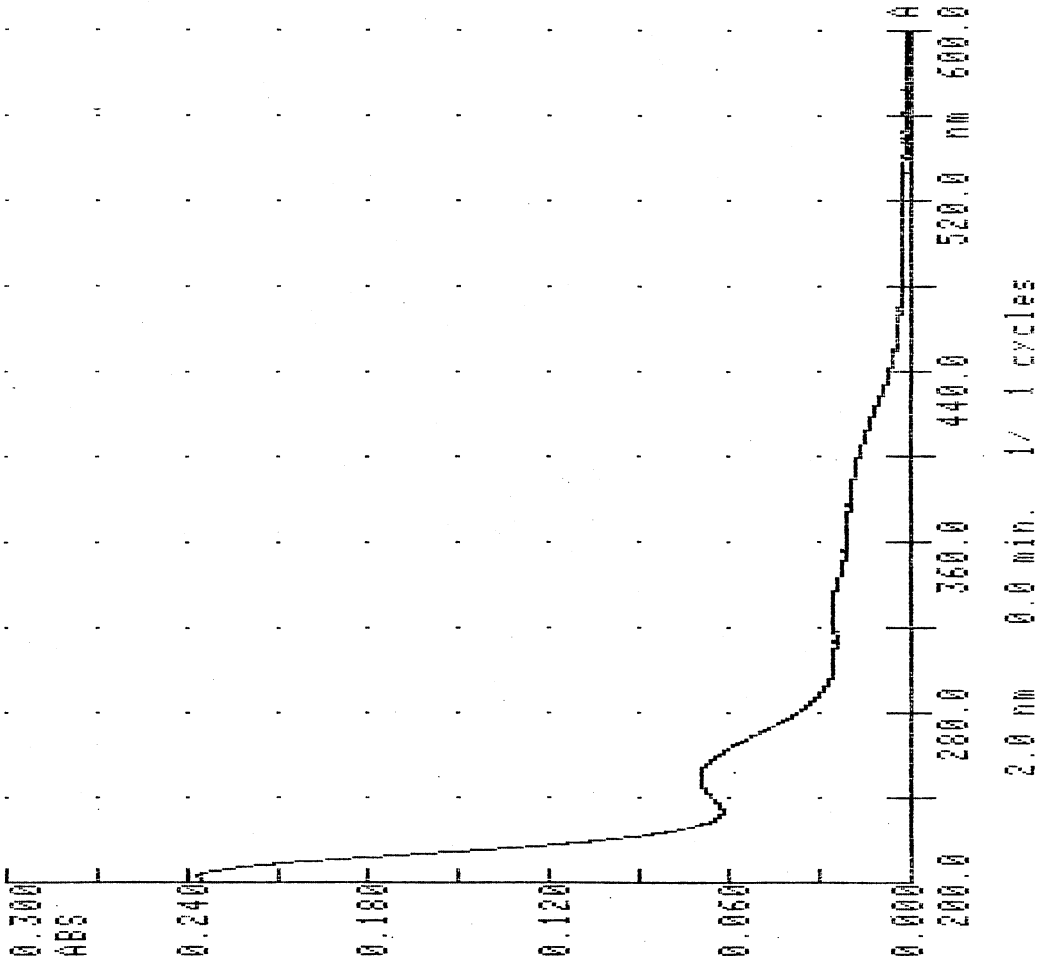

Figure 41. UV-vis spectrum of an LB film of **CPS-1**.

Na^+ and in doing so yields anions, unencumbered by strong solvation forces, which are potent nucleophiles. Sulfuric acid was chosen for the hydrolysis reaction of **3** because of the possible reaction of hydrochloric acid with the ether functional group.

Previously, the alkylation reaction was performed to the product, 4-(4-hydroxypiperidino)benzaldehyde, obtained from the reaction of **1** and 4-fluorobenzaldehyde. In this case, low yield of **5** was obtained because it was necessary to remove unreacted bromohexane and starting material by column chromatography before it could be recrystallized from ethanol-H_2O mixture. After this step, the amount of **5** decreased considerably. Moreover, the presence of a competing reaction which involved the aldehyde functional group was evident from the ^1H NMR. It showed a smaller peak ratio of the aldehydric H. With the presence of a small amount of H_2O, NaH is converted to NaOH which can eventually be used for Cannizzaro reaction of benzaldehyde. Therefore, the alkylation should be done prior to the reaction of the amine to 4-fluorobenzaldehyde. The route chosen to synthesize **5** was found to work well since the crude product precipitated when the reaction mixture was poured into H_2O. The crude solid can then be recrystallized without the removal of excess bromohexane by chromatography.

In the classic version of the Wittig reaction, arylmethyl halides are treated with triphenylphosphine and the corresponding phosphorus ylide is then reacted with aryl aldehydes. The stilbenes usually are formed as a mixture of cis and trans isomers. Some of the drawbacks of the classic Wittig reaction are avoided in the Horner-Emmons and Wadsworth-Emmons reaction.[21] The arylmethyl halides are heated with trialkyl phosphites to give the phosphonates. Reaction of aryl aldehydes with the anion of phosphonates formed in situ with sodium hydride or an alkoxide gives *trans*-stilbenes, with only a small amounts or none of the cis isomers. Baker and Sims[22] reported that the addition of a catalytic amount of 15-crown-5 in the formation of the stilbene greatly facilitates the reaction. Reactions are carried out in short reaction times (about two hours)

and at lower temperatures than those conventionally used (0 - 25 ^{o}C instead of 80 ^{o}C). The preparation of the stilbene methyl esters, **9** and **10**, was performed using the modified Wittig reaction. This procedure has proved to be useful in preparing sensitive olefins not preparable by standard Wittig synthesis. In addition, it is not particularly sensitive to atmospheric oxygen, thus allowing simpler experimental procedures, is, in general, less expensive, and furnishes the trans isomers stereospecifically.

Transesterification reaction is usually conducted under acidic or basic conditions. In an earlier experiment, the use of concentrated H_2SO_4 as catalyst gave low yield for monomer, **MNR-1**. On the other hand, the ^{1}H NMR spectrum of the product obtained from the transesterification of **10** showed the decomposition of the starting material. The four doublets in the aromatic region corresponding to the 8 aromatic H's disappeared. N,N-Dimethylaminopyridine (DMAP)[23] as catalyst was also used for **9** but failed to give the corresponding product. DMAP is used in the transesterification of the more reactive acid derivatives, acid halides and acid anhydride. The failure of the previous procedures made me look for a better catalyst that would involved the use of substrates with similar functional groups present in our materials. Takai and Shibata[18] patented a transesterification procedure using nickel acetylacetonate, $Ni(acac)_2$, as catalyst for the reaction of methyl acrylate and 2-(N, N-dimethylamino)ethanol. This procedure was followed and it gave high yields and good purity of the monomers, **MNR-1** and **MNR-2**. In this reaction, the Ni coordinates with the carbonyl oxygen, making the carbonyl carbon susceptible to nucleophilic attack.

The commercial poly(hydromethyl)siloxane (PHMS) and the copolymer of 50 - 55% (hydromethyl)siloxane - 45 - 50% (dimethyl)siloxane (PHMS-PDMS) used in the preparation of the side-chain polysiloxanes are normally polydisperse. There is also the question of statistical distribution of the $SiMe_2$ and Si(Me)H groups for the copolymer backbone. The ^{29}Si NMR spectrum of PHMS-PDMS indicated that the repeat units are arranged statistically, which is comparable to previously reported spectrum[15] of random

copolymers of PHMS-PDMS. These materials are usually manufactured to meet some viscosity requirement, and not to have a specific value of DP or M_w/M_n.[24] The reported M_w/M_n for commercial PHMS is normally 2.3 while M_w/M_n for PHMS-PDMS is 1.9.[25] These M_w/M_n values are similar to what I have obtained, as presented in Table VII. The DP values are usually quite low, particularly for copolymer backbones (DP < 30). Even for commercial PHMS, the DP ranges from 35 to 60 (Petrarch) or 45 to 90 (Wacker). Thus, the SCLC polysiloxanes produced are in the molecular weight range in which their liquid crystalline properties are dependent upon DP. It is, therefore, important that the characterization of the polysiloxanes used and the side chain polymer are specified.

In the hydrosilylation reaction of my SC polysiloxanes, hexachloroplatinic acid ($H_2PtCl_6 \cdot xH_2O$) was chosen as a catalyst instead of divinyltetramethyldisiloxane platinum. The latter catalyst has been used successfully in other laboratories[26-28] for the preparation of SCLC polysiloxanes. However, in my case, several attempts at hydosilylation failed to give the desired polymers. During the reaction of **MNR-1** with either the homo- or the copolysiloxane in the presence of the latter catalyst, precipitation of the polymer occurred. Since the yellow solid obtained was also insoluble in all organic solvents including chloroform, it is concluded that a cross-linked polymer was made. The nature of the cross-linking is not clear. Gray and his coworkers[29] have suggested that cross-linking could involve Pt catalyzed reactions leading to the splitting of Si-C bonds or a reaction such as

$$2\ \text{–SiH} + \text{Pt (II)} + [\text{O}] \longrightarrow \text{–Si–O–Si–} + \text{Pt (0)} + \text{H}_2 \uparrow$$

The problem of cross-linking can be overcome by the use of freshly prepared Speier's catalyst ($H_2PtCl_6 \cdot xH_2O$ in isopropyl alcohol) and the use of no more catalyst than is needed to give an effective hydrosilylation. If fresh solutions are used, it was suggested that $PtCl_6^{2-}$ may be the catalyst whereby SCLCP without blackish color may be made

reproducibly and without cross-linking. However, with aged catalyst, most of the Pt is in the form of Pt (II). Then, metallic Pt appears to form and makes the polymer dark. It is therefore important to prepare the Speier's catalyst just before the hydrosilylation step. The yellow color of our polymer showed no evidence of metallic Pt forming in our reaction. The low solubility of **HPS-1** in most organic solvents is due to its semicrystalline character. With the degree of polymerization (DP) equal to 60 and having a strong dipole-dipole interaction of the stilbene mesogens, solvent must overcome a sizeable crystal lattice energy to dissolve the polymer. The improved solubility of **HPS-2** is due to the increased flexibility of the hexyloxypiperidino end of the side chain.

Doping studies show that very small amount of low-molecular weight materials have a profound effect on the polymer properties. The phase transitions of polymer contaminated with monomer, as observed in the DSC, show broad peaks, and the transition temperatures are lower than the polymer alone. Total removal of the SC precursor depends critically on the nature of the polymer and the number and efficiency of the precipitations used in the work-up. Gray and his coworkers[30] showed that three precipitations (the number often regarded as sufficient) of the SCLC polysiloxane, shown below, are usually not enough to rid the polymer of the alkene.

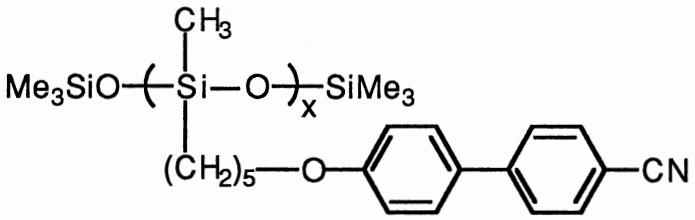

The above mentioned authors showed that after three precipitation in which alkene is still detectable by TLC, the glass transition temperature, T_g, and the isotropization temperature, T_i, values varied appreciably and the peak widths obtained at several analyses for the isotropization transition were fairly broad. However, after 8 - 10 precipitations (no alkene

detectable by TLC), the T_g values were more or less constant, and 3-10 °C higher than the reported values after three precipitations. The T_i values were also 5-9 °C higher, and represented a narrower distribution. The peak widths were also narrower, that is, the biphasic peak was narrowed through the removal of alkene. There is no evidence that the removal of alkene causes any change in DP or M_w/M_n of the polymer. In my case, the work-up and six or seven precipitations did not remove all of the unreacted alkene as detected by GPC. The highest monomer content is in **HPS-2** and **CPS-2**. Apparently, the solubility of **MNR-2** is very much the same as that of the corresponding polysiloxanes. This was evident on the GPC analysis of the polymer obtained after each precipitation. There was very small amount of monomer removed in each precipitation. Therefore, it is important to be aware of the possible effects of these unreacted alkenes on the glass transitions and mesophase transition temperatures.

The molecular weights of the SC polysiloxanes are only relative since they were determined by GPC using a calibration plot constructed with polystyrene standards. These values are much lower that the real molecular weights. The theoretical M_n of **HPS-1** with a DP of 60 and taking into account the end groups, unreacted Si-H groups and the octyl groups as side chain, is either 27 500 (^{1}H NMR analysis) or 22 500 (EA). On the other hand, the value obtained by GPC measurements is only 6800. The same observation holds true for **HPS-2** in which the theoretical M_n is 36 200 (^{1}H NMR analysis) or 25 000 (EA), while the value obtained by GPC is 19 400. The difference in the GPC and calculated M_n is much bigger in **HPS-1** than in **HPS-2** because the mesogenic side chains of the former polymer are less solvated, giving rise to a compact shape. This resulted to a smaller effective volume in solution, thus lower value of M_n. On the other hand, the side chains of the latter polymer are more flexible because of the incorporation of the hexyloxypiperidino end, making the structure more of a random coil. The mesogenic side chains of **HPS-2** experienced greater solvation, giving rise to a larger effective volume in solution. There was not much difference between the theoretical M_n

and the GPC values for **CPS-1** and **CPS-2**. Duran and Strazielle[19] reported that the molecular weights of a series of SCLC polymethacrylates which were measured by the classical size exclusion chromatography (SEC) technique calibrated with polystyrene standards, were systematically lower than those obtained by light scattering (LS) methods.

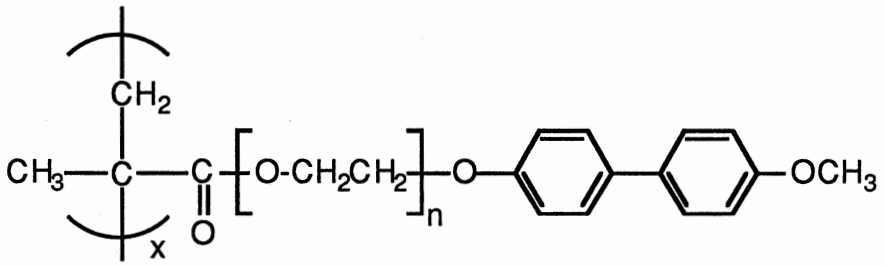

n = 0 - 4

The LS M_W values were 1.5-2.5 times larger than the SEC M_W values. This large difference is understandable when one considers that the SEC separation process is not governed by the mass but by the hydrodynamic volume, that is, the product $[\eta]_i M_i$ of the fraction, where $[\eta]_i$ is the intrinsic viscosity of a fraction of mass (M_i) associated with an elution volume $(V_e)_i$. In another study, Lang and Burchard[31] showed that for the same molecular weight, V_e is shifted to larger values as the average number of branches is increased (using linear PMMA chains as the reference polymer).

It is important to define the DP, M_W/M_n and purity of SCLCPs. Otherwise the structural correlations with liquid crystal and other physical properties are uncertain. The trend that is generally accepted consists of the enlargement of the temperature range of the mesophase with an increase of the polymer molecular weight. Sagane and Lenz[32-34] illustrated that SCLC poly(vinyl ether)s display various mesophases at different molecular weights in the range of 1300 to 18000. A broad M_W/M_n polymer sample showed the disappearance of smectic phase, and all the observed transition temperatures (e.g., T_g and

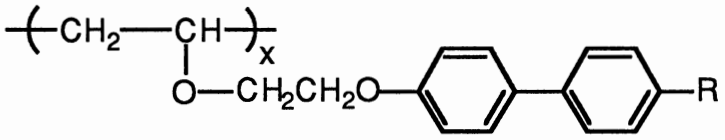

R = H , OC_nH_{2n+1} , CN

T_i) were higher than those for the narrower M_W/M_n polymer sample. Percec and Lee[35] observed that SCLC poly(vinyl ether)s with cyanobiphenyl mesogenic groups having DP from 1 to 30 and M_W/M_n approximately equal to 1.1, showed a continuous change of the mesomorphic - isotropic phase transitions (i.e., from nematic - isotropic to smectic - isotropic) on increasing their molecular weight. Stevens and his coworkers[36] investigated the extent to which the degree of polymerization influences the liquid crystalline state of SCLC oligomers with siloxane backbone. With each additional lengthening of the siloxane backbone, T_i increased steeply up to DP $\leq$ 10. Thereafter, DP has a slight effect on T_i. The T_g and the mesophase-to-mesophase transition temperature (T_{lc}) also shift to higher temperatures with increasing DP, but not as strongly as the corresponding T_i.

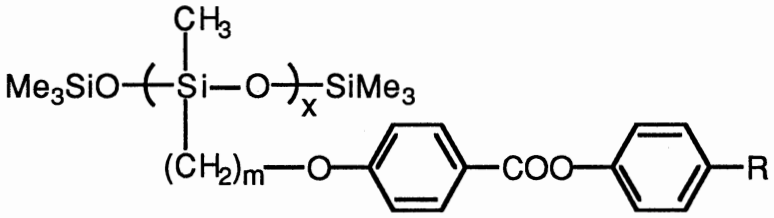

m = 3 - 6
R = OCH_3 , $COOCH_2C^*H(CH_3)(C_2H_5)$

At DP > 10, T_g and T_{lc} remained nearly constant. The authors demonstrated that at DP > 100, the liquid crystal range remained constant and the phase transition temperatures were independent of DP. Varying the molecular weight has little influence on the nature and number of mesophases exhibited by polymers with very flexible backbones such as polysiloxanes, except when comparing oligomers with very low molecular weights.

Similar results were obtained by Gray and his coworkers[25] for the SCLC polysiloxane, shown below, in which the transition temperatures increased with increasing DP at approximately constant M_w/M_n values and approached constancy only at around DP

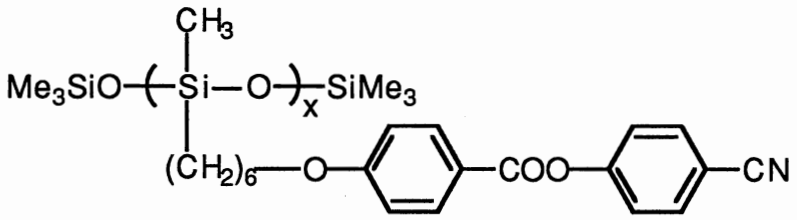

of 100. It has been found by the same group that the effect of M_w/M_n for SCLC polysiloxanes was different in that there was an increasing trend of T_g and T_i as the M_w/M_n values decreased. Changes in M_w/M_n from 1.9 to 1.25 caused increases in T_g and T_i by approximately 5 °C. Since the molecular weights of my SC polysiloxanes are relative, they can only be used to estimate whether they are below or above the minimum needed for molecular weight independent phase transitions. **HPS-1** and **HPS-2** have high enough molecular weights to expect little dependence of phase transitions on molecular weight. It is thus possible to discuss in a semiquantitative manner the effect of the change of the amino groups on the phase transitions for the SC homopolysiloxanes. The addition of 1-octene to mop up the remaining Si-H will make little difference in the physical properties of the polymers made because less than 12% of the substituted Si-H contained the octyl group as calculated from the ^1H NMR. Aside from the slight influence of molecular weight on the phase behavior of **CPS-1** and **CPS-2** due to low DP, the side chain composition also affects the phase transitions of the copolymers. Since the copolymers are mixtures with different SC distributions, the mesophase transitions are likely to be associated with broader biphasic regions. Percec and Lee[37] demonstrated that the transition temperatures and mesophases depend on the composition of SCLC

copolymers at constant M_n and M_w/M_n equal to 1.1. Thus, it is essential to be aware of these effects when discussing the phase behavior of the SC copolysiloxanes.

Liquid Crystal Phases. It is not surprising that **MNR-1** does not form a liquid crystalline phase. Compounds exhibiting liquid crystalline properties usually have an anisotropic rigid core and flexible chains on each end of the core. The dimethylamino group in **MNR-1** is not long enough to make it flexible. However with the change to hexyloxypiperidino group, the required flexibility at the amino end is fulfilled. The appearance of only smectic phases in **MNR-2** was consistent of what has been observed by Dave and Patel.[38] When the alkyl chains are short, the systems are either non-mesomorphic or nematic. As the chain length increases, smectic properties begin to appear and as the smectic phase increases, the nematic phase decreases with each successive chain increment until in the higher homologous series, only smectic phases are found. However, it is hard to postulate the exact length of the alkyl chain in which the appearance of the smectic phases is observed. The long undecylenyl ester and hexyloxypiperidino groups on each side of the stilbene segment were enough to induce the smectic properties of **MNR-2**.

In some cases, the attachment of non-mesogenic molecules like **MNR-1** as side chains on a polymer main chain leads to liquid crystalline properties. The polymer backbone enhances the tendency of low molar mass compounds toward mesomorphism by depressing or even canceling the ability of low molar mass compounds to crystallize after polymerization. Percec and Keller[39] illustrated that T_i (i.e., the mesophase-isotropic transition temperature) is less than the melting temperature, T_m, (i.e., crystal-isotropic transition temperature) for low molecular weights. Since the T_i is below the corresponding T_m for monomer, the monomer displays only a virtual mesophase (pontentially possible mesophase, which is thermodynamically less stable than the crystalline phase at the same temperature, therefore unrealizable both on the heating and on cooling). Therefore, the production of nematic **HPS-1** can be explained by the

attachment of **MNR-1** to a polymer backbone and by the restriction of packing possibilities of the side chains due to the large DP. Because of the polar substituents, antiparallel dipole attraction between the side chains is expected. However, with the large DP, the dipolar attraction of the side chains is affected by steric hindrance and so ordering in layers is less favored (Figure 42a). The insertion of $SiMe_2$ segments in **CPS-1** gives it a larger volume fraction of flexible chains, compared with **HPS-1**, which in turn allows more ordered packing of the side chains, as shown in Figure 42b, into the smectic phase. If, however, the monomer already shows liquid crystalline properties, the SC polymer will show a shift to more ordered mesophases compared to the side-chain precursor, or if both show the same phases, the SCLCP isotropization transition temperature may be higher and the crystal to LC transition lower. Contrary to what is expected, nematic phase was observed in the high temperature mesophase of **HPS-2**, instead of S_A phase as observed in **MNR-2**, which can be attributed to insufficient volume fraction of flexible chains for the mesogens to order into smectic layers. Although, the less ordered nematic phase was observed, the S_B to nematic phase transition and isotropization temperatures of **HPS-2** are higher than those observed in **MNR-2**. The specific volume of the material is lowered by polymerization, that is, the packing density of the mesogenic groups increases.[36] The specific volume at constant temperature decreases with increasing DP. An analogy in the behavior of the phase transition temperatures can be observed for low molar mass LCs, where specific volume decreases with increasing pressure and for oligomers, where the specific volume decreases with increasing DP. Consequently, the phase transition temperatures shift considerably to higher values. Percec and Keller[39] explained that upon increasing the molecular weight from monomer to polymer, the entropy of the isotropic phase (S_i) decreases. However, the decrease of entropies of LC (S_{lc}) and crystal (S_c) is lower than that of S_i. Therefore, the phase transition temperatures increase with increasing molecular weight up to a certain range of molecular weight

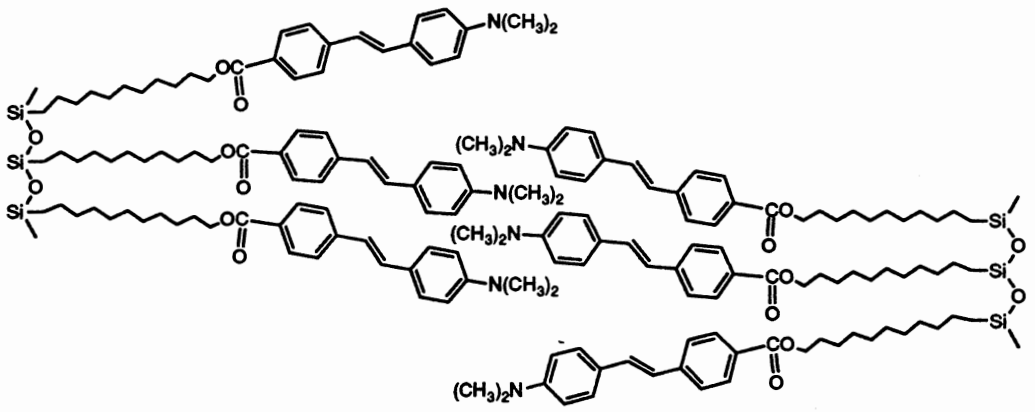

(a)

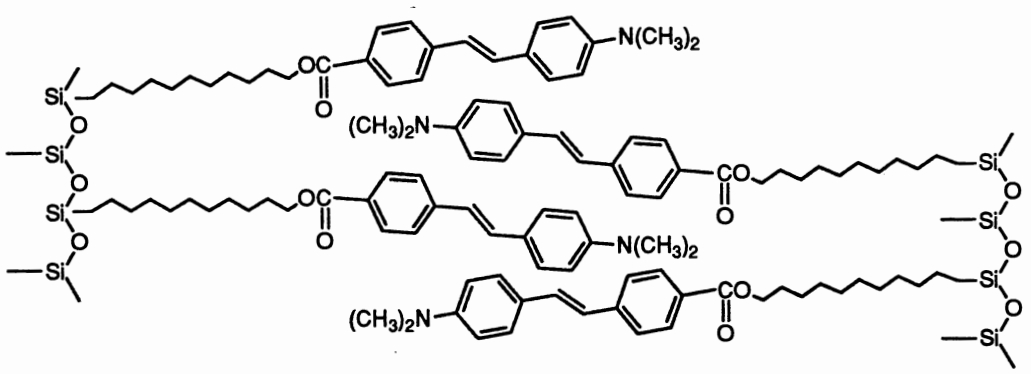

(b)

Figure 42. (a) Lack of molecular ordering of **HPS-1** in a bilayer packing. (b) Molecular ordering in the bilayer smectic A phase of **CPS-1**.

values, and the increase in T_i is steeper than that that of T_{lc} with respect to molecular weight, as shown in Figure 43.[36] This effect has been repeatedly labeled the "polymer effect", especially in the case of SCLCPs. As expected, **CPS-2** showed the same smectic phases as in **MNR-2** and exhibited higher transition temperatures. It is generally observed that homopolymers exhibit higher phase transition temperatures than copolymers

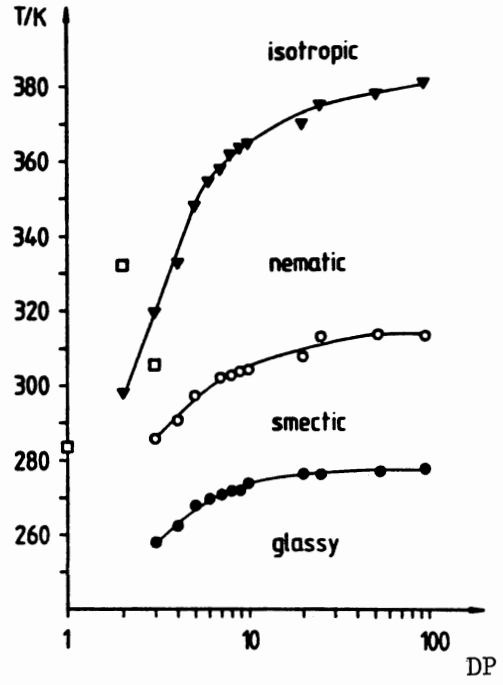

Figure 43. Phase transition temperatures as a function of degree of polymerization, DP. (Taken from Stevens and coworkers, ref. 36).

because the packing density is great in homopolymers. **HPS-1** and **HPS-2** showed high viscosities even in the isotropic state as observed in the polarizing microscope in which the flowing of the material was very slow above the isotropization temperature. The low mobility present in homopolysiloxanes explains the difficulty in producing recognizable microscopic textures even after annealing the polymer for days at 5 °C below T_i.

The identification of nematic and different smectic phases by optical microscopy is more difficult for polymers than for low molecular weight materials due to high viscosity

of polymers. Therefore, X-ray data are very important in reaching unambiguous classifications. For powder samples which were used in my study, the X-ray patterns give all the reticular spacings but no information about the spatial orientation of these planes. Thus, it is possible to distinguish between the nematic and smectic phases of liquid crystals but difficult to differentiate an S_A phase from an S_C phase. However, because of the tilt angle in S_C phase, the layer spacings, *d*, are smaller than the molecular length. Therefore, to have a way of understanding the molecular packing within the layers, the molecular length of the most stable conformation of the molecule was calculated by computer molecular modeling program (PCMODEL, Version 4.3). The calculated molecular length is used as comparison with the *d* spacings obtained from the X-ray data. The observed *d* spacings (see Table XIIIA) for **MNR-1** at 135 °C and at 40 °C with an orthorhombic crystal structure are greater than the calculated length of the molecule (~27.8 Å). The molecules are thought to be arranged in an antiparallel orientation in such a way that a small portion of the flexible undecylenyl ester end is sticking out, as shown in Figure 44a, giving rise to an increase in the layer spacing as compared to the molecular length. The *d* spacing increased as the temperature is increased. The possible explanation is that the molecules have a little mobility at higher temperature and the intermolecular attraction is reduced, allowing the molecules to protrude (Figure 44b) thus, the layer spacing is increased. On the other hand, the *d* spacings for **MNR-2** at 177 °C and 165 °C in S_A and S_B phases, respectively, are smaller than the calculated molecular length (~37.5 Å) as shown in Table XIIIB. The molecules are thought to be completely aligned antiparallel with each other, as shown in Figure 45, however, the flexible ends on each side of the rigid stilbene core are somewhat bent, thus the layer spacings are smaller than what is calculated. The *d* spacing for **MNR-2** at 30 °C, having an orthorhombic crystal structure, is almost equal to the molecular length. This is consistent with the proposed packing in which the molecules lie completely antiparallel with each other and at lower temperature the flexible ends are fully extended in an all-trans conformation.

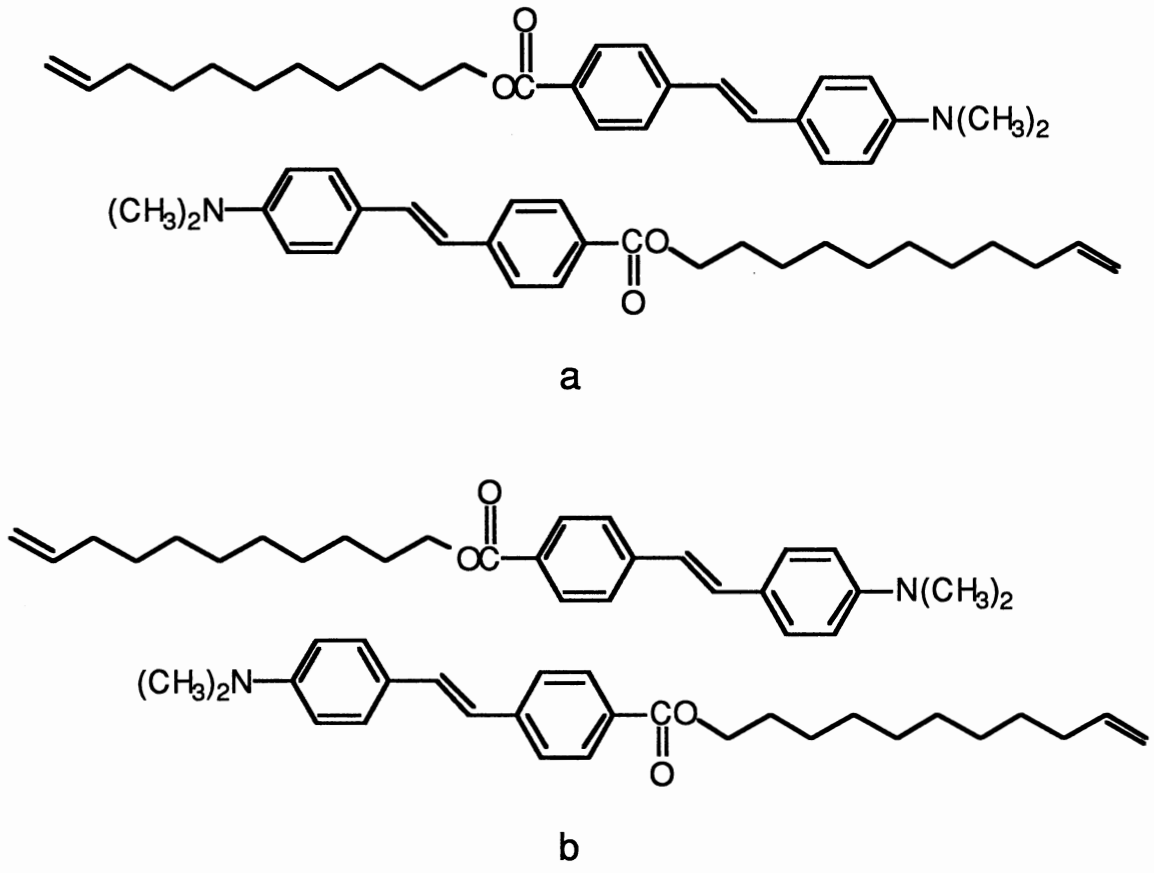

Figure 44. Depiction of antiparallel ordering of molecules such that (a) the layer spacing is slightly greater than the molecular length; (b) the layer spacing increased as the temperature is increased.

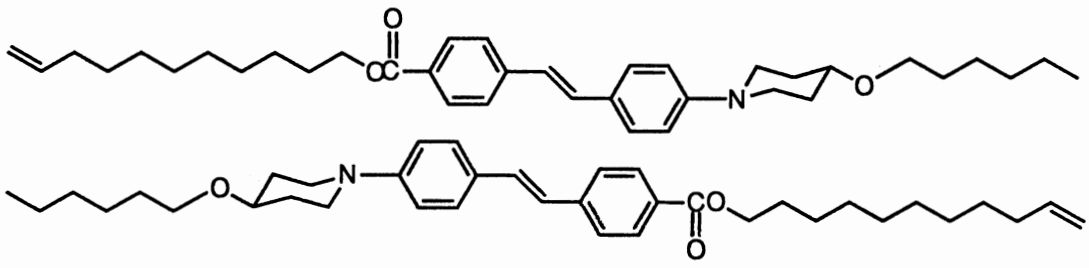

Figure 45. Depiction of antiparallel ordering of molecules such that the layer spacing is equal to the molecular length.

Table XIIIA. X-ray Diffraction Data of **MNR-1**, **HPS-1** and **CPS-1**

Sample	Temp, °C	*d* spacing, Å	(hkl)	unit cell[a]		
MNR-1[b]	135	32.49	(001)	a (Å)	=	8.0
		16.49	(002)	b (Å)	=	5.5
		10.97	(003)	c (Å)	=	32.5
		8.28	(004)	V (Å^3)	=	1430.0
		4.55	(110)	D_x (g/cm)	=	0.97
		3.99	(200)			
		3.24	(210)			
	40	30.26	(001)	a (Å)	=	7.8
		15.34	(002)	b (Å)	=	5.6
		10.28	(003)	c (Å)	=	30.3
		4.55	(110)	V (Å^3)	=	1323.5
		3.88	(200)	D_x (g/cm)	=	1.05
		3.19	(210)			
HPS-1	210	4.87				
	150	35.35	(001)	a (Å)	=	7.9
		18.72	(002)	b (Å)	=	5.4
		4.47	(110)	c (Å)	=	35.4
		3.94	(200)	V (Å^3)	=	1510.0
		3.22	(210)	D_x (g/cm)	=	1.06
CPS-1	180	37.44	(001)			
		4.63				
	136	40.90	(001)	a (Å)	=	7.9
		20.84	(002)	b (Å)	=	5.5
		4.52	(110)	c (Å)	=	40.9
		3.95	(200)	V (Å^3)	=	1777.0
		3.22	(210)	D_x (g/cm)	=	1.02

[a]V and D_x were calculated from the values of a, b, c. Z = 2, which was obtained from the product of a and b (~43 Å^2, which is equal to the molecular area of two molecules or mesogenic side chains per unit cell). [b]Calculated length ≈ 27.8 Å.

Table XIIIB. X-ray Diffraction Data of **MNR-2**, **HPS-2** and **CPS-2**

Sample	Temp, °C	*d* spacing, Å	(hkl)	unit cell[a]		
MNR-2[b]	177	33.72	(001)			
		18.26	(002)			
		4.86				
	165	34.25	(001)			
		18.72	(002)			
		4.53				
	30	38.09	(001)	a (Å)	=	8.2
		19.04	(002)	b (Å)	=	5.4
		11.95	(003)	c (Å)	=	38.1
		9.49	(004)	V (Å^3)	=	1687.0
		4.54	(110)	D_x (g/cm)	=	1.10
		4.08	(200)			
		3.26	(210)			
HPS-2	230	4.61				
	120	4.47				
	30	45.08	(001)	a (Å)	=	8.2
		4.52	(110)	b (Å)	=	5.4
		4.11	(200)	c (Å)	=	45.1
		3.20	(210)	V (Å^3)	=	1997.0
				D_x (g/cm)	=	1.03
CPS-2	205	40.90	(001)			
		21.87	(002)			
		4.65				
	171	45.53	(001)			
		24.54	(002)			
		4.57				
	30	50.19	(001)	a (Å)	=	8.2
		24.41	(002)	b (Å)	=	5.5
		4.58	(110)	c(Å)	=	50.2
		4.11	(200)	V (Å^3)	=	2264.0
		3.26	(210)	D_x (g/cm)	=	1.01

[a]V and D_x were calculated from the values of a, b, c. Z = 2, which was obtained from the product of a and b (~44 Å^2, which is equal to the molecular area of two molecules or mesogenic side chains per unit cell). [b]Calculated length ≈ 37.5 Å.

Several studies[40-43] on the X-ray diffraction of some SCLC polysiloxanes showed that the *d* spacings were much smaller than the calculated length between two polysiloxane backbones. They gave a number of possible explanations for the reduction in the spacing which involve either tilting or interdigitation. There are three possible arrangements and these are shown in Figure 46. The first involves the tilting of the mesogenic side chains which is typical of a S_C phase. The second also involves tilting but this has a herring bone motif. The third involves interdigitation in which there is overlapping of the mesogenic side chains. Sutherland and his coworkers[44] observed that the interlayer spacings of a series of terminally cyano-substituted side chain polysiloxanes in the smectic A phase were considerably smaller than twice the calculated length of the mesogenic side chains, assuming that the mesogenic groups lie perpendicular to the main polymer chain. They eliminated smectic C phase since there was no evidence for this from the X-ray photographs. For the herring bone motif, a tilt angle between 44° and 52° is required to explain the observed d spacing. These tilt angles would greatly reduce the contact between the polarizable side chains of neighboring mesogenic units. Thus, the proposed model is that of the interdigitated bilayer S_A structure with the overlap of the polarizable side chains. On the basis of packing, an interdigitated structure is favored for a number of polymeric materials which showed a similar reduction in the layer spacing, especially with polar side chains. The observed *d* spacing for the **CPS-1** at 180 °C is considerably smaller than the distance between polysiloxane backbones. For a smectic C phase or herring bone motif, the obtained *d* spacing would mean that the tilt angle of the mesogenic side chains with respect to the layer plane need to be on the order of 60°, an unreasonably large angle, thus restricting the dipole-dipole interactions of the side chains. The most sensible structure at this temperature is the interdigitated bilayer S_A which can easily account the *d* spacing and it allows the overlap of the polar side chains. The same mesophase is assigned for **CPS-2** at 205 °C because of the significant reduction of the *d* spacing as compared to the calculated distance between the backbones.

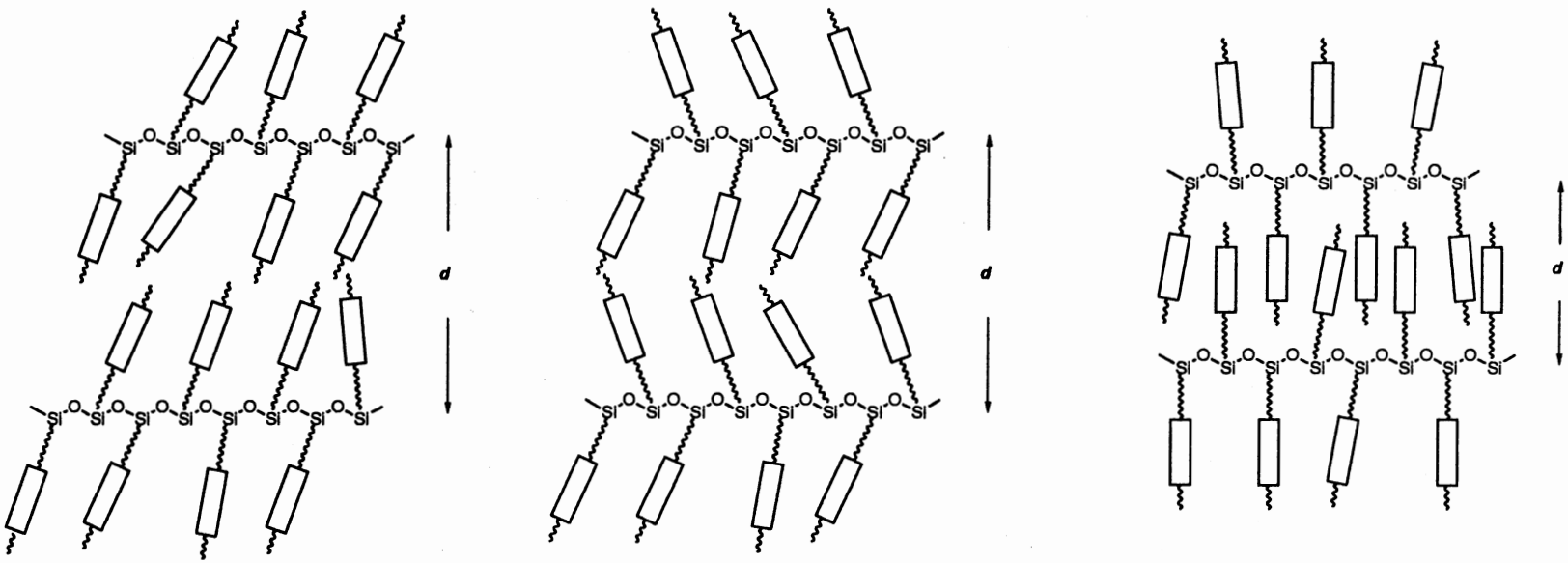

Figure 46. Schematic representation of the molecular packing: (a) tilted as in a smectic C phase; (b) tilted with a herring bone motif; (c) interdigitated bilayer smectic A structure.

The low temperature smectic phase was assigned S_B for **MNR-2** and **CPS-2** because of the strong reflection in the wide angle region, indicating hexagonal order of the molecules within the smectic layers. Smectic B and not smectic F or I was chosen for this phase because it has been observed with other substances that dimorphism can be realized with the transformation of an S_B phase to an S_A phase with increasing temperature but not with transformation of an S_F or S_I phase to an S_A phase. The explanation to this observation is that the mesogenic groups in both S_A and S_B phases are oriented normal to the smectic layers. On the other hand, S_F and S_I phases are tilted and so the transformation of either of these phases to an S_A phase is accompanied with the change of orientation of the molecules. When these phases are present, the sequence of liquid crystalline phase is S_F phase, S_I phase, S_C phase and S_A phase, if present. Trimorphism having the sequence S_E S_B S_A is also possible. There is no substance known with a S_E phase that also possesses smectic H, G, F or I phases.[45] Therefore, I cannot rule out the possibility that the assigned orthorhombic crystalline structure is a S_E phase. Like the orthorhombic crystalline structure, the powder X-ray diffraction pattern of S_E phase also shows the three peaks in the wide angle region corresponding to the 110, 200 and 210 reflections. Sutherland and Ali-Adib[46] also observed these three reflections below the S_A phase of terminally bromo-substituted SCLC polysiloxanes and interpreted it either as S_E phase or orthorhombic crystal.

Monolayers. The small mean molecular area per repeat unit obtained for **HPS-1** corresponds to the expected value of a close-packed array of benzene rings arranged perpendicular to the water surface. The Π - A isotherm of 4-cyano-4"-n-pentyl-p-terphenyl was reported by Daniel and his coworkers[47] and showed the collapse of the monolayer at 22 mN/m with

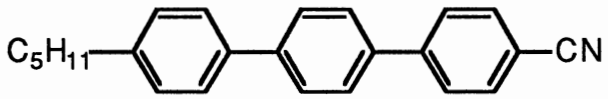

an average molecular area of 23 Å^2/molecule. A space-filling molecular model showed that the estimated minimum cross-sectional area is about 20 Å^2/molecule. Albrecht and his coworkers[48] studied monolayers of rod-shaped liquid crystalline compounds. The Π - A

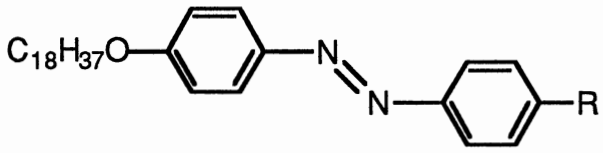

R = COOH , NO_2 , CN

diagrams showed a tight packing of the hydrocarbon chains at the collapse point. They explained that the collapse area of 20 Å^2 could be related to the vertical orientation of the aromatic chromophores at the water surface. This agrees with what I have postulated earlier about the large hydrodynamic volume of **HPS-1**. The strong dipolar interactions of the mesogenic side chains give rise to an extended orientation of the side chains. However, the mean molecular areas of the other three SC polysiloxanes are very much higher than the expected value. The Π - A isotherms of alkyl-cyano biphenyl monolayers were reported to show collapse areas in the range of 34 to 36 Å2/molecule.[49] The increase in collapse area relative to that of the terphenyl compound indicated that the CN biphenyl cores are tilted further from the layer normal at the collapse point. In the case of **CPS-1**, the side chains have more available space due to the $SiMe_2$ segment and can assume a tilted arrangement of the aromatic chromophores at the water space. The amino group at the end of the side chain of my polysiloxanes is assumed to be attracted to the water surface with the stilbene core also slightly attracted, giving rise to a tilted orientation. The polysiloxane backbone is located away from the water surface. UV/vis spectroscopic studies on monolayers of a cyano-substituted azobenzene pointed to such arrangement of the chromophores at the water surface.[48] The addition of the piperidino ring in **HPS-2** and **CPS-2** has a marked effect on the molecular packing. The bulky ring system reduced

packing efficiency, giving a much larger mean molecular area. The $SiMe_2$ segment in the SC copolysiloxanes reduced the surface viscosity of the polymers and so there is little hysteresis observed in isotherms of **CPS-1** and **CPS-2**. Furthermore, the stability of the monolayers of the SC copolysiloxanes is better than the SC homopolysiloxanes, although Figures 31 and 33 showed an unusual behavior of the monolayers of **CPS-1** and **CPS-2**. **CPS-1** showed an increase in the mean molecular area from about 40 minutes to about 80 minutes. This may possibly be due to temperature fluctuations or rearrangement of the polymer chains or side chains. The discontinuity observed at about 53 mN/m in the Π - area isotherm (Figure 23) of **CPS-1** might not be due to the collapse of the monolayer, but instead the polymer might just be undergoing reorientation of the main chains or side chains. The isotherm was reproducible thus, the discontinuity in the isotherm cannot be attributed to temperature variations. **CPS-2** also showed this unusual behavior in the isobaric experiment, however, it is not as obvious as in **CPS-1**.

Conclusion

All of the SC polysiloxanes showed thermotropic liquid crystalline properties from their thermal analysis, optical microscopy, and X-ray diffraction. **HPS-1** and **CPS-1** exhibited enantiotropic nematic and smectic A (S_A) phases, respectively. With the replacement of the dimethylamino group with *n*-hexyloxypiperidino group, an additional low transition temperature mesophase, smectic B (S_B), was observed for **HPS-2** and **CPS-2**. With DP = 60 in SC homopolysiloxanes, the antiparallel dipole attraction of the mesogenic side chains is restricted, thus layer formation is less favored. **HPS-1** and **HPS-2** exhibited the less ordered nematic mesophase while the SC copolysiloxanes, **CPS-1** and **CPS-2**, exhibited the more ordered smectic A phase. The low molecular weight mesogen, **MNR-2** showed similar liquid crystalline phases (S_B and S_A phases) as the corresponding SC polysiloxanes while **MNR-1** showed only melting transition.

The monolayers of **CPS-1** and **CPS-2** showed better stability on water as compared to the monolayers of **HPS-1** and **HPS-2**. The small mean molecular area per repeat unit of **HPS-1** indicates vertical orientation of the aromatic chromophore at the water surface while the other three polysiloxanes are somewhat tilted with the stilbene core also attracted to the water surface. Low transfer ratios of **CPS-1** and **CPS-2** monolayers onto hydrophobic substrate were obtained. The addition of a small amount of monomer was thought to help stabilize the monolayers but the opposite was observed. When the dipping rate was reduced, I was able to transfer monolayers of the copolysiloxanes. Thus, slower dipping might still improved the deposition of the monolayers of my polysiloxanes. Carr and Goodwin[50] used aqueous subphase of pH 5.5 at 20 ^{o}C on their LB experiments on SCLC copolysiloxanes. It is then possible that the lowering of the temperature will greatly improve the stability of the monolayers. Another possibility is the lowering of the pH of the subphase (water), which will protonate the amino group. If the latter case improve the stability of the monolayers, it can be concluded that the amino group is attracted to the water surface and the polysiloxane backbone is sticking out of the water-air interface. Horizontal lifting method was used by Carpenter and his coworkers[51] when transferring SCLCP onto a glass substrate. This might also be a better method for my SCLC polysiloxanes, specially for the homopolysiloxanes which have high viscosity. However, it is also possible that the failure to deposit multilayers of the polymers onto a substrate is simply because not all stable monolayers can be transferred onto a substrate.

Spin-coated films from dibromomethane solution of the polysiloxanes gave cloudy samples. Thus, these polymers cannot be used for SHG measurements, unless the optical quality of the films will improve once the chromophores are oriented by dc electrical poling, either contact or corona poling. Therefore, the preparation of acentric LB films is the best bet for possible study of the SHG response of my polysiloxanes.

REFERENCES

1. Prasad, P. N.; Williams, D. J. *Introduction to Nonlinear Optical Effects in Molecules and Polymers*; John Wiley & Sons, Inc.: New York, 1991.
2. McArdle, C. B., Ed. *Side Chain Liquid Crystal Polymers*; Blackie and Sons: Glasgow, U. K., 1989.
3. Griffin, A. C.; Bhatti, A. M.; Hung, R. S. L. *Proc. SPIE* **1986**, 682, 65-69.
4. Stamatoff, J. B.; Buckley, A.; Calundann, G.; Choe, E. W.; DeMartino, R.; Khanarian, G.; Leslie, T.; Nelson, G.; Stuetz, D.; Teng, C.-C.; Yoon, H.-N. *Proc. SPIE* **1986**, 682, 85-92.
5. Le Barny, P.; Ravaux, G.; Dubois, J. C.; Parneix, J. P.; Njeumo, R.; Legrand, C.; Levelut, A. M. *Proc. SPIE* **1986**, 682, 56-64.
6. Leslie, T. M.; DeMartino, R. N.; Choe, E. W.; Khanarian, G.; Haas, D.; Nelson, G.; Stamatoff, J. B.; Stuetz, D. E.; Teng, C.-C.; Yoon, H.-N. *Mol. Cryst. Liq. Cryst.* **1987**, 153, 451-477.
7. DeMartino, R. N.; Choe, E. W.; Khanarian, G.; Haas, D.; Leslie, T.; Nelson, G.; Stamatoff, J.; Stuetz, D.; Teng, C. C.; Yoon, H. In *Nonlinear Optical and Electroactive Polymers*; Prasad, P. N., Ulrich, D. R., Eds.; Plenum Press: New York, 1988; pp 169-186.
8. Esselin, S.; Le Barny, P.; Robin, P.; Broussoux, D.; Dubois, J. C.; Raffy, J.; Pocholle, J. P. *Proc. SPIE* **1988**, 971, 120-127.
9. Griffin, A. C.; Bhatti, A. M.; Hung, R. S. L. In *Nonlinear Optical and Electroactive Polymers*; Prasad, P. N.; Ulrich, D. R., Eds.; Plenum Press: New York, 1988; pp 375-391.

10. McCulloch, I. A.; Bailey, R. T. *Proc. SPIE* **1989**, 1147, 134-140.

11. Ore, Jr., F. R.; Hayden, L. M.; Sauter, G. F.; Pasillas, P. L.; Hoover, J. M.; Henry, R. A.; Lindsay, G. A. *Proc. SPIE* **1989**, 1147, 26-35.

12. Pfeiffer, M.; Haase, W.; *Proc. SPIE* **1990**, 1337, 234-245.

13. Zhao, M.; Bautista, M.; Ford, W. T. *Macromolecules* **1991**, 24, 844-849.

14. Ford, W. T.; Bautista, M.; Zhao, M.; Reeves, R. J.; Powell, R. C. *Mol. Cryst. Liq. Cryst.* **1991**, 198, 351-356.

15. Gray, G. W.; Hawthorne, W. D.; Lacey, D.; White, M. S.; Semlyen, J. A. *Liq. Cryst.* **1989**, 6, 503-513.

16. Emerson, W. S.; Heimsch, R. A. *J. Am. Chem. Soc.* **1950**, 72, 5152-5155.

17. Tournilhac, F.; Nicoud, J. F.; Simon, J.; Weber, P.; Guillon, D.; Skoulios, A. *Liq. Cryst.* **1987**, 2, 55-61.

18. Takai, Y.; Shibata, Y. Jpn. Kokai Tokkyo Koho JP 63 101 350, 1988; *Chem. Abstr.* **1988**, 109, 129828.

19. Duran, R.; Strazielle, C. *Macromolecules* **1987**, 20, 2853-2858.

20. Friedzon, Y. S.; Boiko, N. I.; Shibaev, V. P.; Plate, N. A. as reported by Noel, C. In *Side Chain Liquid Crystal Polymers*; McArdle, C. B., Ed.; Blackie and Sons: Glasgow, U. K., 1989; p 184.

21. Becker, K. B. *Synthesis* **1983**, 341-368.

22. Baker, R.; Sims, R. J. *Synthesis* **1981**, 117.

23. Hofle, G.; Steglich, W.; Vorbruggen, H. *Angew. Chem. Int. Ed. Engl.* **1978**, 17, 569-583.

24. Gray, G. W. In *Side Chain Liquid Crystal Polymers*; McArdle, C. B., Ed.; Blackie and Sons: Glasgow, U. K., 1989; pp 106-129.

25. Gray, G. W.; Hawthorne, W. D.; Hill, J. S.; Lacey, D.; Lee, M. S. K.; Nestor, G.; White, M. S. *Polymer* **1989**, 30, 964-971.

26. de Marignan, G.; Teyssie, D.; Boileau, S.; Malthete, J.; Noel, C. *Polymer* **1988**, 29, 1318-1322.

27. Suzuki, T.; Okawa, T.; Ohnuma, T.; Sakon, Y. *Makromol. Chem., Rapid Commun.* **1988**, 9, 755-760.

28. Lee, M. S. K., Gray, G. W.; Lacey, D.; Toyne, K. J. *Makromol. Chem., Rapid Commun.* **1989**, 10, 325-331.

29. Gray, G. W.; Lacey, D.; Nestor, G.; White, M. S. *Makromol. Chem., Rapid Commun.* **1986**, 7, 71-76.

30. Nestor, G.; White, M. S.; Gray, G. W.; Lacey, D.; Toyne, K. J. *Makromol. Chem.* **1987**, 188, 2759-2767.

31. Lang, P.; Burchard, W. *Makromol. Chem., Rapid Commun.* **1987**, 8, 451-455.

32. Sagane, T.; Lenz, R. W. *Polymer J.* **1988**, 20, 923-931.

33. Sagane, T.; Lenz, R. W. *Polymer* **1989**, 30, 2269-2278.

34. Sagane, T.; Lenz, R. W. *Macromolecules* **1989**, 22, 3763-3767.

35. Percec, V.; Lee, M. *Macromolecules* **1991**, 24, 1017-1024.

36. Stevens, H.; Rehage, G.; Finkelmann, H. *Macromolecules* **1984**, 17, 851-856.

37. Percec, V.; Lee, M. *Macromolecules* **1991**, 24, 4963-4971.

38. Dave, J. S.; Patel, P. R. *Mol. Cryst.* **1966**, 2, 103-114.

39. Percec, V.; Keller, A. *Macromolecules* **1990**, 23, 4347-4350.

40. Keller, K. N. *Macromolecules* **1989**, 22, 4597-4599.

41. Davidson, P.; Levelut, A. M.; Achard, M. F.; Hardouin, F. *Liq. Cryst.* **1989**, 4, 561-571.

42. Noel, C. In *Side Chain Liquid Crystal Polymers*; McArdle, C. B., Ed.; Blackie and Sons: Glasgow, U. K., 1989; pp 159-195.

43. Tinh, N. H.; Achard, M. F.; Hardouin, F.; Mauzac, M.; Richard, H.; Sigaud, G. *Liq. Cryst.* **1990**, 7, 385-394.

44. Sutherland, H. H.; Ali Adib, Z.; Gray, G. W.; Lacey, D.; Nestor, G.; Toyne, K. J. *Liq. Cryst.* **1988**, 3, 1293-1300.

45. Demus, D.; Diele, S.; Grande, S.; Sackmann, H. In *Advances in Liquid Crystals*, Vol 6; Brown, G. H., Ed.; Academic Press: New York, 1983; pp 1-107.

46. Sutherland, H. H.; Ali-Adib, Z. *Liq. Cryst.* **1991**, 9, 899-902.

47. Daniel, M. F.; Lettington, O. C.; Small, S. M. *Thin Solid Films* **1983**, 99, 61-69.

48. Albrecht, O.; Cumming, W.; Kreuder, W.; Laschewsky, A.; Ringsdorf, H. *Colloid Polym. Sci.* **1986**, 264, 659-667.

49. Daniel, M. F.; Lettington, O. C.; Small, S. M. *Mol. Cryst. Liq. Cryst.* **1983**, 96,373-385.

50. Carr, N.; Goodwin, M. J. *Makromol. Chem., Rapid Commun.* **1987**, 8, 487-493.

51. Carpenter, M. M.; Prasad, P. N.; Griffin, A. C. *Thin Solid Films* **1988**, 161, 315-324.

CHAPTER III

ESTIMATION OF SECOND ORDER NONLINEAR OPTICAL POLARIZABILITY

Introduction

The design of new materials for second order nonlinear optical (NLO) applications requires a knowledge of the contribution of the molecules constituting the medium to its nonlinear polarization. The common technique for measuring molecular second order polarizabilities, β, is electric field induced second harmonic generation (EFISH).[1] The value of β for molecules is determined from measurements on liquids or solutions. In this method, a strong dc electric field is applied across a solution of the compound causing a bias on the average orientation of the molecules due to the interaction of the field with the permanent dipoles of the molecules. A laser beam is passed through the solution, and the intensity of the generated second harmonic light is then measured. However, this method requires elaborate and expensive instruments to make these time-consuming measurements. The equipment for EFISH is as complicated as the one used for second harmonic generation (SHG) measurements on poled polymer films since both require the use of high-voltage power supply and laser beam.

An alternative approach is the calculation of β by the use of the two-level model which takes into account the contribution to β of charge-transfer resonance states within a molecule containing delocalized π-electron system.[2,3] This model assumes that the electronic properties of the molecule are determined by a ground state and a low-lying charge-transfer excited state. For most organic molecules that are of interest for SHG,

this model is a good approximation because the energy difference between the ground and the first excited state is considerably less than that between the ground and higher excited states: there is a first excited state low in energy. For molecules having electron-donor and acceptor groups linked through a π-electron system, the transition to the low-lying charge-transfer state (first excited state) is usually in the visible or near-UV region of the spectrum. Also, most of these molecules have the donor and acceptor groups located such that the charge transfer takes place primarily along the axis of the permanent ground state dipole moment of the molecule (x-axis). Thus, the dominant component of the tensor β_{ijk} is β_{xxx}. The second-order polarizability of a molecule arising from the charge-transfer contributions using the two-level model can be approximated by using the following equation[4]

$$\beta_{xxx}(2\omega) = \left(\frac{3}{2\hbar^2}\right) \frac{\mu_{eg}^2 (\mu_e - \mu_g) \omega_{eg}^2}{(\omega_{eg}^2 - \omega^2)(\omega_{eg}^2 - 4\omega^2)} \qquad (1)$$

where ω is the angular frequency of laser beam, ω_{eg} is the angular frequency of transition from ground to first excited state, μ_{eg} is the transition dipole moment between ground and excited state, μ_g is the permanent dipole moment of the ground state, μ_e is the permanent dipole moment of the excited state, ω is the laser frequency, and $\hbar$ is Planck's constant divided by 2π. A simple method for evaluating the parameters in eq 1 is based on solvatochromism, which is the solvent-dependence of electronic spectra.[5] That is, the UV-vis absorption or emission spectrum of a compound (particularly with large dipole moments) in the vapor state can exhibit characteristic differences in the positions and intensities of the bands from the spectrum of the same compound in solution, and these differences depend on the solvent.

A macroscopic second order nonlinearity can be induced in certain polymeric materials containing dipolar chromophores.[6] To achieve noncentrosymmetric ordering of

the chromophores, electric field poling of the bulk medium can be used. The poling process involves raising the temperature of a film of the polymer to near its glass transition temperature and applying a dc electric field to the film. The permanent dipoles experience a force tending to align them in the direction of the field. The system is cooled under the influence of the field and the alignment is retained in the rigid state. The conversion efficiency to the second harmonic frequency of a thin uniaxial film on a substrate can then be determined as follows.[7,8]

$$\frac{I^{2\omega}}{I^{\omega}} = \frac{2\,\omega^2\, d_{eff}^2 L^2}{c^3\,\varepsilon_o\,(\eta^{\omega})^2\,(\eta^{2\omega})}\; I^{\omega}\; \frac{\sin^2\left\{\frac{\Delta k\, L}{2}\right\}}{\left\{\frac{\Delta k\, L}{2}\right\}^2} \qquad (2)$$

where

$$d_{eff} = (d_{33}\sin^2\theta^{\omega} + d_{31}\cos^2\theta^{\omega})\,\sin\theta^{2\omega} + 2\,d_{31}\cos\theta^{\omega}\sin\theta^{\omega}\cos\theta^{2\omega} \qquad (3)$$

is the effective nonlinear optical coefficient, L is the film thickness, I is the light intensity, Δk is the phase mismatch between the incident fundamental and generated second harmonic wave, η is the refractive index, c is the speed of light, ε_o is the permittivity of vacuum, and d_{33} and d_{31} are the nonlinear coefficients parallel and perpendicular to the poling directions, respectively. The transmitted second harmonic intensity, $I^{2\omega}$, depends upon the angle θ between the incident fundamental beam and the film normal. In this method, the thin film is rotated about an axis perpendicular to the laser beam, giving rise to a fringe (Maker fringe) pattern. The fringes are caused by the angular dependence of the Δk between the incident and harmonic waves.

This study presents the estimation of β of the monomers, **MNR-1** and **MNR-2**, by the solvatochromic method of Paley and coworkers.[9] Preliminary results on the SHG

experiments on films of a SCLC polyacrylate containing a $(CH_2)_{10}$ spacer chain and a 4-dimethylaminostilbene-4'-carboxylic ester mesogen, **P-10**, are given.

Experimental

Solvatochromic method. Solutions of each monomer, **MNR-1** and **MNR-2**, at four concentrations were prepared using eight solvents (dried for 24 h over 5 Å molecular sieve, 8-12 mesh) of different polarity. The solvents selected for this experiment were cyclohexane (C_6H_{12}), ethyl acetate (EtOAc), acetonitrile (CH_3CN), methyl ethyl ketone (MEK), toluene (C_7H_8), chloroform ($CHCl_3$), N,N-dimethylformamide (DMF), and dimethyl sulfoxide (DMSO). UV-vis spectra were scanned in the range of 200 - 600 nm using a Varian DMS 200 spectrophotometer.

Preparation of poled polymer. A transparent film of **P-10** with a thickness of 1.5 μm was obtained by spin coating a solution of the polymer in 1,4-dioxane onto an indium tin oxide (ITO)-coated glass. The film was covered with a second sheet of ITO-coated glass, and wires were cemented to each of the conductive surfaces with electrically conductive epoxy resin (Zymet SL 100-ZX). On a microscope hot stage the film was heated above its isotropization temperature (T_i = 125 °C) for 10 min, and a dc electric field of 800 kV/cm was applied. The sample was cooled at 0.2 °C/min to a temperature 5 °C below T_i, maintained there for 24 h, and then cooled quickly to room temperature before the field was turned off. After poling, the sample was clear at the center with small ripples near the edges. The SHG experiments were performed after the sample had been kept at room temperature for 3 days. After hundreds of laser pulses at 1064 nm, the film showed visible damage in the form of black spots. All data reported were obtained at exposures well below the damage threshold.

Results

Determination of μ_{eg}. The frequency of transition, $\tilde{\upsilon}_{eg}$, for each monomer in each solvent was determined from the band maximum of the UV-vis absorption. The molar extinction coefficient, ξ, was obtained by means of linear regression fit of the data to Beer's Law. The transition dipole moment, μ_{eg}, is related to the intensity of the transition and is obtained from the area under the band by means of[5]

$$\text{area} = \int \xi \, M \, d\omega = \frac{2\pi^2 \tilde{\upsilon}_{eg} N_o \eta \mu_{eg}^2 M}{3\,(2.303)\,\varepsilon_o\, c\, h} \qquad (4)$$

where M is the concentration, N_o is the Avogadro's number, η is the solvent refractive index, and the integral is over the entire absorption band (MKS units). The area (m^{-2}) was calculated from the extinction coefficient, α, at the maximum and the half width at half maximum, $\Delta X_{1/2}$, of the band. The band shape was treated as a Lorentzian function, hence the area under the band was obtained using eq 5[10]

$$\text{area} = \frac{1}{2} \pi \alpha \Delta X_{1/2} \qquad (5)$$

where both α and $\Delta X_{1/2}$ have the unit of m^{-1}. The value of μ_{eg} of each monomer in the eight solvents was then computed by means of eq 4. The results are summarized in Tables XIVA and XIVB.

Determination of μ_e. The frequency of transition, $\tilde{\upsilon}_{eg}$, for each monomer in each solvent was measured from the absorption maximum. The solvatochromic shift is expressed as follows[11]

$$\tilde{\upsilon}_{eg} = \tilde{\upsilon}_{eg}^{\S} + A\left(\frac{\eta^2 - 1}{2\eta^2 + 1}\right) + B\left[\left(\frac{\epsilon - 1}{\epsilon + 2}\right) - \left(\frac{\eta^2 - 1}{\eta^2 + 2}\right)\right] \qquad (6)$$

Table XIVA. UV-vis Absorption Data for Calculation of the Transition Dipole Moment, μ_{eg}, of **MNR-1**

solvent	$\tilde{\upsilon}_{eg}$ (10^6 m^{-1})	α (10^{-2} m^{-1})	$\Delta X_{1/2}$ (10^5 m^{-1})	area (10^7 m^{-2})	concn (10^{-2} mol m^{-3})	μ_{eg} (10^{-29} C m)
C_6H_{12}	2.6681	0.781	4.567	5.603	2.11	2.673
EtOAc	2.6434	0.855	4.807	6.456	2.11	2.939
CH_3CN	2.6302	0.721	4.889	5.537	1.78	3.002
MEK	2.6199	0.775	4.681	5.698	2.00	2.842
C_7H_8	2.6123	0.605	4.681	4.448	1.85	2.510
$CHCl_3$	2.6110	1.104	4.681	8.117	3.08	2.674
DMF	2.5800	0.678	4.700	5.006	1.88	2.718
DMSO	2.5517	0.587	4.777	4.405	1.66	2.682

Table XIVB. UV-vis Absorption Data for Calculation of the Transition Dipole Moment, μ_{eg}, of **MNR-2**

solvent	$\tilde{\upsilon}_{eg}$ (10^6 m^{-1})	α (10^{-2} m^{-1})	$\Delta X_{1/2}$ (10^5 m^{-1})	area (10^7 m^{-2})	concn (10^{-2} mol m^{-3})	μ_{eg} (10^{-29} C m)
EtOAc	2.7130	0.667	5.231	5.480	1.72	2.961
CH_3CN	2.7042	0.887	5.384	7.501	2.23	3.079
MEK	2.6882	0.705	5.159	5.714	2.02	2.795
$CHCl_3$	2.6932	0.815	5.384	6.892	2.18	2.884
DMF	2.6504	0.770	5.169	6.252	2.10	2.836
DMSO	2.6205	0.495	5.210	4.051	1.88	2.385

where $\tilde{\upsilon}^{\S}_{eg}$ is the frequency of transition in vacuum (gas phase), ϵ is the dielectric constant of the solvent, A and B are constants. The dielectric constants and refractive indices of the solvents at 25 °C (Table XV) were obtained from Riddick, Bunger and Sakano's *Organic Solvents.*[12]

Table XV. Dielectric Constants and Refractive Indices of Solvents at 25 °C

solvent	η	ϵ
C_6H_{12}	1.42354	2.015
EtOAc	1.36978	6.02
CH_3CN	1.34163	35.94
MEK	1.37685	18.51[20]
C_7H_8	1.49413	2.3807
$CHCl_3$	1.44293	4.806[20]
DMF	1.42817	36.71
DMSO	1.47754	46.45

The data were substituted in eq 6 and the best-fit values of A and B, reported in Table XVI, were obtained using least squares approximate solution.

Table XVI. Best-fit Values of A, B and $\tilde{\upsilon}^{\S}_{eg}$ in Equation 6*

parameters	**MNR-1**	**MNR-2**
A	-1.8149×10^4	-1.8042×10^4
B	-0.1049×10^4	-0.1238×10^4
$\tilde{\upsilon}^{\S}_{eg}$	3.0215×10^4	3.1021×10^4

*Equations from cyclohexane and toluene are not included.

The dipole moment change, $\mu_g - \mu_e$, was then calculated from the expression for B which is[11]

$$B = \left(\frac{2}{4\pi\epsilon_o c h a^3}\right) \mu_g (\mu_g - \mu_e) \qquad (7)$$

where *a* is the radius of a spherical cavity in the solvent occupied by the molecule (MKS units). The value of *a* (8.7 Å) was obtained from the reported *a* for 4-N,N-dimethylamino-4'-nitrostilbene (DANS) by Paley and his coworkers.[9] They assumed that *a* equals 0.7 times the donor-to-acceptor length of the molecule. An estimate of the ground state dipole moment, μ_g, was calculated from the Hammett substituent constants, σ_p.[13]

$$\Sigma\sigma_p = \sigma_p (CO_2CH_2CH_3) - \sigma_p [N(CH_3)_2] \qquad (8)$$

Ulman[14] plotted calculated dipole moments, μ_{calcd}, of several donor-acceptor substituted stilbenes as function of $\Sigma\sigma_p$ and observed a linear relationship between μ_{calcd} and $\Sigma\sigma_p$.

$$\mu_{calcd} = 3.76\ \Sigma\sigma_p + 2.87 \qquad (r = 0.97) \qquad (9)$$

He also found a linear relationship between the gas-phase calculated and experimental dipole moments, μ_{expt} (measured in benzene or dioxane) of mono and disubstituted stilbenes.

$$\mu_{expt} = 0.8\ \mu_{calcd} + 0.13 \qquad (r = 0.97) \qquad (10)$$

Using both eqs 9 and 10, the approximate value of μ_g of the stilbene chromophore was obtained.

Determination of β_{xxx}. The data for ω_{eg}, μ_{eg}, μ_g, and μ_e were then used to calculate values of β_{xxx} from eq 1 for each monomer in the six solvents for laser wavelength 1064 nm, and the results are summarized in Table XVII.

Table XVII. Second Order Polarizabilities of the Monomers in Different Solvents Calculated by the Solvatochromic Method[a]

solvents	ω_{eg} (10^{15} s^{-1})		β_{xxx} (10^{-30} esu)	
	MNR-1	**MNR-2**	**MNR-1[b]**	**MNR-2[c]**
C_6H_{12}	5.0259	-	85	-
EtOAc	4.9794	5.1105	107	115
CH_3CN	4.9545	5.0939	114	126
MEK	4.9351	5.0637	104	106.4
C_7H_8	4.9208	-	82	-
$CHCl_3$	4.9184	5.0732	93.6	112.4
DMF	4.8599	4.9926	102	116.3
DMSO	4.8066	4.9363	104.6	86.5

[a]The fundamental wavelength, λ, = 1064 nm, and the ground state dipole moment, μ_g, = 2.0904 x 10^{-29} C m. [b]The excited state dipole moment, μ_e, = 5.7445 x 10^{-29} C m. [c]μ_e = 6.4013 x 10^{-29} C m.

Sample Calculation

1. Calculation of ground state dipole moment, μ_g

$$\Sigma\sigma_p = \sigma_p (CO_2CH_2CH_3) - \sigma_p [N(CH_3)_2]$$

$$\Sigma\sigma_p = 0.45 - (-0.83) = 1.28$$

$$\mu_{calcd} = 3.76\ \Sigma\sigma_p + 2.87$$

$$\mu_{calcd} = 3.76\ (1.28) + 2.87 = 7.68\ D$$

$\mu_{expt} = 0.8\,\mu_{cacld} + 0.13$

$\mu_{expt} = 0.8\ (7.68\ D) + 0.13 = 6.78\ D$

$\mu_{expt} = 6.78\ D \times 3.334 \times 10^{-30}\ C\ m / D = 2.0904 \times 10^{-29}\ C\ m$

2. Calculation of dipole moment change, $\mu_g - \mu_e$

$(\mu_g - \mu_e) = B\,(4\,\pi \in_o c\,h\,a^3)\ (1/2\,\mu_g)$

Consider parameters for **MNR-1**

parameters: $B = -0.1049 \times 10^4\ cm^{-1}$

$\in_o = 8.854 \times 10^{-12}\ C^2\ N^{-1}\ m^{-2}$

$c = 2.998 \times 10^{10}\ cm\ s^{-1}$

$h = 6.626 \times 10^{-34}\ N\ m\ s$

$a = 8.7 \times 10^{-10}\ m$

unit analysis: $(cm^{-1})\ [(C^2\ N^{-1}\ m^{-2})\ (cm\ s^{-1})\ (N\ m\ s)\ (m^3)]\ (C^{-1}\ m^{-1}) = C\ m$

$(\mu_g - \mu_e) = (-0.1049 \times 10^4)\ (4\,\pi)\ (8.854 \times 10^{-12})\ (2.998 \times 10^{10})\ (6.626 \times 10^{-34})$

$(8.7 \times 10^{-10})^3\ [1/2\ (2.0904 \times 10^{-29})] = -3.6525 \times 10^{-29}\ C\ m$

3. Calculation of transition dipole moment , μ_{eg}

$\mu_{eg} = (area / \bar{\upsilon}_{eg}\,\eta\,M)^{1/2}\ [3\ (2.303)\ \in_o c\,h / 2\,\pi^2\,N_o]^{1/2}$

Consider parameters for **MNR-1** in ethyl acetate

parameters: $area = 6.4557 \times 10^7\ m^{-2}$

$\bar{\upsilon}_{eg} = 2.6434 \times 10^6\ m^{-1}$

$\eta = 1.36978$

$M = 2.11 \times 10^{-2}\ mol\ m^{-3}$

$N_o = 6.022 \times 10^{23}\ mol^{-1}$

unit analysis: $[m^{-2} / m^{-1}\ (mol\ m^{-3})]^{1/2}\ [(C^2\ N^{-1}\ m^{-2})\ (m\ s^{-1})\ (N\ m\ s) / (mol^{-1})]^{1/2}$

$= C\ m$

μ_{eg} = [(6.4557 x 10^7) / (2.6434 x 10^6) (1.36978) (2.11 x 10^{-2})]$^{1/2}$ [3 (2.303) (8.854 x 10^{-12}) (2.998 x 10^{10}) (6.626 x 10^{-34}) / 2 π (6.022 x 10^{23})]$^{1/2}$

= 2.9391 x 10^{-29} C m

4. Calculation of molecular second order polarizability, $\beta_{xxx}(2\omega)$

$$\beta_{xxx}(2\omega) = \left(\frac{3}{2\hbar^2}\right) \frac{\mu_{eg}^2 (\mu_e - \mu_g) \omega_{eg}^2}{(\omega_{eg}^2 - \omega^2)(\omega_{eg}^2 - 4\omega^2)}$$

Consider parameters for **MNR-1** in ethyl acetate

parameters: μ_{eg} = 2.9391 x 10^{-29} C m (2.998 x 10^9 $cm^{3/2}$ $g^{1/2}$ s^{-1} / C) (10^2 cm / m)

= 8.8114 x 10^{-18} $cm^{5/2}$ $g^{1/2}$ s^{-1}

ω_{eg} = $\tilde{\upsilon}_{eg}$ (2π) = 4.9794 x 10^{15} s^{-1}

(μ_e - μ_g) = 3.6525 x 10^{-29} C m = 1.0950 x 10^{-17} $cm^{5/2}$ $g^{1/2}$ s^{-1}

ω = (1 / 1064 nm) (10^7 nm / 1 cm) (2.998 x 10^{10} cm / s) (2π)

= 1.7704 x 10^{15} s^{-1}

$\hbar$ = h / 2π = 1.0546 x10^{-34} kg m^2 s^{-1}) (1000 g / 1 kg) (10^4 cm^2 / m^2)

= 1.0546 x10^{-34} g cm^2 s^{-1}

unit analysis: [($cm^{10/2}$ $g^{2/2}$ s^{-2}) ($cm^{5/2}$ $g^{1/2}$ s^{-1}) (s^{-2})] / [($g^{4/2}$ $cm^{8/2}$ s^{-2}) (s^{-2}) (s^{-2})]

= $cm^{7/2}$ $g^{-1/2}$ s = cm^4 / statvolt = esu

where statvolt = $cm^{1/2}$ $g^{1/2}$ s^{-1}

$\beta_{xxx}(2\omega)$ = [3 / 2 (1.0546 x10^{-34})^2] [(8.8114 x 10^{-18})^2 (1.0950 x 10^{-17}) (4.9794 x 10^{15})^2] / {[(4.9794 x 10^{15})^2 - (1.7704 x 10^{15})^2] [(4.9794 x 10^{15})^2 - 4 (1.7704 x 10^{15})^2]} = 107.09 x 10^{-30} esu

Determination of $I^{2\omega}/I^{\omega}$.[15] SHG experiments on **P-10** were performed by Dr. Roger Reeves of the Physics Department with a modelocked Nd:YAG laser producing 20 ps single pulses at 1064 nm. The absolute conversion efficiency was determined by measuring the ratio of the 532 and the 1064 nm signal intensities and applying corrections

for the relative responses of the monochromator and photomultiplier tube to the two wavelengths.

The conversion efficiency of **P-10** film sample was measured as function of input intensity at an angle of $\theta = 50^{o}$, and the results obtained are shown in Figure 1. Absolute efficiencies approach 10^{-7}, which are typical values for organic polymer films.

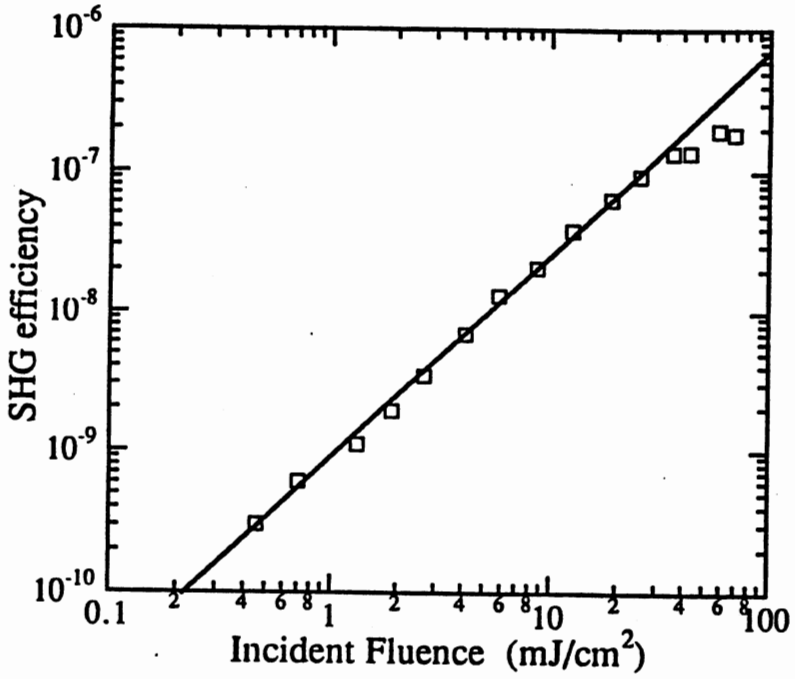

Figure 47. SHG efficiency of a film of **P-10** as a function of input intensity at $\theta = 50^{o}$.

Discussion

The measurements from cyclohexane and toluene were not included in the calculation of the best-fit values of A, B, and $\tilde{\upsilon}_{eg}^{\S}$ in eq 6 because the values obtained from $\{[(\epsilon - 1) / (\epsilon + 2)] - [(\eta^2 - 1) / (\eta^2 + 2)]\}$, the coefficient of B in eq 6, for the two

solvents are so close to zero that the calculated value of B could have a large random error. Although, the inclusion of C_6H_{12} and C_7H_8 data gives better solvatochromic data because it covers a greater range of polarity, there was no significant change in the value of B when data from C_6H_{12} and C_7H_8 were included. Therefore, these two solvents were not used in the solvatochromic measurements of **MNR-2**.

The expression for the solvatochromic shift that Paley and his coworkers[9] found useful is that of McRae[11] (eq 6). In the calculation of the μ_e, eq 7, they have assumed that the cavity radius, *a*, equals 0.7 times the length of the donor-to-acceptor length of the molecule; this is somewhat arbitrary choice gives good fit to McRae's equation and gives values of μ_e that compare well with available literature values. In a paper by Stiegman and his coworkers[16], the constant B is equal to $2\,\mu_g\,(\mu_g - \mu_e) / h\,c\,a^2$ and the unit of B is esu. The Onsager radius, *a*, was estimated from crystal structure data as the volume of an ellipse whose long axis was taken as the donor-to acceptor length of the molecule and whose short axis was taken as the in-plane width of the molecule at the largest point. It is the uncertainty in estimating *a*, as well as the various assumptions made in deriving eq 6, that make the solvatochromic method of calculating μ_e less accurate than EFISH measurements. I have chosen the method of Paley and his coworkers in evaluating the value of μ_e. The values of β_{xxx}, obtained from solvatochromic method, are not expected to be equal to those of β_x, obtained by EFISH, eq 11. They are two different quantities; β_x is the vector part of a tensorial property, whereas β_{xxx} is only one component of the tensor.

$$\beta_x \equiv \beta_{xxx} + 1/3\,(\beta_{xyy} + 2\,\beta_{yxy} + \beta_{xzz} + 2\,\beta_{zxz}) \qquad (11)$$

A direct comparison of the absolute magnitudes of these two quantities is not very informative. Paley and his coworkers compared the trend in the values of β_{xxx} with the trend in the values of β_x. They observed an excellent agreement at 1064 and 1907 nm.

Thus, β_{xxx} can be used as well as β_x for evaluating the relative merit of small organic compounds for SHG. The β_{xxx} values obtained were found to be dependent on the solvents employed.

The position and intensity of an electronic spectra can be influenced by solvents. In a solution, molecules having a permanent dipole moment cause an electric dipole field and this field acts on the surrounding solvent molecules. If the solvent molecules have a permanent dipole moment, they orient themselves with their dipole moment parallel to the field. Although, not all the solvent molecules are ideally oriented at any time since orientation is opposed by thermal motion. If the solvent molecules have no permanent dipole moment, a dipole moment is induced in the dipole field of the dissolved molecule. From the permanent and induced dipole moments of the solvent molecules, this in turn produces a dipole field in its environment and acts on the dissolved molecule in the same way as an external field. The extinction coefficient of an absorption band whose transition moment is parallel to the dipole moment increases in a field, while that of a band whose transition moment is perpendicular to the dipole moment decreases. The electronic excitation of a molecule is also associated with the change in the dipole moment, $\mu_g - \mu_e$, which leads to a field-dependent shift of the band. The band shift leads to a broadening of the absorption band in a field, and since this broadening is unsymmetrical, the maximum of the band is also shifted.

The energy absorbed in the ultraviolet region produces changes in the electronic energy of the molecule resulting from transitions of valence electrons in the molecule. These transitions consist of the excitation of an electron from an occupied molecular orbital to the next higher energy orbital. The energy absorbed is dependent on the energy difference between the ground state and the excited state; the smaller the difference in energy, the longer the wavelength of absorption. In the six solvents, the λ_{max} of **MNR-1** is always about 10 nm greater than the corresponding λ_{max} of **MNR-2**. This means that the energy difference between the ground state and the excited state of **MNR-1** is less

than that of **MNR-2.** The chromophore of **MNR-1** is flat, thus the delocalization of the π-electrons from the amino to the ester groups is effective, giving rise to lower energy of the $\pi \rightarrow \pi^*$ transition. On the other hand, the piperidino ring in **MNR-2** must be twisted, as shown in Figure 48, to obtain a flat conformation of the chromophore. At times when the piperidino ring is not in the twisted conformation, the delocalization of the π-electrons is not as effective as it should be, therefore **MNR-2** absorbs at a shorter wavelength.

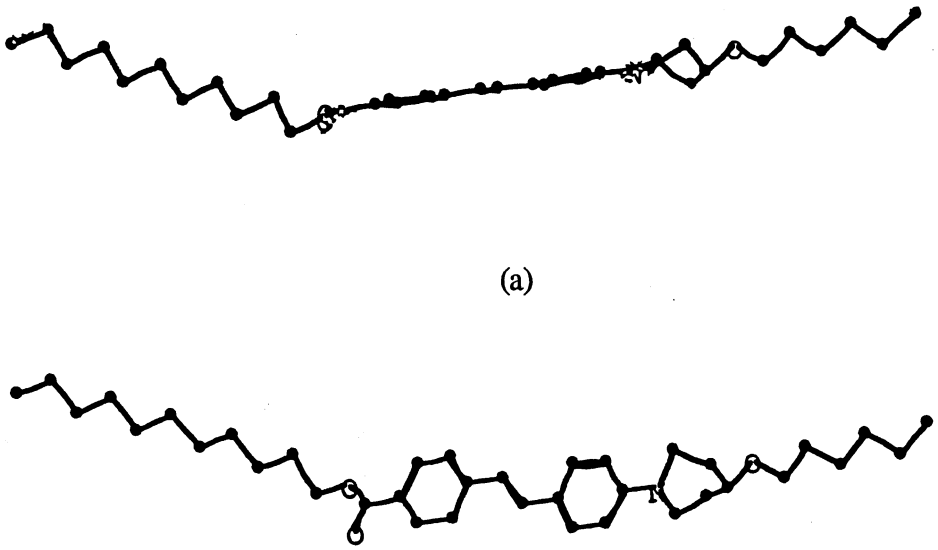

(a)

(b)

Figure 48. Computer drawings of the most stable conformation of **MNR-2**, viewed from (a) the side and (b) the top.

Preliminary experiments showed that **P-10** has strong picosecond SHG responses at 1064 nm. The molecular contribution d_{33} to $\chi^{(2)}$ of **P-10**, after it was corrected for path length and number density, is a factor of 5.6 less than that of DANS doped in PMMA. This is not surprising since DANS has a strongly electron-withdrawing nitro group as compared to a moderately electron-withdrawing carboxylic ester group in **P-10.**

This agreed with the solvatochromic data in which the β_{xxx} values obtained for **MNR-1** and **MNR-2** are 3x less than that of the β_{xxx} obtained for DANS (300 x 10^{-30} esu). The SCLC polysiloxanes do not give transparent films when spin coated onto indium tin oxide (ITO)-coated glass. It is not known whether these translucent film will become transparent upon alignment of the chromophore. Unless these films become transparent, there is no way one can use this method for SHG experiments. The polysiloxanes will not have problems in attaining high degree of alignment. However, maintaining alignment for a long period after electrical poling might not be possible since the T_g's of the polysiloxanes are below room temperature, unless the anisotropic ordering can be frozen in the crystalline phase, which is observed at room temperature.

In comparison to the SCLC copolysiloxanes studied by Carr and Goodwin[17], in

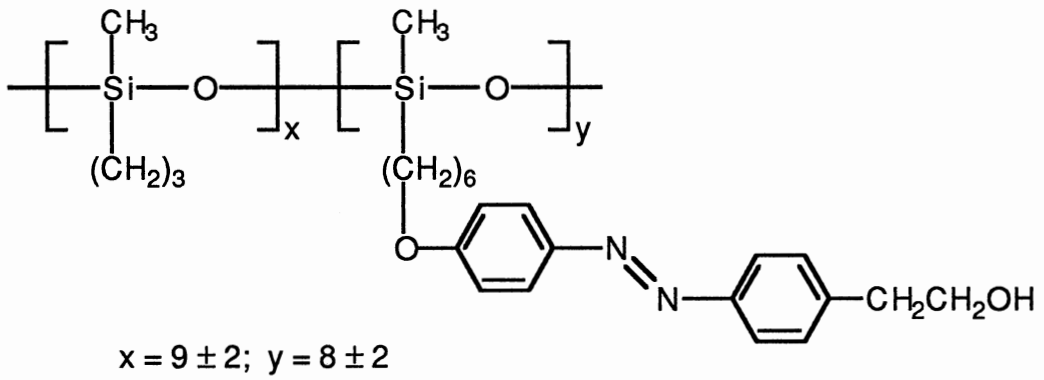

which they reported a β_z value of 8.4 x 10^{-29} esu for the repeat unit, I believed that the LB films of my copolysiloxanes will give higher SHG signal because it has better electron donor-acceptor substituents on each end of the stilbene. In addition, the UV-vis spectrum (Figure 40) of the LB film of **CPS-2** showed a shift in the λ_{max} to a lower wavelength, which will possibly give a nonresonant $\chi^{(2)}$.

REFERENCES

1. Levine, B. F.; Bethea, C. G. *J. Chem. Phys.* **1975**, 63, 2666-2682.
2. Levine, B. F. *Chem. Phys. Lett.* **1976**, 37, 516-520.
3. Oudar, J. L.; Chemla, D. S. *J. Chem. Phys.* **1977**, 66, 2664-2668.
4. DeQuan, L.; Ratner, M. A.; Marks, T. J. *J. Am. Chem. Soc.* **1988**, 110, 1707-1715.
5. Liptay, W. *Angew. Chem., Int. Ed. Engl.* **1969**, 8, 177-188.
6. Meredith, G. R.; Van Dusen, J. G.; Williams, D. J. *Macromolecules* **1982**, 15, 1385-1389.
7. Jerphagnon, J.; Kurtz, S. K. *J. Appl. Phys.* **1970**, 41, 1667-1681.
8. Prasad, P. N.; Williams, D. J. *Introduction to Nonlinear Optical Effects in Molecules and Polymers*; John Wiley & sons, Inc.: New York, 1991; pp 117-121.
9. Paley, M. S.; Harris, J. M.; Looser, H.; Baumert, J. C.; Bjorklund, G. C.; Jundt, D.; Twieg, R. J. *J. Org. Chem.* **1989**, 54, 3774-3778.
10. Frazer, R. D. B.; Suzuki, E. In *Physical Principles and Techniques in Protein Chemistry*, Leach, S. J., Ed.; Academic Press: New York, 1973; p 323.
11. McRae, E. G. *J. Phys. Chem.* **1957**, 61, 562-572.
12. Riddick, J. A.; Bunger, W. B.; Sakano, T. K. *Organic Solvents: Physical Properties and Methods of Purification*, John Wiley & Sons: New York, 1986.
13. Hine, J. S. *Physical Organic Chemistry*, McGraw-Hill Book Company: New York, 1962; p 87.
14. Ulman, A. *J. Phys. Chem.* **1988**, 92, 2385-2390.
15. Ford, W. T.; Bautista, M.; Zhao, M.; Reeves, R. J.; Powell, R. C. *Mol. Cryst. Liq. Cryst.* **1991**, 198, 351-356.

16. Stiegman, A. E.; Graham, E.; Perry, K. J.; Khundkar, L. R.; Cheng, L.-T.; Perry, J. W. *J. Am. Chem. Soc.* **1991**, 113, 7658-7666.

17. Carr, N.; Goodwin, M. J. *Makromol. Chem., Rapid Commun.* **1987**, 8, 487-493.

APPENDIX

SELECTED NMR SPECTRA

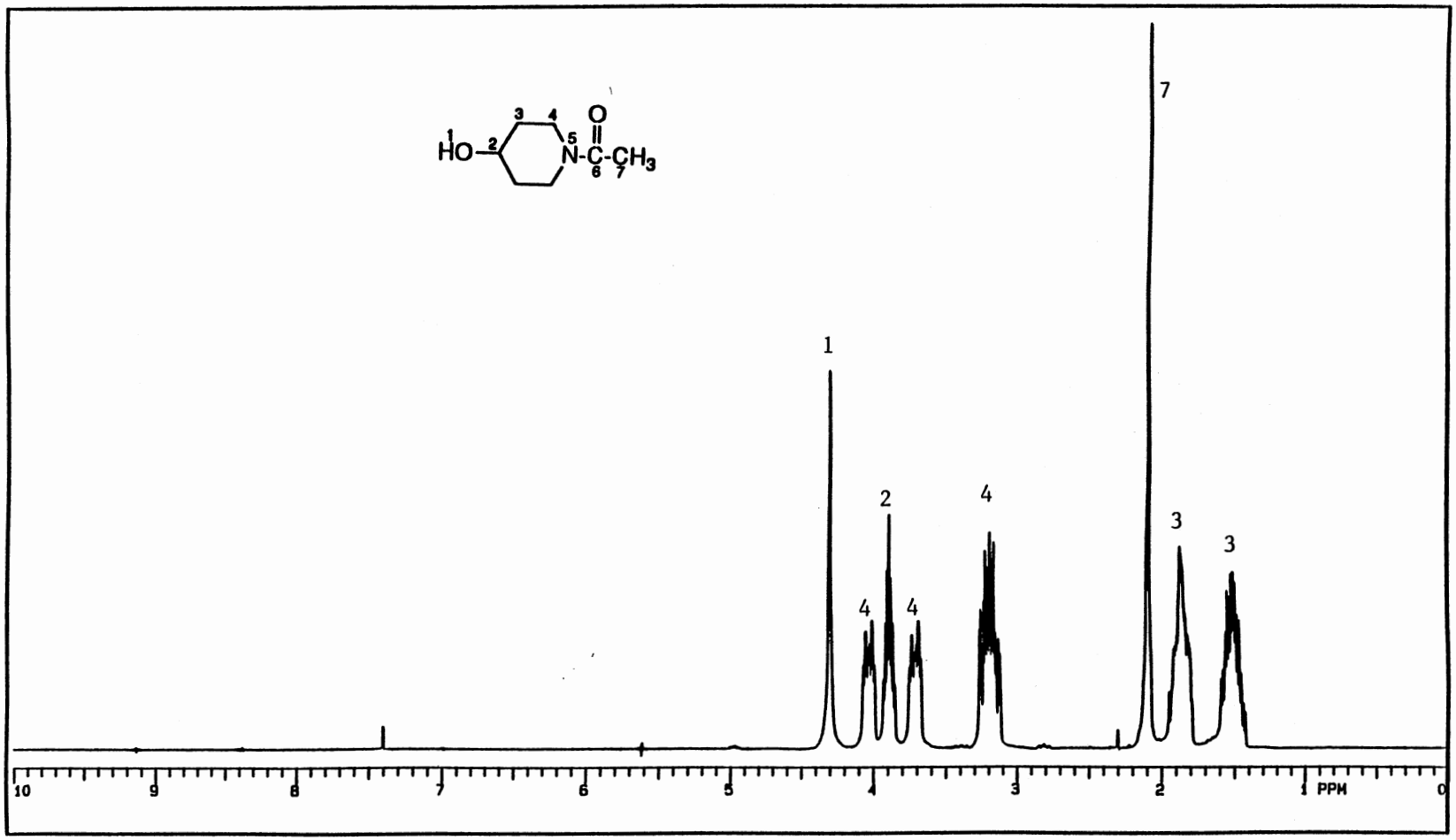

Spectrum 1. ^{1}H NMR Spectrum of N-acetyl-4-hydroxypiperidine, **2.**

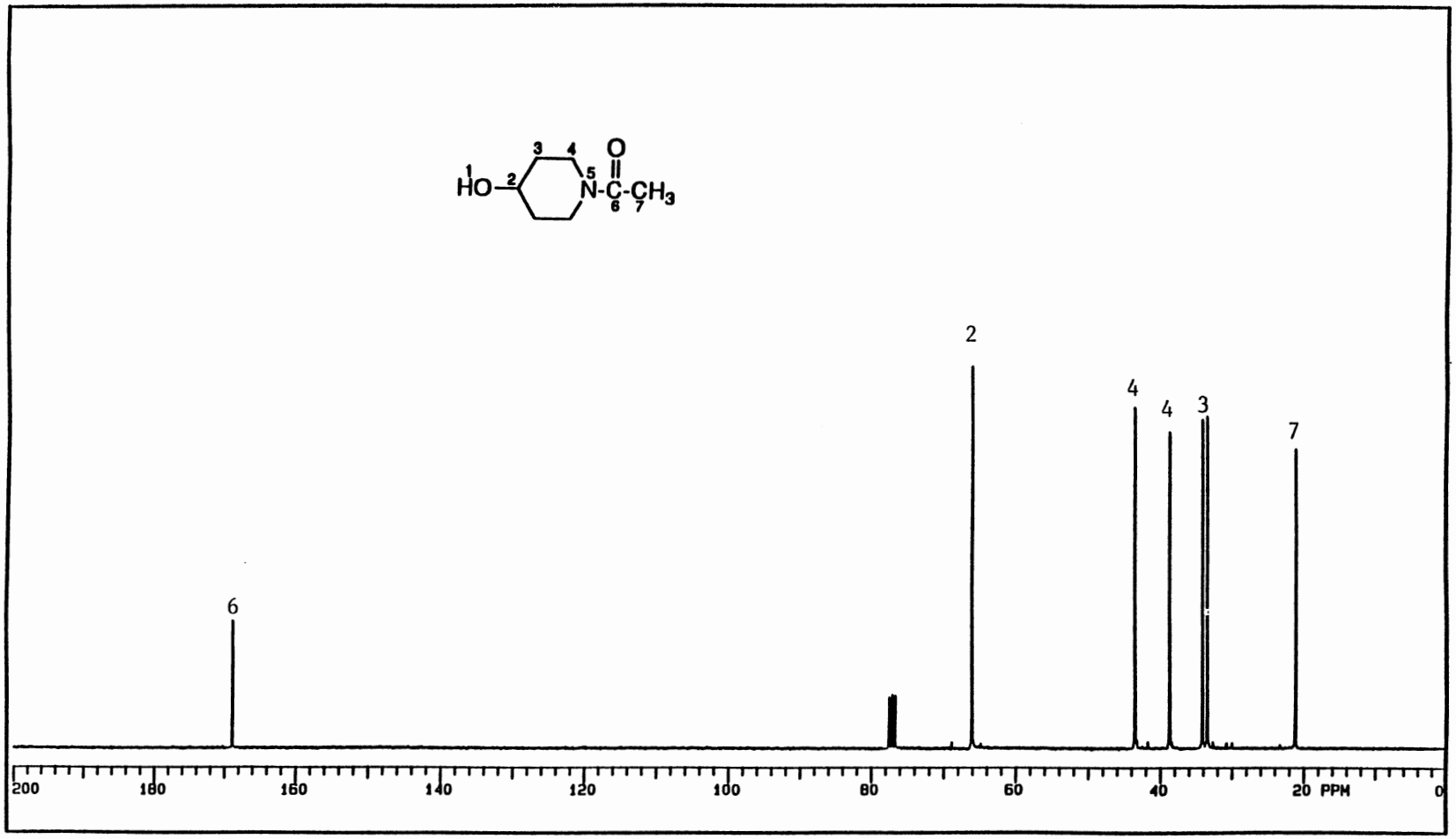

Spectrum 2. ^{13}C NMR Spectrum of N-acetyl-4-hydroxypiperidine, **2**.

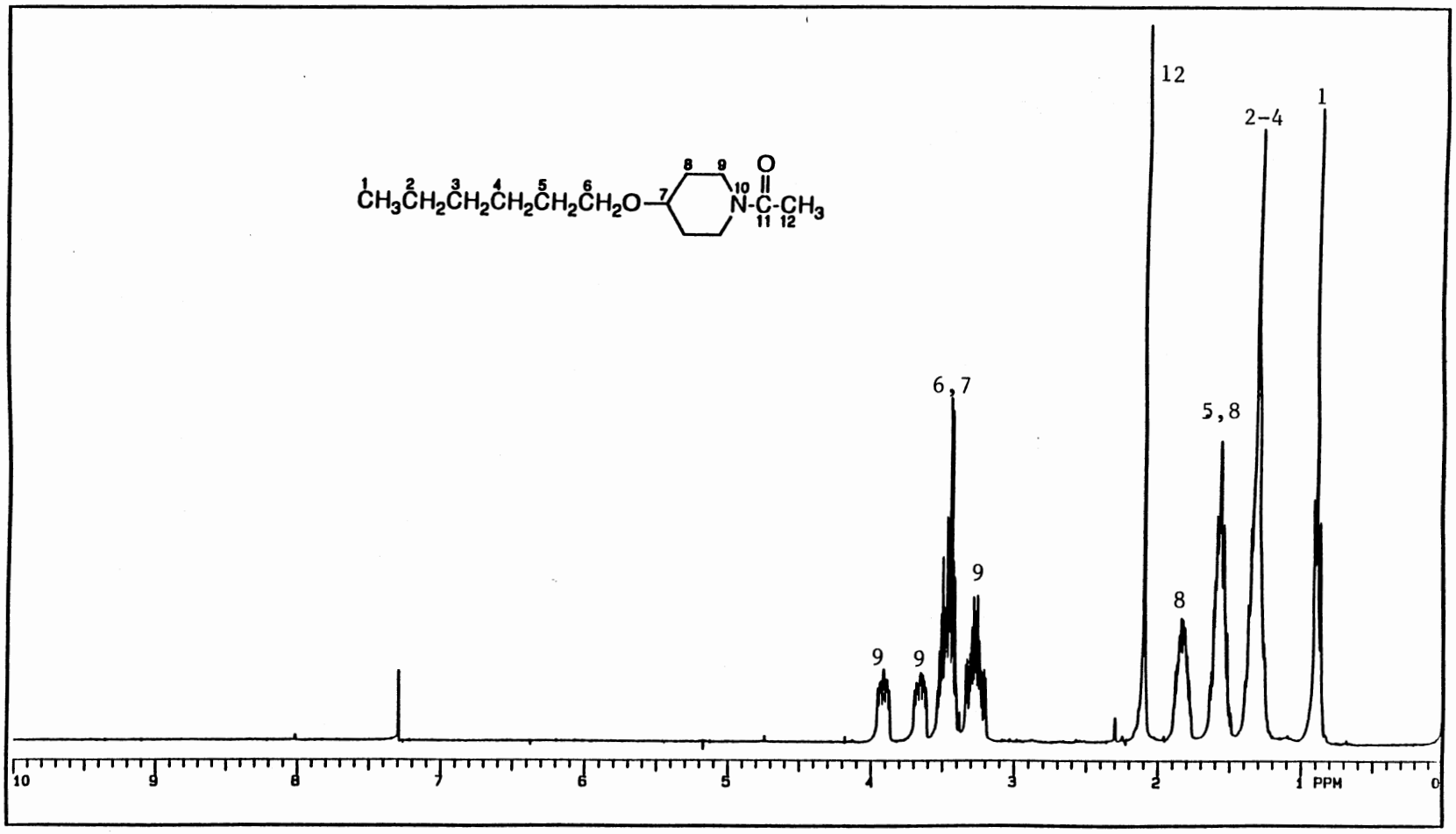

Spectrum 3. ^{1}H NMR Spectrum of N-acetyl-4-hexyloxypiperidine,**3**.

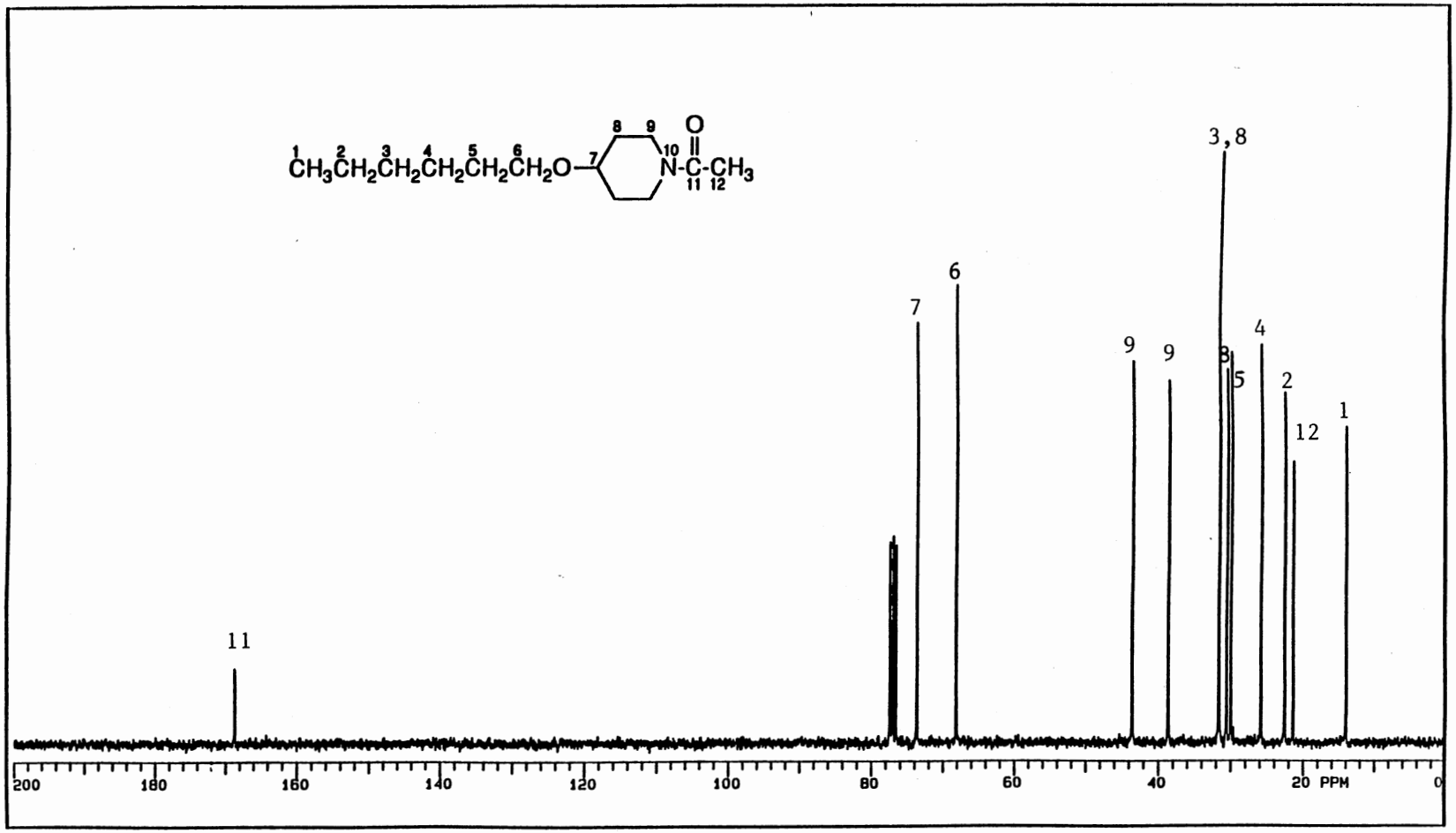

Spectrum 4. ^{13}C NMR Spectrum of N-acetyl-4-hexyloxypiperidine, **3**.

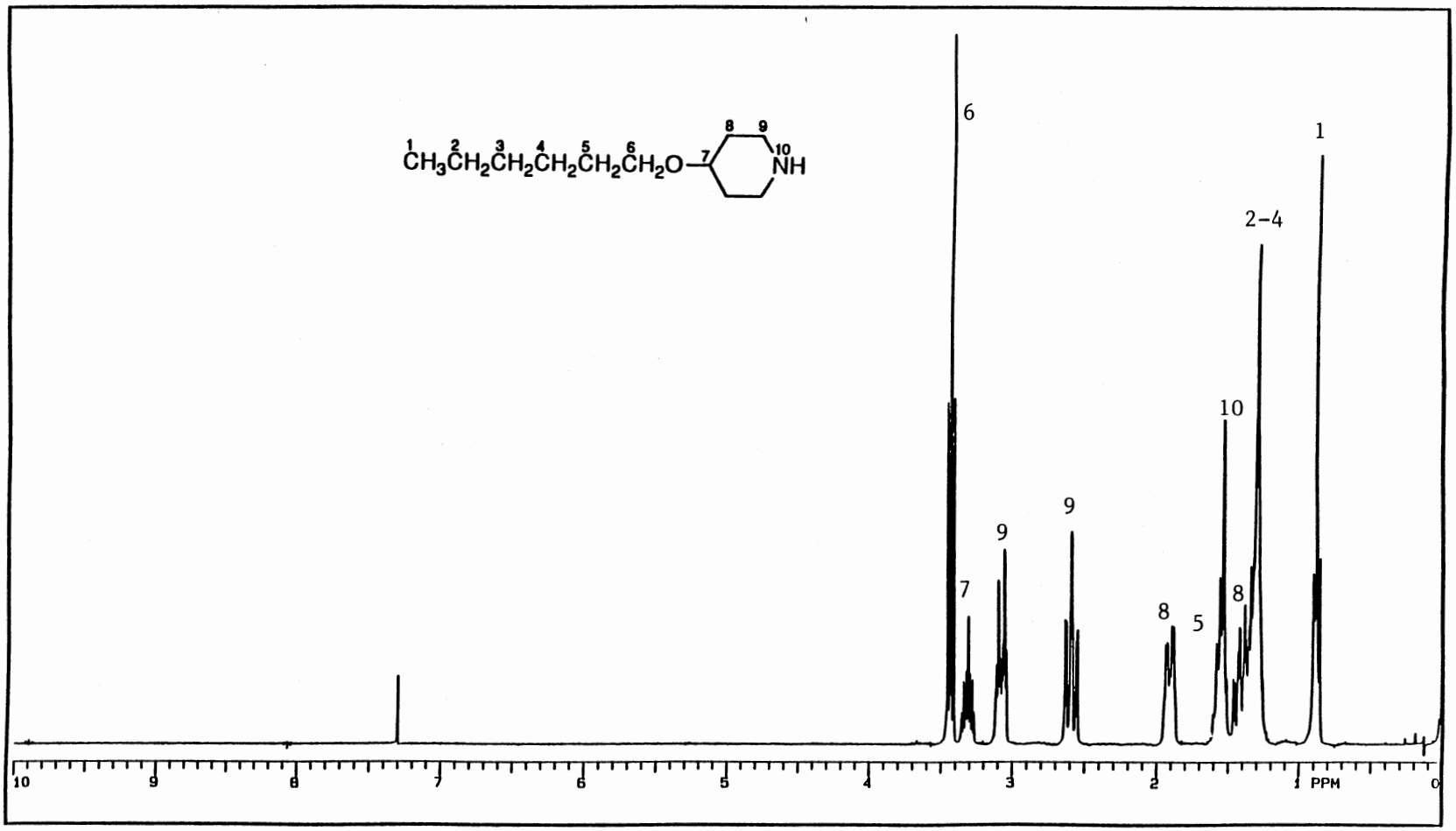

Spectrum 5. ^{1}H NMR Spectrum of 4-hexyloxypiperidine, **4**.

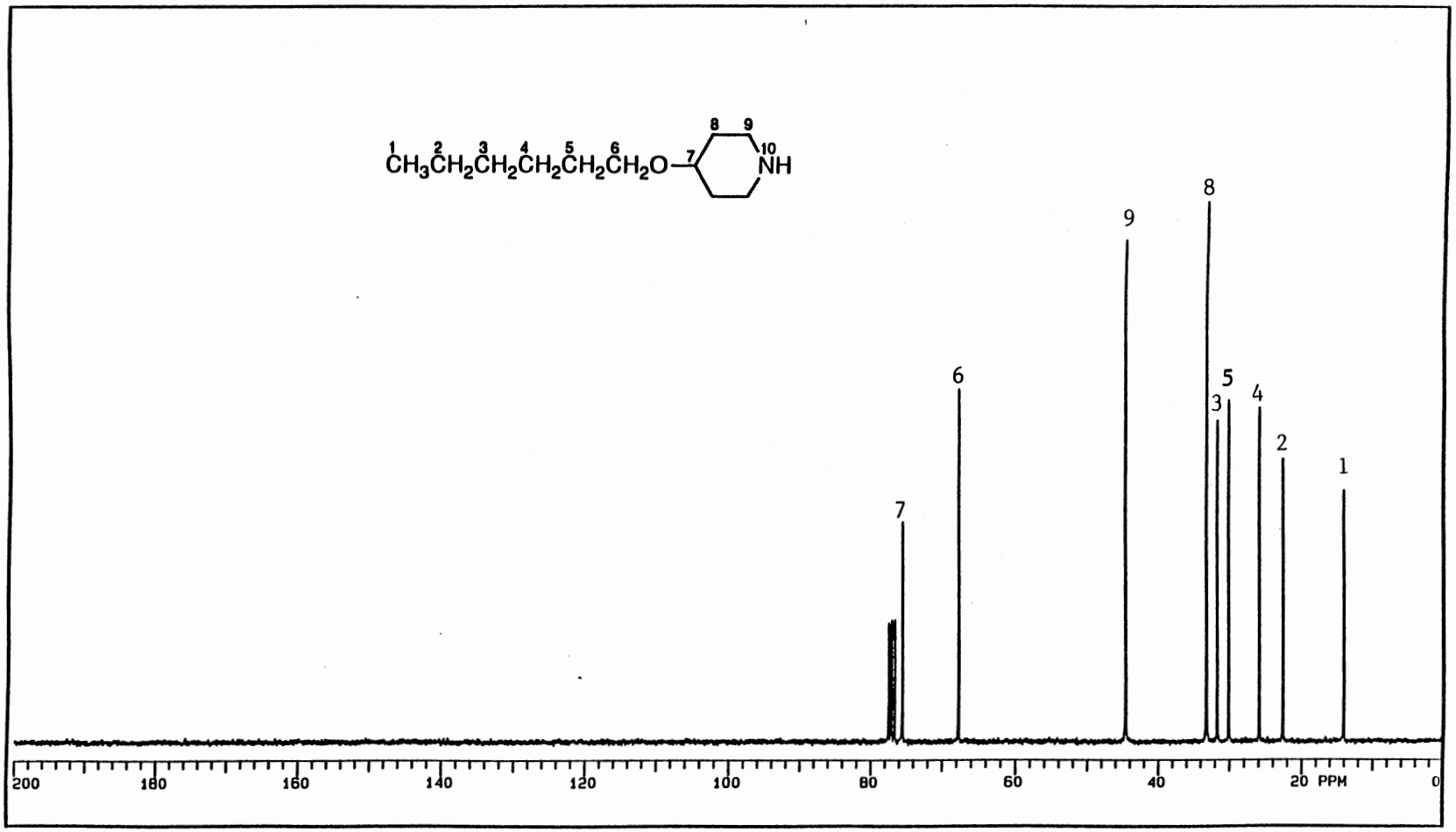

Spectrum 6. ^{13}C NMR Spectrum of 4-hexyloxypiperidine, **4**.

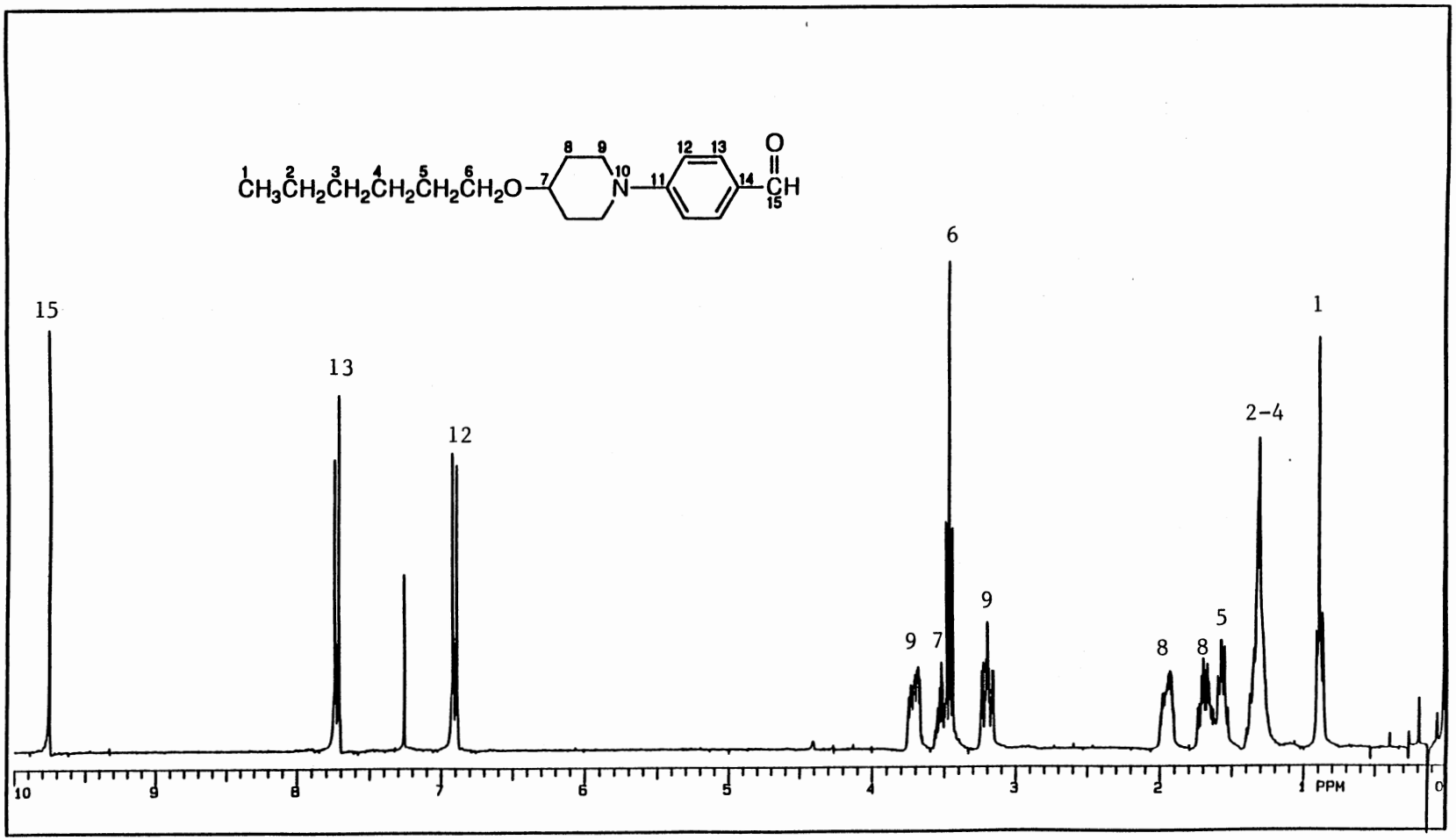

Spectrum 7. ^{1}H NMR Spectrum of 4-(4'-hexyloxy-1-piperidino)benzaldehyde, **5**.

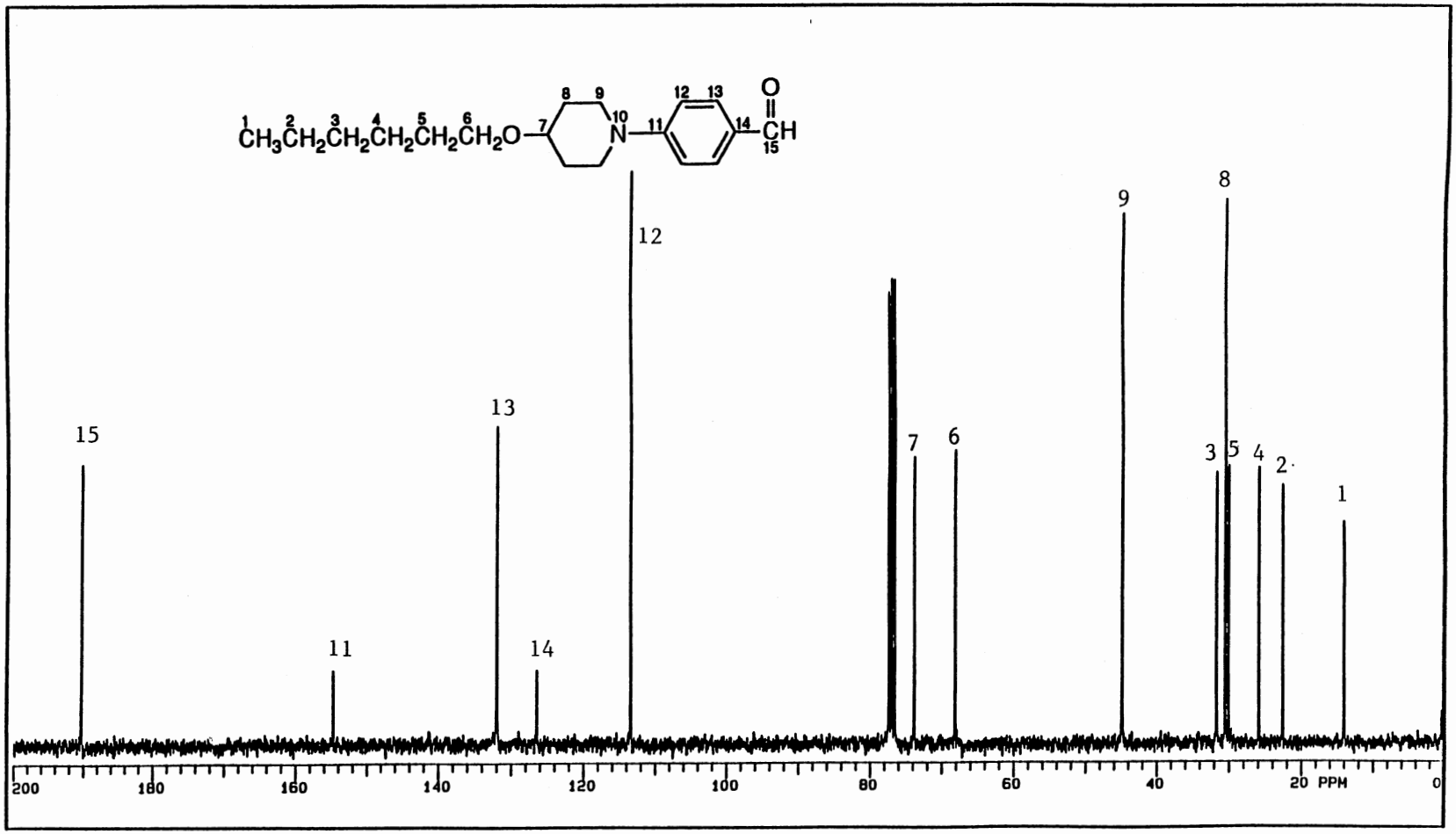

Spectrum 8. ^{13}C NMR Spectrum of 4-(4'-hexyloxy-1-piperidino)benzaldehyde, **5**.

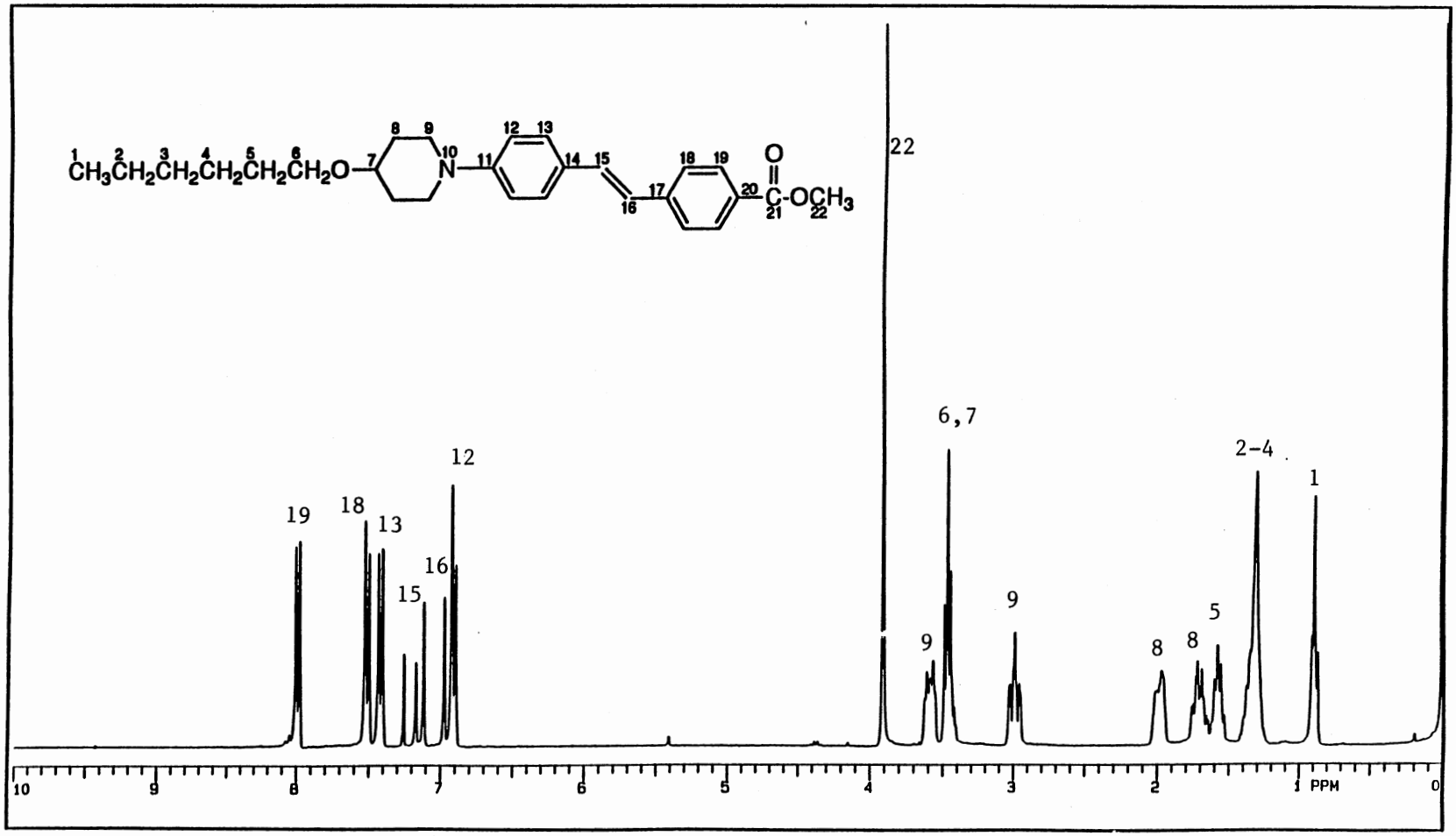

Spectrum 9. ^{1}H NMR Spectrum of 4-(4-hexyloxy-1-piperidino)-4'-carbomethoxy-*trans*-stilbene, **10**.

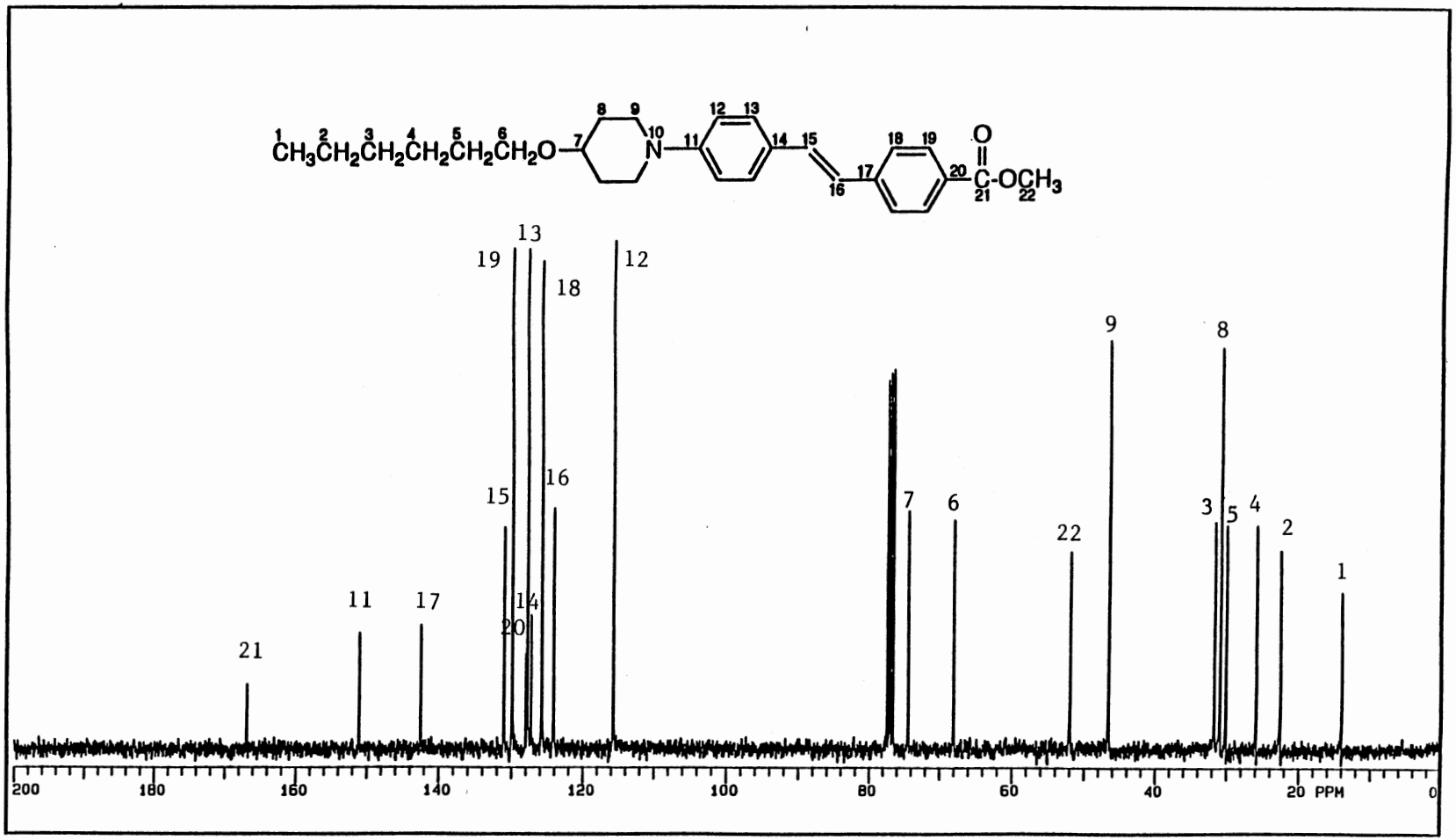

Spectrum 10. ^{13}C NMR Spectrum of 4-(4-hexyloxy-1-piperidino)-4'-carbomethoxy-*trans*-stilbene, **10**.

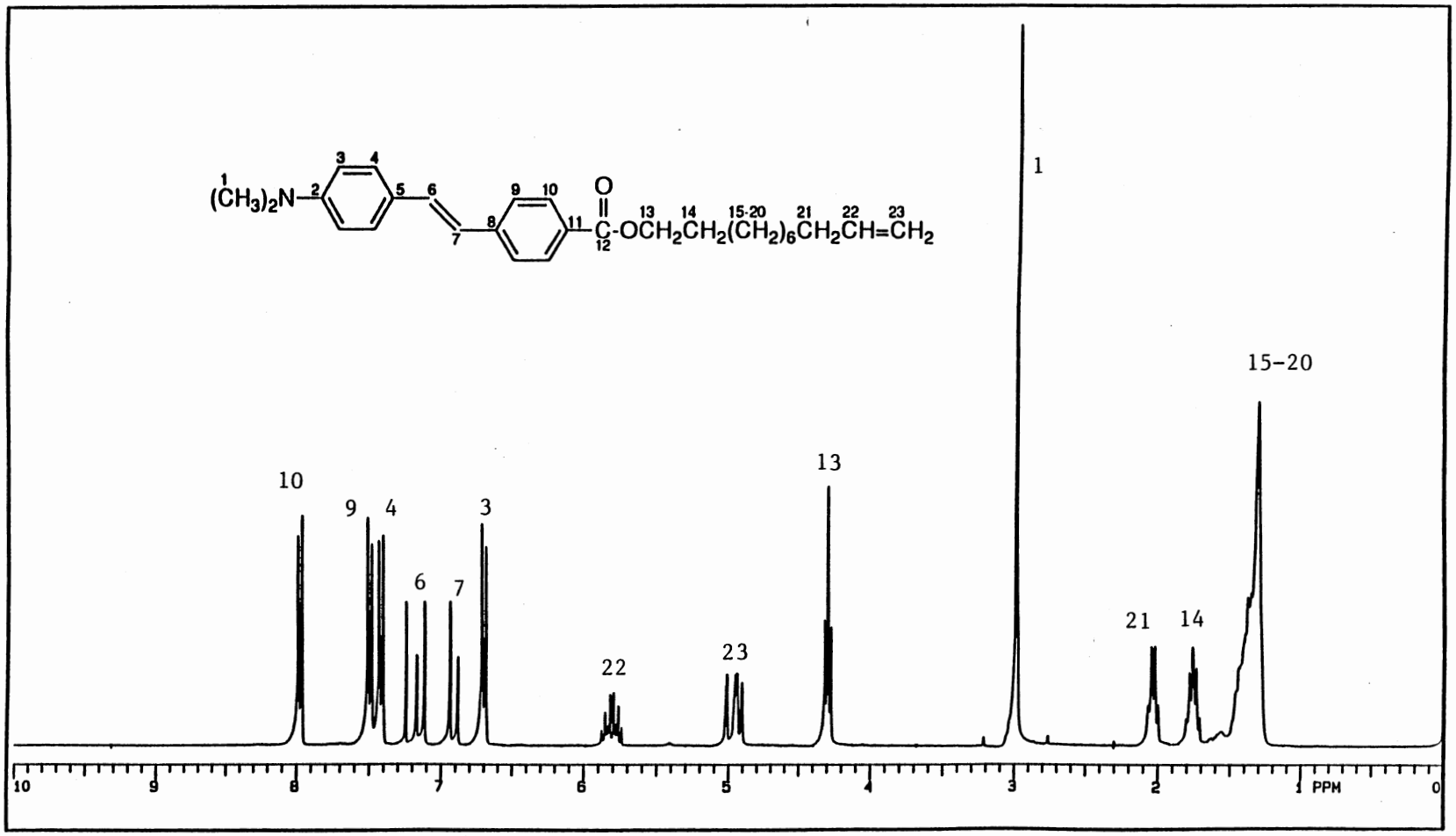

Spectrum 11. ^{1}H NMR Spectrum of 10-undecen-1-yl-4-(N,N-dimethylamino)-*trans*-stilbene-4'-carboxylate, **MNR-1**.

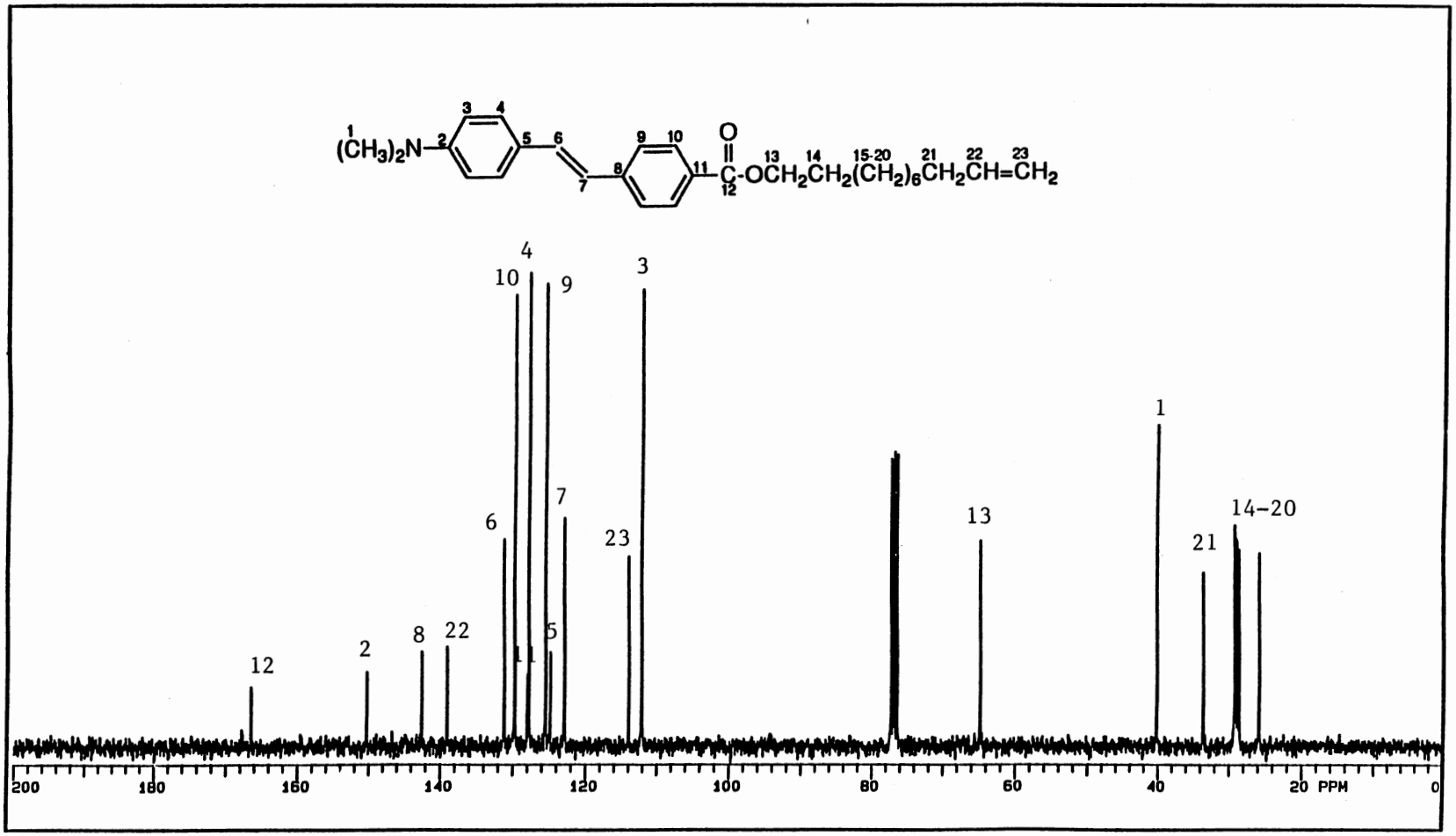

Spectrum 12. ^{13}C NMR Spectrum of 10-undecen-1-yl-4-(N,N-dimethylamino)-*trans*-stilbene-4'-carboxylate, **MNR-1**.

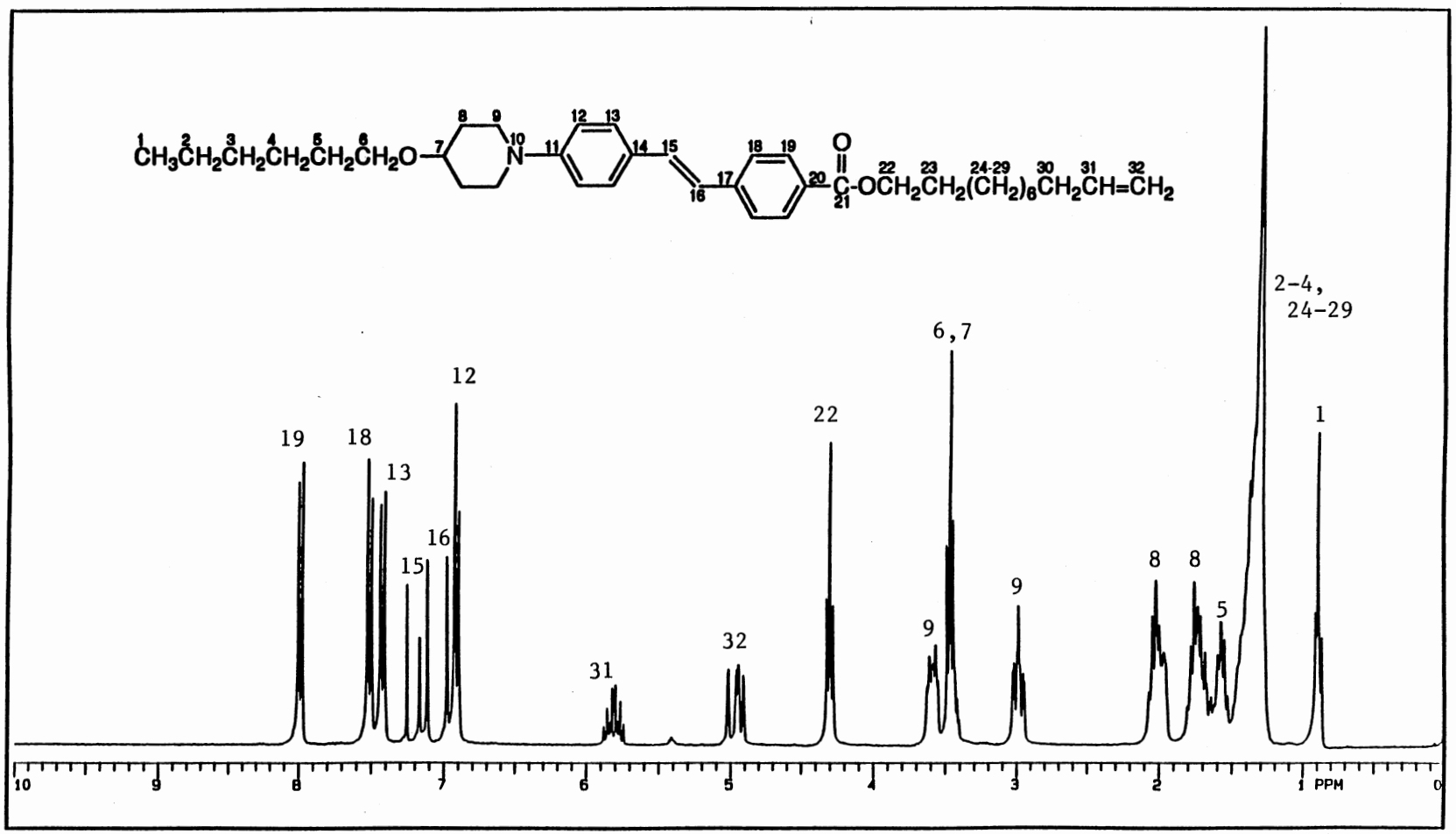

Spectrum 13. ^{1}H NMR Spectrum of 10-undecen-1-yl-4-(4-hexyloxy-1-piperidino)-*trans*-stilbene-4'-carboxylate, **MNR-2**.

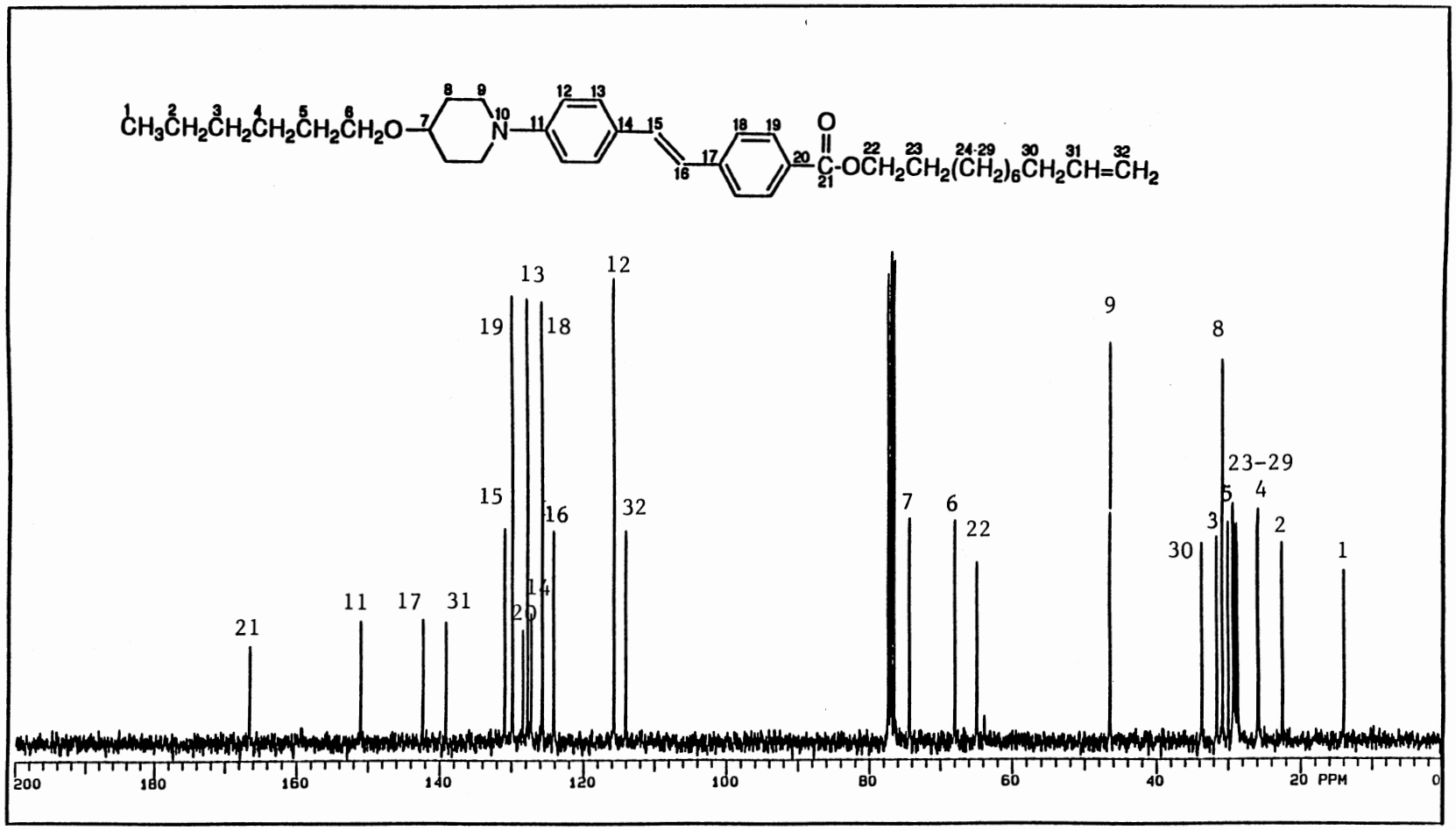

Spectrum 14. ^{13}C NMR Spectrum of 10-undecen-1-yl-4-(4-hexyloxy-1-piperidino)-*trans*-stilbene-4'-carboxylate, **MNR-2**.

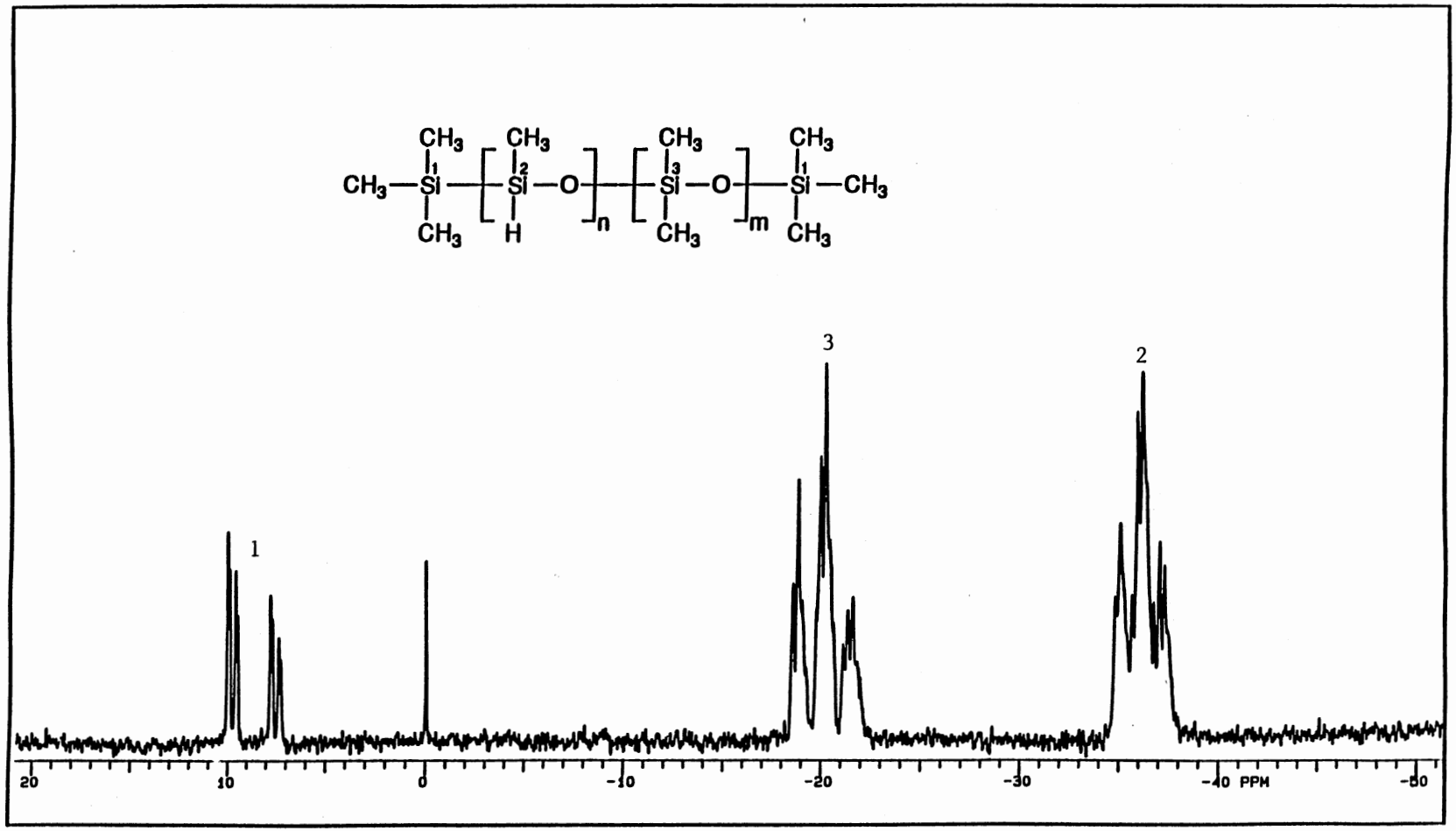

Spectrum 15. ^{29}Si NMR Spectrum of poly(hydromethylsiloxane-co-dimethylsiloxane (50-55% wt% hydromethyl).

VITA

Marietta O. Bautista

Candidate for the Degree of

Doctor of Philosophy

Thesis : LIQUID CRYSTALLINE SIDE CHAIN POLYSILOXANES WITH 4-AMINO-4'-STILBENE-CARBOXYLIC ESTER MESOGENS

Major Field: Chemistry

Biographical:

Personal Data: Born in Dagupan City, Philippines, March 4, 1961, the daughter of Paulino and Nenita Bautista

Education: Graduated from Dagupan City National High School, Dagupan City, Philippines, in April, 1978; received Bachelor of Science in Chemistry from University of the Philippines at Los Banos, Los Banos, Philippines, in October, 1982; completed requirements for the Doctor of Philosophy Degree at Oklahoma State University, Stillwater, Oklahoma, U.S.A., in May, 1992.

Personal Experience: Instructor, Institute of Chemistry, University of the Philippines at Los Banos, Los Banos in October, 1982 to June, 1986; Teaching Assistant, Department of Chemistry, Oklahoma State University, August, 1986 to May, 1990.